Maximum Power Point Tracking of PV System Using ANFIS Prediction and Fuzzy Logic Tracking

by

Abdulaziz Aldobhani

School of Computing, Faculty of Computing
Sciences and Engineering, De Montfort University, UK

Dissertation submitted in partial fulfillment
of the requirements for the degree of

Doctor of Philosophy

in Computer Engineering

September, 2008

Abstract

Operating faraway from maximum power point decreases the generated power from photovoltaic (PV) system. For optimum operation, it is necessary to continually track the maximum power point of the PV solar array. However with huge changes in external influences and the nonlinear relationship of electrical characteristics of PV panels it is a difficult problem to identify the maximum power point as a function of these influences. Many tracking control strategies have been proposed to track maximum power point such as perturb and observe, incremental conductance, parasitic capacitance, and neural networks. These proposed methods have some disadvantages such as high cost, difficulty, complexity and non-stability.

This thesis presents a novel approach based on Adaptive Neuro-Fuzzy Inference System (ANFIS) to predict the maximum power point utilising the actual field data, which is performed in different environmental conditions. The short circuit current and open circuit voltage are used as inputs to PV panels instead of solar irradiation and cell junction temperature.

The predicted V_{max} from ANFIS model is used as a reference voltage for fuzzy logic controller (FLC). The FLC is used to adjust the duty cycle of the electronic switch of two types of DC-DC converter. These DC-DC converters are used to interface between the load voltage and PV panels. The duty cycle of the electronic switch of the DC-DC converter is adjusted until the input voltage of the converter tracks the predicted V_{max} of the PV system.

FLC rules and membership functions are designed to achieve the most promising performance at different environmental conditions, different load types and different rate of changes in the duty cycle of Buck-Boost and Buck converters. The membership functions and fuzzy rules of FLC are designed to balance between different required features such as quick tracking under different environmental conditions, high accuracy, stability and high efficiency.

Declaration

I declare that the work described in this thesis is original work undertaken by me for the degree of Doctor of Philosophy, at the School of Computing, Faculty of Computing Sciences and Engineering, at De Montfort University, Leicester, United Kingdom.

No part of the material described in this thesis has been submitted for the award of any other degree or qualification in this or any other university or college of advanced education.

Abdualziz M. Aldobhani
Leicester, United Kingdom
September, 2008

List of Publications

Published papers:

Abdulaziz M. S. Aldobhani and Robert John, "Maximum Power Point tracking under Different Environment Conditions for Solar Photovoltaic Panels Using ANFIS Model" JOURNAL OF SCIENCE AND TECHNOLOGY , Year 2007 Volume(12) Number(1)

Abdulaziz M. S. Aldobhani and Robert John, "Maximum Power Point Tracking of PV System Using ANFIS Prediction and Fuzzy Logic Tracking" The 2008 IAENG International Conference on Control and Automation Hong Kong, 19-21 March, 2008.

Abdulaziz M. S. Aldobhani and Robert John, "Using ANFIS Model and Fuzzy Logic Controller to Track Maximum Power Point of PV System,IEEE Industrial electronics, The 20th chinese control decision conference, 2-4 July, 2008.

Abdulaziz M. S. Aldobhani and Robert John, "A novel ANFIS Model and Fuzzy Logic Controller for Maximum Power Point Tracking of PV Systems, American Institute of Physics for the IMECS 2008, IAENG Transactions on Engineering Technologies (Accepted).

Dedication

To my mother and father:

The two uneducated persons who taught me,

for their endless love.

To my family:

Who have supported me while they had to

be extremely patient during the research years.

Acknowledgements

First and foremost, my deepest gratefulness goes to GOD for all his blessings without which nothing of my work would have been done.

I would also like to express my sincere gratitude to my supervisor Prof. Robert John at De Montfort University, Leicester, UK, for his guidance, ideas, valuable directions and support throughout my research study. I am deeply indebted to him for his insights and suggestions to the thesis topic and for valuable supervision at various stages of my work. Many thanks also to my second superervisor Prof. Marwan Al-Akaidi for all support I have received from him.

I would also like to thank my sponsor University of Science and Technology (UST) in Yemen, especially Prof. Abdulraqib Asaad, Prof. Dawood Alhodabi, Dr. Abdo Almakalah, Eng. Mohamed Alhothely, Pof. Abdualziz Alkabib, Prof Tawfic Sofyan and all my colleagues there who supported me in order to complete this thesis.

Special thank to my wife, Zolika for her great support during the research years. Also, for my son Omar and my daughter Asma who help me during data collection time.

Finally I would like to express my gratefulness to my friends and colleagues Mr. Moussa Barkhadleh, Mr Abdulakider Aroa, Mr. Ammar Alzahary, and Mr. Mohammed Alshaddadi who helped me to overcome many troubles during the research years.

List of Acronyms

A	Ideality factor
η	Efficiency
G	Irradiance level
I	Elictrical current
I_D	Dark current
I_{max}	Maximum power point current
I_O	Output current
I_{op}	Operating current
I_{PH}	Photo current
I_S	Saturation current
I_{SC}	Short circuit current
K_B	Boltzmann's gas constant
P_{max}	Maximum power point power
q	Electronic charge
R	Electrical Resistance
R_P	Electrical Resistance
R_S	Electrical Resistance
t_{on}	On time
T_a	Ambient temperature
T_C	Cell junction temperature
T_S	Cell temperature
V	Electrical Voltage
V_{in}	Input voltage
V_{max}	Maximum power point voltage
V_O	Output voltage
V_{OC}	Open circuit voltage
V_{op}	Operating voltage
V_{ref}	Referance voltage

ANFIS	Adaptive Neuro-Fuzzy Inference System
D	Duty cycle
DC	Direct Current
FIS	Fuzzy Inferance System
FLC	Fuzzy Logic Controller
Genfis	Generate Fuzzy Inference System
IEEE	Institute of Electrical and Electronics Engineers
LSE	Least Square Estimation
MFs	Membership Functions
MOSFET	Metal Oxide Semiconductor Field Effect Transistor
MPP	Maximum Power Point
MPPT	Maximum Power Point Tracking
NOCT	Nominal Operating Cell Temperature
PWM	Pulse Width Modulator
PV	Potovoltaic
RMSE	Root Mean Square Error
STC	Standard Test Condition
T	Period time

Contents

List of Tables

List of Figures

Chapter 1

Introduction

1.1 Overview

Solar energy has become an essential source for many applications in the last four decades. It is difficult to supply electrical energy to small applications in remote areas from the utility grid or from small generators. Stand alone photovoltaic (PV) systems are the best solutions in many small electrical energy demand applications such as communication systems, water pumping and low power appliances in rural areas [76] [8]. In general, the cost of electricity from the solar array system is more expensive compared to electricity from the utility grid [27] [52]. For that reason, it is necessary to study carefully the efficiency of the entire parts to design an efficient PV system to cover the load demands with lower cost.

There are many external and internal influences which have an effect on the efficiency of the PV panel. Solar irradiance, ambient temperature and wind are the main external influences, which affect the maximum power and the voltage of maximum power point of PV panel. These external influences also change the position of the maximum power point on the current voltage (I-V) curve. Furthermore, load is the main internal factor that can drive the PV panels to operate at a strict point on the I-V curve in direct coupled systems. The intersection between the different load line and I-V curves under different environmental conditions identifies the operating point on I-V curves. Hence, it is necessary to continually track the maximum power point (MPP) of the solar array [49]. However, the tracking control of MPP is a complicated problem. Many tracking control strategies have been proposed to overcome this problem such as: perturb and observe, incremental conductance, parasitic capacitance, constant voltage and neural networks [86][73]. The drawbacks of these methods comes from their high cost, difficulty, complexity, and non-stability [70]. In

the main methods these controlling mechanisms use is to adjust the duty cycle of the shunt metal oxide semiconductor field effect transistor (MOSFET) of maximum power point tracking (MPPT) converter. The MPPT converter is used to maintain the PV array's operating point at the MPP. MPPT controller does this by controlling the PV array's voltage or power independently of the load.

1.2 Motivation

The cost of electricity from the PV system is more expensive than from the utility grid. The PV panels are the main part and cost of a PV system, of the system. Poor operation of PV panels obliges the designers to increase the number of PV panels to cope with the energy demand for the load. This leads to the design of an uneconomic system. Studying the influences that affect the maximum power operation assists in building the optimum PV system. A large amount of power is saved by the optimum design of PV system thus reducing the total cost of PV system. Accordingly, the PV system becomes feasible for many applications, especially in rural areas.

In addition, during monitoring a Grundfos solar water pump in Yemen a high fluctuation is observed in MPPT control system that is used with this solar pump in cloudy days. The control system which use a traditional MPPT system also fluctuates during the wind movements [11]. This high oscillation in MPPT system decreases the live time of electronic devices, which control the duty cycle of DC-DC converters which interface between the PV panels and the loads. Hence, the developed approach in this thesis is designed to overcome this problem.

Generally, the designers add a constant percentage drop in power generated to compensate the drop in power due to temperature effect [27] [26]. However, there are high differences in the generated power from PV panels in different ambient temperatures. These differences in power generated can be more than 30% in enclosed areas [12]. Hence, studying the behaviour of PV panels in different regions is essential to improve the performance of PV panels in different environmental conditions. Sufficient data in different environmental conditions will help model the behaviour of PV

panels.

Insufficient input parameters, the lack of data and the difficulty in measuring the cell temperature and solar irradiance are drawbacks in many MPPT approaches. Hence, these provide additional motivation to introduce an approach that has sufficient and appropriate parameters to solve the above mentioned problems. In addition, the difference between actual MPP and computed MPP at different environmental conditions in several approaches gives encourage for introducing an approach which tracks the maximum power point with low error between actual MPP and predicted point.

1.3 Research Hypothesis, Aims and Objectives

The research hypothesis addressed in this thesis can be summarised in five questions:

- How can the MPP of PV panels be located in different environmental conditions?
- What are the problems associated with locating the MPP?
- Is it possible to collect data that will help the MPPT system model the behaviour of PV panels?
- Has the adaptive neuro-fuzzy inference system (ANFIS) approach the ability to overcome the drawbacks of locating MPP in other techniques?
- Can fuzzy logic provide a good MPPT system that operates in different environmental conditions and with different types of load?

The main aim in this thesis is to introduce an MPPT system which can predict and track the MPP of PV system under high changes of environmental conditions in short time with minimum error and low oscillation. This aim is achieved by the following seven objectives.

1. Collect adequate data which represents the behaviour of PV panel under different environmental conditions.

2. Analysing the core data of PV panels by using statistical analysis tools to clarify the relationships between different parameters of PV panels and confirming the use of short circuit current (I_{SC}) and open circuit voltage (V_{OC}) to predict the MPP location. In addition, the statistical analysis assists in initiating the primary membership functions (MFs) of ANFIS models.

3. Developing the ANFIS models to reach the minimum error between the actual data and predicted data.

4. Using the initial output of the ANFIS model with test data to determine the gaps in the data and improve the collected data to provide a feedback for the ANFIS model.

5. Improving the developed ANFIS model with per unit (PU) data to be applied with all single crystal and polycrystalline PV system.

6. Utilising the experiences in different components of MPPT system to identify the problems of the PV system with MPPT. Consequently, utilise this identification to design the MFs and rules of fuzzy logic controller (FLC).

7. Use simulation models to evaluate the performance of FLC with different types of load and with Buck-Boost and Buck converter to improve and generalise the MPPT system.

1.4 Significant research contributions

There are four major contributions:

1. **A novel ANFIS based approach applied to predict the MPP** utilising the actual field data in different environmental conditions. A number of ANFIS models are tested to reach the best model that can predict accurate V_{max}.

Subtractive clustering is applied to determine the number of rules and the best values of antecedent membership functions parameters, and then uses a linear least squares estimation to determine each rule's consequent parameters. Furthermore, the ANFIS models were tested three times during data collection. More data was added after evaluating the performance of ANFIS models in different irradiance levels and PV cell temperatures.

In addition, to avoid the limited implementation of the developed ANFIS model the selected ANFIS model with a few rules is developed and generalised with PU data. The developed general ANFIS model is tested with the data of two panels, and the predicted output voltage error is less than 2%. Moreover, the general model is tested with different PV panels and it has an error of only 1% with three types of PV panels.

2. **The novelty of the developed FLC is the methodology of utilising the MFs design incorporate with rules** to provide a solution for several problems that can be solved by increasing the number of rules. The MFs of the developed FLC are selected and designed to give a solution for problems faced by the MPPT system. The FLC has been developed with minimum number of rules to provide fast and stable tracking for MPP of PV system. The FLC rules and MFs are designed to work well with the large changes in weather conditions. In addition, the MFs are modified related to the rate of changes in duty cycle of Buck-Boost converter and Buck converter at different input voltages.

The developed FLC can be adjusted easily to control the duty cycle of DC-DC converters depending on the requirements of each converter and the appropriate converter that should be used to interface between the PV panel and different types of load.

Furthermore, the membership functions and fuzzy rules of FLC are designed to balance between different required features like quick tracking under different

environmental conditions, high accuracy, stability, and high efficiency.

3. **A systematic design of data collection and it is evaluation** in this thesis presents sufficient and appropriate parameters to give a solution for the shortage in parameters, the lack in data and the difficulty in measuring the cell temperature and solar irradiance, which demonstrate the drawbacks in many approaches. The evaluation of data in different environmental conditions and different seasons provide a comprehensive learning data set for the MPPT system.

4. **The fourth contribution is the methodology of selecting the inputs and outputs of the ANFIS model and FLC** in this thesis. The behaviour of the PV panels in different environmental conditions during data collection and the statistical analysis methods are utilising to study the PV parameters relationships. Hence, the short circuit current and open circuit voltage are used as inputs to PV panels instead of solar irradiation and cell junction temperature. The reason for this substitution is the difficulty of measuring the cell junction temperature. In addition, the simplicity of I_{SC} measurement gives a solution for the problem of having to deploy a solar irradiance external sensor.

   In addition, the input and output parameters of FLC are selected to recognise the behaviour of all parts of MPPT system. Moreover, the input and output of FLC are selected carefully to give sufficient and simple information for the FLC. The input voltage of DC-DC converters and the predicted output of ANFIS model V_{max} are used to detect the deflection of operating point on the I-V curves. In addition, I_{SC} is utilised to recognise the irradiance level and the amount of power that can be generated from the PV panels. Furthermore, I_{SC}, is utilised in assembling the activated rule at certain irradiance level.

1.5 Research methodology

The following five phases form the methodology of achieving the objectives of this research:

- The research started with a literature review. Thus, the drawbacks in different literature are recognised. In addition, three publications that I have been published in [11] [12] [10] before starting the PhD research provided an understanding of the problems of locating the MPP and the research requirements.

- The data is collected in two seasons in four areas. These choices have been made to provide comprehensive learning data. In addition, the behaviour of PV panels under different environmental conditions is observed. After that the data is sorted and the core data is obtained.

- The data is analysed using statistical tools to study the relationships between various parameters of PV panels.

- The ANFIS model is established and it is evaluated by the test data to confirm the performance of ANFIS model and determine the gaps in collected data.

- The actual data is evaluated more than one time. During these evaluations the ANFIS models are tested with new points and learning data is added until reaching wide-ranging ANFIS models.

- After that the subtractive clustering is used to generate new ANFIS models to be compared with other models.

- The final selected model is improved by Least square estimation using ANFIS function in Matlab.

- The selected ANFIS model is developed and generalised with PU data of two types of PV panels.

- The final general ANFIS model is tested with different types of PV panels.

- The output of the developed ANFIS model is used as a reference voltage of FLC. The FLC is designed to achieve the best promising performance in different environmental conditions, different load types, and two types of DC-DC converters. The developed controller is modified to apply for all single crystal and polycrystalline PV models. A few modifications are executed to construct an extensive FLC for all PV system with mentioned panels.

- Two simulation models using Matlab tools are designed to test and improve the performance of final FLCs. Hence, the MFs and rules are modified to achieve the best performance and to provide the MPPT system requirements.

- Check data is used to test the performance of all parts of MPPT system. In addition, the developed MPPT system is compared with the direct coupled system.

1.6 Thesis outline

This thesis is organised into eight chapters:

Chapter 2 presents the background of the MPPT configuration and the tools used in the developed approach. The following items are included in this chapter: PV system, DC-DC converter, fuzzy inference system, ANFIS, linear correlation analyses and clustering methods.

Chapter 3 investigates other MPPT approaches reported in the literature. It starts with conventional searching techniques such as perturb and observation methods, incremental conductance methods and computational methods. Furthermore, the chapter introduces three applied artificial intelligent techniques for the MPPT system. In addition, a comparison between on line and off line fuzzy methods is discussed in this chapter. Finally the chapter gives an introduction to the developed approach.

Chapter 4 discusses data collection.

1.6 Thesis outline

Chapter 5 introduces several ANFIS models, which are assembled to predict the maximum power point voltage of PV panels. Furthermore, statistical analysis methods are utilised to identify the relationships between different parameters of PV panels.

In chapter 6 the FLC is developed to solve the problems that face the MPPT system of PV system. In addition, the maximum power point problems are described in this chapter. Finally, the two general FLC are designed to control the duty cycle of Buck-Boost converter and Buck converter.

Chapter 7 includes the MPPT system simulation models description and the test of developed maximum power point tracking system results which take account of the different situations of input data.

Chapter 8 highlights the conclusions, recommendations and future work.

Chapter 2

Background

2.1 Solar energy and solar electricity

Solar radiation is composed of discrete packets of energy known as photons. The range of wavelengths that the sun emits is known as the solar spectrum. The majority of solar radiation lies within the wavelength range of 0.2 and 2.5 mm. The intensity of solar radiation (J/s or W/m^2) is known as the Radiant Flux Density, often referred to as irradiance or insolation. The irradiance level outside the Earths atmosphere is approximately1.367 kW/m^2. The surface of the Earth irradiance levels is lower than this value. For example, the equator at sea level irradiance is approximately $1kW/m^2$ [40]. Solar radiation reaching the surface of the Earth has two components – direct or beam radiation and diffuse radiation. The beam radiation is the radiation that arrives directly from the sun. The diffuse radiation is the portion of solar radiation which is scattered in the Earth's atmosphere. On a clear day beam radiation makes up about 90% of the total reaching the Earth's surface [40]. The ratio of direct and diffuse radiation changes with the quantity of cloud and haze in the atmosphere. The solar collectors that convert radiation into electricity can be either flat-plane collectors or focusing collectors [52] [40].

Solar electricity is the technology of converting solar radiation into electricity. This electricity is generated using photovoltaic (PV) cells. PV refers to an electric voltage caused by light. Solar electricity is already used in many applications such as lighting, water pumping, and powering telecommunications stations [76] [8]. Photovoltaic systems are solar energy supply systems, which either supply power directly to the electrical equipment or feed energy into the public electricity grid. The PV system in many applications generally consists of three main parts: PV panels, loads, and control unit. The PV panel is the most important part of a PV system

[76]. Photovoltaics are generally considered to be an expensive method of producing electricity. However, in the off-grid situations photovoltaics are very often the most economic solution to provide the required electricity service. The growing market all over the world indicates that solar electricity has entered many areas in which its application is economically viable [8] [76].

2.1.1 Photovoltaics cells and photovoltaic generator

Photovoltaic materials produce electrical power from sunlight. The basic component of photovoltaic power conversion is the solar cell. The most common solar cell is a p-n junction, where the p-type is a semiconductor positive material and the n-type is a semiconductor negative material. Solar cells are most commonly fabricated from silicon, however other materials such as cadmium and gallium may also be used. Four types of silicon semiconductor devices are in use: single crystal, polycrystalline, thin film polycrystalline and amorphous [51]. Single crystal silicon has a highly ordered atomic structure and cells made from it have the highest photovoltaic conversion efficiencies (18%). Polycrystalline silicon consists of many crystalline grains; the conversion efficiency of a solar cell manufactured from polycrystalline silicon is around 13%. A standard solar cell is typically cut from a large ingot of polycrystalline silicon and is typically between 200 and 400 microns thick. The photovoltaic (PV) cell is simply a diode of large area forward bias with photovoltaic as explained in [8] [76].

Photovoltaic cell operation

Kirchoff's law states the relationship between three main variables voltage (V), current (I) and resistance (R). The mathematic expression of Kirchoff's law is:

$$I = \frac{V}{R} \tag{2.1}$$

The electrical current I changes linearly with V. The slope of this linear relationship depends on electrical resistance R, which equals (1/R). The voltage of main electricity

remains constant; therefore, the current changes according to resistance magnitudes. The power delivered to the load is being calculated from Equation 2.2:

$$P = V * I \tag{2.2}$$

The relationship between current, voltage and power of PV panels is not simple as in electrical traditional sources. The load resistance affects the output voltage and current of the PV cell. When the resistive load is decreased the voltage decreases and current increases. Hence, when the resistance equals zero, the terminal voltage of PV cell equals zero and current is maximised. This point is called the short circuit current point (I_{SC}). Point M on Figure 2.1 represents the short circuit current point. In addition when the resistance is increased until high Ohms value, the current decreases until it reaches zero and the voltage is maximised. The maximum voltage point is called open circuit voltage point (V_{OC}). Point N on Figure 2.1 represents the open circuit voltage point. The current flow from the PV cell is affected by the load voltage. The relationship between load voltage and cell current is a decreasing relationship and this relationship is not linear as seen on the current voltage curve (I-V curve) of PV cell in Figure 2.1. When the PV cell is loaded, the created load voltage acts as a reverse voltage opposite the PV cell voltage. This voltage generates a reverse current called a dark current (I_D), which flows in the opposite direction of the generated photo current (I_{Ph}) from the PV cell. Accordingly, the output current of PV cell is the difference between these two currents.

PV cell, equivalent circuit and characteristics

The simplified equivalent circuit of a PV cell that is shown in Figure 2.2 consists of a current source which is connected parallel with a diode, internal series resistance of PV cell (R_S) and a shunt resistance (R_P). This resistance represents the electrical resistance between the PV solar cell and the PV panel frame. The current source generates the photo current I_{Ph}, which is directly proportional to the irradiance level.

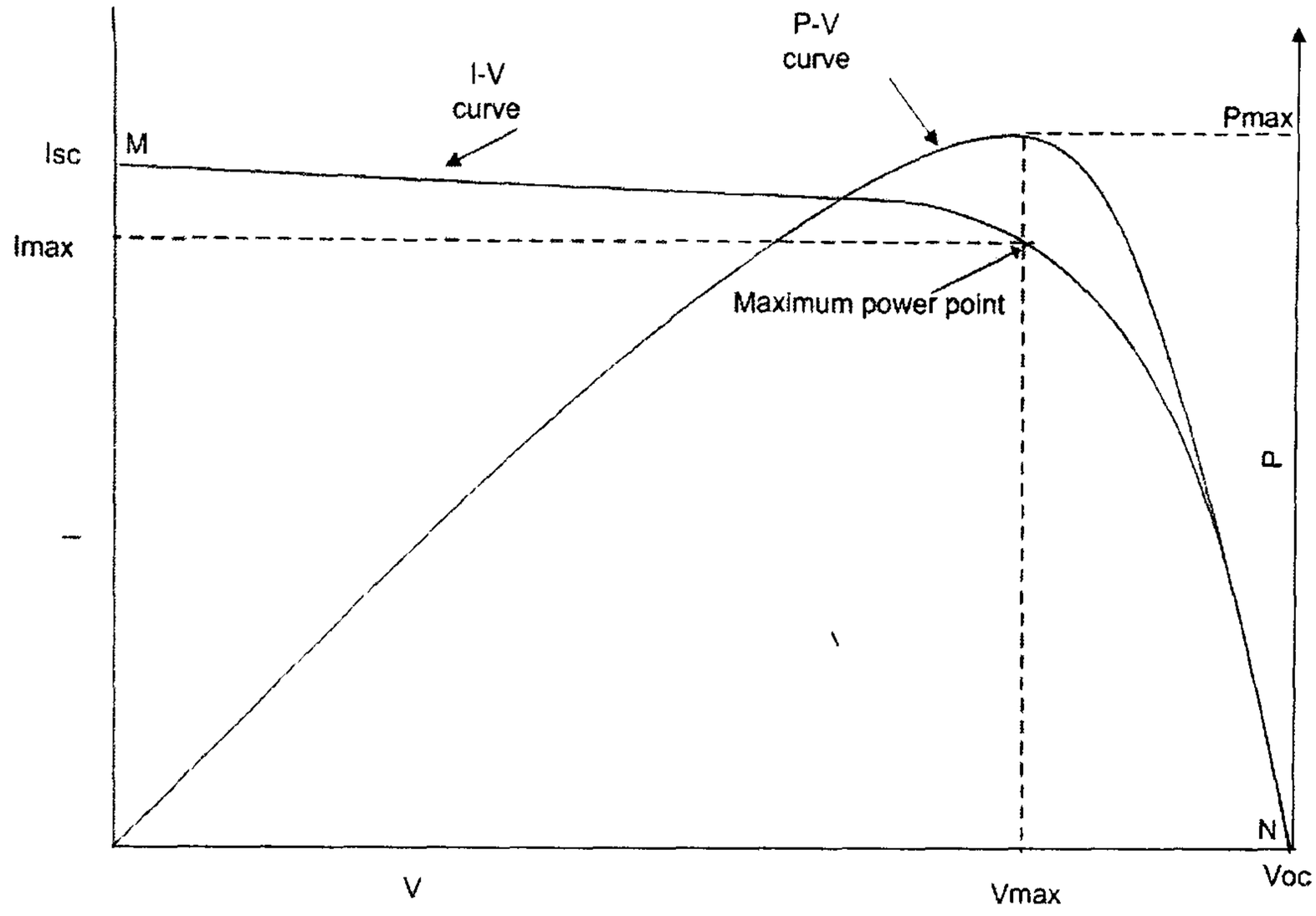

Figure 2.1: I-V curve and P-V curve of a PV cell

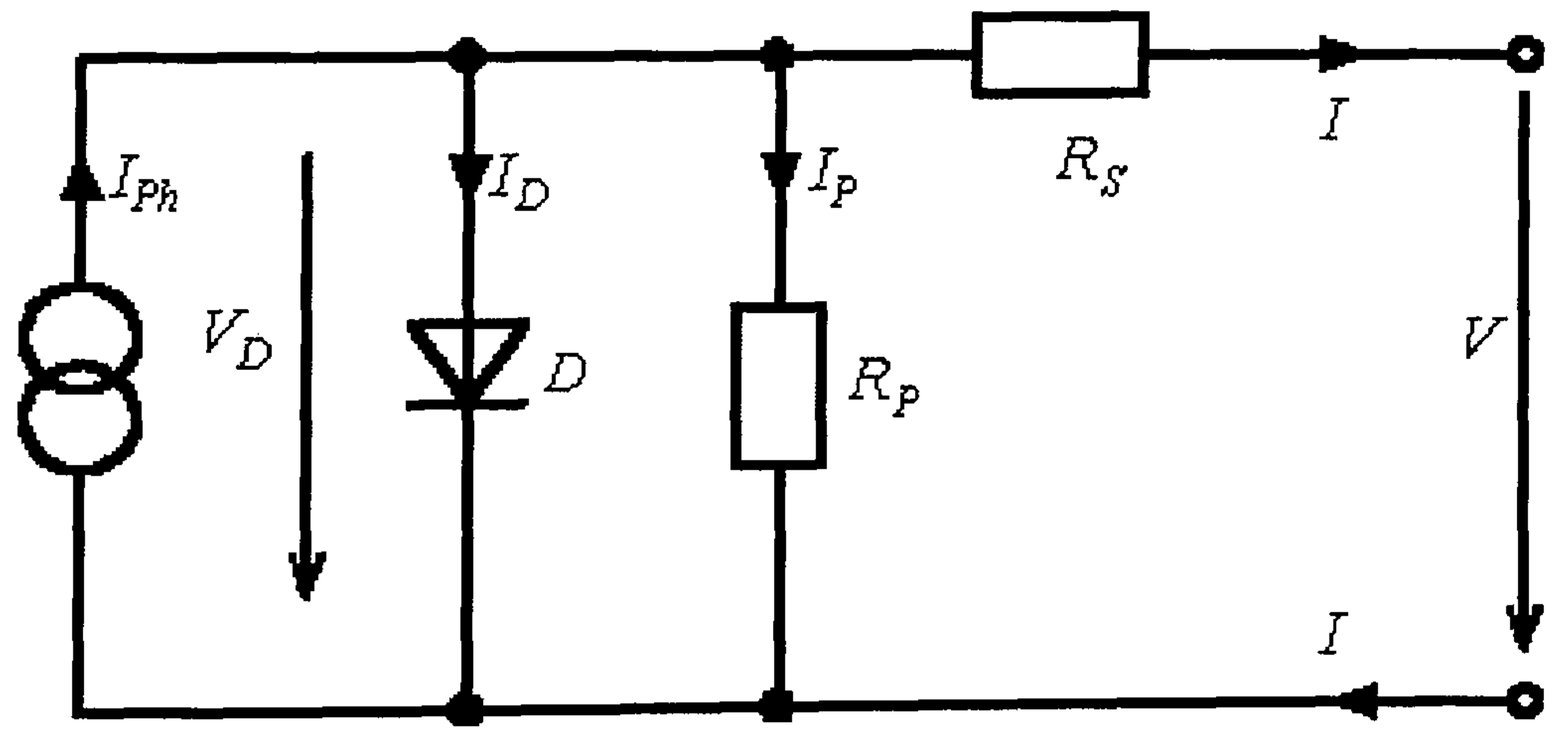

Figure 2.2: The simplified equivalent circuit of a PV cell

2.1 Solar energy and solar electricity

The relationship between PV cell current and load voltage is an exponential relationship as seen in Equation 2.3 and Equation 2.4:

$$I = I_{Ph} - I_D \tag{2.3}$$

$$I = I_{ph} - I_o \left[\exp(\frac{q(V + R_S I)}{AK_B T_C}) - 1\right] - \frac{V + IR_S}{R_P} \tag{2.4}$$

Where

$$I_D = I_S \left[\exp(\frac{q(V + R_S I)}{AK_B T_C}) - 1\right] - \frac{V + IR_S}{R_P} \tag{2.5}$$

Where I is output current, I_D is the diode current which equals the dark current. I_S is the saturation current, A is the ideality factor, q(C) is the electronic charge, K_B(J/K) is Boltzmann's gas constant and T_C is the cell junction temperature. The simplified equivalent circuit in Figure 2.2 can be represented in Equation 2.4. The output current of solar cell in Equation 2.4 is a function of output cell voltage considering all constant parameters shown in Figure 2.2 [51] [52]. Normally, the series resistance is very low. Also, with good isolation between the PV cell and the panel frame, R_P becomes very high at normal operating voltage. Therefore R_S and R_P is neglected in Equation 2.4. Hence, the ideal PV cell equation can be expressed as:

$$I = I_{ph} - I_o \left[\exp(\frac{q(V)}{AK_B T}) - 1\right] \tag{2.6}$$

The PV cells are connected in series and parallel to generate a sufficient voltage and current for the load. These connected cells are called a PV generator or PV.

Photovoltaic Generator

The PV generator is normally composed of N panels in series and M panels in parallel. The most common panels have 30 to 36 crystalline silicon cells in series. All cells in PV panels are identical [76]. When PV cells are connected in series, the total current remains constant, which is equivalent to the current of one cell, however the voltage is multiplied. In contrast, if the cells are connected in parallel, the current will increase

and the voltage remains constant. Hence, I-V curve characteristics of one panel can be derived by scaling the characteristic of one cell voltage with the number of cells in series. In addition, the I-V characteristics of the whole generator can be derived by scaling the characteristics of one panel with a factor N in voltage and M in current.

2.1.2 Electrical I-V curve characteristics

I-V curve characteristics describe the PV cell electrical terminal characteristics under the influence of environmental conditions such as irradiance and ambient temperature. The PV cell can operate at any point on the I-V curve depending on the intersection between I-V curves and load line curves. Short circuit current, open circuit voltage and maximum power point (MPP) are three significant points that identified the I-V curve and P-V curve of PV cells.

Short circuit current and Open-circuit voltage

When the positive terminal is connected with the negative terminal directly the operating voltage of PV cell is approximately zero. Therefore, the output current is the short circuit current. At normal level irradiance and ambient temperature, the short circuit current equivalents the I_{Ph}. So the short circuit current is directly proportional with the irradiance level G (W/m^2) as seen in Equation 2.7

$$I_{SC} = I_{Ph} = K * G \tag{2.7}$$

Where K is a constant depending on cell area and PV cell type efficiency and G is the irradiance level (mW/cm^2)

When the PV cell is disconnected from any external load, the external current I equals zero and the generated photovoltaic current by the incident radiation circulates back through the diode.

Let I = 0 in Equation 2.6 the open circuit voltage of the PV cell can be obtained

from Equation 2.8:

$$V_{OC} = \frac{AK_BT_C}{q} \ln(\frac{I_{ph} + I_S}{I_S}) \tag{2.8}$$

The open-circuit voltage corresponds to the voltage drop across the p-n junction when it is traversed in the I_{Ph}. The photo current increases linearly with irradiance, therefore the open circuit voltage in Equation 2.8 increases logarithmically with irradiance level. Also, from Equation 2.8 the open circuit voltage decreases linearly with increases in cell junction temperature.

Maximum-power operation

Maximum power point (P_{max}) is obtained when the multiplication of voltage and current is maximum. The maximum operation voltage and current at this point are V_{max} and I_{max}. As shown in Figure 2.1, the PV cell operates at maximum power point at only one point on I-V curve. When the solar cell is loaded, the PV cell can operate at any point on I-V curve. The power delivered to the load changes according to the intersection between PV curves and load curves. Matching between PV systems is very difficult due to continuous changes in maximum power point with different environmental conditions.

2.1.3 Effect of environmental influences on PV curves characteristics

Irradiance level, ambient temperature and wind speed are the main environmental factors that affect PV systems. I_{SC}, V_{OC}, V_{max} and I_{max} are the main characteristics that specify the I-V curves of PV panels [51] [52] . I-V curve characteristics and cell junction temperature of PV panels are adjusted due to any changes in environmental conditions. This section will demonstrate how PV output characteristics and cell junction temperature changes with environmental conditions. Furthermore, the effect of cell junction temperature on electrical characteristics of PV curves panels will be addressed in this section.

Effect of irradiance level on PV curves characteristics

There is a directly proportional relationship between irradiance level and the output power of PV panels [51] [26]. Figure 2.3 shows how I-V curves change with irradiance. In addition, Figure 2.3 shows how maximum output power increases with the irradiance level when the cell temperature remains constant. The change in irradiance level leads to changes in voltage and current those specify the MPP. Generally, any increment in solar radiation increases I_{max}. Maximum power voltage increases theoretically with solar radiation when there are no changes in cell junction temperature [51] [52]

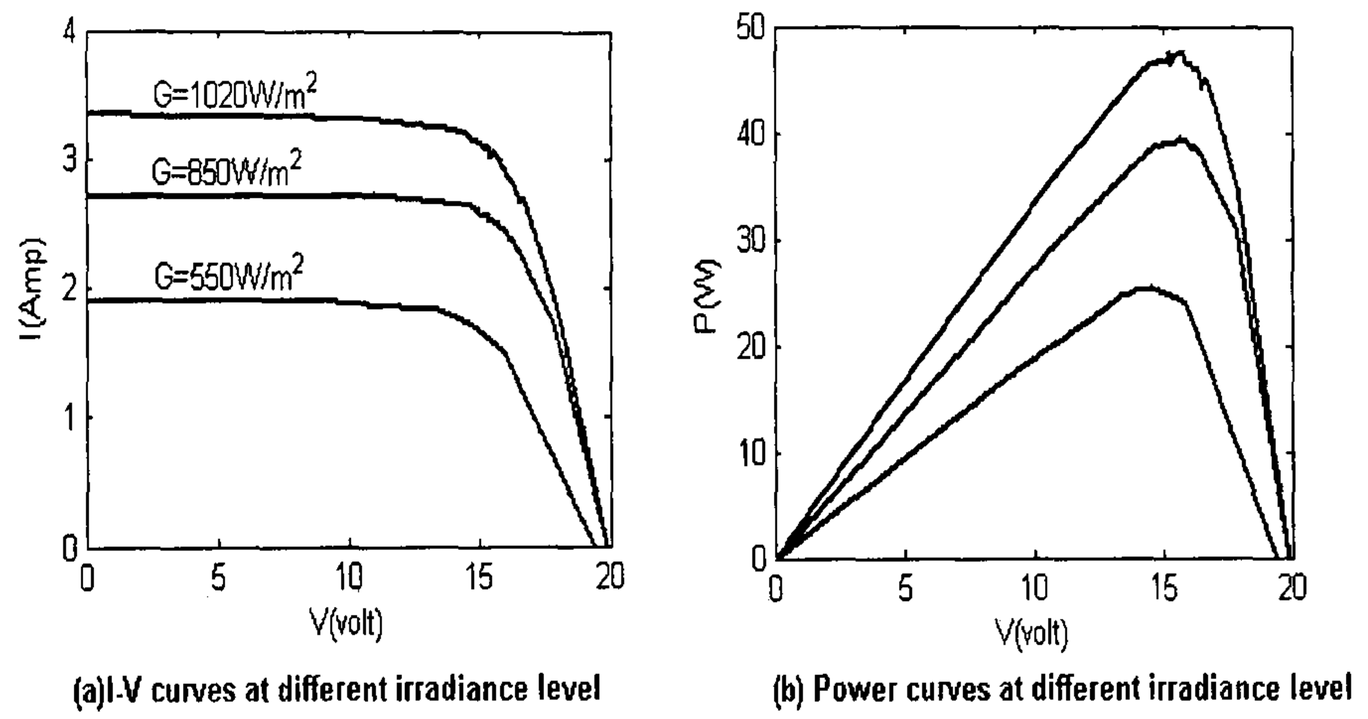

Figure 2.3: I-V and P-V curves at different irradiance level

The short circuit current of solar cells depend exclusively and linearly on the irradiance level [52]. It is of the order of 30mA/cm^2 for an irradiance of 1kW/m^2 for single-crystal silicon cell at 25 ^{O}C. The photocurrent increases 0.1% per ^{O}C which is neglected at normal operating conditions [51]. The I-V curve in Figure 2.3 shows how I_{SC} increases with solar irradiation. Equation 2.8 shows a logarithmic relationship between V_{OC} and irradiance level [51]. After sunrise the V_{OC} increases slightly with increase in irradiance level. It is of the order of 590mV for 1KW/m^2 of irradiance and 25 ^{O}C cell temperature for a single crystal silicon cell [27] [51] .

Effect of environment conditions on cell junction temp

"The working temperature of the PV cells depends exclusively on the irradiance and ambient temperature, according to the following linear relationship" E. Lorenzo, page number 96 [52].

$$T_S = T_a + C * G \tag{2.9}$$

- T_S Cell temperature in ^{O}C
- T_a Ambient temperature in ^{O}C
- G Irradiance level (mW/cm^2)

The value of the constant C is between 0.27 and 0.32^{O}C/(mW/cm^2) for modules currently in the market. This assumption leaves aside the effect of wind velocity on Ts. There is a constant increase in PV cell temperature with solar irradiation when the wind effect is neglected. In other words, heat dissipation from the cells to the environment is taken to be dominated by conduction through the encapsulation, rather than convection from the surface by wind effect. Generally, the wind decreases the surface temperature of the solar cell which finally decreases the cell junction temperature [52].

Effect of cell junction temperature on MPP and V_{OC}

Ambient temperature and current flowing through PV solar cells increases the PV cell junction temperature. Junction cell temperature is the main factor that reduces the maximum power output of the PV panel [51]. Figure 2.4 shows how the I-V curves and power curves (P-V curves) change with surface temperature of PV cell as a result with cell junction temperature. It is observed from power curves in Figure 2.4 how maximum power generated from a PV panel decreases due to the increase in cell temperature when the irradiance remains constant. In addition, Figure 2.4 shows how V_{max} decreases with cell junction temperature [51] [52].

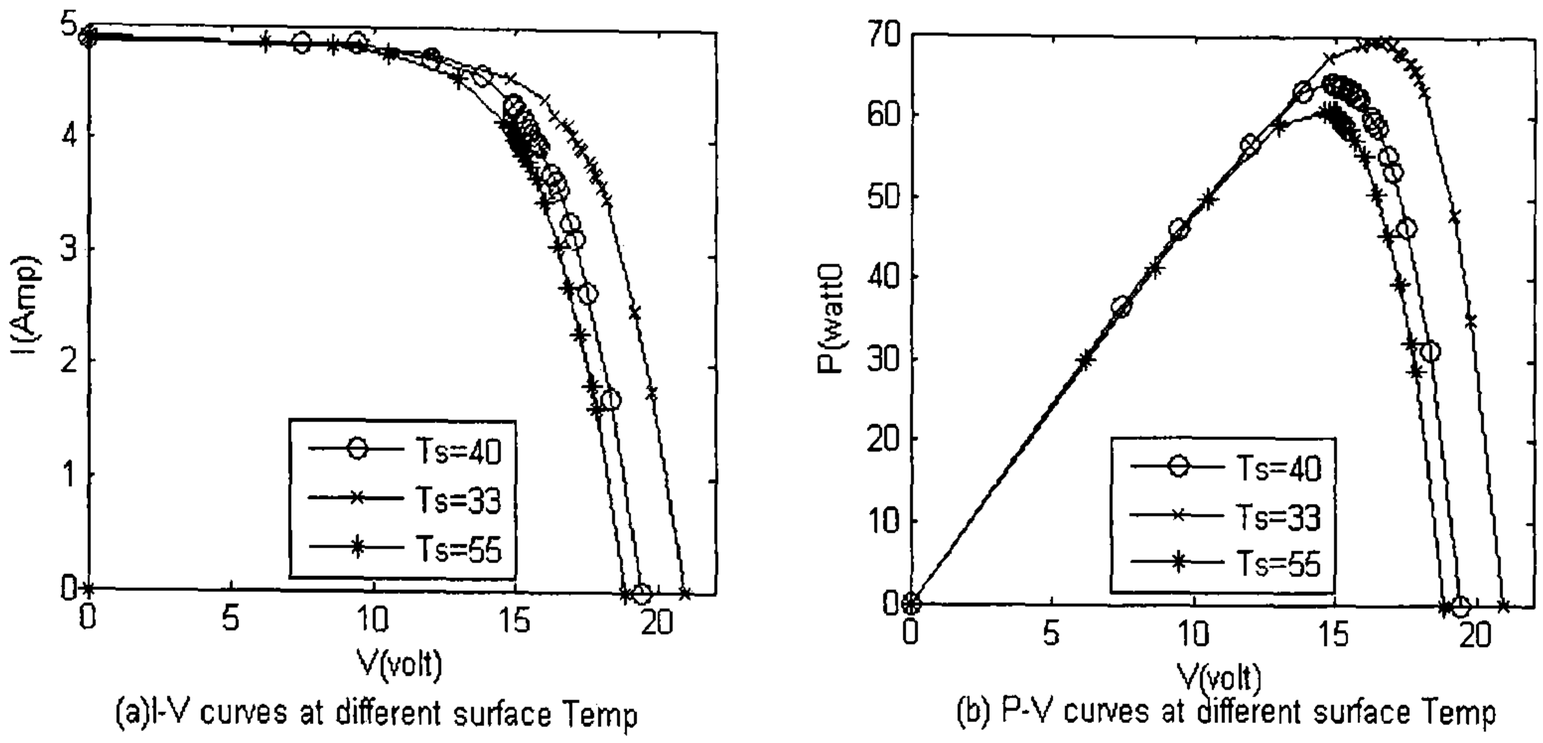

Figure 2.4: I-V and P-V curves at different surface temperature

The cell junction temperature increases due to ambient temperature and solar irradiance in Equation 2.9. Therefore, this increase in junction temperature reduces the V_{OC} as shown in Figure 2.4. There is strong linear dependence between V_{OC} and cell junction temperature as shown in Equation 2.8. The V_{OC} would decrease by 2.3mV/^{O}C between 20^{O}C and 100^{O}C when irradiance remains constant [51] [52]. Neglecting the wind effect at constant irradiance it is easy to compute the cell junction temperature from the drop in V_{OC} of PV cell.

To compute the operating points on I-V curves it is necessary to measure the irradiance level and cell junction temperature. The irradiance level can be measured using an external sensor. However, the problem is the difficulty of measuring or deducing the cell junction temperature from different environment factors or electrical parameters.

There are three main difficulties in finding a relationship between V_{OC} and irradiance level and cell junction temperature:

1. A nonlinear relationship between irradiance and open circuit voltage.

2. Effect of ambient temperature and irradiance level on cell junction temperature.

3. The difficulty of measuring wind effect on the cell junction temperature as a result on V_{OC}.

2.1.4 Load effect in operating point of PV solar panels curves

The load has no effect on I-V curve characteristics, however the load affects the operating point on I-V curves. When the load is directly coupled to the PV panel this leads to a mismatch between the actual and the optimum operation voltage (V_{max}) of the solar generator which decreases the generated power from PV panels. Operating voltage (Vop) and operating current (Iop) on I-V curves are load dependent points. The intersection between the different load line and I-V curves under different environmental conditions identifies the operating point on I-V curves as shown in Figure 2.5 for resistive and battery loads. If there are any changes in environmental conditions, the I-V curve is modified, as a result the operating voltage and current continuously changes. Mostly, these intersection points are not the P_{max} as shown in Figure 2.5. Hence, the load drives the PV panels to operate faraway from maximum power point as will be discussed in chapter 7 .

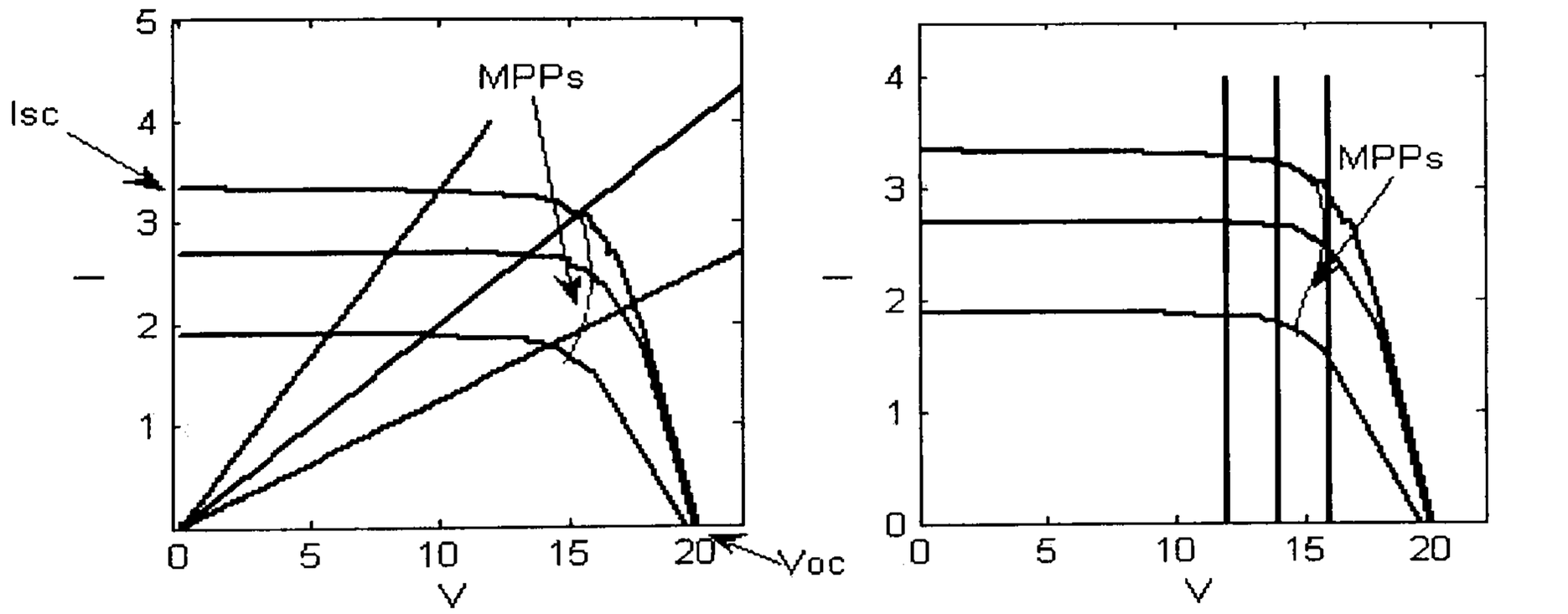

(a) IV curves with resistance load lines **(b) IV curves with battery load lines**

Figure 2.5: I-V curves with different types of load

Type of load strongly affects the range that locates the operating point in I-V curves. There are two main types of load that can be supplied from the PV system: constant voltage load such as battery load, and resistive load such as DC pumps. Battery is the most common load in a stand alone PV system. When

12V lead acid battery is at full discharge, the open circuit voltage is approximately 11.5V. During charging time the battery voltage raises to 14.6 V when the battery is in full charge [26] [22]. Maximum power point voltage of 36 series single crystal panel and polycrystalline panel at normal environment operating is between 12V and 18V. Figure 2.5 shows the intersection between battery load curves and I-V curves in different situations. It is observed from the constant linear voltage curves of the battery load that the battery voltage is varied in the range near to the MPP location. However, resistive load drives the PV panel to operate in a wide interval on I-V curves due to the linear relationship between current and voltage that concludes from Kirchoff's law as seen in Equation 2.10:

$$\frac{1}{R} = \frac{I}{V} \tag{2.10}$$

Thus, the I-V curves of PV panels and the resistive load curves can only intersect at MPP when V_{max} and I_{max} pass through a value that is given in Equation 2.11:

$$R = \frac{V_{max}}{I_{max}} \tag{2.11}$$

The changes in V_{max} and I_{max} position due to continuous changes in environmental conditions leads to low chance of operating the PV system in the maximum power point that is recognised in Equation 2.11. In addition, Figure 2.5 shows how resistive load curves could operate the PV panels faraway or close to the maximum power point.

2.2 DC-DC converters

DC-DC converters are widely used in photovoltaic generating systems as an interface device between the photovoltaic panel and the load. It is used for matching between load voltages and maximum power point voltages of PV panels. The main role of the DC-DC converter is primarily to convert an input power $P_{in}= V_{in}*I_{in}$ into output power $P_O= V_O*I_O$ with the best possible efficiency. The DC-DC converter is used to

step up or step down the input voltage. The efficiency (η) of the DC-DC converter can be calculated from equation 2.12:

$$\eta = \frac{P_O}{P_{in}} = \frac{V_O * I_O}{V_{in} * I_{in}} \tag{2.12}$$

Therefore, the relationship between input and output parameters can be expressed as in Equation 2.13

$$V_O * I_O = \eta * V_{in} * I_{in} \tag{2.13}$$

The efficiency remains roughly constant at certain values of converter voltage and current. Any increase in V_{in} or I_{in} in Equation 2.13 lead to either increase in V_O or I_O. Three converters demonstrate the main types that have been used to step up and step down the input voltage of DC-DC converter:

1. Buck converter or step down converter.

2. Boost converters or step up converter.

3. Buck-Boost converter or step up/ step down converter.

All of the above converters have an inductor capacitance (LC) electrical circuit. The LC circuit in different types of DC-DC converters is governed electronically. The duty cycle (D) of the electronics switch is controlled using a pulse width modulator (PWM). The duty cycle of the electronics switch can be expressed in Equation 2.14:

$$D = \frac{t_{on}}{T} \tag{2.14}$$

Where

- T is the switch oscillation period or time period of square pulse that controls the electronics switch.

- t_{on} is the on time of controlling square pulse.

2.2 DC-DC converters

The DC-DC converters can operate in two separate modes: continuous current conduction and discontinuous current conduction. These two modes have significantly different characteristics. The relationship between duty cycle of electronics switch and voltage ratio is simpler in continuous mode operation. If the current through the inductor remains greater than zero, the converter will operate in continuous mode. The frequency of PWM pulse signal times the inductor inductance (L) should be enough higher than the load resistance to prevent the current of inductor to reach zero value. Hence, the converter parameters and its control frequency should be designed to operate in selected mode. This design has to consider the maximum and minimum required current and voltage of appliances. In most applications, the converter is designed to operate in continuous current conduction. To operate in this mode, the converter parameters are selected to maintain the current through the inductor does not reach the zero stipulation. [65].

The following summary specifies the three earlier mentioned DC-DC converters. It has assumed the converters are designed to operate in continuous mode conduction [88] [62].

2.2.1 Buck converter step-down converter

This type of converter is used in applications that required stepping down the input voltage. A simple relationship between voltages is obtained by supposing that no voltage drops across a transistor or diode in Figure 2.6 during the on time. Applying the Buck converter in circuit that is shown in Figure 2.6 the voltage ratio ($\frac{V_o}{V_{in}}$) can be obtained from Equation 2.15:

$$\frac{V_O}{V_{in}} = D \tag{2.15}$$

Where D lays between 0 and 1

A linear relationship between voltage ratio and duty cycle can be observed From Equation 2.15. That means the duty cycle changes with constant rate with respect to the change in voltage ratio.

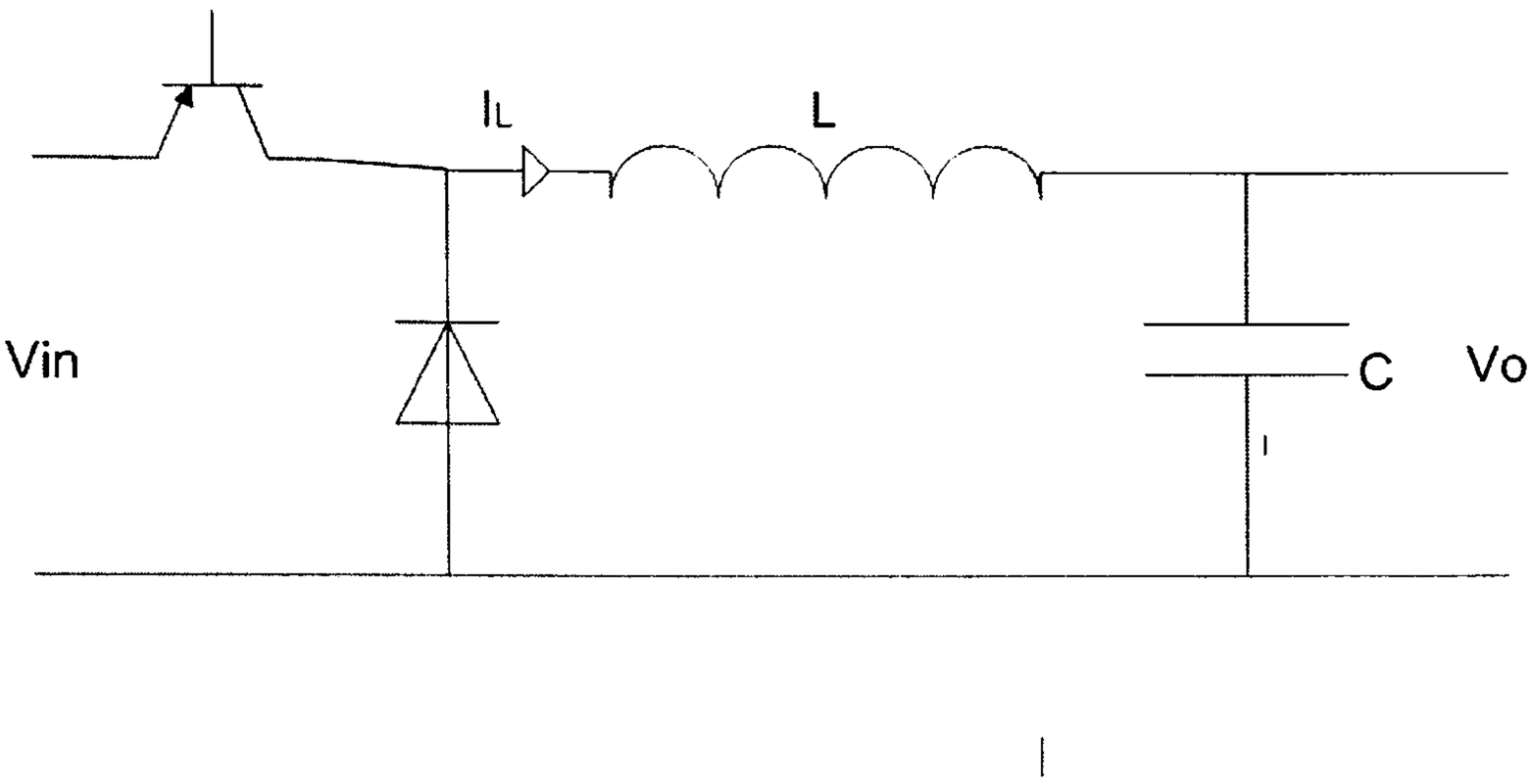

Figure 2.6: Buck converter circuit

2.2.2 Boost converter step-up converter

The schematic in Figure 2.7 shows the basic boost converter. This circuit is used when a higher output voltage than input is required. The voltage ratio can be obtained from Equation 2.16:

$$\frac{V_o}{V_{in}} = \frac{1}{1-D} \tag{2.16}$$

The duty cycle in Equation 2.16 changes between 0 and 1. Therefore, the voltage ratio is always greater than 1 and that means this converter is used to step-up the input voltage. The relationship between voltage ratio and duty cycle is shown in Figure 2.8.

Figure 2.8 shows a nonlinear relationship between voltage ratio and duty cycle of Boost converter. This relationship shows a higher change in voltage ratio due to changes in the duty cycle when voltage ratio becomes bigger.

2.2.3 Buck-Boost converter

With continuous conduction operation the voltage ratio of Buck-Boost converter in the Figure 2.9 is expressed in Equation 2.17:

$$\frac{V_o}{V_{in}} = \frac{D}{1-D} \tag{2.17}$$

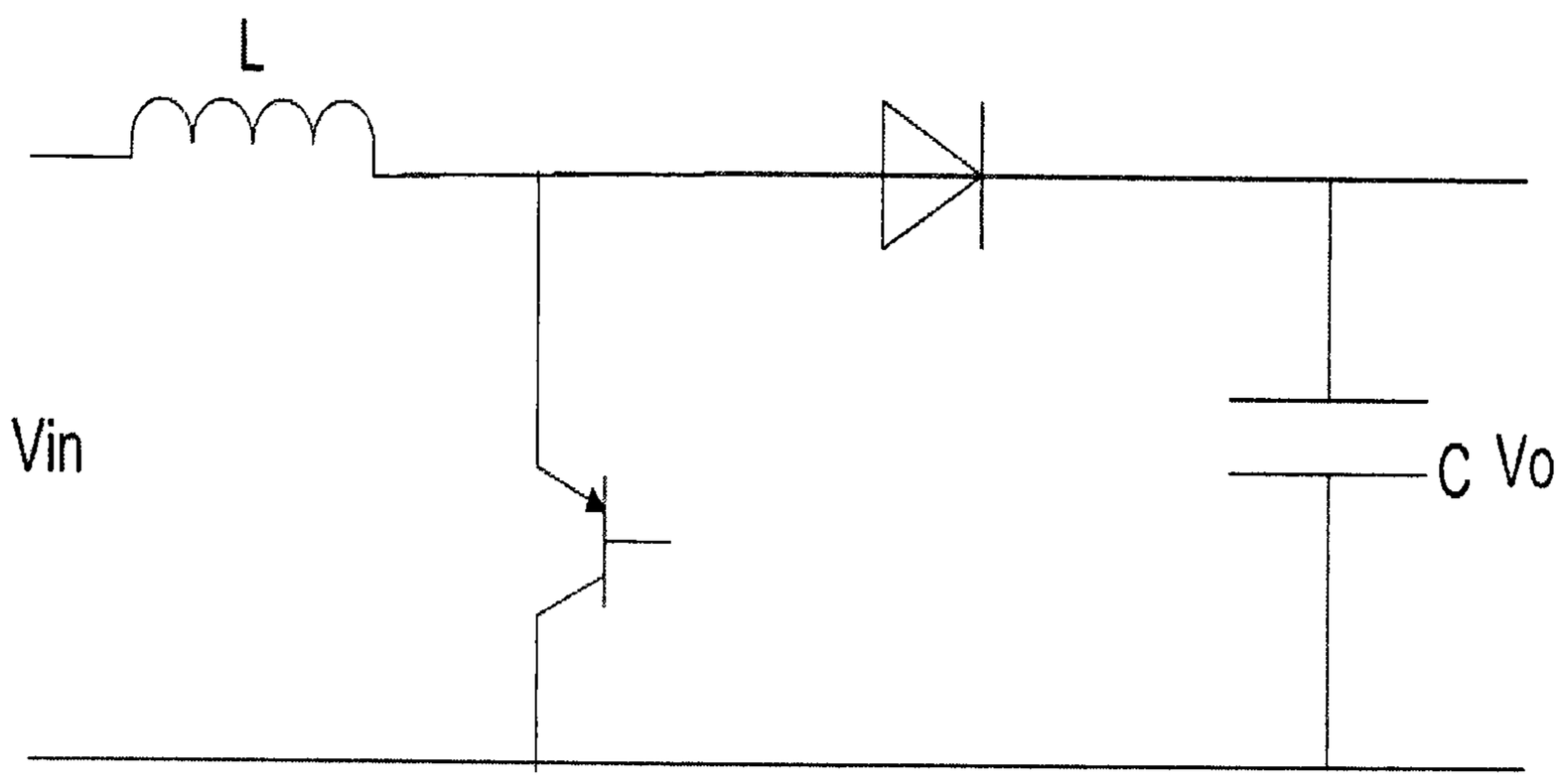

Figure 2.7: Boost converter circuit

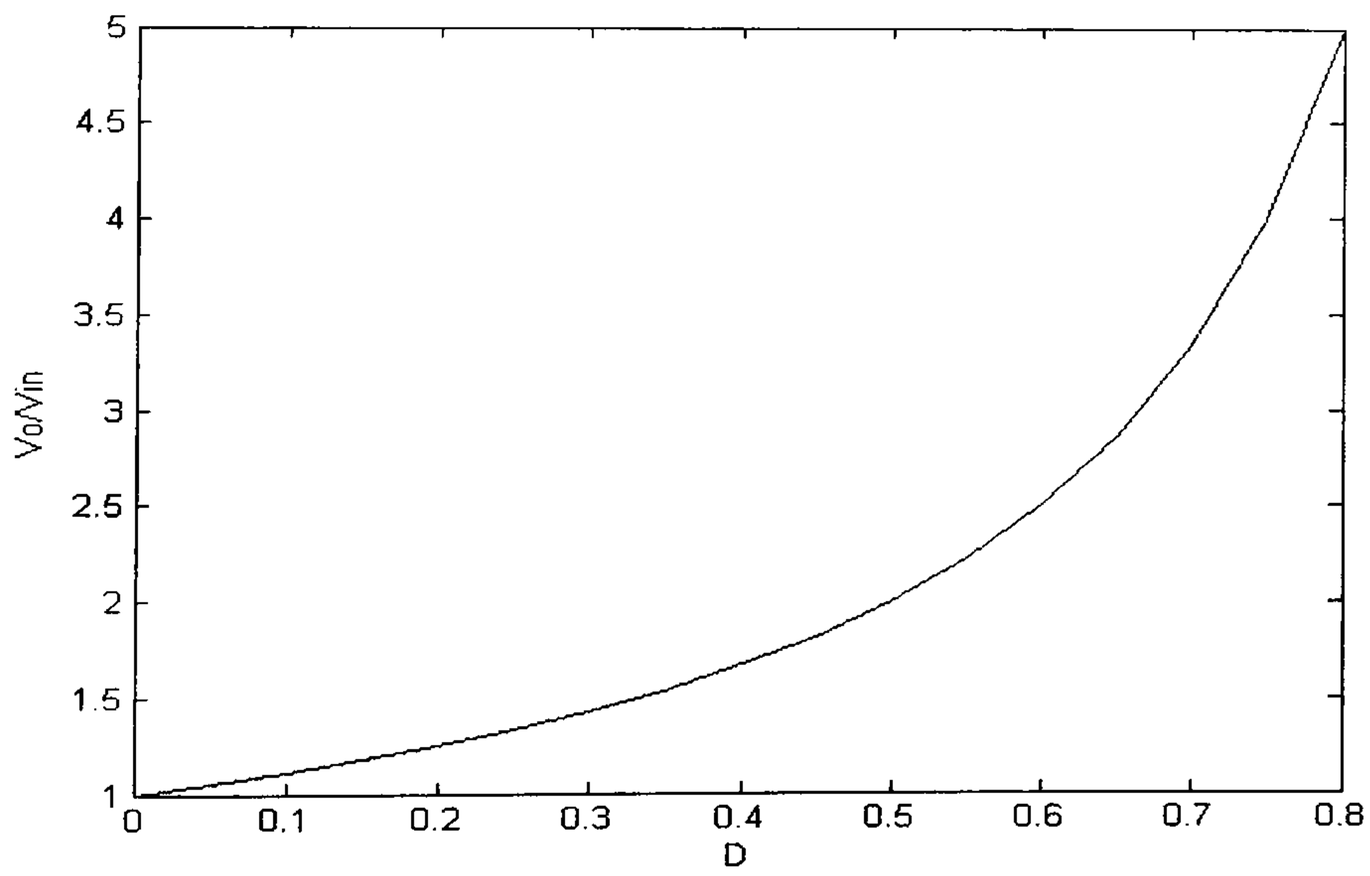

Figure 2.8: Relationship between duty cycle and voltage ratio of Boost converter

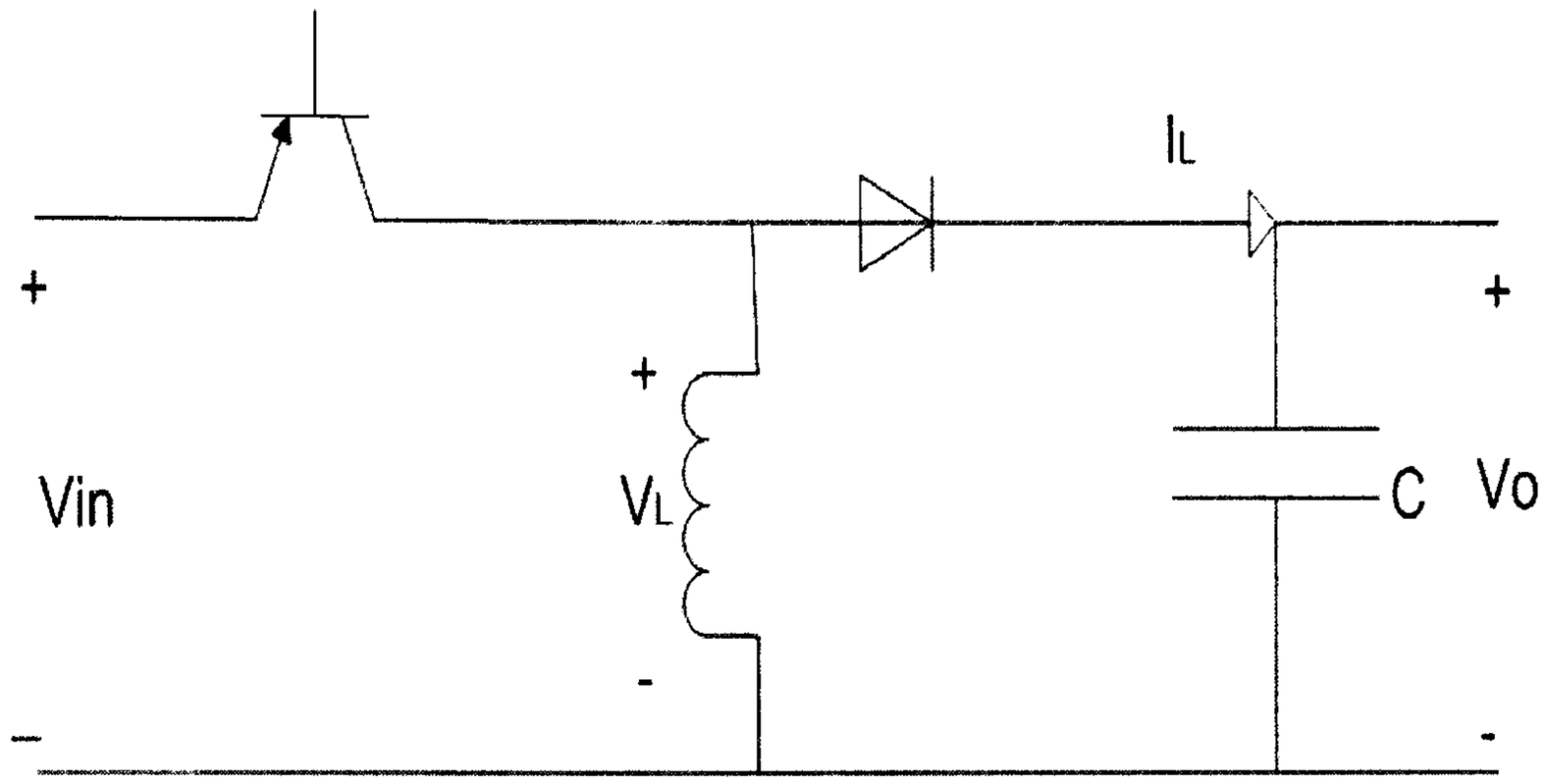

Figure 2.9: Buck-Boost converter circuit

This type of converter can be used to step up and step down the input voltage. The main application of the buck-boost converter is in regulated power supplies, where the output load voltage can be either higher or lower than the power supply voltage. The converter works as a step up when the duty cycle change between 0.5 and 1 and as a step down when the duty cycle changes between 0 and 0.5. Figure 2.10 shows how the voltage ratio changes with changes in the duty cycle.

2.2.4 Select and sizing of DC-DC converters

To select the appropriate DC-DC converters that is required to interface between the PV panels and the desired load voltage, five main criteria should be studied carefully [62] [65].

1. Maximum and minimum input voltage of PV system.

2. Maximum and minimum output load voltage.

3. Maximum and minimum input and output current.

4. Efficiency and cost of DC-DC converters that is useful for a specific load.

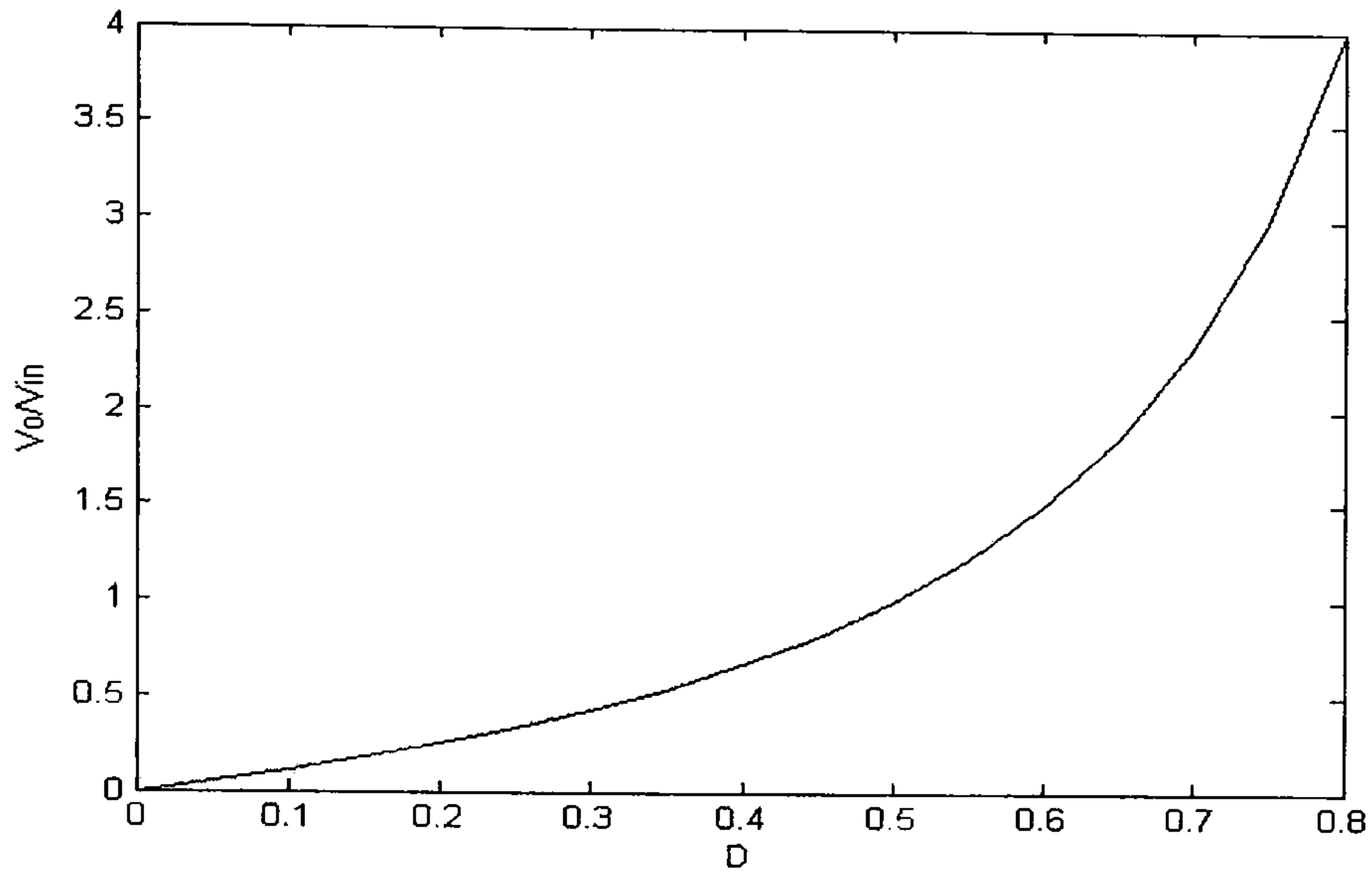

Figure 2.10: Relationship between duty cycle and voltage ratio of Buck-Boost converter

5. The energy that can be saved by different available converters.

"Practically, the Buck-Boost converter which has a MOSFET electronics switch and a very low resistance inductor, achieving efficiencies in regards to input power higher than 95% and hardly 2 or 3% lower than the buck and boost topologies" J.M. Enrique *et al*, page number 18 [25]. This difference in efficiency comes from electronics switch utilisation factor Po/P_T, where Po is the output power and P_T is the rated power of the electronics switch. "The switch utilisation of the Buck and the Boost converter is very good. However, the Buck-Boost switch has a poor utilisation factor. The maximum switch utilisation factor is 0.25 at D=0.5, which corresponds to the unity voltage ratio" Mohan *et al*, page number 195 [65]. If it is necessary to compare both higher and lower output voltages with the input voltage, the Buck-Boost converter should be used. Otherwise it is preferable to use buck or boost converters depending on the application requirements. The design of DC-DC converters requires compromise among switching frequency, inductor sizes, and switching losses [25].

Most PV system applications need the Buck-Boost converter which can be used for step up/step down the voltage of PV systems. In addition, the Buck converter can be used for the battery load applications which can be operated on voltages less than V_{max} especially in low ambient temperature regions. Moreover, Buck converters is more efficient than Buck-Boost converters. Hence, we will focus on these two converters in chapter 6 for the above reasons.

DC-DC converters are applied in PV systems to match between load voltage and the V_{max} of the PV system. Different techniques are implemented to control the duty cycle of the electronics switch such as perturb and observation, incremental conductance, computational and computational artificial intelligence. Fuzzy logic is an artificial intelligence technique which achieves a good performance in several applications. It can be applied to control the duty cycle of different DC-DC converters to track the maximum power point at different load types and in different environmental conditions.The FLC is nonlinear and adaptive in nature. Morevere, the FLC gives a robust performance under parameter variations. In next section we will introduce an overview of fuzzy inference system, which can be utilised as a control system for the duty cycle of DC-DC converters.

2.3 Fuzzy inference systems

Fuzzy logic deals with the concept of the values between completely true and completely false. Fuzzy logic has mostly been applied in control systems [79]. Fuzzy controllers apply decision rules (if-then rules) by making use of critical variables to interpolate the output between the crisp boundaries [79] [83].

Fuzzy rule based systems or fuzzy inference systems are the most important modelling tool based on fuzzy set theory. The systems can be applied in many applications such as automatic control, expert systems, pattern recognition, data classification and time series prediction [79] [39]. The main five construction operations of fuzzy rules based system can express as follow[38] [36] [79]:

1. A database which defines the membership functions of the fuzzy sets used in

the fuzzy rules.

2. A fuzzification interface which transforms the crisp inputs into degrees of match with linguistic values.

3. A rule base containing a number of fuzzy if-then rules.

4. A decision-making unit which performs the inference operations on the rules.

5. A defuzzification interface which transform the fuzzy results of the inference into a crisp output.

The block diagram in Figure 2.11 shows the construction operations of fuzzy inference system (FIS) [39] [79].

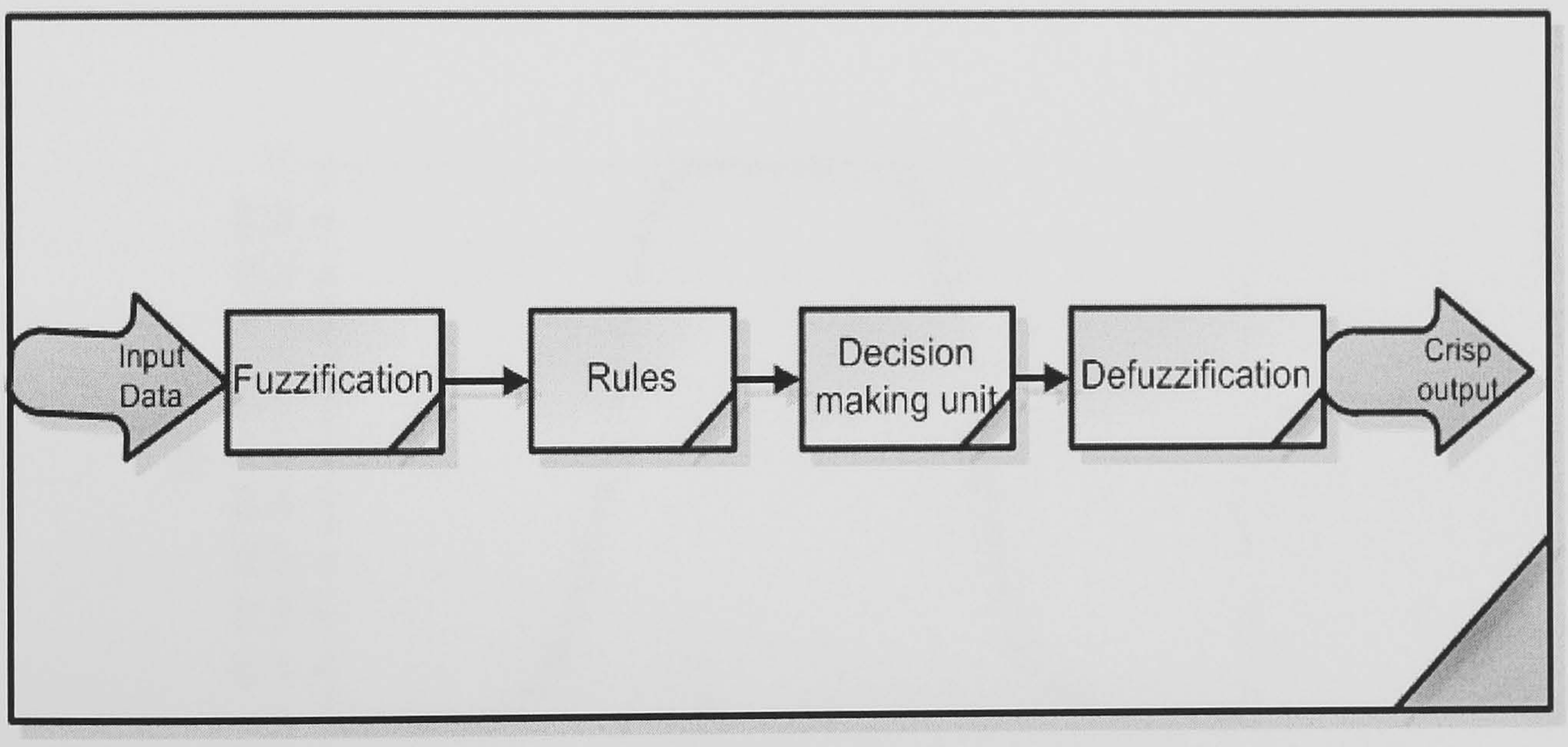

Figure 2.11: The block diagram of FIS system

2.3.1 Fuzzification

Fuzzification is the process of converting crisp inputs to fuzzy memberships in order for them to be used in a fuzzy inference system. Fuzzy memberships functions(MFs) can takes various form of fuzzy set shapes such as triangular MFs which have many

shapes like normal fuzzy and subnormal or convex or nonconvex. In addition, fuzzy MFs can takes other forms such as Gaussian MFs, General bell MFs and sigmoidal MFs [79]. The MFs that are used to give a good response in the fuzzy system are determined by the expertise knowledge.

Here we describe the general Bell MF. Three parameters that specify the bell MF in Figure 2.12 are a, b and c. The centre of bell is determined by the constant c. When constant a increases the width of bell MF will increase. Third constant b controls the slope of the step up and step down of bell MF. This slope can be obtained from: (slope=$\frac{b}{2a}$). The MF of crisp x can be obtained from Equation 2.18:

$$\mu = \frac{1}{1 + \left|\frac{x-c}{a}\right|^{2b}} \tag{2.18}$$

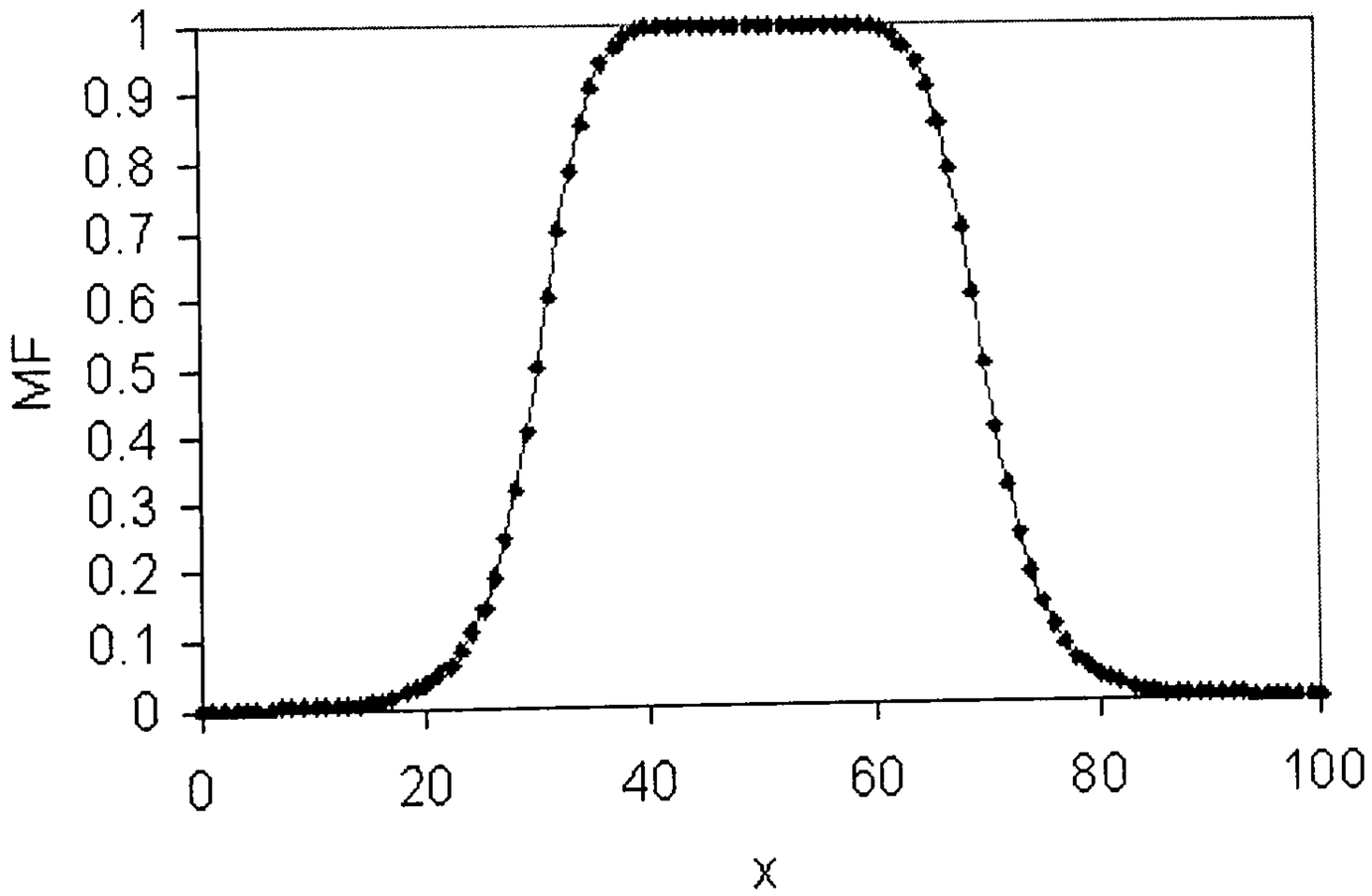

Figure 2.12: Bell MF

2.3.2 Fuzzy rule-based systems

The antecedents of the rules may include any number of terms conjoined by "and" or disjoined by "or". The fuzzy rules are used in the area of automatic control, a fuzzy controller has to able to act on fuzzy input data to create fuzzy output data. In this case the rule base which comprises the process information comes in the form [79]:

$Rule_i$ **If** x_1 **is** A_{1i} **and** x_2 **is** A_{2i} **.....and** x_n **is** A_{ni} **Then** y_i **is** B_i

Where A_{ji}, B_i are fuzzy sets and x_j, y_i are crisp values in these sets.

We can write many rules if there are many antecedents and as a result many consequents. Furthermore, the rules can state multi antecedents and multi consequent.

2.3.3 Fuzzy Inferencing

Fuzzy outputs need to be converted into a scalar output quantity so that the nature of the action to be performed can be determined by the system. Within the process of converting the fuzzy output, there are several types of fuzzy reasoning [36]. Here two types of fuzzy inference system will be introduced. These two types have been widely employed in various applications. The differences between these two fuzzy inference systems lie in the consequents of their fuzzy rules, and thus their aggregation and defuzzification procedures differ accordingly [39] [79].

The Mamdani approach

There are different types of t-norm which can be used for the connectives of antecedents. The Mamdani method gives up different fuzzy collective consequents for the rules used. For example max-min is used as the inference method in the Mamdani approach using either scalar values or graphical techniques. The Mamdani inference system has two rules and two inputs as inputs (x and y) that are fuzzified by two MFs groups of sets, (A_1,A_2) and(B_1,B_2), and one output of MFs sets (C_1,C_2). The inference system can be expressed in scalar technique as follows:

$Rule_1$: If x is A_1 and y is B_1 Then z is C_1

$Rule_2$: If x is A_2 and y is B_2 Then z is C_2

By applying min Conjunction connective (Λ) the output W_1 and W_2 can be obtained from:

$W_1 = \mu\ A_1\ (\mathrm{x})\ \Lambda\ \mu\ B_1\ (\mathrm{y})$

$W_2 = \mu\ A_2\ (\mathrm{x})\ \Lambda\ \mu\ B_2\ (\mathrm{y})$

and

$\mu\ Cf_1\ (\mathrm{x}) = W_1\ \Lambda\ \mu\ C_1\ (\mathrm{z})$

$\mu\ Cf_2\ (\mathrm{x}) = W_2\ \Lambda\ \mu\ C_2\ (\mathrm{z})$

Where μ is the membership function of different variables.

Finally max Disjunction connective (V) is applied:

$\mu\ \mathrm{C}\ (\mathrm{z}) = \mu\ Cf_1\ (\mathrm{x})\ \mathrm{V}\ \mu\ Cf_2\ (\mathrm{x})$

This can be applied for n numbers of fuzzy sets and k numbers of rules.

In addition, the graphical Mamdani (max-min) inference methods with two crisp inputs and two rules is shown in Figure 2.13 [39]. The overall fuzzy output is derived by applying Mamdani operation to the qualified fuzzy outputs and it uses the appropriate defuzzification method to find the crisp output. The different defuzzification techniques will be explained later in this section [39] [79].

The Takagi-Sugeno approach

The Takagi-Sugeno method is a type of a fuzzy system, which avoids defuzzification. This method was proposed to develop a systematic approach to generate fuzzy rules from a given input-output data set [36] [78]. Typical rules in a Takagi-Sugeno model have two inputs x_1 and y_1, and outputs z_1 and z_2 have the form:

Rule 1 x_1 is A_1 and y_1 is B_1 Then $z_1 = f_1(x_1,y_1)$

Rule 2 x_1 is A_2 and y_1 is B_2 Then $z_2 = f_2(x_1,y_1)$

Where z_1,z_2 are crisp functions in the consequent which are usually polynomial. The output level Z_i of each rule is weighted by the firing strength W_i of the rule. For example, for an AND rule with input x_1 and input y_1, the firing strength is:

$W_1 = \mu\ A_1(x_1)\ \Lambda\ \mu\ B_1(y_1)$

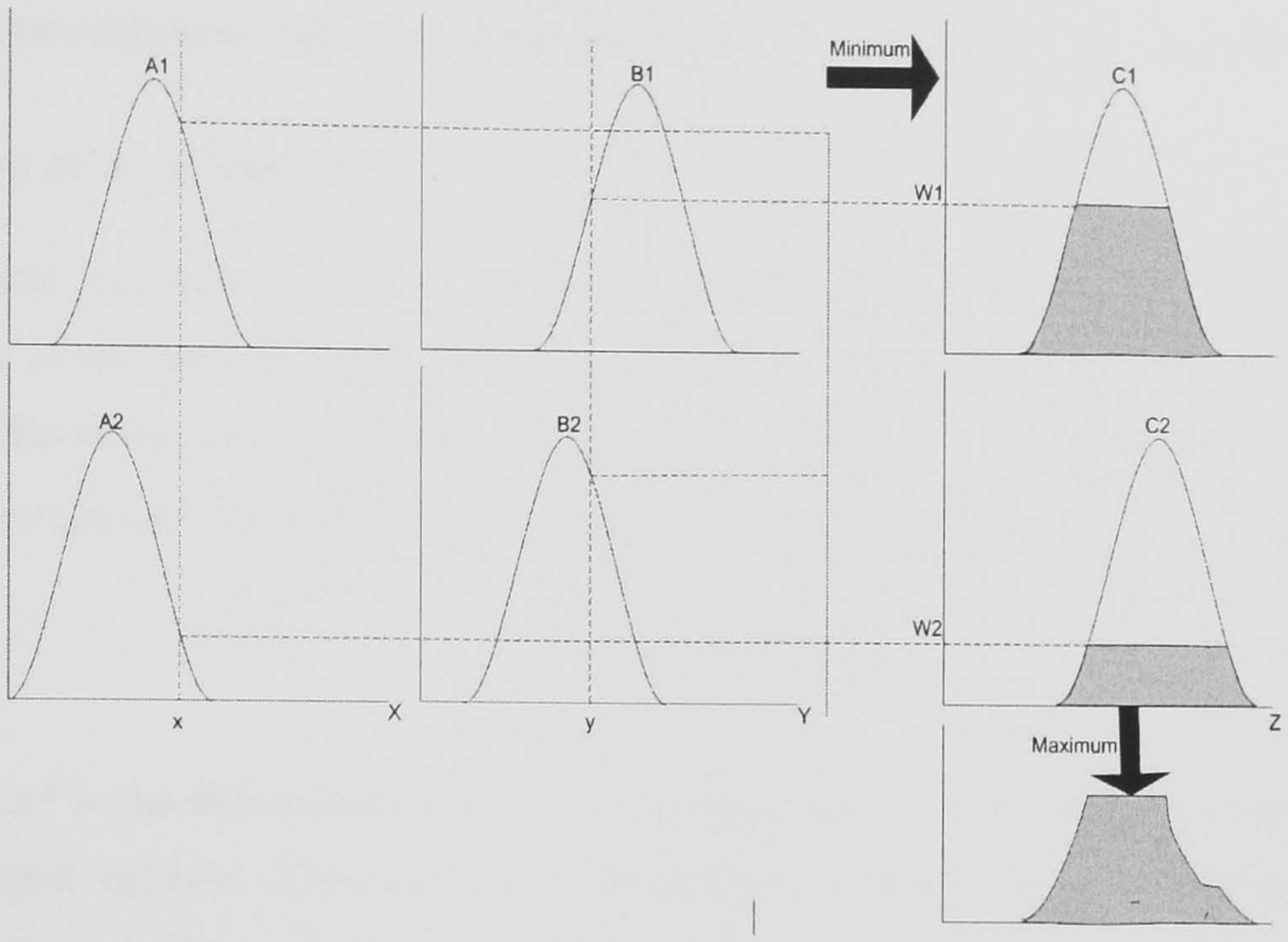

Figure 2.13: Mamdani max-min fuzzy inference model

$W_2 = \mu\ A_2(x_1)\ \Lambda\ \mu\ B_2(y_1)$

$$Z = Z_1 * W_1 + Z_2 * W_2 \tag{2.19}$$

Where W_1 and W_2 are obtained using the same method that was shown in the Mamdani approach in Figure 2.13. It is devious from Equation 2.19 that there is no need for defuzzification, because we get a crisp value in the output. This method avoids the time consuming process of defuzzification [36].

2.3.4 Defuzzification

The process of converting the fuzzy output to crisp values is called defuzzification. Before an output is defuzzified all the fuzzy outputs of the system are aggregated with union operator as described in the Mamdani approach. There are many different methods of defuzzifying fuzzy output function such as: max membership principle, centroid method (centre of area method), weighted average method, mean max membership, centre of sums method, centre of largest area and first or last of maxima [79]

[47]. Two important defuzzifications methods will be presented in this section.

Centre of area method

The most common method is the centre of area method which finds the centre of gravity of the solution fuzzy sets. This technique was developed by Sugeno in 1985 [79]. This is the most commonly used technique and is very accurate[79].

The centroid defuzzification technique can be expressed as:

$$\mathrm{x}* = \frac{\int \mu_{\mathrm{i}}\ (x)x dx}{\int \mu_{\mathrm{i}}\ (x)dx} \tag{2.20}$$

Where x^* is the defuzzified output, μ_i is the aggregated membership function and x is the output variable. The boundary of integration is determined as the accumulative integration of each underline area in Figure 2.13.

Max membership principle

The max membership principle gives the output with the highest membership function as seen in Figure 2.14 [95]. This defuzzification technique is very fast but is only accurate for peaked output [79]. This technique is given by Equation 2.21:

$$\mu_A(\mathrm{x}*)\ \geq \mu_{\mathrm{A}}(\mathrm{x}) \tag{2.21}$$

for all $\mathrm{x} \in \mathrm{X}$ where x^* is the defuzzified value

2.4 ANFIS: Architecture and learning algorithm

"An innovative approach to constructing a computationally intelligent system has just come in to the limelight. These intelligent systems are supposed to possess humanlike expertise within a specific domain, adapt themselves and learn to do better in a changing environment such as; Neural networks that recognise patterns and a adapt themselves to cope with changing environment; fuzzy inference system that incorporate human knowledge and perform inferencing and decision making. The

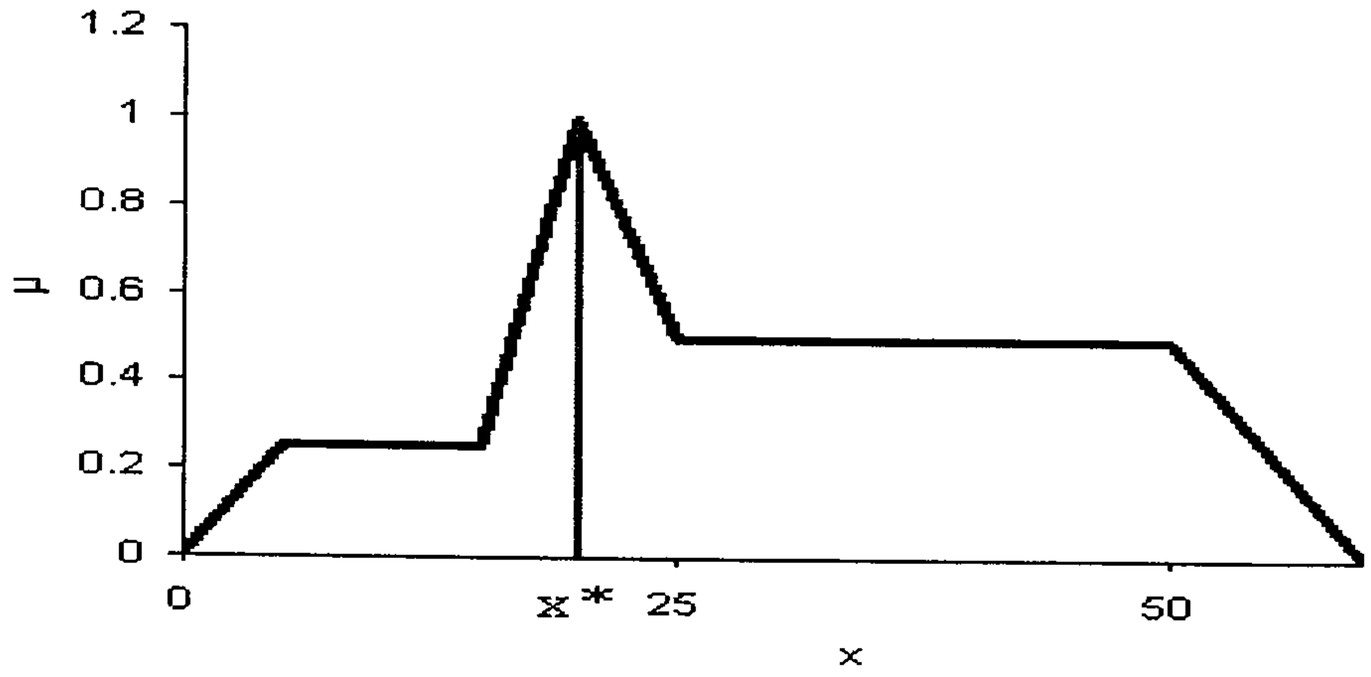

Figure 2.14: Max membership

complementary approaches, when used together with certain derivative-free optimisation techniques, result in a novel discipline called neuro-fuzzy and soft computing" Jang, page number 1 [39].

2.4.1 ANFIS architecture

ANFIS has a network-type structure similar to that of a neural network, which maps inputs through input membership functions and associated parameters. ANFIS uses a hybrid learning algorithm to identify parameters of Sugeno-type fuzzy inference systems [36]. Figure 2.15 represents the ANFIS architecture with x and y inputs and f output. A_1 and A_2 are the fuzzy memberships that fuzzified input x. In addition, B_1 and B_2 are the fuzzy memberships that fuzzified input y [36] [39]. Sugeno ANFIS has rules of the form [71]:

$$If\ x\ is\ A_1\ and\ y\ is\ B_1 \quad THEN\ f_1 = p_1x + q_1y + r_1$$

$$If\ x\ is\ A_2\ and\ y\ is\ B_2 \quad THEN\ f_2 = p_2x + q_2y + r_2$$

For the training of the network, there is a forward pass and a backward pass. We now look at each layer in turn for the forward pass. The forward pass propagates the

2.4 ANFIS: Architecture and learning algorithm

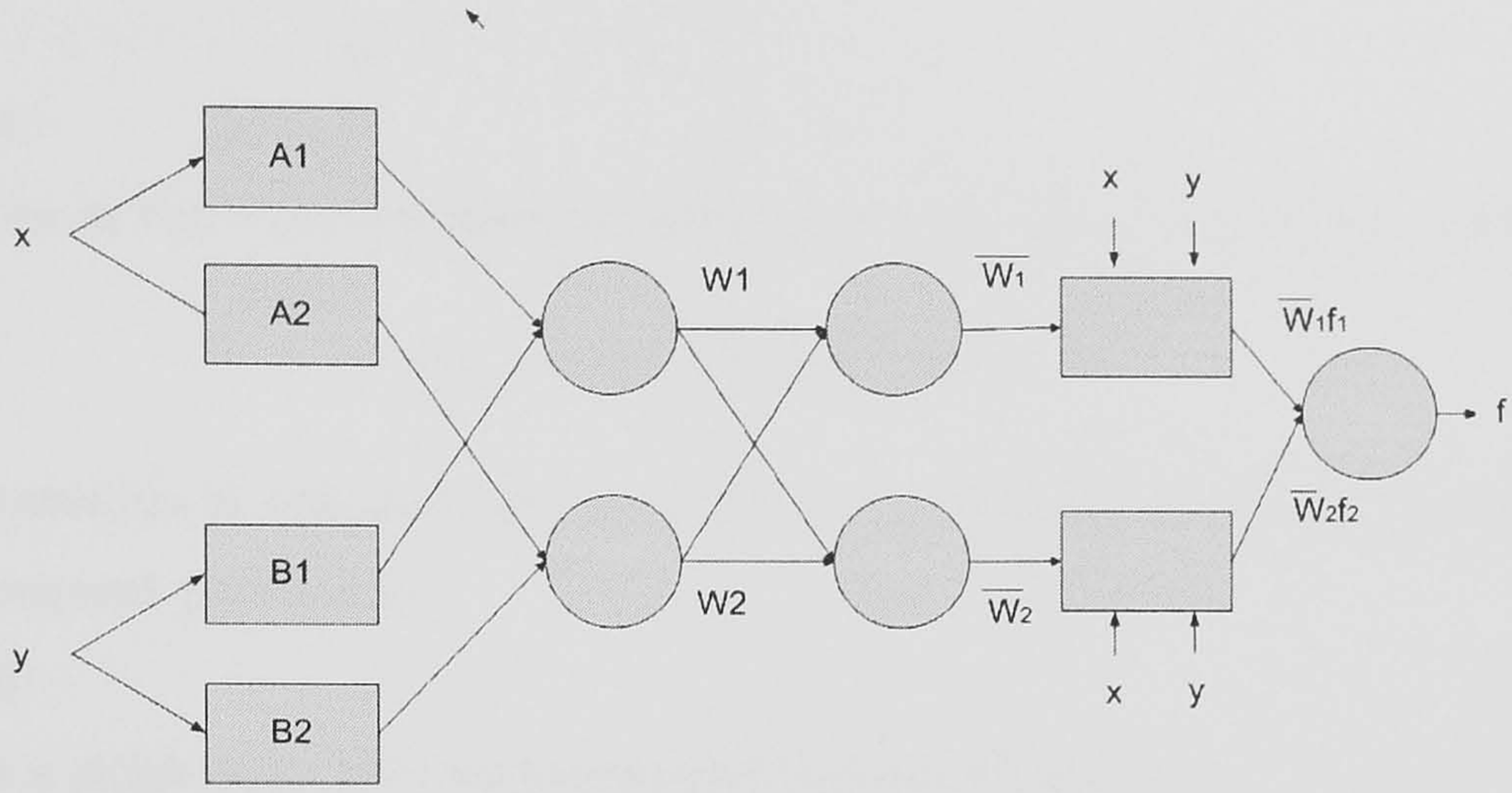

Figure 2.15: An ANFIS architecture for a two rule Sugeno system

input vector through the network layer by layer. In the backward pass, the error is sent back through the network in a similar manner to backpropagation [71].

Layer 1:

The output of each node is:

$$O_{1,i} = \mu_{A_i}(x) \qquad for\ i = 1, 2$$

$$O_{1,i} = \mu_{B_{i-2}}(x) \qquad for\ i = 3, 4$$

So, the $O_{1,i}(x)$ is essentially the membership grade for x and y. The membership functions could be any shaped function like that described before. The parameters of membership function are called the premise parameters.

Layer 2:

Every node in this layer is fixed. This is where the t-norm is used to 'AND' the membership grades - for example the product:

$$O_{2,i} = w_i = \mu_{A_i}(x)\mu_{B_i}(x), \qquad i = 1, 2$$

Layer 3:

Contains fixed nodes which calculate the ratio of the firing strengths of the rules:

$$O_{3,i} = \overline{w}_i = \frac{w_i}{w_1 + w_2}$$

Layer 4:

The nodes in this layer are adaptive and perform the consequent of the rules:

$$O_{4,i} = \overline{w_i} f_i = \overline{w_i}(p_i x + q_i y + r_i)$$

The parameters in this layer (p_i, q_i, r_i) are to be determined and are referred to as the consequent parameters.

Layer 5:

There is a single node here that computes the overall output:

$$O_{5,i} = \sum_i \overline{w_i} f_i = \frac{\sum_i w_i f_i}{\sum_i w_i} \tag{2.22}$$

2.4.2 Learning algorithm

In general, ANFIS is used to predict the output data parameters from inputs. ANFIS uses training data to adapt the Sugeno-type model to perform a high accuracy in output data prediction. The Sugeno-type model has two type of parameters [37] [39]:

- Nonlinear parameters or membership functions parameters (premise parameters).
- Linear parameters or rules parameters (consequent parameters).

The input output training data is used with different learning algorithm strategies to adapt the premise parameters and consequent parameters. The least-squares estimate (LSE) method and the backpropagation gradient descent method are used for training FIS membership functions parameters to estimate a given training data set [39].

LSE learning algorithm calculates the square error between training data output and predicted output that is obtained from the Sugeno-type model. This error is utilised to adapt the consequence parameters of the Sugeno parameters.

The backpropagation gradient descent method uses the error between output training data and predicted output in backward pass to calculate the error in different nodes. Accordingly, the learning rate is calculated to adapt the Sugeno parameters. There are four methods are used to update the parameters. These methods are listed below according to their computational complexities [39] [44]:

1. Gradient descent only: all parameters are updated by the gradient descent.

2. Gradient descent and one pass of LSE: the LSE is applied only once at the very beginning to get the initial values of the consequent parameters and then the gradient descent takes over to update all parameters.

3. Gradient descent and LSE: this is the proposed hybrid learning rule.

4. Sequential approximate LSE only.

The selection of above methods should be based on the trade-off between computation complexity and resulting performance. Jang in [36] used the third method, which achieves a high performance. In hybrid learning rule algorithm, ANFIS uses a two pass learning algorithm:

1. Forward pass: here consequent parameters are computed using a LSE algorithm and premise parameters are unmodified.

2. Backward pass: here premise parameters are computed using a gradient descent algorithm and consequent parameters are unmodified.

2.5 Statistical analysis

Statistical techniques are very important in data analysis. Correlation analysis and data clustering are two important statistical techniques which are utilised to analyse and group data in many control strategies. Dividing the data into different numbers of clusters helps to reduce the complexity of understanding the system behaviour. Correlation analysis can inspect the relationship between different data that affect

each other in the system boundary. In this section, these two statistical methods are discussed.

2.5.1 Correlation analysis

Correlation analysis is a statistical technique that evaluates the relationship between two variables. In linear correlation analysis there is a mathematical approach that compute a constant called a correlation coefficient which represents the degree of linear functionality between two variable parameters in specific system [89] [90]. The correlation coefficient is computed in the following stages: If one parameter is X and the second is Y and the two parameters have n time values. The sum of the products of the deviations of the two distributions is computed from covariance Equation 2.23 [91]:

$$\sum_{i=1}^{n}(X_i - \overline{X})(Y_i - \overline{Y}) \tag{2.23}$$

Where $\overline{X}$ and $\overline{Y}$ are the average value of X and Y values. The sum of squared deviations of the X distribution and the Y distribution is computed from:

$$\sqrt{(\sum_{i=1}^{n}(X - \overline{X})^2)(\sum_{i=1}^{n}(Y_i - \overline{Y})^2)} \tag{2.24}$$

Finally the correlation coefficient is computed from a combination of above Equations:

$$\frac{\sum_{i=1}^{n}(X_i - \overline{X})(Y_i - \overline{Y})}{\sqrt{(\sum_{i=1}^{n}(X - \overline{X})^2)(\sum_{i=1}^{n}(Y_i - \overline{Y})^2)}} \tag{2.25}$$

The value of a correlation coefficient lies in a range of between +1.0 and -1.0. The correlation coefficient is dimensionless. The positive sign means that the two variables vary in the same direction. The negative sign means that the two variables vary in opposite directions [91]. If the absolute value of correlation coefficient is close up unity that means a high relationship between variables.

2.5.2 Data clustering

Cluster analysis is a technique used to examine similarities and dissimilarities of observations or objects [94]. The main objetive of clustering is to identify natural groupings of data from a large data set to produce a concise representation of a system's behaviour. Several fields of study, such as engineering, medicine, linguistics and marketing, have contributed to the development of clustering techniques and the application of such techniques [58]. The literature describes several kinds of clustering analysis. These kinds of clustering analysis have different features. The kind of clustering that can be utilised to deal with data in different systems depends on following influences[39] [58]:

1. Volume of data and estimated data relationships.

2. The specifications of clusters that we need to assemble.

3. The purpose that we need to achieve from using data clustering analysis.

This is a summary of some of the popular kinds of clustering:

1. "Subtractive clustering, is a fast, one-pass algorithm for estimating the number of clusters and the cluster centres in a set of data" Matlab help, Fuzzy clustering [58]. In this type of clustering we should have a clear idea of how many clusters there are for a given set of data. Also the radius of the cluster centre is determined, and the ratio between clusters radii. The first cluster centre is determined by iteration. This centre is determined by counting a point that has the highest potential of points within setting radius. After that the point in the first cluster is removed to compute the second cluster centre depending on the radii ratio and the process that has been applied to the first cluster. This type of clustering is a one-pass method to take input-output training data and generate a Sugeno-type fuzzy inference system that models the data behavior. [19] [58] [39] [92].

2. Fuzzy C-means is a data clustering technique where in each data point belongs to a cluster to some degree that is specified by a membership grade. This technique was originally introduced by Jim Bezdek in [14] as an improvement on earlier clustering methods [58] [77].

3. K-means clustering can best be described as a partitioning method. "K-means is more suitable for clustering large amount of data. K-means clustering is a partitioning method that treats observations in your data as objects having locations and distances from each other. It partitions the objects into K mutually exclusive clusters, such that objects within each cluster are as close to each other as possible, and as far from objects in other clusters as possible. Each cluster is characterised by its centroid, or centre point. The distances used in clustering often do not represent spatial distances" Matlab help, Fuzzy clustering [58].

2.6 Summary

This chapter discussed the PV system and MPPT system. The PV panels and DC-DC converter are the main parts that are required to discuss in the MPPT system design. Fuzzy logic inference system, ANFIS and statistical analysis are the tools that are required in assembling the MPPT system in chapter 5 and chapter 6. In chapter 3, several MPPT approaches that have been implemented in literature will be discussed.

Chapter 3

Tracking Maximum Power Point Approaches for PV panels

This chapter reports on MPPT approaches in the literature. It starts with conventional searching techniques such as perturb and observation methods, incremental conductance methods and computational methods. Furthermore, this chapter introduces three applied computational artificial intelligent techniques in MPPT. In addition, a comparison between on-line and off-line methods is included in fuzzy inference system approaches. Finally this chapter gives an introduction to the developed approach in this research.

3.1 Introduction

The cost of electricity from the solar array system is generally more expensive compared to electricity from the utility grid [27] [8]. For this reason, it is necessary to study carefully the efficiency of the entire solar system to design an efficient system that meets the load demands with lower cost. Solar irradiance, ambient temperature and speed of the wind are the main external influences that affect the maximum power that can be generated from a PV panel. These external influences also change the position of the maximum power point on the I-V curve as explained earlier in chapter 2. Furthermore, in direct coupled systems, load is the main internal factor that can drive PV panels to operate at a strict point on I-V curve, as demonstrated in Figure 2.5. If there is any small change in external influences, the position of maximum power point changes. Operating faraway from maximum power point decreases the output power of PV system. Therefore, it is necessary to continually track the maximum power point of a PV solar array. However, with huge changes in external influences the electrical parameters of PV panels are modified continuously and thus

there is a difficulty in measuring these parameters. Accordingly, it is difficult to locate the maximum power point mathematically as a function of the internal and external influences. Many control techniques have been proposed to track the maximum power point of a PV system with traditional and artificial intelligence techniques.

3.2 MPPT approaches

For many years, research has focused on many maximum power point control algorithms to extract the maximum power of PV panels. These techniques mostly utilise different research methods with different control strategies. The main directions of these MPPT techniques can be categorised in four main methods; perturb and observation, incremental conductance, computational and computational artificial intelligence.

The characteristics that are required in the MPPT techniques can be expressed as follow:

1. Has low tracking iterations under different environmental conditions.
2. Stability
3. Simplicity
4. Low cost
5. Efficiency.
6. Has been evaluated in different climatic conditions.
7. Can be used with different types of loads and can be adapt for different types converters.

3.2.1 Perturb and observation method

The perturb and observation method has been widely used because of the simple feedback structure and there are few measured parameters [85]. This method

is an iterative approach [72] [50]. In this method the operating voltage of PV panel is decreased or increased to find the correct direction of change toward maximum power point. The output power of PV panels is measured in each voltage stage. Power in each stage is compared with the previous perturbation. If the output power is increased the voltage will change in this direction, otherwise the voltage will change in the other direction. Maximum power is achieved by forcing the derivative of the power to be equal to zero under power feedback control [20]. Three main problems are associated with this method:

(a) This method needs to measure the PV current in each stage and this increases the power losses in the control unit. As a result, these losses decrease the system efficiency.

(b) This method needs a high number of iterations to track the MPP and it oscillates around the MPP [55] [33].

(c) Fluctuation around maximum power point due to the difficulty of the zero derivative calculation of $\frac{dP}{dV}$ or $\frac{dP}{dI}$.

Many techniques are proposed to defeat these problems. Hsiao in [98] developed a three-point weight comparison method that avoids the oscillation problem of the perturbation and observation algorithm. Also, the perturbation and observation method is proposed in [42] and [43] with an identification of capacitor for the maximum power point tracking in a photovoltaic power system. Capacitance is estimated and is used to correct the variations of duty ratio to obtain the highest performance of MPPT along with avoiding the degradation of PV panels.

The incremental conductance method in [1] [55] is an attempt to improve the perturb and observation method under rapid change in environmental conditions [33].

3.2.2 Incremental conductance method

Incremental conductance method is independent of device physics. It uses the source incremental conductance $\frac{dI}{dV}$ of PV panel as its maximum power point locating [85]. This method depends on a positive slope of P-V curve below V_{max} and negative slope of P-V curve above V_{max}. To demonstrate how this algorithm of incremental conductance works, the power equation (P=I*V) is differentiated as shown in Equation 3.1:

$$\frac{dP}{dV} = I + V * \frac{dI}{dV} \tag{3.1}$$

Dividing by V

$$\frac{1}{V} * \frac{dP}{dV} = \frac{I}{V} + \frac{dI}{dV} \tag{3.2}$$

In Equation 3.2 $\frac{I}{V}$ is a positive quantity. The slope of I-V curve of PV panels $\frac{I}{V}$ is always negative. Therefore, we can conclude from Equation 3.2 three rules as follow:

- If V $< V_{max} \Longrightarrow \frac{dP}{dV} > 0$, therefore $\frac{I}{V} > |\frac{dI}{dV}|$
- If V$> V_{max} \Longrightarrow \frac{dP}{dV} < 0$, therefore $\frac{I}{V} < |\frac{dI}{dV}|$
- If V$= V_{max} \Longrightarrow \frac{dP}{dV} = 0$, therefore $\frac{I}{V} = |\frac{dI}{dV}|$

The three rules above are used to track the maximum power point of PV panels. The incremental conductance method is proposed in [1] [55] [16]. The method has better performance than perturb and observation method in the case of rapid changes of environmental conditions. However, the current has to be measured continuously and that leads to more losses in the generated power. This method tracks the maximum power point without reference point. Therefore, the traditional controller which depends on perturb and observation or incremental conductance still takes a long time to reach the maximum power point, especially with rapid changes in environmental conditions. In addition, this type of controlling unit can be oscillated around the maximum power point.

A combination of the modified constant voltage control and the incremental conductance method is introduced in [41], which provides good efficiency, especially at low irradiance level [49].

The high power consumption, the oscillation around V_{max} and instability due to changes in environmental condition are the main problems that are observed with perturb and observation and incremental conductance. Avoiding these problems in these methods leads to more complexity with the conventional control unit [66] [85] [67] [57]. Control approaches with the computational method are the best ways to minimise the problems in perturbs and observation and incremental conductance methods.

3.2.3 Computational methods

In computational methods, electrical parameters of maximum power point are obtained using different influences that affect the PV cells. Locating the maximum power point voltage and current is the main aim in this method. This method has good performance with rapid changes in the environmental conditions [15]. This method works with different search methods to locate the maximum power point such as hill climb search. The main problem with this method is the degree of accuracy of locating maximum power point parameters. The degree of accuracy depends on the influences which are used to obtain the maximum power point parameters. In addition, stability and quick maximum power point tracking depend on the approach that is used along with computational methods.

The curve-fitting technique is a computational method which depend on the solar panel characteristics, so an explicit mathematical function describing the output characteristics can be predetermined [20]. This method is proposed in [46] and [84], which is based on fitting the operating characteristic of the panel to the loci of the maximum power point of the PV systems. Although this technique attempts to track the maximum power point without computing the

voltage-current product explicitly for the panel power, it cannot predict the characteristics including other complex factors such as aging, temperature, and a possible breakdown of individual cells [20] [46].

Maximum power points are computed at different environmental conditions in many approaches as a function of either irradiance level or cell open circuit voltages or cell short circuit currents. In [57] Masoum analysed theoretically and experimentally two different computational techniques. A voltage-based approach is the first technique that is proposed in [32], which calculates V_{max} as a function of V_{OC}. A current-based approach is the second technique which is proposed in [34], which calculate I_{max} as a function of I_{SC}. Masoum in [57] has concluded two important aspects which are summarised as follows:

- The current-based maximum power locating is a more accurate approximation of the actual nonlinear PV characteristics compared to the linear voltage function of the voltage-based technique.
- The voltage-based maximum power locating is naturally more efficient and has less circuit losses.

The low accuracy of voltage-based techniques comes from neglecting the irradiance level effect on open circuit voltage at different temperatures.

Solar radiation is used in [29] instead of short circuit current to obtain a reference P_{max} and V_{max}. The reference voltage (V_{max}) is also obtained in [53] as a function of V_{OC}.

Generally, there is a nonlinear relationship between I-V electrical characteristics of PV panels and external influences. Therefore, computing the maximum power point parameters as a function of one or more of environmental influences or as a function of the PV electrical parameters suffer from low accuracy especially with large changes in environmental conditions. In addition, it is difficult to continuously measure the environmental conditions and PV cell temperature. A statistical analysis with field data in chapter 5 will investigate the

relationships between these parameters and the method of improving the relationships between electrical parameters of PV panel. Neural networks as an artificial intelligence method is also used to improve the accuracy of locating the maximum power point in PV systems.

3.2.4 computational artificial intelligence methods

Generally, artificial intelligent approaches are used to map highly non-linear relationships between input and output to the system. Neural networks, fuzzy logic inference systems and adaptive neuro fuzzy inference systems which are implemented in several pieces of research are used to track maximum power point parameters.

Neural networks

A neural network is an example of artificial intelligence systems which are composed of simple elements operating in parallel. These elements are inspired by biological nervous system [39]. As in the nature, the network function is determined largely by the connections between elements. A neural network can be trained to perform a particular function by adjusting the values of the connections (weights) between elements. A neural network is commonly adjusted, or trained, so that a particular input leads to a specific target output [36] [58].

Neural networks have been used to estimate maximum power point parameters in several articles. Mashaly *et al* proposed a neural network to locate V_{max} from P_{max} in [56].The maximum power is computed as a function of irradiance level. In addition, the estimated V_{max} is used as a reference voltage to track maximum power point using FLC. This approach has been achieved better than conventional controller approaches.

In [23] Alexis used the same technique to locate maximum power point, however

with V_{OC} as an input parameter of the neural network instead of irradiance level. The convergence in error from neural networks in this approach reaches to 2.2% after training process.

Hiyama presented a neural network application in [31] to identify the maximum power point of PV modules and design a PI-type controller for real-time maximum power tracking. Maximum power point voltage is identified through the proposed neural network using the open circuit voltages from monitoring cells. The proposed neural network has provides a highly accurate estimation of maximum power point from the PV modules.

Mummadi *et al* developed a feedforward maximum power point scheme in [66] [80]. Mummadi *et al* located the maximum power point voltage by an off-line trained neural network. In these two approaches a three layer feedforward neural network with back-propagation algorithm is utilised to estimate the reference voltage from irradiance. Neural network model with FLC is implemented to track the maximum power point in [66] [80]. A comparative study of noncoupled and coupled interleaved Boost converter supplied PV systems is made in these approaches. The improvement in the efficiency is about (2-5)% and the observed reduction in load voltage ripple is about (50-70)%.

Generally, the neural networks approaches performs better than the simple mathematical computing methods if the input parameters are sufficient to describe the behaviour of the PV panels. However neural networks transact random data with a lack of human knowledge. It depends on data to learn the network which can lead to a long and complicated process of learning. Thus, the neural networks approach is used as a final alternative that can be selected to solve problems of poor knowledge.

Fuzzy inference system research

Fuzzy logic is appropriate for nonlinear control systems. Therefore, a fuzzy logic controller is used to provide a solution to control problems that cannot be described by mathematical models or need a complex mathematical model [85]. However, the fuzzy logic controller behaviour depends on the membership functions, their distribution, and the rules that influence the relationship between different fuzzy variables in the system. There is no formal method to determine accurately the parameters of the fuzzy controller [85]. Several approaches are implemented using the fuzzy logic controller to track the maximum power point of PV systems [2] [68] [30] [63]. Two main strategies are implemented in the reported research to track the maximum power point. The first strategy tracks the maximum power point directly without reference point like perturb and observation method (on-line approach) [73] [86] [6]. In this method the searching starts from previous point and move toward the target point step by step. In each step new input about current point and the relation between current point and previous point is delivered to the system. The power increment is observed till it reaches the maximum power point. All input parameters are modified in each step. This process is continued until reaching the specification of the target. The second strategy is the off-line approaches [44]. In this approach the maximum power point parameters are located as a reference point using different computation techniques [53] [66]. In this approach the target is delivered only one time and the searching starts from current point until reaching the target. In the rest of this section a brief overview of these approaches which describe MPPT using FLC is provided.

On-line approaches

The approaches that present a FLC to track maximum power point without computing the reference point are called on-line approaches. These approaches

concentrate on minimising the tracking time needed by perturb and observation and avoiding the fluctuation that may occurs in the traditional methods [7].

In [85] Bogdan and Li described two traditional methods for MPPT; the perturbation and observation and incremental conductance methods. The paper describes the benefits of the fuzzy logic controller approach. Bogdan and Li did not give any details regarding the FLC approach.

Altas and Sharaf implemented an FLC in [2] to extract maximum power point from stand alone PV to feed a three phase induction motor. The fuzzy controller that is introduced in [2] uses the change in generated power with respect to current change $\frac{dP}{dI}$ and its variations $\Delta \frac{dP}{dI}$ as input to FLC. The output of FLC is the change in duty cycle of MPPT converter. In this approach, the min-max rule is implemented as a fuzzy inference system to determine the changes in duty ratio ΔD using a pulse width modulator inverter, which controls the electronic switch of the DC-DC converter.

In [73] Senjyu and Uezato proposed a MPPT system using a fuzzy controller to overcome the problem of constant increment in hill climbing methods. Change in power due to variation in duty cycle and rate of change in power at different irradiance. The fuzzy rules are designed to avoid fluctuation in perturb and observation method. This method used the change in power with respect to the duty cycle $\frac{dP}{dD}$ and the change in the slope of P-V curve at different irradiance level to provide a fast tracking. This method provides a good performance with the step-down chopper converter but with a limited operating range and with constant resistive load only. Also, it needs a continuous current measuring which dissipated the generated power from PV system.

Chung *et al* proposed an MPPT in [86] using a fuzzy logic control with step up converter. There are two input variables of the proposed controller in [86], namely error (e) and change of error (Δe) at a sampling instant K where:

$$e(k) = \Delta P$$

$$\Delta e = \Delta P(k) - \Delta P(k-1)$$

The output of fuzzy union is used to control duty ratio of the Boost converter. This approach uses the centre of gravity method to obtain a crisp value of FLC. The simulation and experimental results show the tracking maximum power point performance of fuzzy controller. The FLC in [86] is compared with a controller based on hill climbing method and shows better performance. This method reduces the time required to track the maximum power point and reduces fluctuation of power around during tracking process. The experiment is implemented using a 16 bit microcontroller (80c196kB). More power is generated from PV array compared with the power generated using controller based on hill climbing method.

In [74] Simoes *et al* described analysis, modelling and implementation of fuzzy based PV peak power tracking. The power circuit in [74] is based on a Boost converter while the controller used an RISC microcontroller with fuzzy algorithm that searched for the optimum duty cycle to track the peak power from the solar array. In [74] the rules of the fuzzy controller are divided in to four groups. The first group controls the normal system operation. The second group is used when I-V curves of PV panels is changing due to environmental conditions only. A third group is implemented when ΔP has constant output in a small interval, which is not maximum power point. The last rules group is implemented when the maximum power point is reached. This approach uses the change in duty cycle ΔD(k-1) and the change in power ΔP as input parameters of FLC. The new result of change of duty ratio is used as the output of the FLC. A simple centre of gravity method is used to get a crisp value for the converter in this approach. The system was implemented in Matlab under different temperatures, different resistive loads and different levels of irradiance. Also, it was implemented in the laboratory with RISC controller type (PIC16174) under different levels of irradiance.

In [75] Simoes *et al* added experimental results curves to the previous mentioned

approach to show the response of pulse width modulator (PWM) cycles at different light-intensity steps. This approach provides fast convergence and robust performance against parameters variation.

In [87] Wu and Chen presented a FLC which controlled a single stage converter with the integration of a bidirectional Buck Boost charger/discharger and a class-d series resonant parallel loaded inverter. The system adjusts the duty cycle by comparing the maximum current (I_{max}) that can be reached by FLC and the direction of the new currents that mutate with environmental conditions. The fuzzy rules are built depending on whether the operating point is under or above the desired value. In addition, the current values are in divergence to the desired value or convergence regarding the slope of current curve toward maximum power point. The min-max operation is adopted to obtain the output fuzzy set. In this approach the MPPT system is implemented in a single-chip microprocessor. The proposed system needs about 70s to reach the maximum power point in which fluctuation in PV array output has been minimised.

In [68] Patcharaprakiti and Sirisuk and in [69] Patcharaprakiti *et al* proposed FLC with lookup table for light-flasher and battery charger applications. Two input variables of the proposed controller, namely error(e = $\frac{\Delta P}{\Delta V}$)and a change in error ($\Delta$e) are used to adapt the duty cycle of a DC-DC converter switch. The lookup table divides the input and output fuzzy parameters to help the FLC realising rules that are designed for MPPT system.

Off-line approaches.

Off-line approaches are the techniques that firstly locate one or more parameters (voltage-current-power) which are affected by the environmental conditions. After that, it compares the current point on the I-V curve of a PV system to give the proper decision for decreasing the tracking time of the maximum power point in on-line techniques. The fuzzy controller in on-line approach starts its

search for new maximum power point, by using a previous maximum power point as starting point to track the new maximum power point. The off-line approach devolvement reduces the number of iterations that is required to reach the MPP, especially if this new MPP is located faraway from the previous one. Hence, the approaches based on off-line techniques avoid the energy wasted in on-line techniques [15] [97]. Generally, the FLC rules are designed to reduce the number of iterations in different approaches that use off-line techniques as seen in the following literatures:

Rohan and Adel introduce in [30] a rule-based fuzzy logic controller to control a PWM inverter. This approach locates P_{max} as a polynomial function of irradiance level. This approach extracts and tracks the MPP from the PV array at different irradiance levels. In [30] power error (e= $\frac{P_{max}-Pop}{P_{max}}$) and rate of change in this error (Δe) are used as input signals to FLC. This FLC controls the duty cycle of the PWM inverter. This approach applied 49 fuzzy rules to change the modulating index, which controls the angle and the duty cycle of the PWM inverter. The proposed fuzzy rule-based controller in [30] is introduced in a software package.

In [28] Gwon *et al* described the effect of temperature on locating the maximum power point. In this approach the temperature is calculated as a function of voltage using a voltage transducer and the temperature values are used to calculate V_{max}(t) as a function of V_{max} at standard test conditions. The value of V_{max}(t) is used in the fuzzy controller as voltage reference (V_{ref}) to calculate the first input of FLC (e= V_{ref} -V_{op}(t)), where V_{op}(t) is the current operating voltage point of the PV panel. The second input of FLC is (Δe). These two inputs are used to modify duty ratio as output of FLC. The experiments compare the proposed FLC with a traditional controller without giving any detail of the results.

Khashab and Nashed presented in [53] a simulation study and an experimental implementation of FLC for a Cuk converter in a stand alone PV energy scheme.

DC-DC converters were used to convert unregulated DC input into a regulator DC output at a desired voltage level. At certain irradiance, the V_{OC} in this approach is obtained as a function of irradiance and I_{SC}. Accordingly, the reference voltage V_{ref} is obtained as a linear function of V_{OC}. This reference voltage is used to calculate the error:

$$e = V_{ref} - V_{op}$$

Error (e) is used as a first input of FLC in this approach. Δe is used as a second input of FLC. These two inputs are used to control the duty cycle of PWM which feeds a switch to the Cuk converter. The system is implemented with different resistive loads and at different irradiance levels. In addition, this approach demonstrates a comparison between the output power of PV panels of direct coupled system and the power of proposed MPPT controller.

In [66] and [80] Mummadi *et al* introduced a feed forward maximum power point scheme which is developed for the interleaved dual Boost converter which feeds a FLC. In this approach the reference voltage is obtained using a neural network. The first input of the FLC is:

$$e = V_{ref} - V_{op}$$

The second input is Δe. These two inputs are used to modify the duty cycle of PWM that feeds a switch of interleaved dual Boost converter. In this approach the controller does not need the tuning of parameters like the conventional controller. The experimental result gives a good result with different types of load (resistive load, battery load and both types). The paper presents a comparison between the proposed controller and the conventional Boost converter. The efficiency about (2-5)% higher than conventional Boost converter and about (15-35)% less ripple content in voltage is achieved in this approach.

In [63] Games and Abdul presented a FLC scheme for the optimal power requirement of a PV system with and without energy storage. In this approach

the MPP is located using a genetic algorithm to track it using fuzzy logic controller. The second and third inputs of FLC are the state of charge of the battery and the load current. The FLC rules are designed in [63] to control the following parameters:

- The output load elements (load curtailment or addition) depending on the optimal power tracked and the rating of the PV panel.
- The injection of optimal current into the battery to achieve the optimal operating conditions of the PV system during the storage of energy.

In addition, the fuzzy design scheme in this approach is developed around an in-house PV program using Matlab software. The normalised control variable for the FLC is used to control the duty cycle of the PWM converter. In addition, in [4] Altas presents simulated load matching for maximum power utilisation. This approach introduces a PV standalone energy utilisation scheme feeding hybrid DC electric loads and fully controlled by a dual controller using dynamic multi loop online error driven classical PI controller and FLC. The proposed hybrid PI and FLC action is studied in two cases for maximum power point tracking and specific load control.

In [48] and [49] Kottas *et al* presented a novel MPPT method, which uses fuzzy sets theory in close cooperation with fuzzy cognitive maps (FCMs). The FCM represents essential operational (voltage, current, irradiance level, temperature) and it controls the current of PV system. The node interconnection weights are determined using data, which covers the operation of a PV system under a wide range of different simulated climatic conditions. The nodes values in FCMs are fuzzy and the weights of the interconnections belong in [1,-1]. The proposed system was trained by a simulated climatic data of a one year. It had a 0.78% error in energy production when compared with the theoretical expected production of a commercially available photovoltaic array.

A comparison of on- line and off-line methods

Udayakumar *et al* in [97] introduced a comparison between different strategies of tracking maximum power point. This paper studies the benefits of the MPPT controller with reference point (off-line approaches) and without reference point (on-line approaches). Furthermore, the paper proposed a FLC with different numbers of MFs to prevent overshooting from maximum power point and it designed the rules to control the rate of change of the duty cycle. The controller uses the following parameters as input of a FLC:

$$\Delta V(k)$$

and

$$\Delta V(k) - \Delta V(k-1)$$

The FLC in this approach tracks the maximum power point under rapid changes of environmental conditions. In addition, this approach confirms the problems of power wasted in on-line techniques. However, a complicity of maximum power point computing in many techniques and the external environment sensors in other techniques represent the drawbacks in off-line approaches. Udayakumar *et al* prefer the simplicity of on-line techniques. On the other hand, Mummadi in [66] and Theodores in [15] choose the off-line method due to the high accuracy in maximum power point prediction, such as the neural network that was proposed in [66] and fuzzy cognitive maps in [15].

Adaptive neuro fuzzy inference system

In [59] Mellit, in [60], Mellit and Kalogirou and in [61] Mellit and Benghanem proposed an ANFIS models to estimate the output of PV systems. In these papers, an ANFIS model is used for modelling the different components of the PV system. Additionally, the ANFIS was developed to model the delivered and consumed power by the PV system. The ANFIS model trained using data

from the various input signals of the PV system. This database is created from an experimental data acquisition. The developed model can predict and simulate the different electrical signals of the PV power supply system from only the ambient temperature, solar irradiation and humidity. Results obtained indicate that a satisfactory accuracy is obtained between the measured and estimated electrical signals. The papers conclude that the ANFIS system can be implemented to help the maximum power point tracker controller deliver the maximum energy from the PV array.

In [67] and [68] Patcharaprakiti and Premrudeepreechacharn proposed a method of MPPT using adaptive FLC for a grid connected PV system. This approach is an on-line search technique. The proposed system in this approach composes of a Boost converter single phase inverter which is connected to the utility grid. The MPPT control is based on adaptive fuzzy logic to control the MOSFET switch of the Boost converter and the single phase inverter uses to predict current control. The grid connection PV system that is presented in this approach can directly feed energy into the existing Ac grid system. The MFs in this approach are assigned to the linguistic variables using seven fuzzy subsets. The inputs parameters are: e $= \frac{\Delta P}{\Delta I}$ and change of error Δe. These two inputs are normalised by the input scaling factor β and β^*. In this approach the inputs are scaled between 1 and -1. The purpose of the learning mechanism is to learn the environmental parameters as a result modifying the fuzzy logic controller parameters. Accordingly, the outcome of the overall system is close to the optimum operation point. The learning is composed of an inverse fuzzy model and knowledge base modifier. The basic operation of the inverse fuzzy modifier is to change the shape of membership to make fast tracking under different irradiance levels. The simulation results show, how the proposed system has fast response and good transient performance insensitive to variations in external disturbances. In addition, the results of simulation show how the MPPT controller by using adaptive FLC has provided more power than simple fuzzy

logic controller.

MPPT approaches summary

Several approaches that were mentioned earlier in this chapter compute the maximum power point parameters depending on irradiance level. However, the solar irradiance cannot describes the behaviour of the maximum power point voltage, as we will clarify in the statistical analysis in chapter 5. In addition, there is more than one approach with includes the temperature effect on electrical parameters of P-V and I-V curves. These approaches were used to test the system in a limited range of solar radiation and ambient temperature. However, these approaches do not consider the wind effect on cell temperature, which strongly affects the maximum power point voltage.

The high power consumption, the oscillation around V_{max} and instability due to changes in environmental condition are the main problems that are observed with perturb and observation and incremental conductance. Avoiding these problems in these methods leads to more complexity with the conventional control unit.

Neural networks provide a high precision in estimation systems.The neural networks approaches performs better than the simple mathematical computing methods if the input parameters are sufficient to describe the behaviour of the PV panels. However neural networks transact random data with a lack of human knowledge. It depends on data to learn the network which can lead to a long and complicated process of learning. A lack of human knowledge in neural network leads to complex structure of the neural network, especially with a low correlation between inputs and outputs data.

The fuzzy logic controller behaviour depends on the membership functions, their distribution, and the rules that influence the relationship between different fuzzy variables in the system. Therefore, fuzzy logic inference system

reduces the time of tracking maximum power point compared with approaches that depend on the simple perturb and observation method [85] [97]. Also, it avoids the fluctuation in power around the maximum power point. "Generally, the FLC is nonlinear and adaptive in nature. Therefore, it gives a robust performance under parameter variation" Mummadi *et al*, page number 970 [66]. "It does not require precise, noise-free inputs and can be programmed to fail safely if a feedback sensor quits or is destroyed. The output control is a smooth control function despite a wide range of input variations" Udayakumar R. *et al*, page number 1421 [97].

Also, different peak power tracking schemes have been proposed by different fuzzy logic researchers . There are three main factors which play a crucial role on the fuzzy logic controller approaches trends. The first factor is regarding the technique of moving towards the MPP whether by using off-line techniques or on-line techniques that are discussed in section 3.2. The second factor is the type of converter that is used. The third factor is the type of fuzzy MFs and the ability of rules to handle the problems under different conditions and, consequently adjusting the rate of duty cycle according to the location of operating point on P-V curves and the slope of the curves under different conditions.

ANFIS is used in maximum power point tracking publications as an on-line searching system. The self-adaptation of ANFIS parameters with different system configuration is very important when the controlling system will be generalised [39]. However, the feedback effect of the load voltage on the output of converter and the type of converter that is used will increase the parameters that are required as input of the ANFIS structure. A large structure of ANFIS makes it more complicated. Therefore, the ANFIS model will be used with fuzzy logic controller in the developed MPPT system as off-line approach.

3.3 Introduction to the developed approach applying ANFIS prediction and FLC tracking

Maximum power point tracking techniques are applied to extract the maximum available power from the PV panel at different environmental conditions and different types of load.It is difficult to design a system that encompasses completely all required characteristics . A successful approach is one that can balance between different features to acquire the best promising performance. On-line systems are generally simpler than off-line systems. However a continuous current measuring during iteration searching time decreases the system efficiency. Furthermore, it is difficult to perform stability in on-line techniques at partially cloudy days. Off-line system precision depends on the accuracy of computational methods that provide the FLC by the reference maximum power point parameters.

The proposed system will use ANFIS to predict the maximum power point voltage with two inputs and one output. The two inputs and output data are selected depending on actual data analysis in chapter 4 and chapter 5. A number of ANFIS models are tested to reach the best model that can predict the accurate V_{max}.

3.3.1 Motivation for using ANFIS

The low CC between I_{SC} and V_{max} and between V_{OC} and V_{max} in chapter 5 confirm the nonlinear relationship between these variables. Moreover, clustering analysis with correlation analysis clarifies the improvement of CCs between V_{OC} and V_{max} when the input data is clustered with respect to I_{SC}. In addition, it is observed the improvement in CCs when there is an overlapping between different clusters. Takagi and Sugeno's fuzzy if-then rules are used when the output of each rule is a linear combination of input variables plus a constant term. The final output is the weighted average of each rule's output [36]. In

addition, as mentioned earlier ANFIS has the ability to adapt MFs and reach the best MFs that can predict the output with minimum error between actual data and predicted data.

3.3.2 Introduction to the developed FLC

The final output of the ANFIS model is used as input parameters of FLC. The FLC will be used to track the maximum power point. A novel FLC is designed to achieve the most features that are mentioned above in this section. In addition, the FLC is designed to avoid the shortages in several MPPT techniques. The MFs of the developed FLC are designed to help solve the problems of the MPPT and reducing the rules that are required in FLC. Thus, the FLC become simple and it overcomes the problems that are ignored in most existing approaches. In addition, the proposed FLC can be adjusted easily to control the duty type of DC-DC converters depending on the requirements of each converter and depending on the appropriate converter that should be used to interface between the photovoltaic panel and different types of load. Two simulation models will be applied to study the behaviour of FLC. The developed MPPT system will be compared with the direct coupled system. Figure 3.1 shows the sequence of MPPT of PV system. The developed system has the following five main features.

- The PV system behaviour is studied and tested with different climatic field data
- The system has been deduced using statistical analysis and mathematical tools.
- Had sufficient time in testing to determine the gaps in learning data and completing these gaps.
- System has been evaluated using the different Matlab tools and simulation models.

- Does not need external sensors to locate and track the maximum power point.

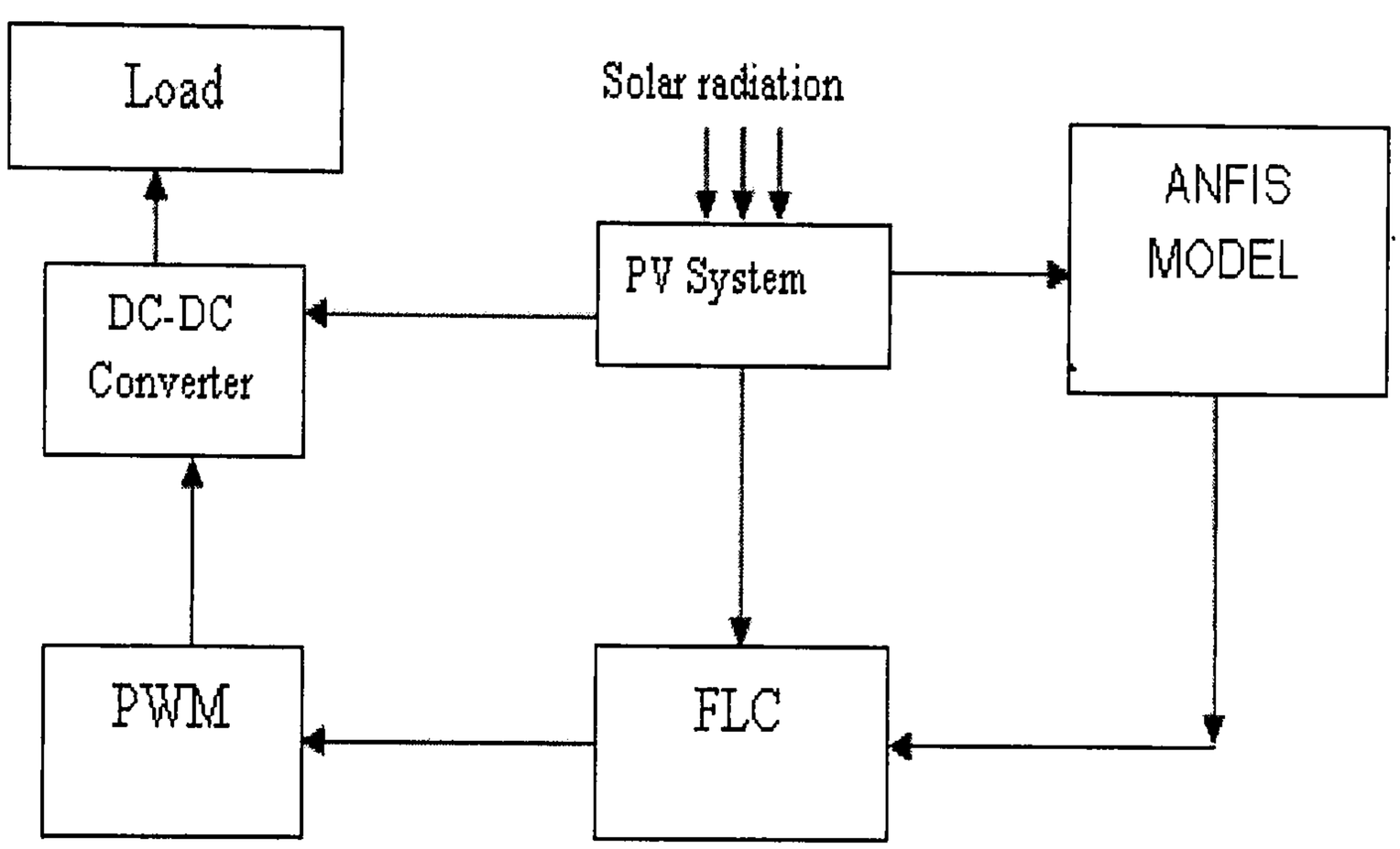

Figure 3.1: Proposed system architecture

3.4 Summary

This chapter presented an overview of the approaches that have been implemented in MPPT system. In addition, This chapter gives an introduction to the developed ANFIS prediction and FLC tracking approach. In the next chapter we present the collected data from different environmental conditions for two types of PV panels. In addition, the data will be analysed in chapter 4 to provide core data for the ANFIS model in chapter 5.

Chapter 4

Data Analysis

4.1 Introduction

PV panels are traditionally tested under standard test conditions (STC). (Irradiance: 1000 W/m^2; Spectrum: AM1.5; and Cell temperature: 25^{o}C). The main parameters that are measured at STC are I_{SC}, V_{OC}, V_{max} and I_{max} which are always included in the manufacturers data sheets. Furthermore, characterisation of the PV module is accomplished by measuring the nominal operating cell temperature (NOCT), which is defined as the temperature that the cell can reach when the PV module is submitted to an irradiance of 800 W/m^2 and an ambient temperature of 20 ^{o}C [51] [26].

To compute the operating points theoretically on I-V curves, it is necessary to measure the irradiance level and cell junction temperature. The irradiance level, as a result a photocurrent, can be measured using an external sensor or by means of the linear relationship between short circuit current and irradiance levels in Equation 2.7. However, the problem is the difficulty of measuring or deducing the cell junction temperatures by using the different environment or electrical parameters.

On sunny days, the ambient temperature increases from 20^{o}C to 45^{o}C, and the irradiance level can reach 100mW/cm^2. By applying Equation 2.9, the 100mW/cm^2 irradiance increases the PV cell temperature to about 30 ^{o}C over the ambient temperature when neglecting wind effect. The PV panel cells temperature is affected environmentally in the different regions as follows:

- Increased due to the irradiance level.

- Increased proportional to the increase in ambient temperature and high humidity.
- Decreased due to the decline in ambient temperature in high altitude regions.
- Decreased due to wind velocity.

The solar radiation affects directly PV panels due to solar power being dissipated in the PV cells. In addition, the high irradiance level lead to increases in the ambient temperature especially in high humidity regions. A high speed of wind movement improves the convection factor effect, which increases the heat dissipation from the surface of the PV panel to the surrounding. It is difficult to measure the convection factor, which strongly affects the PV cell temperature. Furthermore, the generated current in PV cells increases the cell junction temperature of the PV cells. This current increases with increasing in irradiance level.

Any change in environmental conditions affects the PV cell temperature and photo current. If there is a small change in the external influences, the characteristics of the I-V curve are modified. With a huge change in the environmental conditions and the difficulty of measuring the cell junction temperature, it is difficult to predict the maximum power point voltage mathematically.

To study the behaviour of a PV panel, it should be tested in all possible environmental conditions. Considering most environmental conditions that affect cell temperature and electrical parameters of PV panels, field data is collected to be utilised in MPPT, which will be discussed in chapter 5 and chapter 6.

4.2 Field data

Wind, humidity, irradiance level and ambient temperature are the main factors that should be considered when introducing a comprehensive learning data for

the MPPT system. The field data was collected from different environmental conditions in different seasons. Yemen has three main regions with different climates, the first region is the mountain areas, the second is the desert areas, and the third is the coastal areas. All of these areas were considered for data collection. Sanaa and Shuayb are high altitude areas with low ambient temperature, Marib is a desert area with high ambient temperature in summer and Aden is a coastal area with high humidity.

Two thirty-six single crystal and polycrystalline photovoltaic (PV) solar panels were used to obtain the actual field data. The characteristics of these two panels under standard test conditions are shown in Table 4.1.These two types are the most widely used PV solar panels [8]. Two electrical ammeters, two temperature sensors, solar irradiance sensor and humidity sensor are used to measure the output electrical characteristics of PV panels, environmental parameters which affect these PV panels and surface cell temperatures.

Table 4.1: Characteristics of solar panel under standard test conditions

Single crystal panel		**Polycrystalline panel**	
V_{OC}	22 V	V_{OC}	21.2 V
I_{SC}	5.5 A	I_{SC}	3.25 A
I_{max}	4.91 A	I_{max}	3.02 A
V_{max}	17.4 V	V_{max}	16.9 V
P_{max}	85.5 W	P_{max}	51 W

4.2.1 Assumptions of collecting data

The developed system is designed to simulate the results based on the field data described. Table 4.2 describes the acquisition choice for the data. The first three rows in Table 4.2 include normal situations which concern a high proportional relationship between the surface temperature of PV panels with ambient temperature and irradiance level. The next four cases in Table 4.2 consider the effect of the wind and altitude on ambient temperature and the PV

cell temperature. The last two cases in Table 4.2 related to the high humidity area which is associated by low and medium irradiance level and these cases are usually found in coastal areas. These situation are selected to provide the majority of circumstances that can affect the external influences, as a result I_{SC}, V_{OC} and MPP parameters of PV panel.

Table 4.2: Data acquisition choice

G	T_a	T_S	influences	Regions
High	High	High	No	Desert
Medium	Medium	Medium	No	General
Low	Low	Low	No	General
High	High	Miduim	Wind	General
High	Medium	Medium	Wind and altitude	Mountain
High	Medium	Low	Wind and altitude	Mountain
Medium	Low	Low	Wind and altitude	Mountain
Low	Medium	Miduim	High humidity	Coast
Medium	Medium	High	High humidity	Coast
T_S	Cell temperature in ^{O}C			
T_a	Ambient temperature in ^{O}C			
G	Irradiance level (mW/cm^2)			

4.2.2 Core data extracting

The voltage and current of PV panels is measured at different resistance values. This process is done quickly to obtain all points on I-V curves in the same environmental conditions. The actual V_{max} and P_{max} are extracted from I-V curves and voltage power P-V curves using polynomial curve fitting in the Matlab toolbox. Figures 4.1 and 4.2 illustrate the method of extracting the maximum power point voltage and power from P-V curves. If either I_{SC} or V_{OC} change, I-V and P-V curves will modify and as a result the location of MPP will be changed. Change in I_{SC} takes place if the irradiance level changes. V_{OC} is affected by any change in irradiance level or photovoltaic cell temperatures. In addition, the ambient temperature (T_a) and the surface temperature (T_S)

are both obtained during data collection.

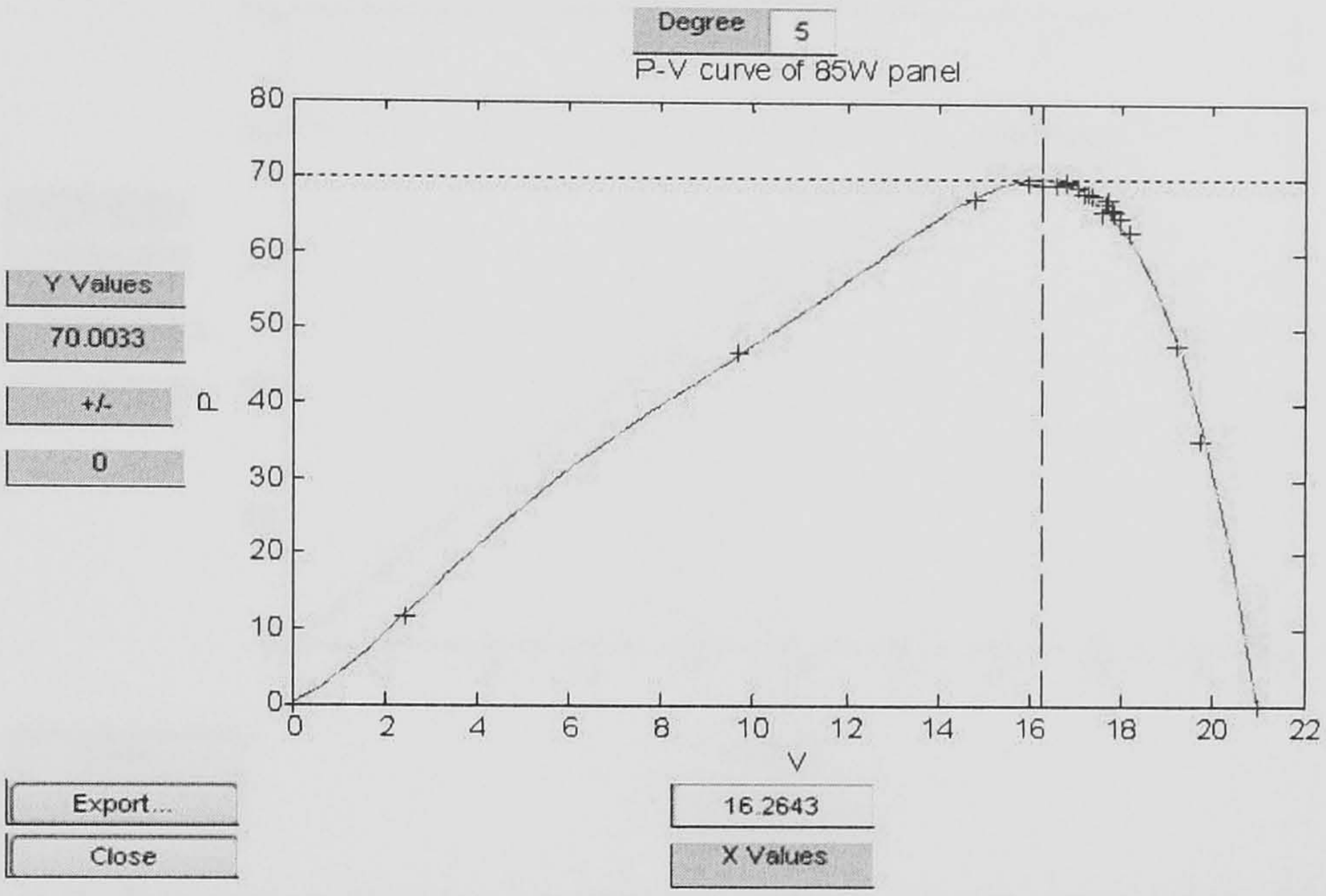

Figure 4.1: Extracting maximum power point from the I-V curve of the 85W panel

Table 4.3 and Table 4.4 represent the core data for the two tested panels. This data was extracted data collected in different selected times between June 2005 and February 2007. The data was collected in high ambient temperature season during June and July 2005 in hot climate regions (Aden and Marib). However, in high irradiance level and low ambient temperature region (Shuayb) the data was collected three times in December and January (winter) and in July (summer) during years 2005 and 2006. In Sanaa the data was collected in several times within 2 years because of variety of environmental conditions in Sanaa during the year. Data was evaluated during this interval and more data has been added later to fill some detected gaps in previous data according to assumptions listed in Table 4.2 and after evaluating the performance of ANFIS models at different irradiance levels and PV cell temperatures. The data was collected in about 35 selected days in different regions and different environmental conditions in the mentioned interval. The data will be utilised

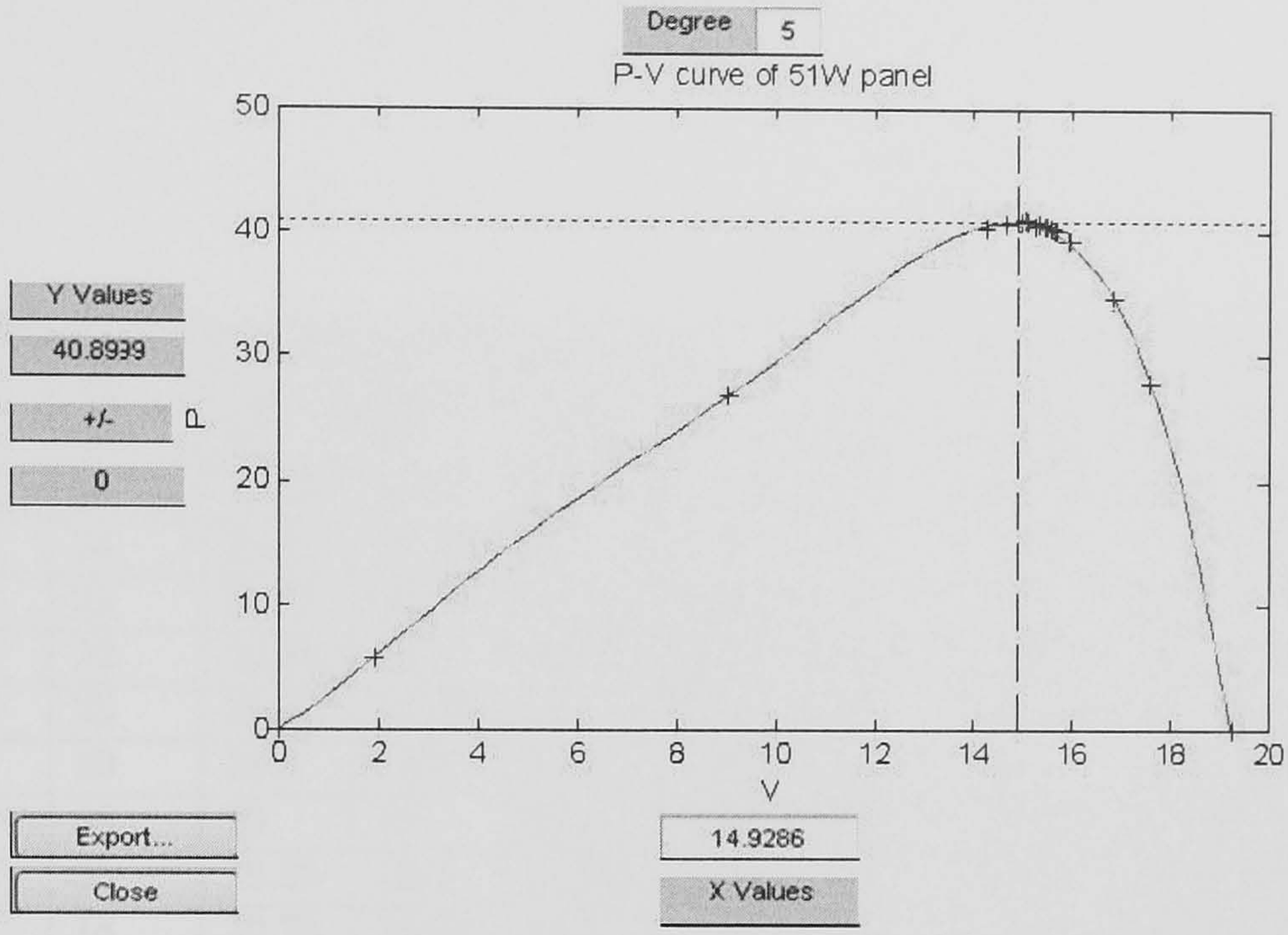

Figure 4.2: Extracting maximum power point from the I-V curve of the 51W panel

in predicted MPP using ANFIS models in chapter 5 and it will be used in the FLCs design.

4.3 Effect of deviating from maximum power point voltage

As explained in section 2.1 the load drives the PV panels to operate on strict point on I-V curves. When the PV panels operate faraway from V_{max}, the generated power decreases. The voltage deflection (Vd) and the percentage drop in operating power against MPP (%Pd) can be calculated from Equation 4.1 and Equation 4.2:

$$V_d = V_{op} - V_{max} \tag{4.1}$$

$$\%P_d = \frac{P_{max} - P_{op}}{P_{max}} \tag{4.2}$$

Where V_{op} and P_{op} represent the operating voltage and power on I-V curves.

4.3 Effect of deviating from maximum power point voltage

Table 4.3: Core data of 85W panel from different environmental conditions

I_{SC}	T_S	V_{OC}	V_{max}	P_{max}	I_{SC}	T_S	V_{OC}	V_{max}	P_{max}
0.26	22	18	12	1.92	4.22	52	19.31	14.47	53.84
0.49	24	19.44	15.4	5	4.25	37	20.14	15.5	58
0.57	25	19.27	15.16	6.3	4.3	54	18.95	14.25	56.5
0.67	22	20.05	16.9	7.77	4.45	55	19.2	14.35	55.7
0.78	22	20.02	16.4	9.85	4.45	52	19.65	15.1	60
0.89	25	19.95	16.29	11	4.45	31	20.75	16	64.1
1	40	18.8	14.8	12.5	4.62	43	19.7	14.87	60.5
1.1	36	19	15	13.2	4.65	27	20.95	16.28	67
1.14	35	19.05	15.1	13.56	4.73	45	20.18	15.4	64.23
1.25	18	20.75	16.85	17.8	4.78	57	19.1	14.15	62.1
1.3	24	20.15	16.6	17.52	4.8	58	18.82	13.93	58.9
1.56	26	19.83	16.7	21.7	4.85	33	20.98	16.35	70.1
1.65	40	19.3	16	21.9	4.88	57	18.86	14.11	61.5
1.82	21	20.81	16.83	26.28	4.88	40	20.16	15.2	65.65
2.08	25	20.5	16.5	29	4.95	54	19.45	14.72	64.23
2.23	41	19.55	15.65	30.4	5.13	39	19.92	14.88	64.6
2.3	24	20.96	17	34	5.2	34	20.9	16.11	75.2
2.35	30	19.72	15.8	32.6	5.3	31	20.9	15.95	76.3
2.45	28	20.35	16.22	35	5.39	45	19.72	14.85	69
2.78	42	19.76	15.7	38.1	5.44	53	19.44	14.65	71.5
2.95	27	21	16.7	44.2	5.5	34	20.7	15.82	77.65
3.2	45	19.49	15.2	42.87	5.5	25	22	17.4	85.5
3.25	40	20.33	15.85	46.2	5.56	51	19.62	14.76	72.6
3.53	40	20	15.53	48	5.9	33	21	16	86.4
3.73	49	19.54	15.32	50.8	5.92	29	21	15.95	85
3.75	21	21.83	16.9	56.5	6.85	34	20.95	16.24	100.84
3.8	47	19.6	15.35	51.6					
4.2	35	20.3	15.66	58.6					

4.3 Effect of deviating from maximum power point voltage

Table 4.4: Core data of 51W panel from different environmental conditions

I_{SC}	T_S	V_{OC}	V_{max}	P_{max}	I_{SC}	T_S	V_{OC}	V_{max}	P_{max}
0.25	24	18.95	17.15	3.6	2.7	31	19.85	15.53	39.2
0.38	19.05	19.05	16.07	5.77	2.75	33	19.87	15.45	39.4
0.42	22	19.65	16.5	6.6	2.8	39	19.12	14.77	38.36
0.42	24	19.3	16.2	6.3	2.84	57	17.8	13.35	34.52
0.5	30	18.95	17.6	7	2.84	40	19.18	14.87	38.75
0.61	25	19.3	16	9.44	2.86	57	17.76	13.36	34.52
0.76	40	18.39	15	10.6	2.86	55	18.1	13.64	34.2
0.95	40	18.46	14.85	12.96	2.87	39	19.1	14.76	39
1.15	18	20.15	16.36	18.48	2.88	53	18	13.55	35.15
1.18	25	19.75	16.1	18.2	2.93	51	18.25	13.8	36.66
1.27	26	19.6	16.14	19.12	2.98	43	19.24	14.93	40.86
1.42	40	18.7	15	19.8	3.05	45	19.09	14.62	41.24
1.52	21	20.1	16.28	23.37	3.05	46	18.9	14.6	40.4
1.55	42	18.6	14.66	20.75	3.1	33	20.03	15.7	44.44
1.7	32	19.53	15.8	25	3.12	54	18.15	13.6	38.46
1.78	43	18.74	14.8	24.1	3.15	31	20.05	15.59	45.1
1.9	33	19.44	15.5	27.2	3.25	56	18.2	13.62	40.29
1.9	35	18.96	14.9	26.5	3.3	34	19.81	15.36	47.2
2.07	35	19.05	15	28.5	3.35	34	19.92	15.47	47.4
2.08	38	19.15	15.15	29.36	3.35	28	20.13	15.55	48.6
2.16	21	20.6	16.4	33.75	3.4	35	19.82	15.22	48.22
2.35	37	19.18	14.94	33.16	3.95	34	20	15.6	56.3
2.4	51	18.34	14	30.6	4.19	34	19.95	15.24	60.7
2.46	38	19.17	14.85	34.3					
2.63	54	17.9	13.52	32.32					
2.67	53	18.14	13.8	32.9					

4.3 Effect of deviating from maximum power point voltage

Figure 4.3 shows the relationship between Vd and %Pd in Equations 4.1 and Equation 4.2. Figures 4.3.a and 4.3.b show the power drop due to +1V and -1V

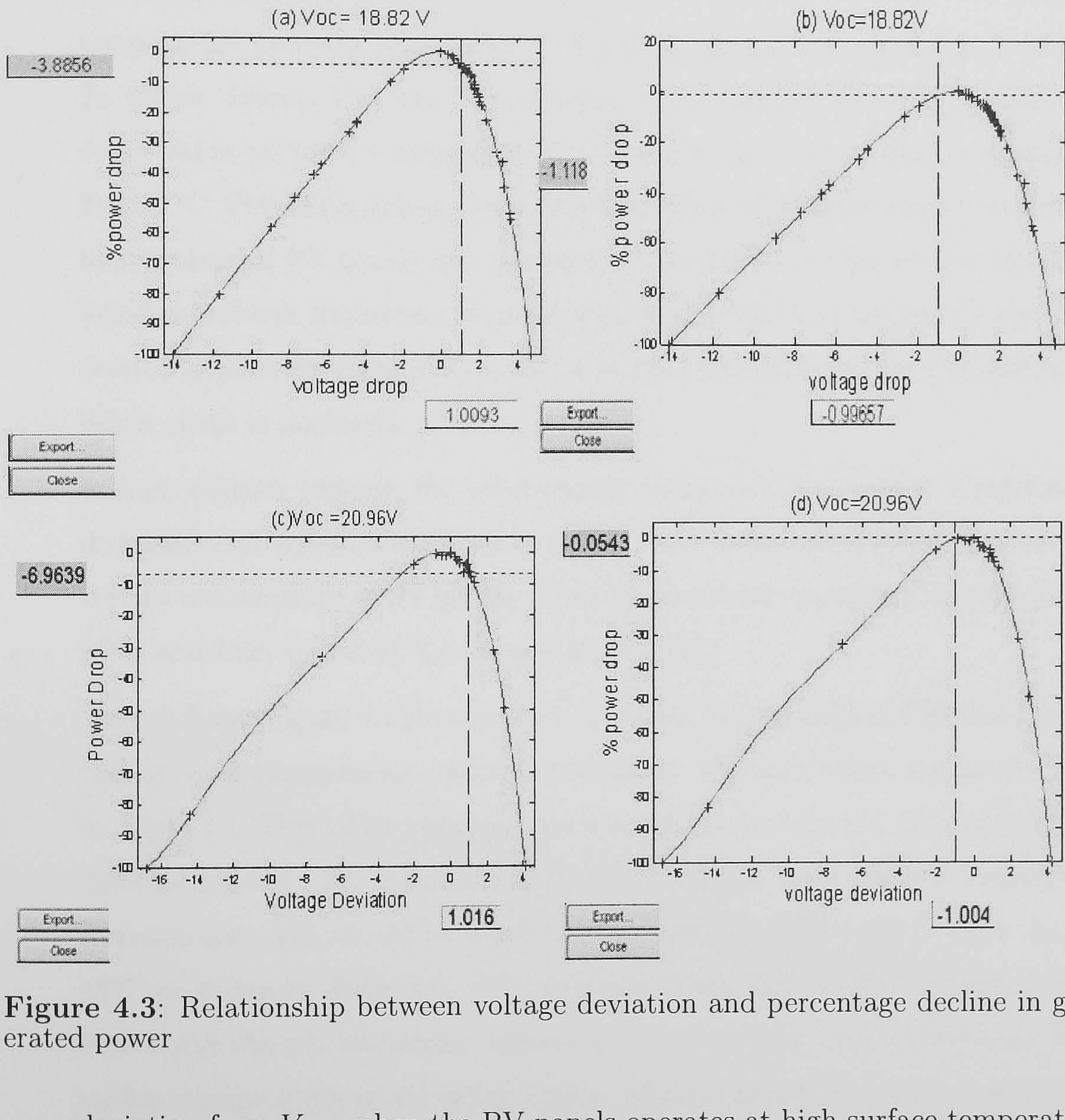

Figure 4.3: Relationship between voltage deviation and percentage decline in generated power

deviation from V_{max} when the PV panels operates at high surface temperature (T_S=55^{o}C and V_{OC} =18.82V). Also, Figures 4.3.c and 4.3.d show the drop in power due to +1V and -1V deviation from V_{max} when the PV panel operates at low surface temperature (T_S= 25^{o}C and V_{OC} = 20.96 Volt). In addition, Figure 4.3 shows how the decline in power due to positive deviation is greater

than that by negative deviation.

4.4 Effect of wind on T_S and V_{OC}

At certain irradiance, the linear relationship between cell temperature, ambient temperature and irradiance level in Equation 2.9 can be utilised to calculate T_S values. Hence, V_{OC} can be calculated approximately from the T_S value as described in section 2.1 using the 2.3 mV drop in V_{OC} that caused by increasing T_S by 1°C. Field data demonstrates the high effect of wind movement on surface temperature of PV panels and consequently on junction temperature and V_{OC}. Wind movement improves the convection factor which decreases T_S and as a result increases the value of V_{OC}. Accordingly, the generated power at maximum power point is improved.

In high altitude regions, the wind usually increases, the ambient temperature decreases and irradiance becomes higher. The wind has strong effect on the surface temperature of PV panels. This improvement appears in the low values of T_S and high values of V_{OC} in mountain areas.

Table 4.5 and Figure 4.4 show how T_S, V_{OC} and P_{max} change in different climate regions with approximate constant irradiance. The wind effect can be observed in Table 4.5. This effect appears from the differences between ΔT_S and ΔT_a in different regions. For example, when the irradiance level remains constant in equation 2.9, ΔT_S should be equal to ΔT_a, however $\Delta T_S = 26°C$ when $\Delta T_a = 18°C$ as shown in Table 4.5. ΔT_S is greater than ΔT_a by 8°C between Marib desert and Shuayb Mountain. Moreover, the wind effect can be observed from surface temperature in the Aden region, which is lower than that in Marib, in spite the fact that the ambient temperature in Aden was higher than that of Marib during data collecting.

Measuring T_S needs an external sensor which can have contact problems with PV cell surface and it also require a delay time to give a response. At constant

irradiance level, if 2.3mV drop in V_{OC} due to the 1^oC increases in T_S is applied, this relationship gives a true result compared with the actual data in Table 4.5. The following calculation confirms this relationship.

V_{OC} (Shuayb)= V_{OC} (Marib)+ Δ T_S (26)* 2.3mV *36 cells

$V_{OC} = 18.82V + 2.15V = 20.97V$

Also, this relationship is true when this relationship is applied between Marib and Aden. Therefore, the open circuit voltage can be used as an indicator for cell junction temperature when the solar radiation changes in small ranges. Measuring open circuit voltage is simple and gives a correct and fast response during changes in the cell junction temperature.

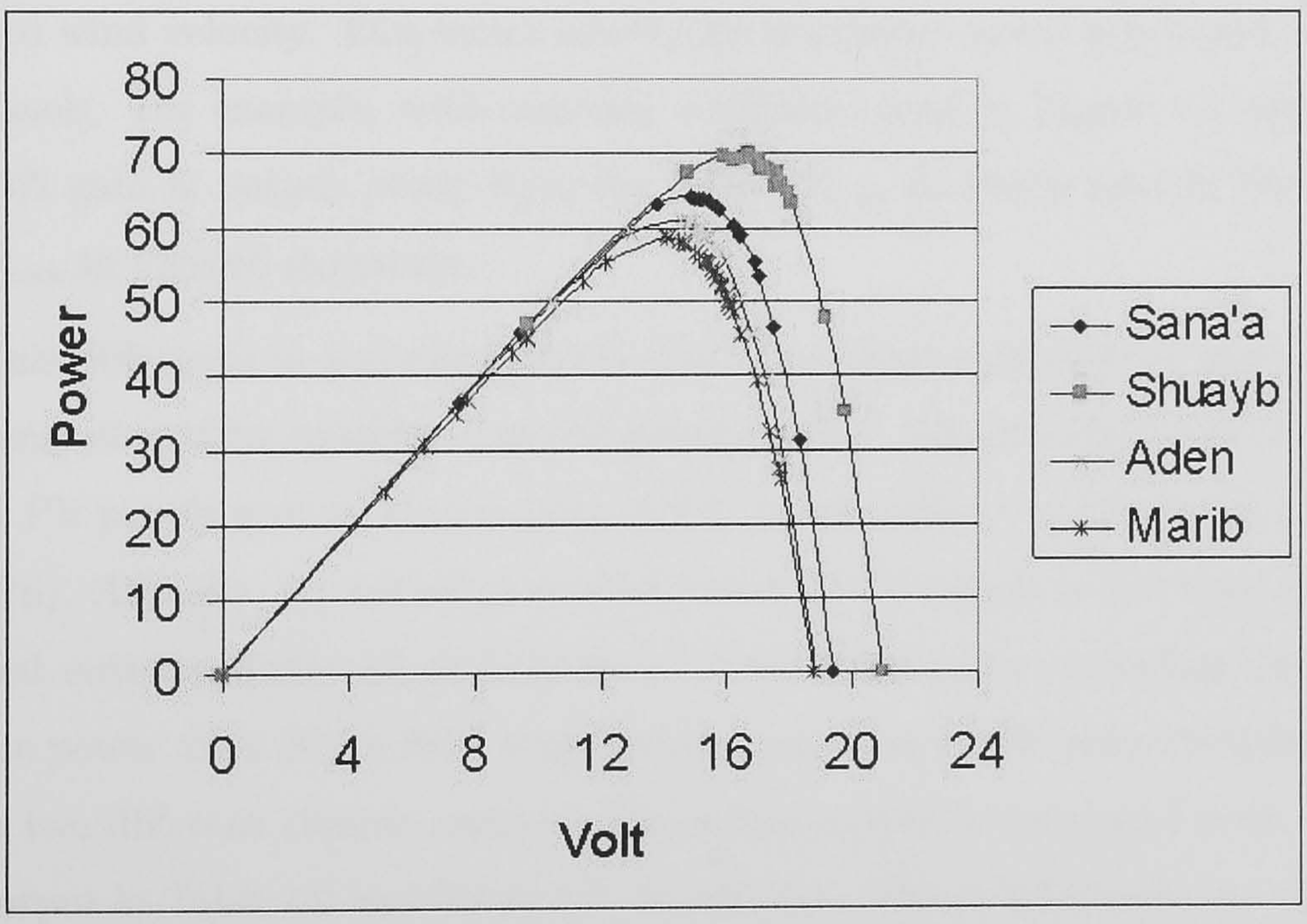

Figure 4.4: Effect of surface temperature on P_{max} and V_{OC} in different regions

Table 4.5: Temperature effect on P_{max} and V_{OC} of PV panels

Region	T_a (^{o}C)	T_S (^{o}C)	I_{SC} (A)	V_{OC} (V)	P_{max} (W)
Marib(1000m)	38	58	4.8	18.82	58.9
Shaiyb(3317m)	20	33	4.85	20.98	70.1
Aden(see level)	40	57	4.88	18.86	61.5
Sana'a(2300m)	32	52	4.95	19.4	64.23

4.5 Maximum power generated in different climate regions

The cooling factor in different regions changes due to ambient temperature and wind velocity. This factor affects the maximum power generated from PV panels. For example, with constant irradiance level in Figure 4.4 there is an 18% gain in output power from the lowest P_{max} in Marib area to the highest P_{max} in Shuayb mountain.

This difference in generated power due to ambient temperature and wind velocity should be considered in PV system design. The standard test conditions of PV panels give an ideal output of PV panels called a nominal output power (Pn). Actually, the actual generated power of PV panels is less than the nominal output. Table 4.6 and Table 4.7 demonstrate the percentage average of the power drop of the 85W single crystal panel and 51W polycrystalline panel in two different climate regions. The actual output is compared with nominal output in Table 4.6 and Table 4.7. In addition, Figure 4.5 shows how this drop in power increases due to increasing in the surface temperature of the 85W single crystal PV panel and 51W polycrystalline PV panel in two different climate regions.

This drop in output power is considered when the PV system is designed as a constant percentage [26] [27]. However, the average drop in power generated shown in Tables 4.6 and 4.7 of two types of PV panels is more than 16% in high

Table 4.6: Maximum power compared with nominal power of 85W single crystal PV panel

85W PV panels at low ambient temperature and wind effect						
I_{SC}	T_S	V_{OC}	V_{max}	P_{max}	**Pn**	%(P_{max}-**Pn**) /**Pn**
1.82	21	20.81	16.83	26.28	28.1	-6.57
2.3	24	20.96	17	34	35.55	-4.35
2.95	27	21	16.7	44.2	45.59	-3.05
4.45	31	20.75	16	64.1	68.77	-6.79
5.3	31	20.9	15.95	76.3	81.90	-6.85
5.5	34	20.7	15.82	77.65	85	-8.65
5.92	29	21	15.95	85	91.49	-7.09
Average of percentage power drop						**-6.2**
85W PV panels at high ambient temperature						
I_{SC}	T_S	V_{OC}	V_{max}	P_{max}	**Pn**	%(P_{max}-**Pn**) /**Pn**
1.1	36	19	15	13.2	17	-22.35
1.14	35	19.05	15.1	13.56	17.6	-23.03
2.23	41	19.55	15.65	30.4	34.46	-11.79
3.2	45	19.49	15.2	42.87	49.45	-13.3
3.73	49	19.54	15.32	50.8	57.65	-11.87
3.8	47	19.6	15.35	51.6	58.73	-12.14
4.22	52	19.31	14.47	53.84	65.22	-17.45
4.78	57	19.1	14.15	62.1	73.87	-15.94
4.88	57	18.86	14.11	61.5	75.42	-18.45
Average of percentage power drop						**-16.23**

4.5 Maximum power generated in different climate regions

Table 4.7: Maximum power compared with nominal power of 51W Polycrystalline PV panel

51W PV panels at low ambient temperature and wind effect						
I_{SC}	T_S	V_{OC}	V_{max}	P_{max}	**Pn**	%(P_{max}-**Pn**) /**Pn**
1.15	18	20.15	16.36	18.48	18.05	2.40
1.27	26	19.6	16.14	19.12	19.93	-4.060
1.52	21	20.1	16.28	23.37	23.85	-2.02
2.16	21	20.6	16.4	33.75	33.89	-0.43
2.7	31	19.85	15.53	39.2	42.37	-7.48
3.15	31	20.05	15.59	45.1	49.43	-8.76
3.3	34	19.81	15.36	47.2	51.78	-8.85
3.35	28	20.13	15.55	48.6	52.57	-7.55
3.4	35	19.82	15.22	48.22	53.35	-9.62
Average of percentage power drop						**-5.15**
51W PV panels at high ambient temperature						
I_{SC}	T_S	V_{OC}	V_{max}	P_{max}	**Pn**	%(P_{max}-**Pn**) /**Pn**
0.76	40	18.39	15	10.6	11.92	-11.12
0.95	40	18.46	14.85	12.96	14.9	-13.065
1.55	42	18.6	14.66	20.75	24.32	-14.69
1.78	43	18.74	14.8	24.1	27.93	-13.72
2.4	51	18.34	14	30.6	37.66	-18.75
2.63	54	17.9	13.52	32.32	41.27	-21.69
2.67	53	18.14	13.8	32.9	41.9	-21.48
2.84	57	17.8	13.35	34.52	44.57	-22.54
Average of percentage power drop						**-17.8**

4.5 Maximum power generated in different climate regions

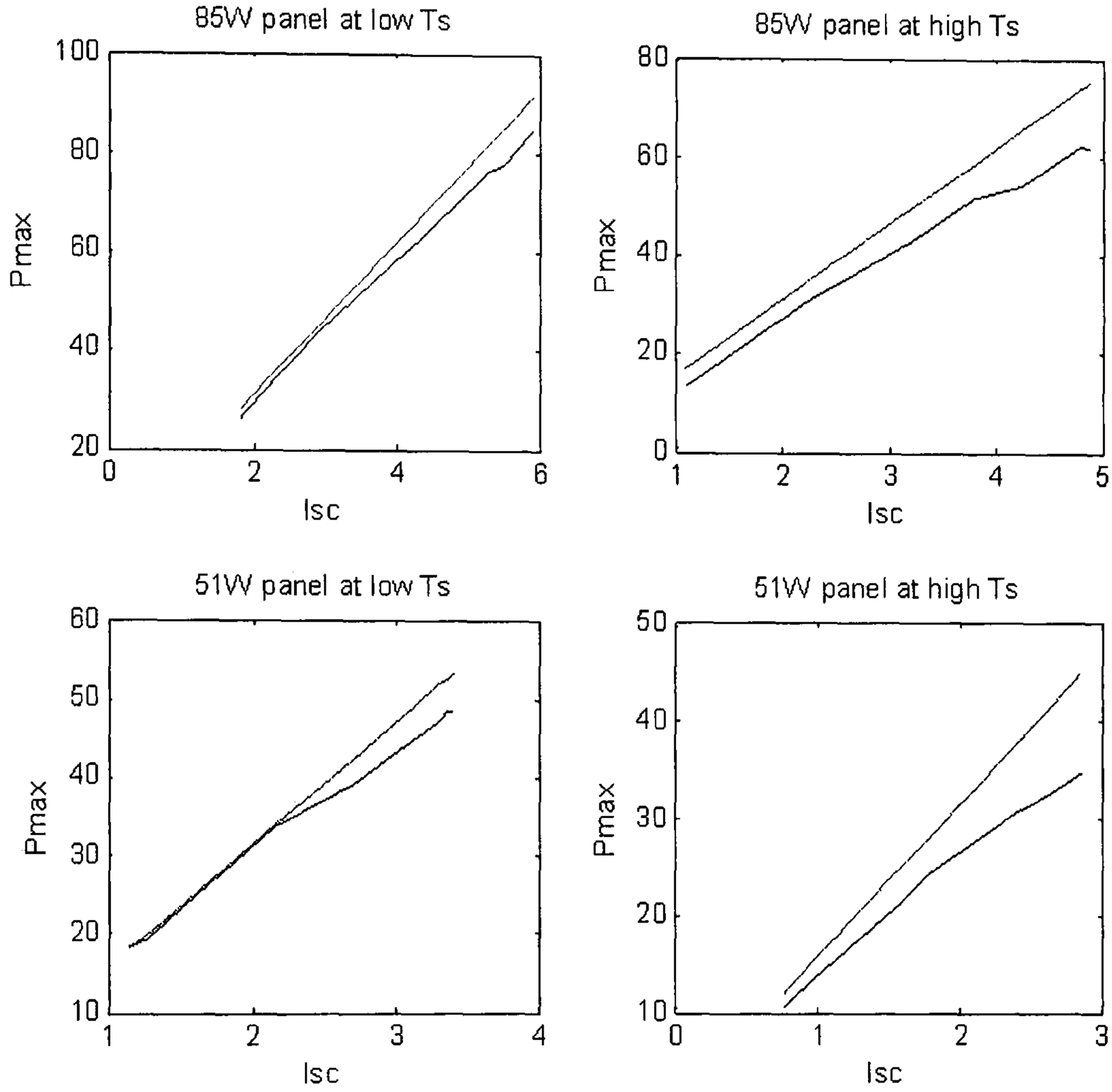

Figure 4.5: Temperature effect on maximum power of 51W PV panels

ambient temperature regions and about 6% in low ambient temperature regions. This drop in power becomes very high in massive ambient temperature areas such as desert areas. The ambient temperature may reach to 50^{O}C in several regions. In these regions a high increasing in cell junction temperature can cause a high drop in the generated power from PV panels, which can be more than the estimated value. Moreover, if the PV system is installed in high solar radiation areas that have low ambient temperature, the estimated energy drop of PV system is greater than the actual drop, which leads to additional cost in system capacity.

4.5 Maximum power generated in different climate regions

The location in which the PV system is installed is very important. This aspect is shown in Figure 4.6, which shows the gain in maximum power generated at midday in different regions. Generally, the differences in altitude affect the irradiance level and cooling factor which finally affects the power generated from PV panels. In high mountain areas, the solar energy increases due to the low solar energy dissipated in atmosphere[40]. In addition the wind decreases the cell temperature of PV panels. In summer, the gain in maximum output power of PV panels reach to 63% between Shuayb and Aden as shown in Figure 4.6. Also, the gain in maximum output power of panels reach to 40% between Shuayb and Sanaa, despite that Shuayb and Sanaa are in the same area. However Shuayb is 1000m higher than Sanaa in altitude. To maintain this acquisition in the generated power, PV panels have to operate at MPP. If the PV panel has more than 1Volt deviation from V_{max}, most generated power will be lost. Hence, operating at V_{max} is necessary to generate maximum power from PV system.

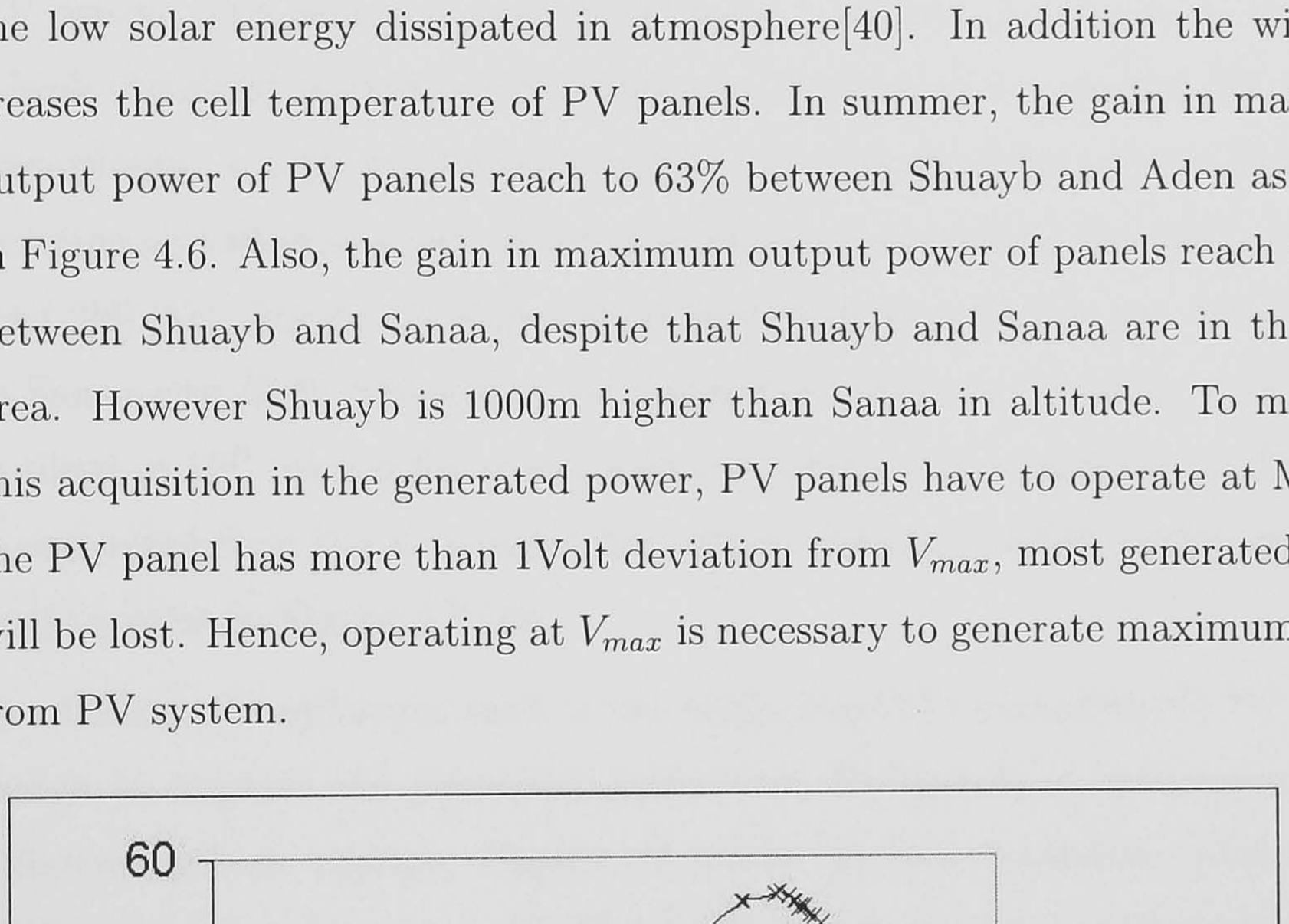

Figure 4.6: P-V curves of 51W PV panel at midday in different climate regions.

4.6 Power Gain of PV System with Sun tracker

The gain in solar energy that is acquired by using a sun tracker is very high, especially in sunny days. Two main advantages are achieved by using one or two axis tracker. The first one is a high gain in total generated power from PV panels. The second to provide sufficient irradiance for the loads that need a high threshold operating irradiance level such as direct coupled DC pumps. Accordingly, a high submitted irradiance level in tracking system during the morning and afternoon time helps on increase the operating time of the resistive load [26] [81]. Figure 4.7 shows the solar radiation incidence per meter square in Sanaa city 15.5^{O} latitude in the begging of December when the solar sensor is tilted at 15^{O} toward the south with sun tracker and without it. A 35% gain is computed from the area under the curves between tracking system and fixed angle system in Figure 4.7 [10].

In addition, the optimum south north angle should be considered in PV system design to improve the generated power from PV panels at optimum angle in different latitude regions. Figure 4.8 shows the solar radiation incidence per meter square in Sanaa city 15.5^{O} latitude in the begging of December when the sun tracker is tilted at optimum angle 31^{O} towards the south with the sun tracker. In addition, Figure 4.8 shows the submitted irradiance when the sensor is fixed at optimum angle toward the south without the sun tracker [9]. A 28% gain is computed from the areas under the curves between tracking system and optimum angle system [10] [82].

4.7 Summary

This chapter presented the core data of two types of PV panels which extracted from a lot of data that is collected in four different regions in Yemen in different selected times in two years. In addition, the maximum generated power from PV system in different environmental conditions is investigated in this chapter.

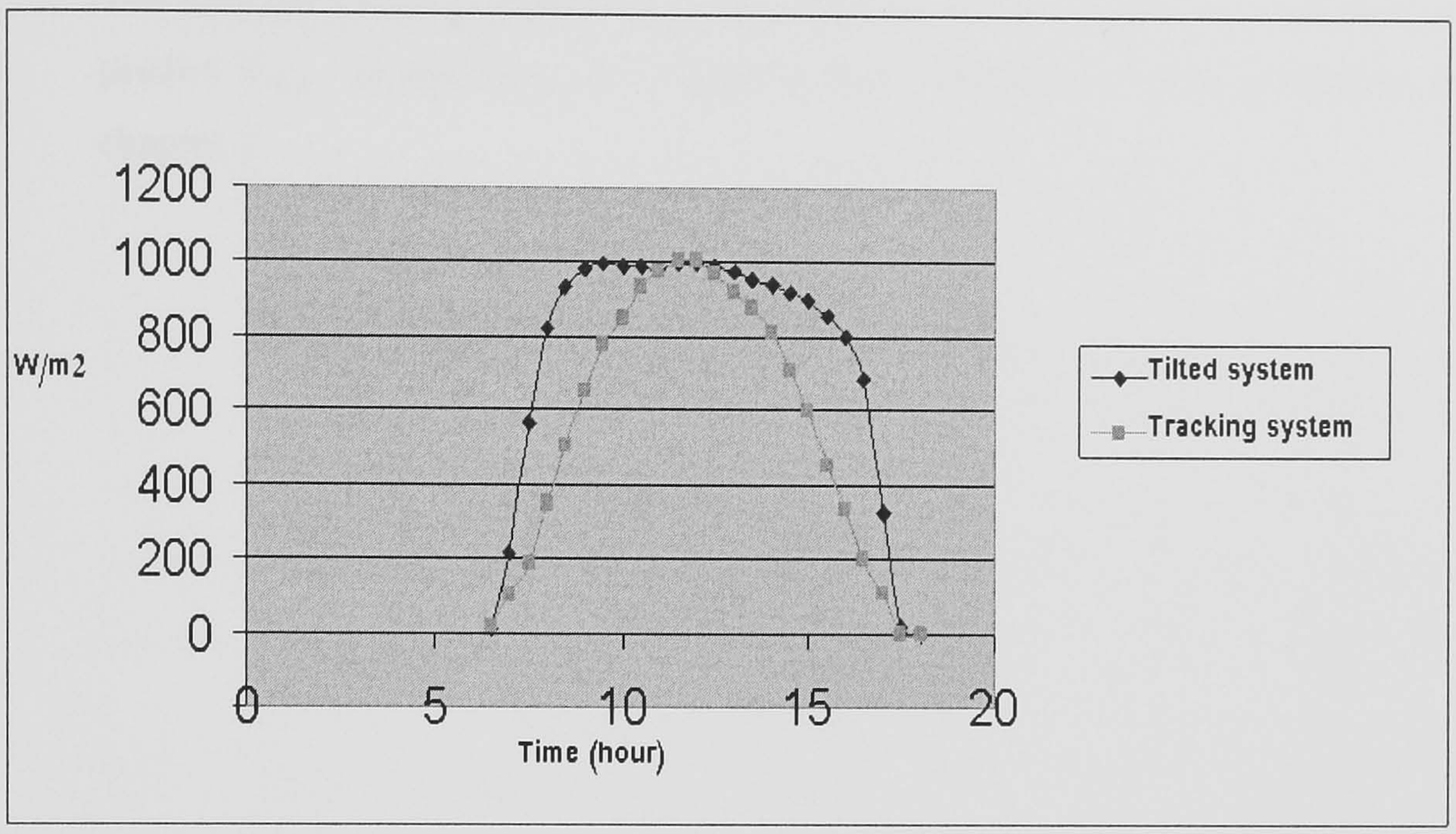

Figure 4.7: Effect of East West 2 axis sun tracker in the total solar energy incident (at tilt 15 ^{O})

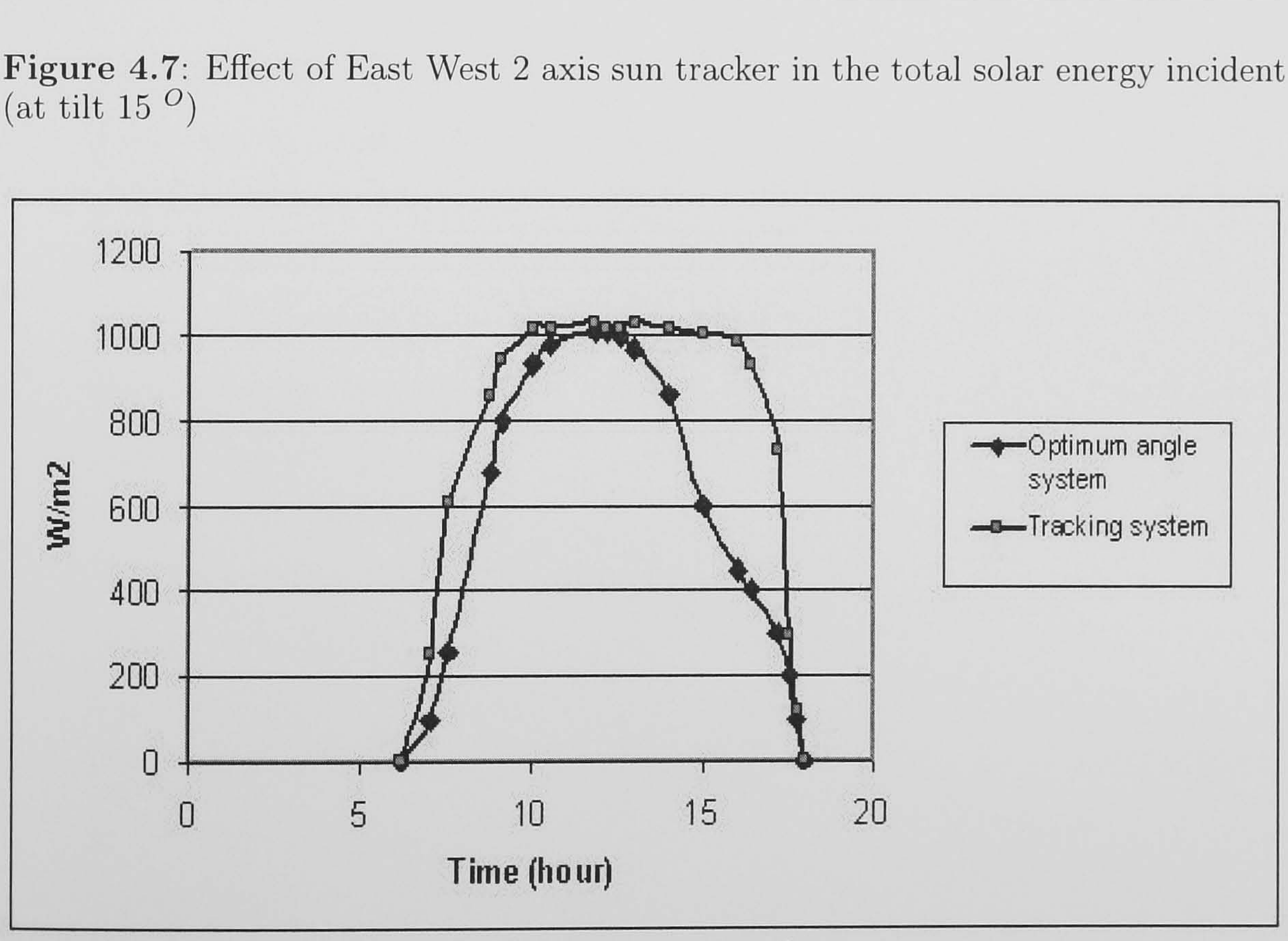

at optimum tilt 31^{O}

Figure 4.8: Effect of East West 2 axis sun tracker in the total solar energy incident (at optimum tilt 31^{O})

4.7 Summary

The core data that is presented in this chapter will be utilised in chapter 5 to predict V_{max}. In addition, the presented data will help in result discussion in chapter 7.

Chapter 5

ANFIS Model

In this chapter, several ANFIS models are assembled to predict the maximum power point voltage of PV panels. Furthermore, statistical analysis methods are utilised to identify the relationships between different parameters of PV panels. This statistical analysis helps us to understand the behaviour of PV panels in different environmental conditions, and therefore, helps with the ANFIS design.

5.1 Introduction

As discussed in chapter 2, the short circuit current of a solar cell depends exclusively and linearly on the irradiance level. In addition, the short circuit current measures solve the problem of the solar irradiance external sensor. Therefore, it is used as an input to ANFIS models instead of irradiance level. Furthermore, the open circuit voltage is used instead of cell junction temperature due to the difficulty of cell junction temperature measured and the simplicity of measuring the open circuit voltage. In addition, the open circuit voltage is used as a second input of solar panels instead of cell temperature due to the linear relationship between V_{OC} and cell junction temperature when irradiance roughly remains constant. Therefore, it is necessary to study the relationships between input and output parameters of PV system to understand the behaviours of PV panels in different environmental conditions. Correlation analysis and data clustering are utilised to find the degree of association between short circuit current and open circuit voltage with maximum power point parameters. In addition, it helps clarify the relationship between different PV parameters.

5.2 Correlation analysis of input data and MPP parameters

Many methods have been used to find the relationships between input and output variables of different control systems. Statistical techniques such as correlation analysis are the most commonly used [17]. Linear correlation analysis is the most direct and simple method that can be used to measure the association of different variables. To investigate the relationships between different parameters of PV panels in Tables 4.3 and 4.4, correlation coefficients (CCs) between these parameters are computed by applying a linear correlation calculation. Tables 5.1 and 5.2 show the correlation coefficients between different output parameters of two panels.

The CCs between I_{SC} and P_{max} of 85W and 51W PV panels are 0.993 and 0.987 respectively. Even though the PV panels are tested in different surface temperatures in four climatic regions, these two values imply high CCs between input I_{SC} which represent the irradiance level and P_{max}. The slight drop of linear relationship between I_{SC} and P_{max} values is due to the drop in V_{max} in high ambient temperature regions which finally reduces the maximum generated power from PV panels at high temperature. Electrically, to operate the PV panels at P_{max}, the panels have to operate at V_{max} and I_{max}.

It is easier and more efficient within maximum power point tracking systems to measure and adjust continuously the operating voltage of PV panels until they get in touch with the maximum power point voltage. Therefore, it is essential to investigate the correlation between the two selected inputs that affect the maximum power point voltage and power.

A poor CC between I_{SC} and V_{max} appears in Tables 5.1 and 5.2. Hence, it is difficult to find a linear relationship between I_{SC} and V_{max} as shown in Figures 5.1 and 5.2.

The CC between V_{OC} and V_{max} is 0.837 for 85W single crystal and 0.717 for 51W

5.2 Correlation analysis of input data and MPP parameters

Table 5.1: Correlation coefficients of the single crystal panel

Correlation coefficient between 85 W Panel parameters					
Character	I_{SC}	**Ts**	V_{OC}	V_{max}	P_{max}
I_{SC}	1.000				
Ts	0.534	1.000			
V_{OC}	0.290	-0.538	1.000		
V_{max}	-0.131	-0.638	0.837	1.000	
P_{max}	0.993	0.450	0.383	-0.046	1.000

Table 5.2: Correlation coefficients of the polycrystalline panel

Correlation coefficients between 51 W Panel parameters					
Character	I_{SC}	**Ts**	V_{OC}	V_{max}	P_{max}
I_{SC}	1.000				
Ts	0.531	1.000			
V_{oc}	0.065	-0.776	1.000		
V_{max}	-0.559	-0.934	0.717	1.000	
P_{max}	0.987	0.398	0.216	-0.436	1.000

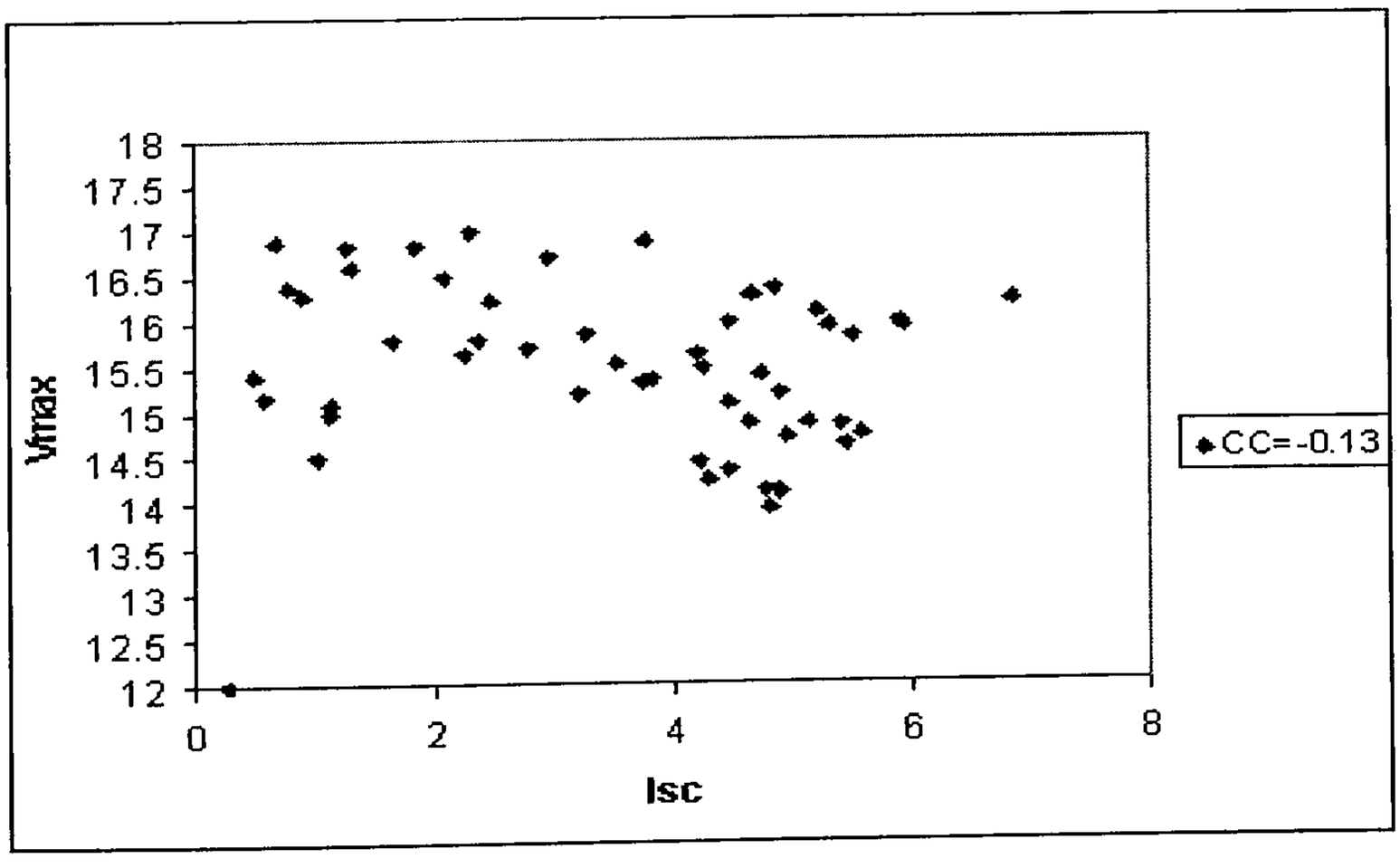

Figure 5.1: Plot of I_{SC} and V_{max} 85W Panel parameters

5.2 Correlation analysis of input data and MPP parameters

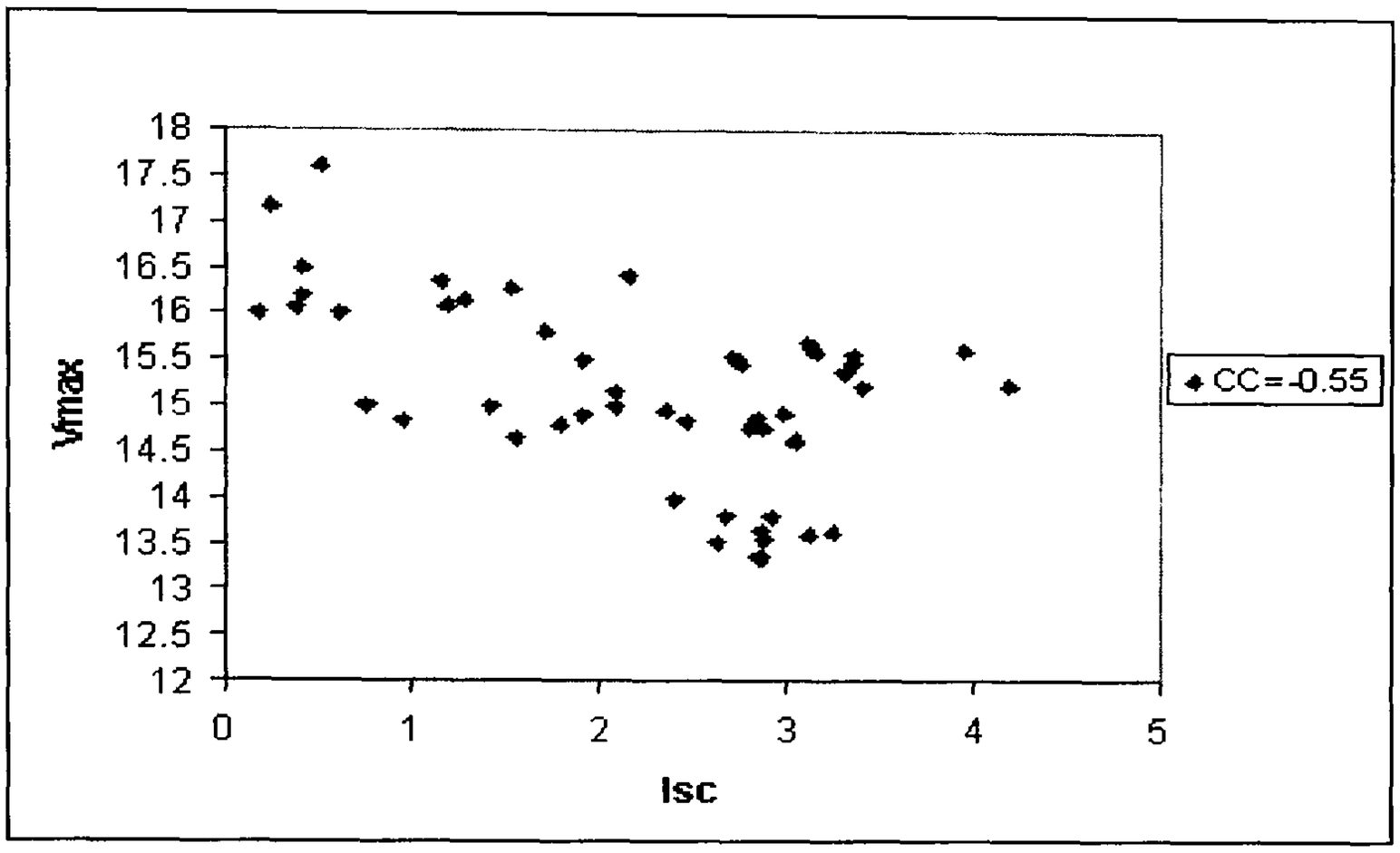

Figure 5.2: Plot of I_{SC} and V_{max} 51W Panel parameters

polycrystalline panel. Based on these low CCs that are also observed in Figures 5.3 and 5.4, V_{max} changes widely when V_{OC} remains constant. Therefore, the CCs are not sufficient to set up a linear relationship between the inputs and outputs of PV panels. Within a small range of I_{SC}, the effect of the logarithmic relationship between V_{OC} and irradiance level can be reduced. Therefore, the linear relationship between cell temperature and V_{OC} becomes more effective and as a result, the association between V_{OC} and V_{max} of PV panels will be improved.

Generally, when a mutual effect between inputs is reduced, the individual relationship between input and outputs becomes more understandable. Hence, the relationship between V_{OC} and V_{max} becomes more apparent when the effect of I_{SC} is reduced by dividing the data in small groups depending on I_{SC} values. With a small change in I_{SC} a CC between V_{OC} and V_{max} is improved. Improving the CCs between V_{OC} and V_{max} can be confirmed by classifying the input data of PV panels and recognising the increments in the CCs of different clusters. Studying the CC of different appropriate clusters is essential to initiate an outstanding control method for locating and tracking the maximum power

point of PV panels.

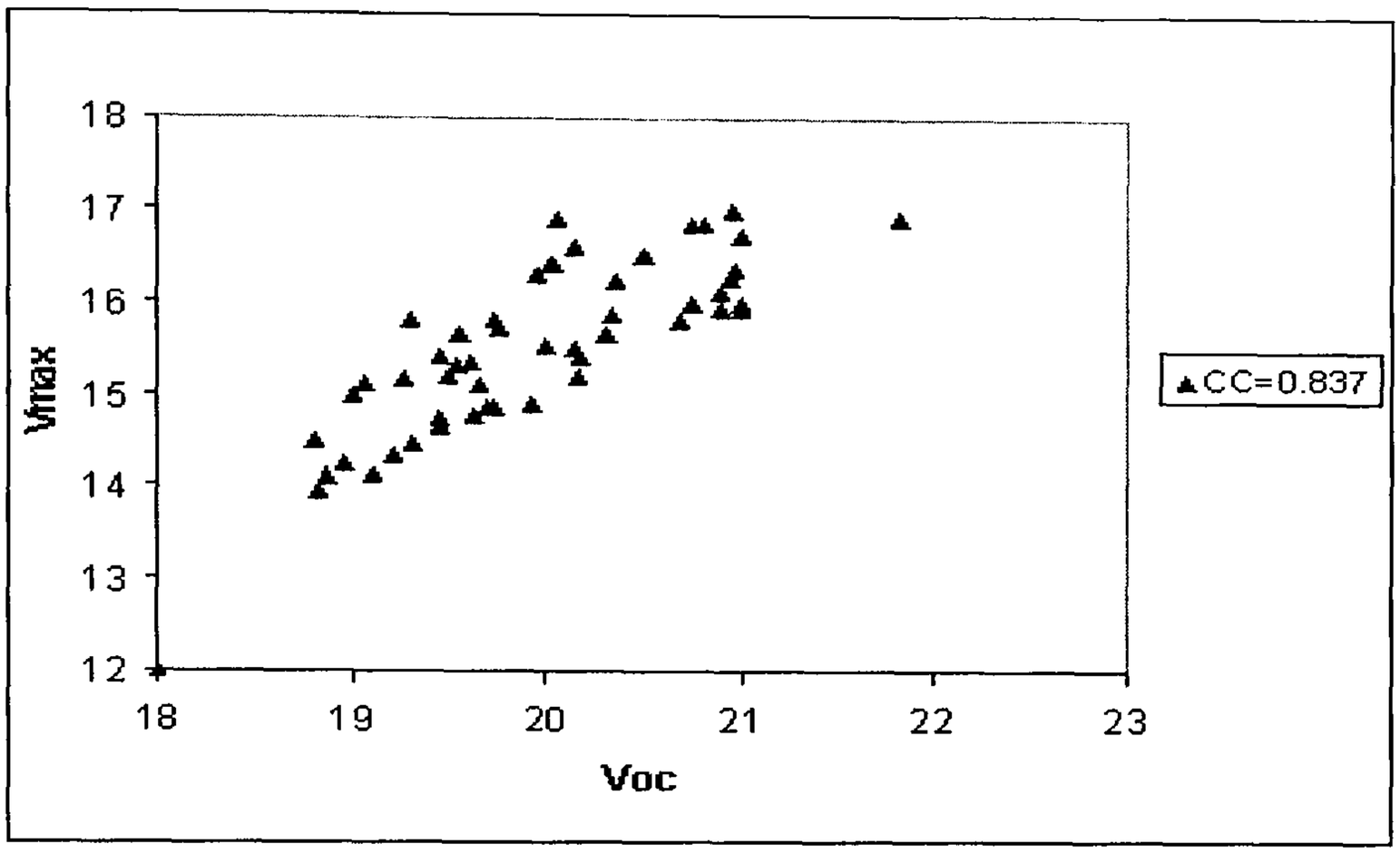

Figure 5.3: Plot of V_{OC} and V_{max} 85W Panel parameters

5.3 Input data clustering

"Clustering of numerical data forms the basis of many classification and system modelling algorithms. The purpose of data clustering is to identify natural groupings of data from a large data set to produce a concise representation of a system's behaviour. Cluster analysis also helps in creating balanced treatment and control groups for a designed study" Matlab help, Fuzzy clustering [58]. The K-means clustering function that was described in chapter 2 partitions the observations of data into K mutually exclusive clusters. However, with different range variations of I_{SC} and V_{OC}, it is necessary to normalise the input data for clustering analysis [24].

Clustering functions should deal with homogenous per unit data of I_{SC} and V_{OC}. Table A.1 in Appendixes shows how the input per unit data is clustered for two types of panels depending exclusively on short circuit current when either data is sorted by I_{SC} or V_{OC}.

5.3 Input data clustering

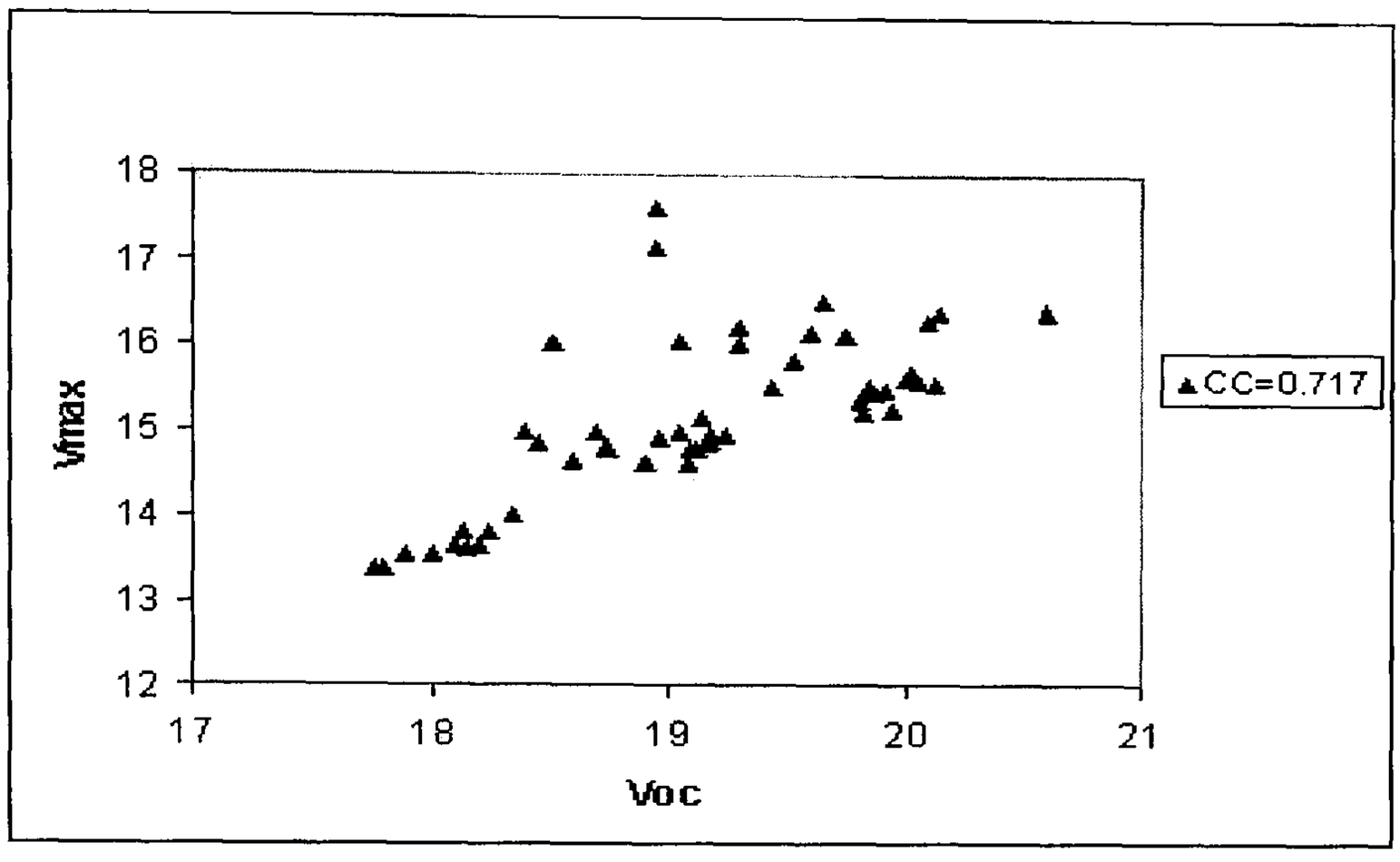

Figure 5.4: Plot of V_{OC} and V_{max} 51W Panel parameters

To understand how input data is distributed in different clusters, it is important to clarify how V_{OC} changes when I_{SC} changes in small ranges. With small changes in I_{SC} (irradiance level), V_{OC} is affected only by cell temperature. For that reason, V_{OC} changes at this irradiance level in a limited range. On the other hand, the limited changes in V_{OC} can be caused by the following two main reasons:

- The association between high irradiance level and high temperature which forces V_{OC} to change into two directions. The first is increasing due to high irradiance and the second is decreasing with high temperature.
- The temperature decreases with low irradiance, therefore, V_{OC} decreases due to the low irradiance and increases owing to the low temperature.

For these reasons, when the open circuit voltage changes in a small range, there are no limitations for short circuit current changes. Therefore, the result of K-means clustering function in Table A.1 shows how the data is clustered in two cases with respect to I_{SC}.

The Matlab program shown in Program B.1 in Appendix B is used to normalise

I_{SC} and V_{OC} data of two panels, and then, it applies the K-means function to group the data in a number of clusters that are set in the program. Finally, the program draws the separate cluster groups of both panels as shown in Figures 5.5 and 5.6 for four clusters, and Figures 5.7 and 5.8 for six clusters.

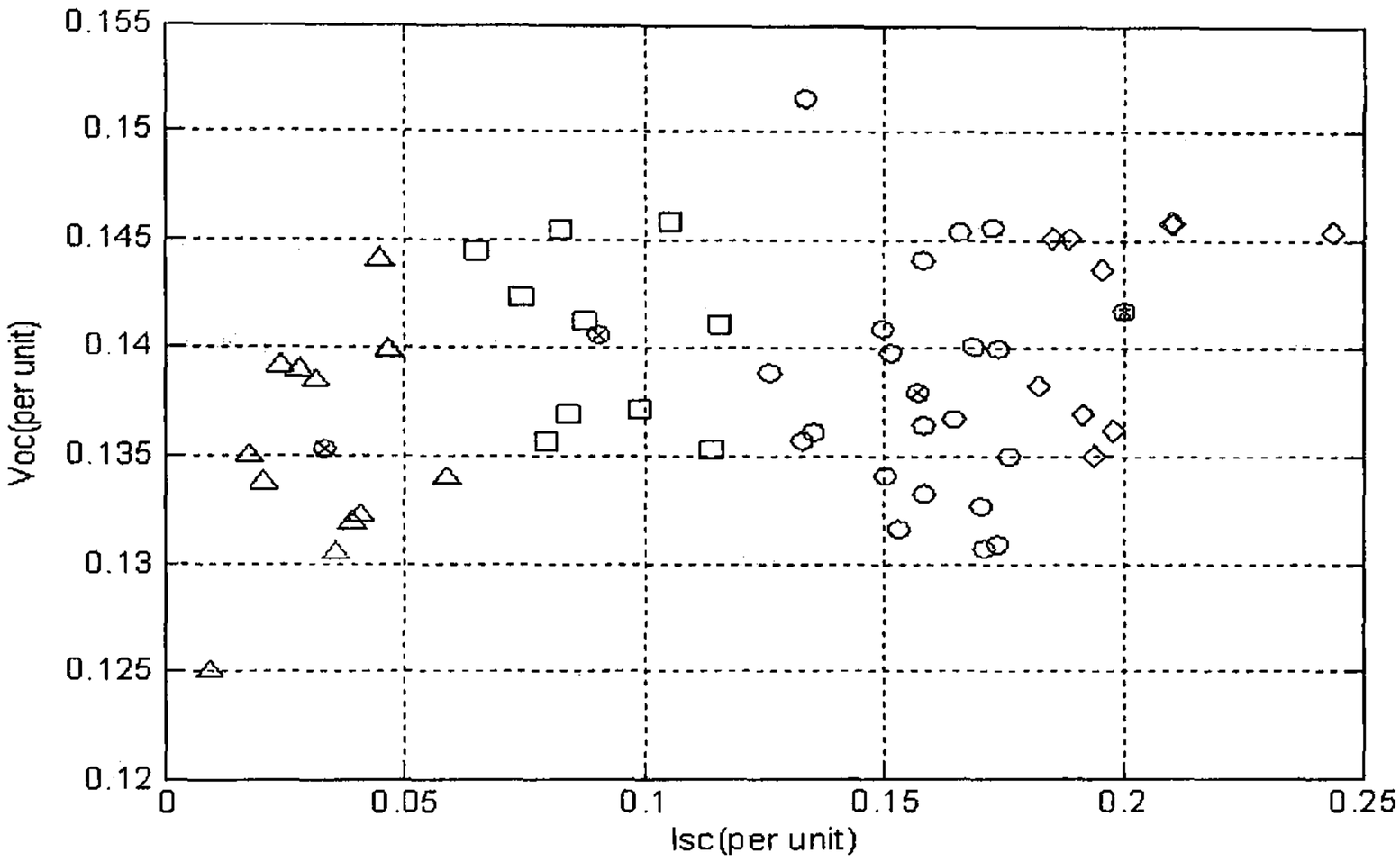

Figure 5.5: Clustering the 85W PV input data in four clusters

When the input data of two panels is clustered into different numbers of clusters, the input data is always clustered regarding I_{SC}. This fact appears when data is clustered in four groups as shown in Figures 5.5 and 5.6. Furthermore, clustering with I_{SC} is recurring when data is clustered in six clusters as shown in Figures 5.7 and 5.8.

In addition, clustering the input data by means of short circuit currents is tested by using CCs between V_{OC} and V_{max} in different clusters. Tables 5.3 and 5.4 show the CCs between V_{OC} and V_{max} in these clusters.

According to Tables 5.1 and 5.2, the CCs between V_{OC} and V_{max} are 0.837 for 85W PV panel and 0.717 for 51 W PV panel. These values are improved when the CCs between V_{OC} and V_{max} are computed in small cluster groups as shown

5.3 Input data clustering

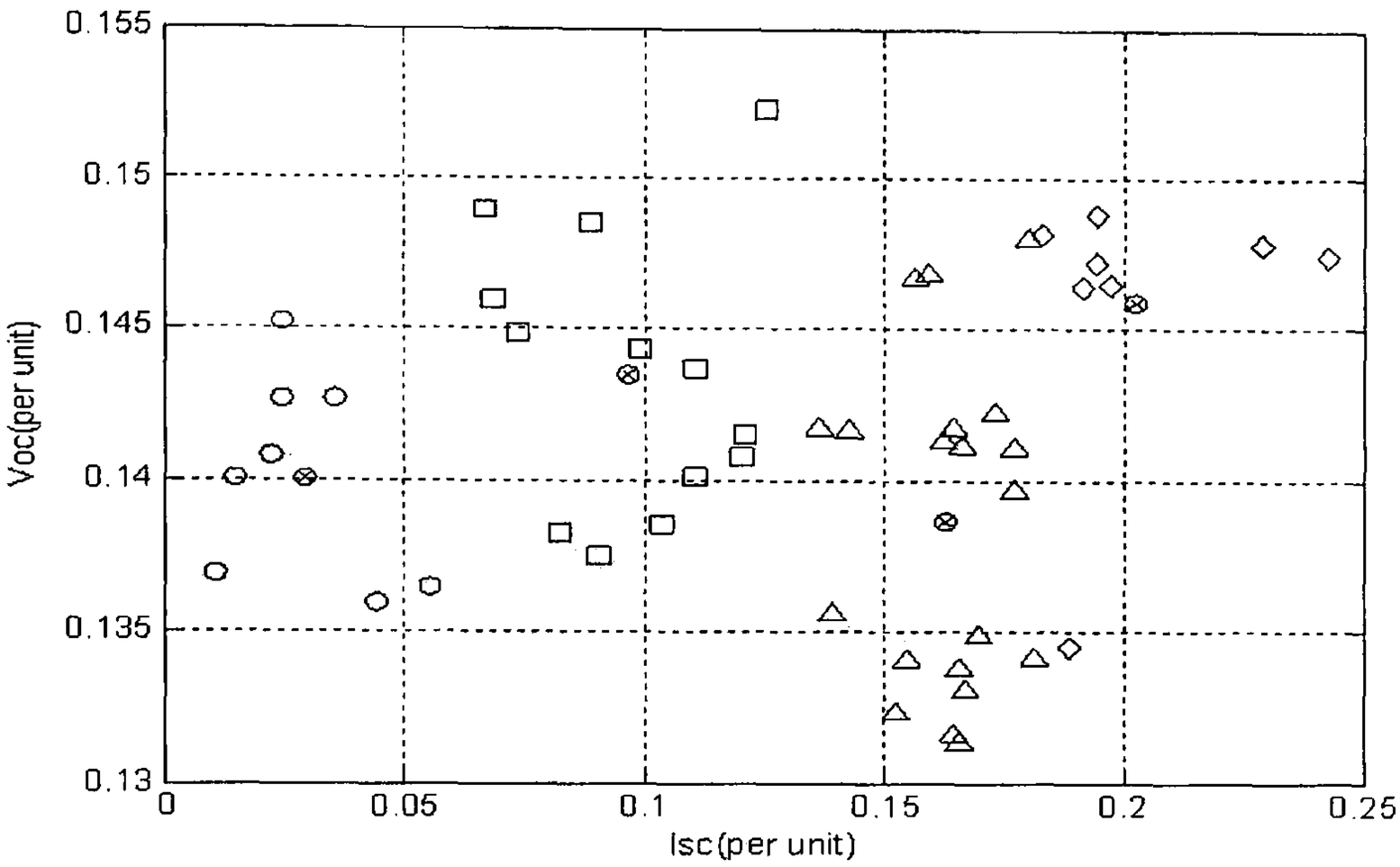

Figure 5.6: Clustering the 51W PV input data in four clusters

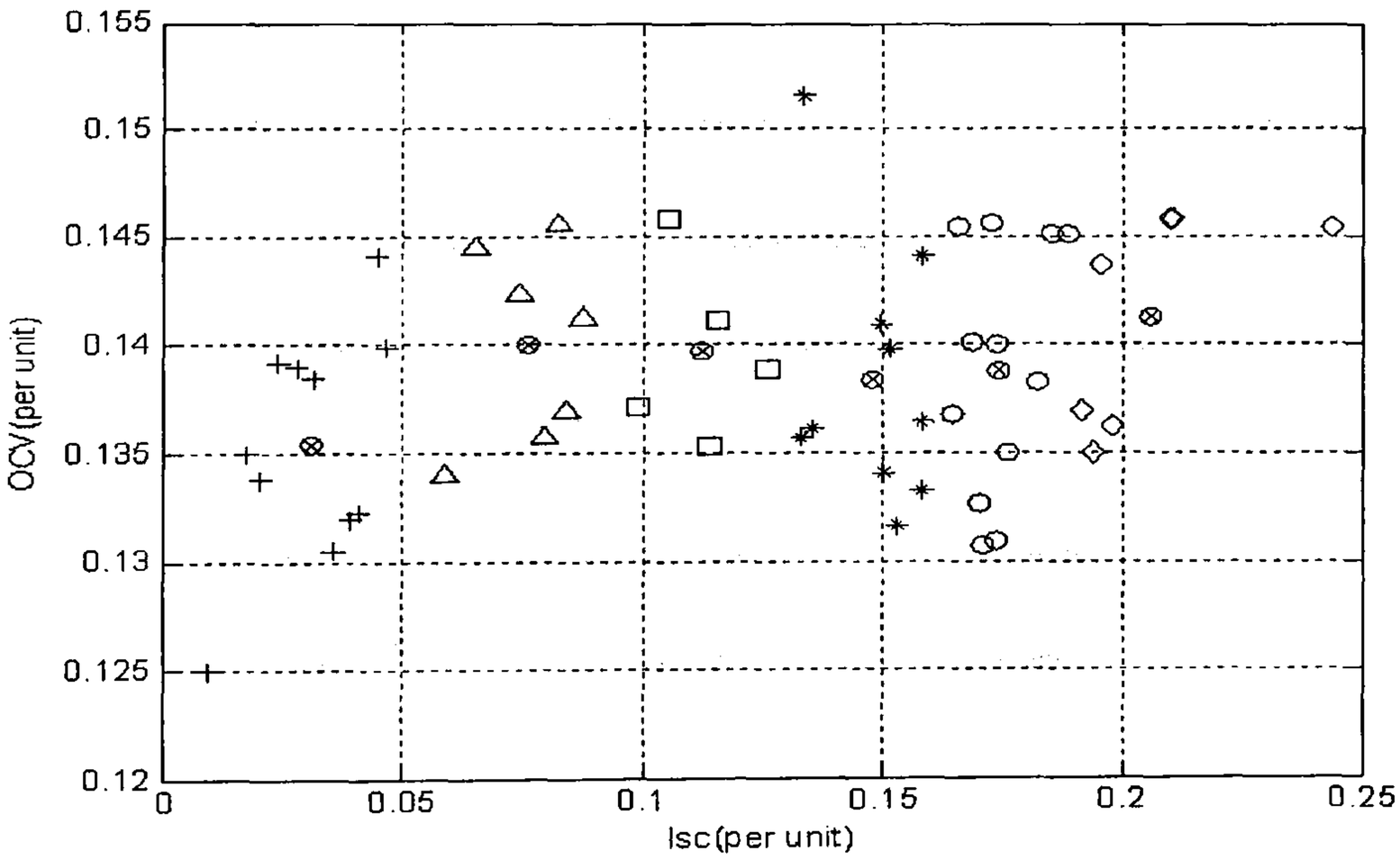

Figure 5.7: Clustering 85W PV input data into six clusters

5.3 Input data clustering

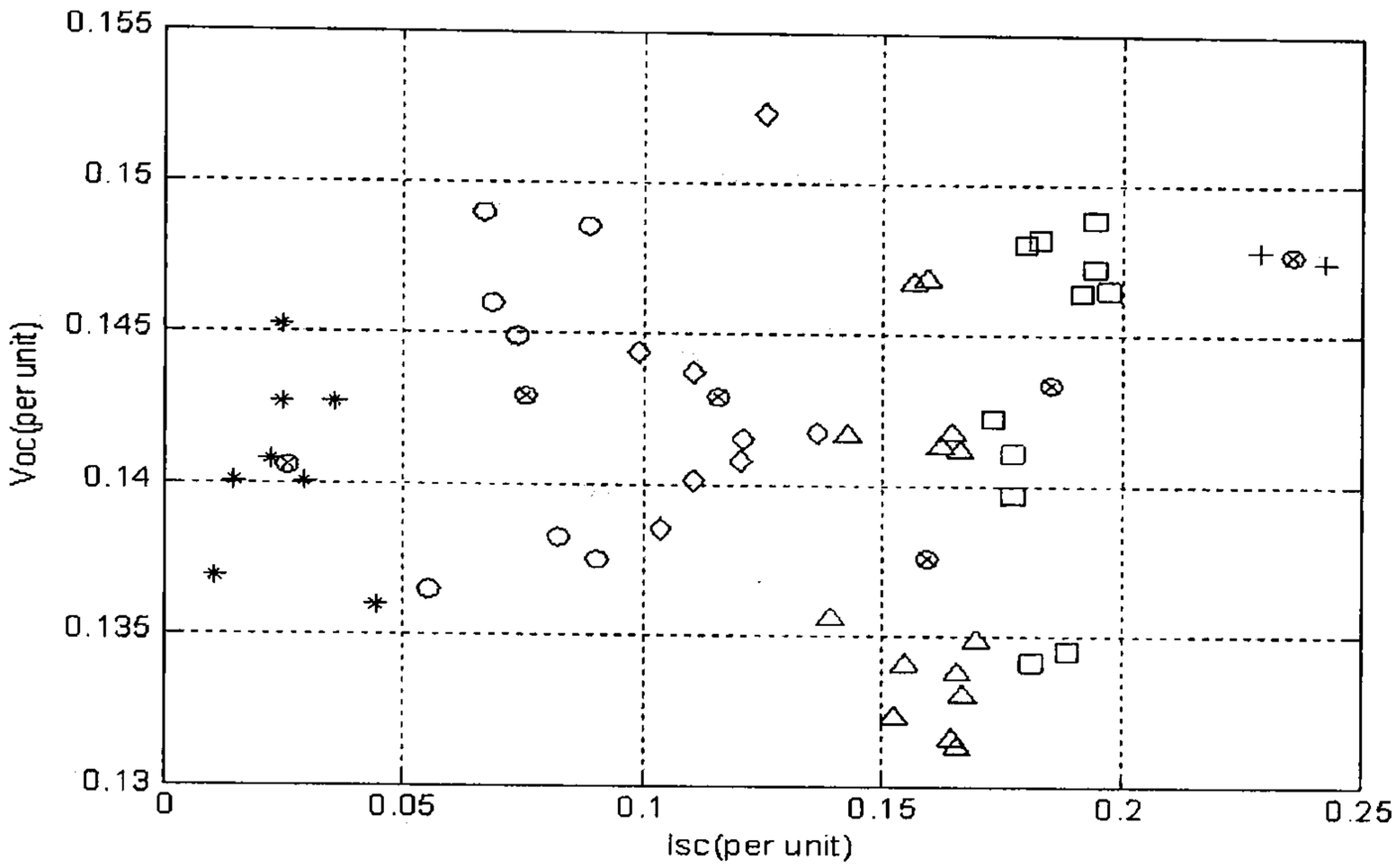

Figure 5.8: Clustering 51W PV input data into six clusters

in Tables 5.3 and 5.4. From Table 5.3, it can be observed the CCs between V_{OC} and V_{max} of the 85W panel are greater than 0.93 for all groups. In addition the CCs increase at high short circuit current groups. Generally, the CCs are greater than 0.95 for all clusters of the 51W polycrystalline panel except in the lowest irradiance level cluster. A low CC at low I_{SC} cluster is caused by a high effect of logarithm relationship of irradiance level on V_{OC} at low irradiance level. At the last two points in this cluster it is not easy to measure the exact I_{max} and V_{max}, as a result P_{max} when the irradiance changes under $100\text{W}/m^2$. Moreover, at low irradiance level one point has abnormal reading of V_{max}, hence, when this three point is removed the CC of the other points becomes more than 0.96 in this cluster. Generally, the CCs in small groups are very high compared to the CC of whole data. In addition, the CC at the high I_{SC} cluster (high irradiance level) is close to unity.

According to Tables 5.3 and 5.4, the CCs in the two cluster groups have unstable values in different clusters. Sometimes the CC is improved when the cluster becomes bigger and it decreases occasionally. This diversity in CCs can be

Table 5.3: CCs between V_{OC} and V_{max} of the single crystal panel in different clusters

CCs in four clusters		CCs in six clusters	
Range of I_{SC}	CCs	Range of I_{SC}	CCs
0 - 6.85	0.837	0 - 6.85	0.837
0.26 - 1.65	0.93	0.26 - 1.3	0.949
1.82 - 3.25	0.945	1.65 - 2.78	0.956
3.53 - 4.95	0.968	2.95 - 3.8	0.978
5.13 - 6,85	0.984	4.2 - 4.95	0.99
———	———	5.13 - 3.92	0.989
———	———	6.85-6.85	1

Table 5.4: CCs between V_{OC} and V_{max} of the polycrystalline panel in different clusters

CCs in four clusters		CCs in six clusters	
Range of I_{SC}	CCs	Range of I_{SC}	CCs
0 - 4.19	0.717	0 - 4.19	0.717
0.18 - 0.26	0.5	0.18 - 0.76	0.35
1.15 - 2.16	0.952	0.95 - 1.55	0.978
2,35 - 3.12	0.996	1.7 - 2.35	0.96
3.15 - 4.19	0.988	2.4 - 2.93	0.998
———	———	2.98 - 3.4	0.989
———	———	3.9 - 4.19	1

referred to the following four reasons:

- Differences in irradiance levels.
- The unbalanced distribution of overall data.
- The diversity of boundaries of V_{OC} and V_{max} in different clusters.
- Number of points in every cluster.

The data is collected environmentally without applying a constant increments, thus, the amount of data in each cluster can not be organised straightforwardly. Therefore, when CCs is computed after increasing or decreasing the boundary of clusters, the CCs change randomly. The data group boundaries are change frequently with small adjustments and the CCs are computed every time, the CCs are increased sometimes and decreased in other times. The best data group distribution can be achieved with more and more iterations. In addition, there are overlaps between data groups, the best possible clusters can be achieved.

The actual learning data is distributed randomly and the groups of data need to be modified frequently with overlapping between different groups. Consequently, the CC should be computed with every modification until it reaches to the best data groups to attain the highest CCs. These processes are time-consuming and required continuous evaluating.

An adaptive neuro-fuzzy inference system is very efficient system, which can carry out this process with expert knowledge using a hybrid learning algorithm. Data fuzzification in different membership functions in ANFIS provides a solution for the problem of frequent changes in cluster boundaries and it can change the overlaps between different clusters until reach the best linear relationships between input output parameters.

5.4 Locating MPP voltage using an ANFIS model

ANFIS structure and adaptation process changes the proposed MFs of input learning data and output linear parameters to minimise the errors between ANFIS output and training data that is used to learn the ANFIS model.

5.4.1 Proposed ANFIS Model analysis

The ANFIS function in Matlab toolbox uses a hybrid learning algorithm to identify the MFs and output rules parameters is the major training routine for Sugeno-type fuzzy inference systems. Prior to apply in the Matlab ANFIS function, Genfis1 (Generate a fuzzy inference system) function in the Matlab toolbox is applied to convert the input crisp data to the selected number and type of membership functions. Genfis1 function generates a Sugeno-type Fuzzy inference system (FIS) structure which initialises the membership function parameters [58]. The ANFIS function uses actual I_{SC} and V_{OC} of PV panels as input parameters and actual V_{max} as output parameter to learn the ANFIS model by adapting the nonlinear parameters of the MFs and output linear parameters of Sugeno output equations.

The parameters of MFs and output linear parameters of a Sugeno-type FIS structure are modified by applying a hybrid learning rule algorithm that is described in chapter 2. All actual data is used as a learning data to train the ANFIS model. Also, this data is used as a test data to find the individual errors between actual data and predicted data. This process is continued in this chapter until achieve the best ANFIS model that give the minimum individual errors. The final selected ANFIS model will be tested by dividing the actual data into learning data and test data. In addition, the performance of final model is tested with new data in chapter 7.

The ANFIS function in Matlab toolbox modifies the ANFIS model parameters according to the selected error criterion or the number of epochs that are set

in the ANFIS function. Figures 5.9 and 5.10 show 4 ×1 Gaussians MFs as a first example of input data fuzzification before and after these MFs are adapted by ANFIS function. The number of generated rules can be computed from all possible connectives between MFs of inputs. Therefore, the number of rules equal the number of MFs of input1 times the number of MFs of input2.

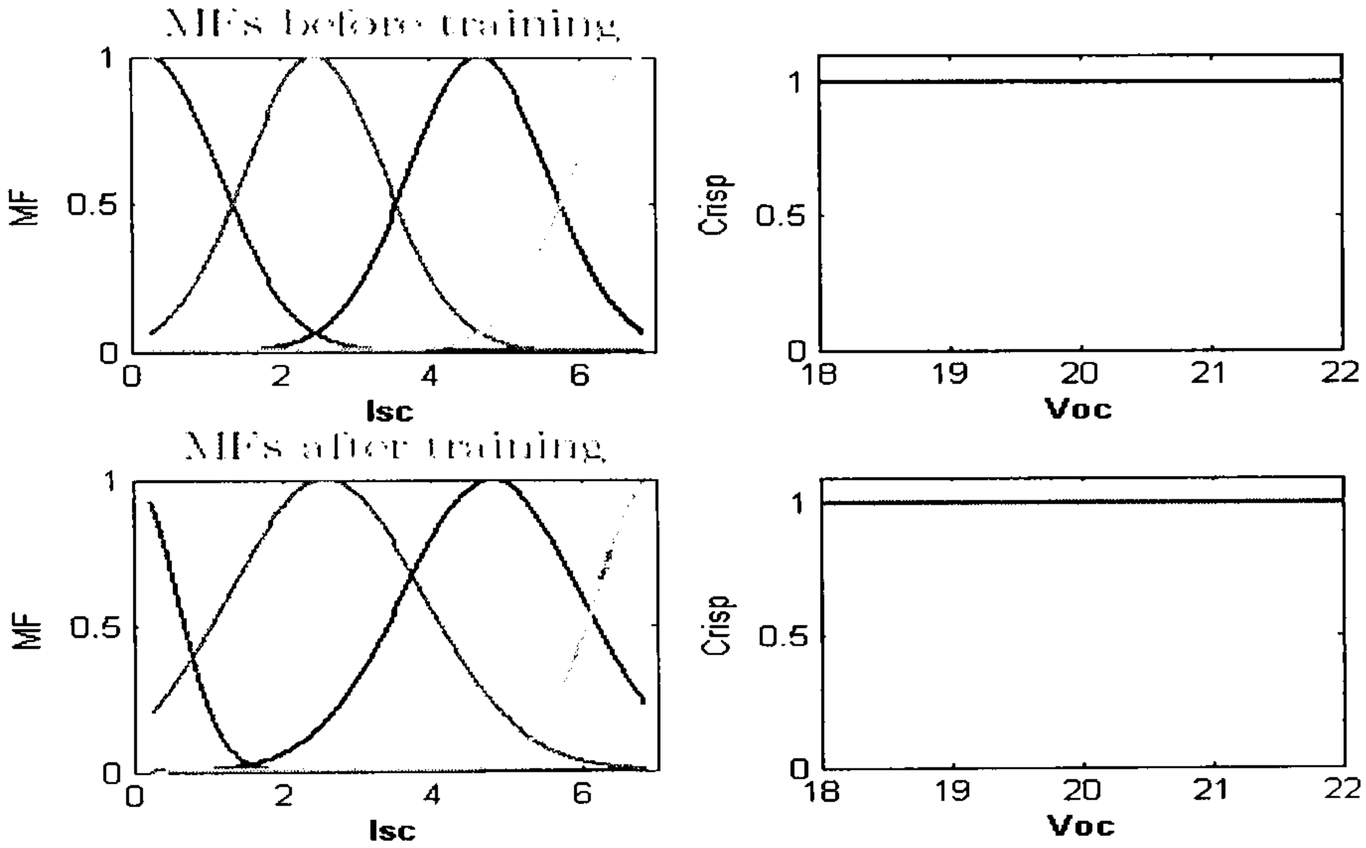

Figure 5.9: 4×1 Gaussians MFs of 85W PV panel

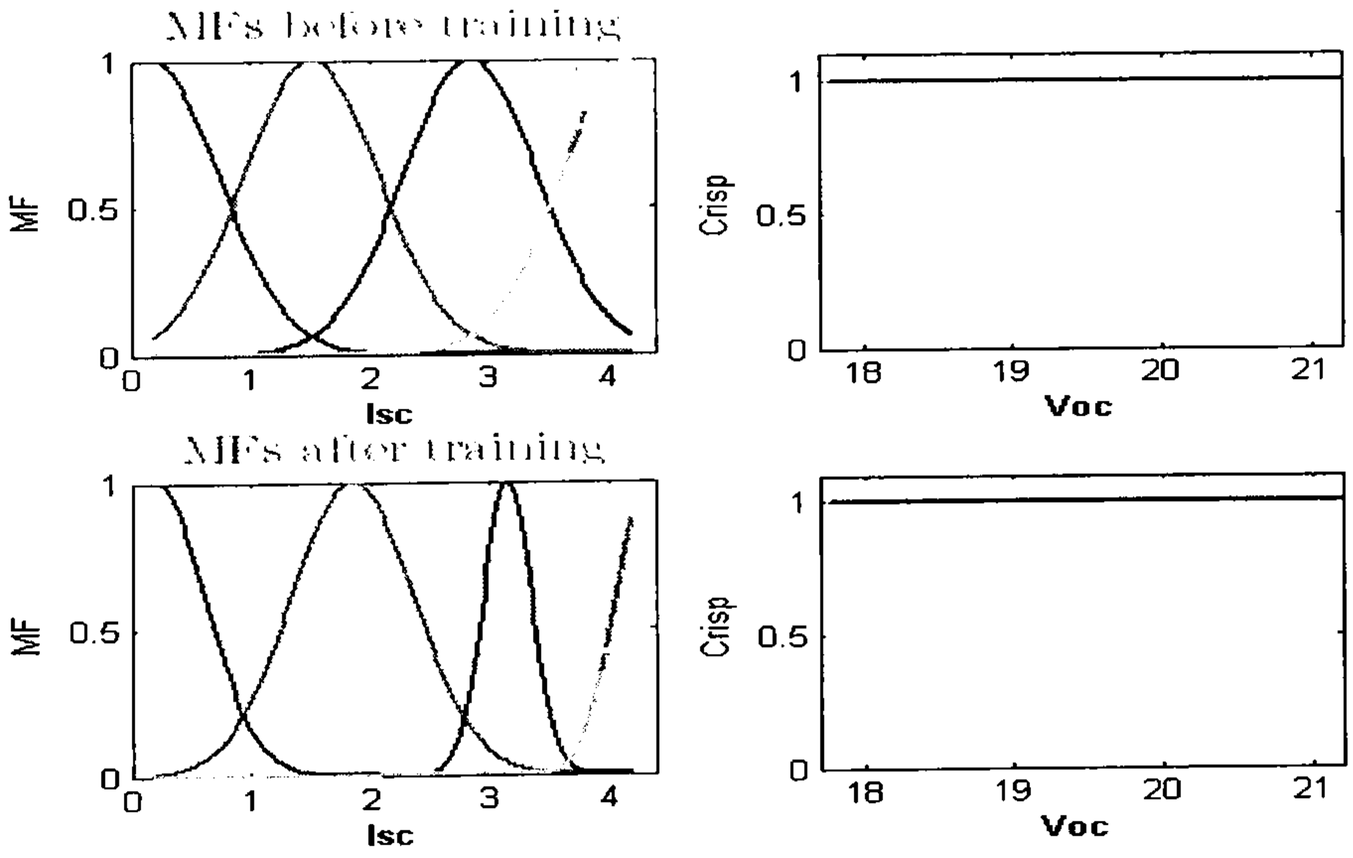

Figure 5.10: 4×1 Gaussians MFs of 51W PV panel

RMSE of different ANFIS models

For different groups of inputs Gaussians MFs, Figures 5.11 and 5.12 show how the root mean square error (RMSE) between the actual V_{max} and the predicted outputs is improved after 100 epochs for 85W panel data and 50 epochs for 51W panel data.

When the data is grouped by means of I_{SC}, the relationship between V_{OC} and V_{max} is improved as clarified in statistical analysis. Thus, when the input I_{SC} data is fuzzified in more than two MFs the RMSE decreases rapidly after a few number of epochs as shown in Figures 5.11.a and 5.12.a. Conversely, a high RMSE is produced when the input data is grouped only by means of V_{OC} as shown in Figures 5.11.b and 5.12.b. Also, there is a poor improvement of RMSE when the data is fuzzified according to V_{OC}.

When the control systems are assembled, two important requirements should be considered:

- The system should be optimised with minimum number of rules to avoid the complexity in system design.
- A maximum accepted error is associating with the system precision requirements according to maximum efficiency required in the control system which is determined by designers.

When only I_{SC} is fuzzified into 3MFs, 4MFs and 5MFs and V_{OC} remains as a crisp, the RMSE reaches its minimum values after a few number of epochs as shown in Figures 5.11.a and 5.12.a. Furthermore, the RMSE is improved due to increasing the number of MFs and consequently, the number of rules, which in this cases equal the number of MFs of I_{SC}. This means that the linear and nonlinear parameters are adapted until they reach their final values that provide these low RMSE values. Accordingly, the differences between actual V_{max} and the ANFIS models output are improved owing to the increasing the number of MFs as a result number of rules.

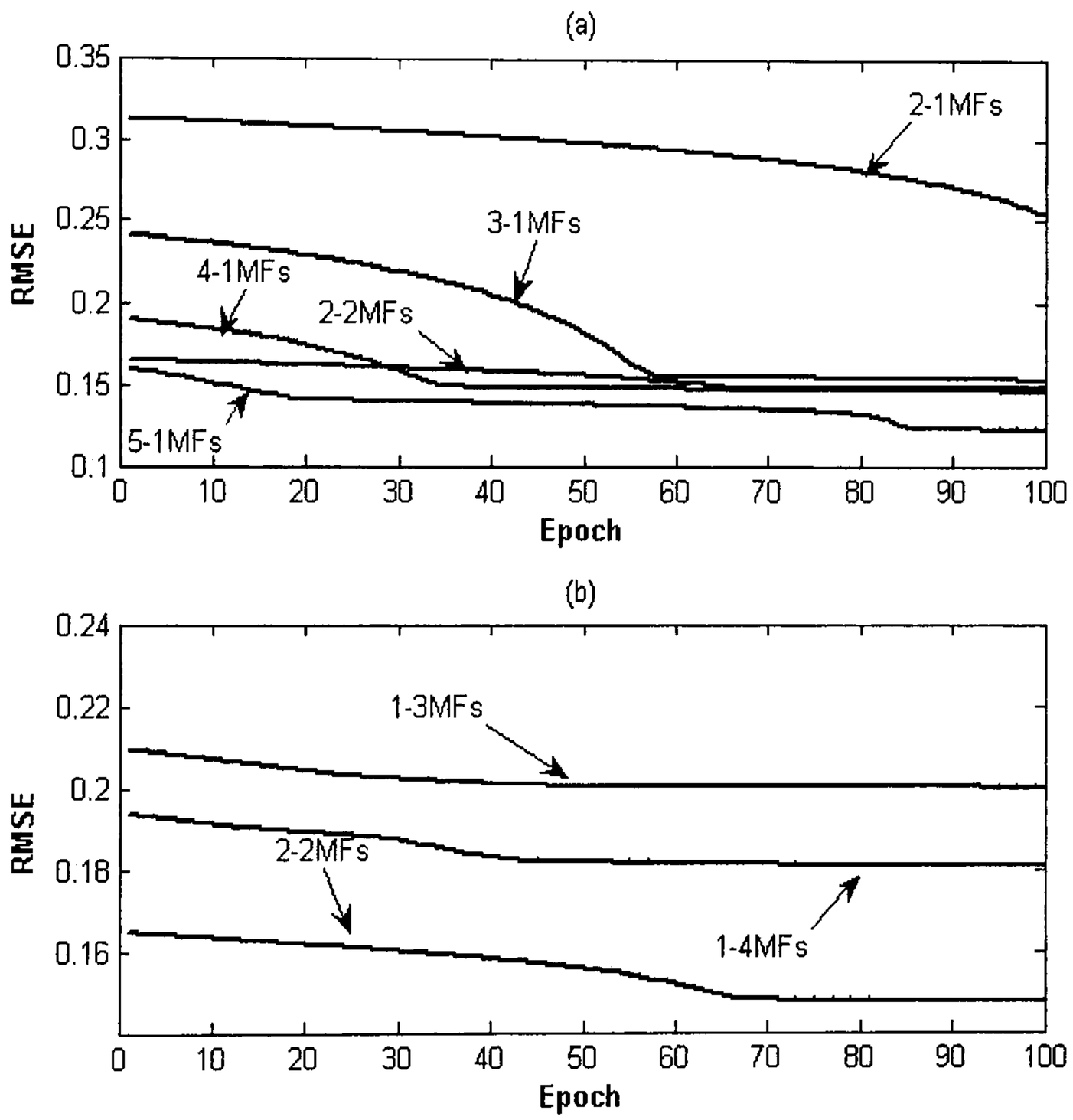

Figure 5.11: Root mean square error of the 85W panel at different MFs

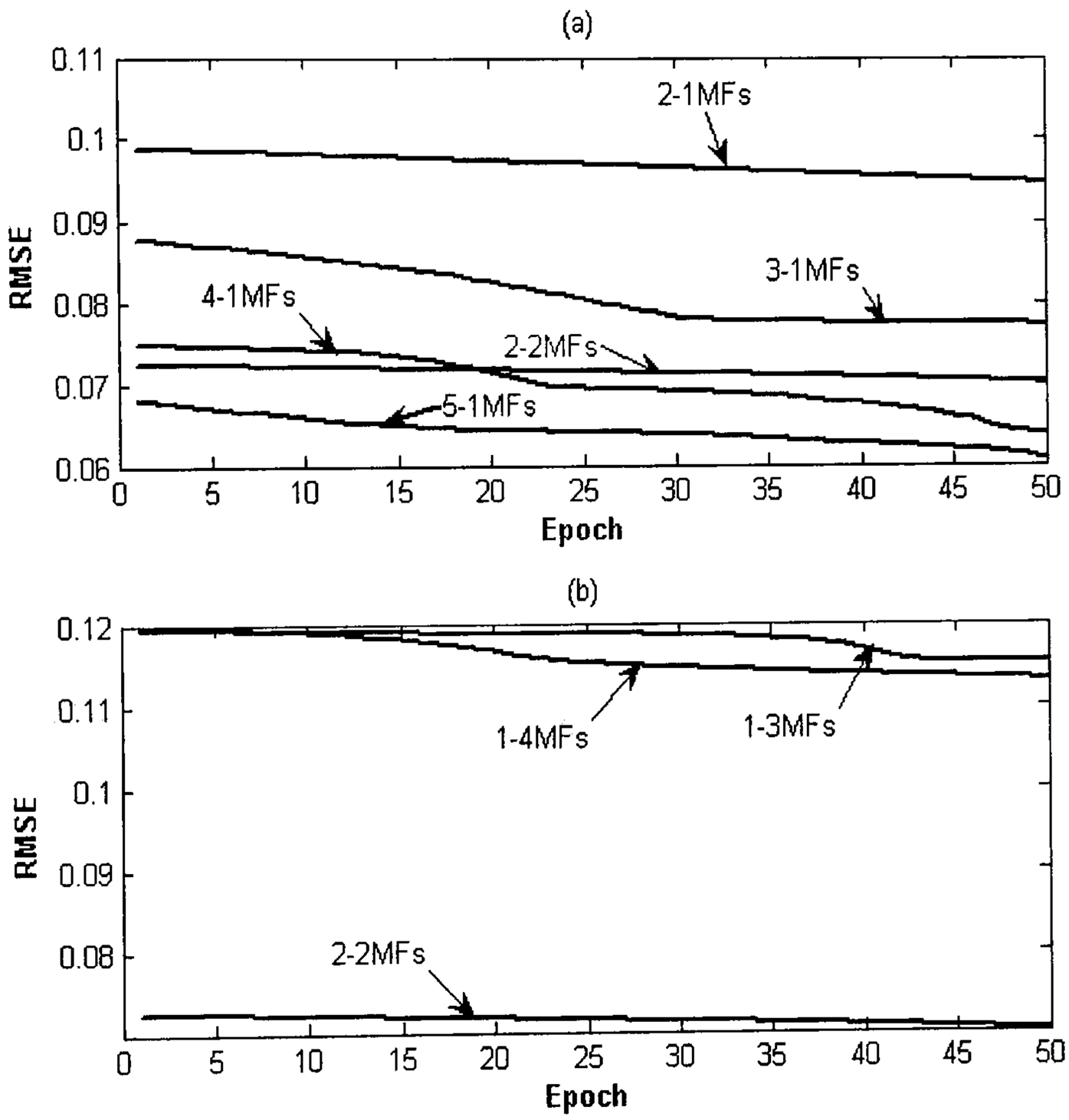

Figure 5.12: Root mean square error of the 51W panel at different MFs

Individual errors of different ANFIS models

Based on Figures 4.3.a and 4.3.b for the two types of PV panels, the generated power from PV panels decreases around 1% when the V_{OP} deviate a 0.3V from V_{max}. This small decline in power does not affect the maximum generated power from the PV panels. Also, this accessibility in voltage deviation is necessary for the MPPT system stability, which is clarified in the next chapter.

According to the previous percentage drop in output power of PV panels due to voltage deviation from V_{max} the individual errors between predicted ANFIS output and actual V_{max} should be computed.

Generally, the RMSE is not high in most models that have been tested in Figures 5.11 and 5.12. A test data is applied in different ANFIS Models to predict V_{max}. The outputs of the different proposed ANFIS models have been compared with the actual experiment output of the PV panels. Three models are selected to predict the V_{max} regarding the low individual errors between the actual data and the predicted output from ANFIS models that is shown in Figures 5.13 and 5.14 and Table A.2, A.3, A.4 and A.5 . The Models that have 4×1MFs, 5×1 MFs and 2×2 achieve high precisions with less than 2% absolute error between the predicted V_{max} and the real measured data. On the other hand a high individual errors between the actual data and the predicted outputs from ANFIS models of more than one point is observed, especially with the models that have less than four MFs (less than four rules) and all ANFIS models that are grouped only by means of V_{OC} data as shown in Figures 5.13 and 5.14 for two panel types.

The individual errors of ANFIS output is between 2% and 5% in many points when V_{OC} only is fuzzified in more than one MFs and I_{SC} data remains as a crisp input. These high errors confirm a low precision in the predicted V_{max} of ANFIS models when dealing with a crisp data of I_{SC}. Also, with the lowest number of MFs in a 2×1 model (minimum number of rules), the RMSE is

0.119 after 200 epochs for the 85W panel and 0.0946 after 50 epochs for the 51W panel. Normally, these RMSE values are accepted, however as shown in Figures 5.13.a and 5.14.a the errors between the actual data and ANFIS output are more than 2% for many points of the 85 W panel data and near 2% for the 51W panel. Accordingly, more MFs of I_{SC} in 4×1 model and 5×1 model reduce the error in these points.

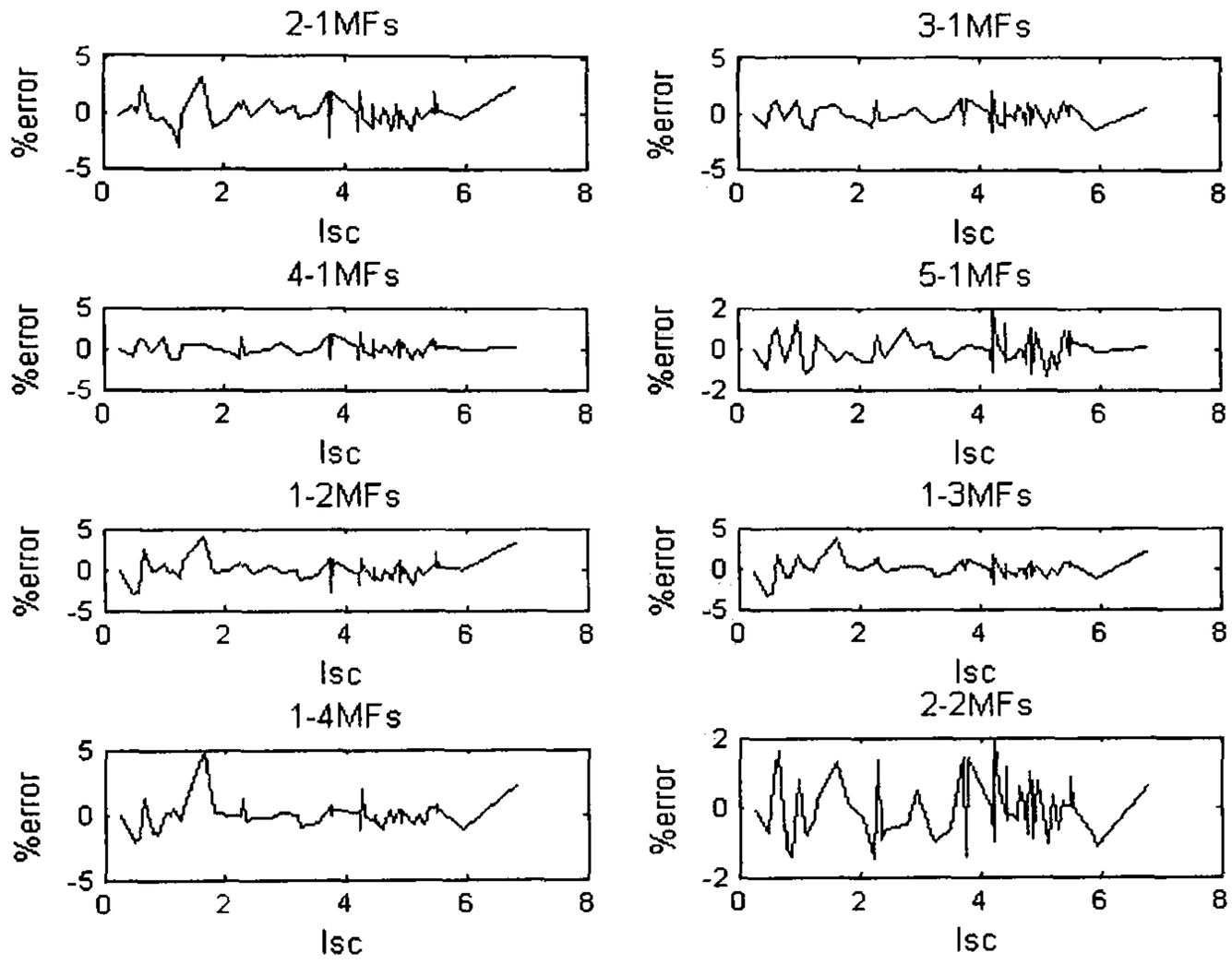

Figure 5.13: Individual errors between the actual data and the outputs of ANFIS models of the 85W panel

A good performance is achieved when the input I_{SC} and V_{OC} data is fuzzified into two MFs (2×2 model). This ANFIS model attains a low initial RMSE. The problem with 2×2 model is that the low improvement is achieved during the learning epochs. Figures 5.15 and 5.16 show how the MFs are modified after 50 epochs and 100 epochs respectively. The RMSE decreases by only -0.004 due to this high modification in MFs parameters.

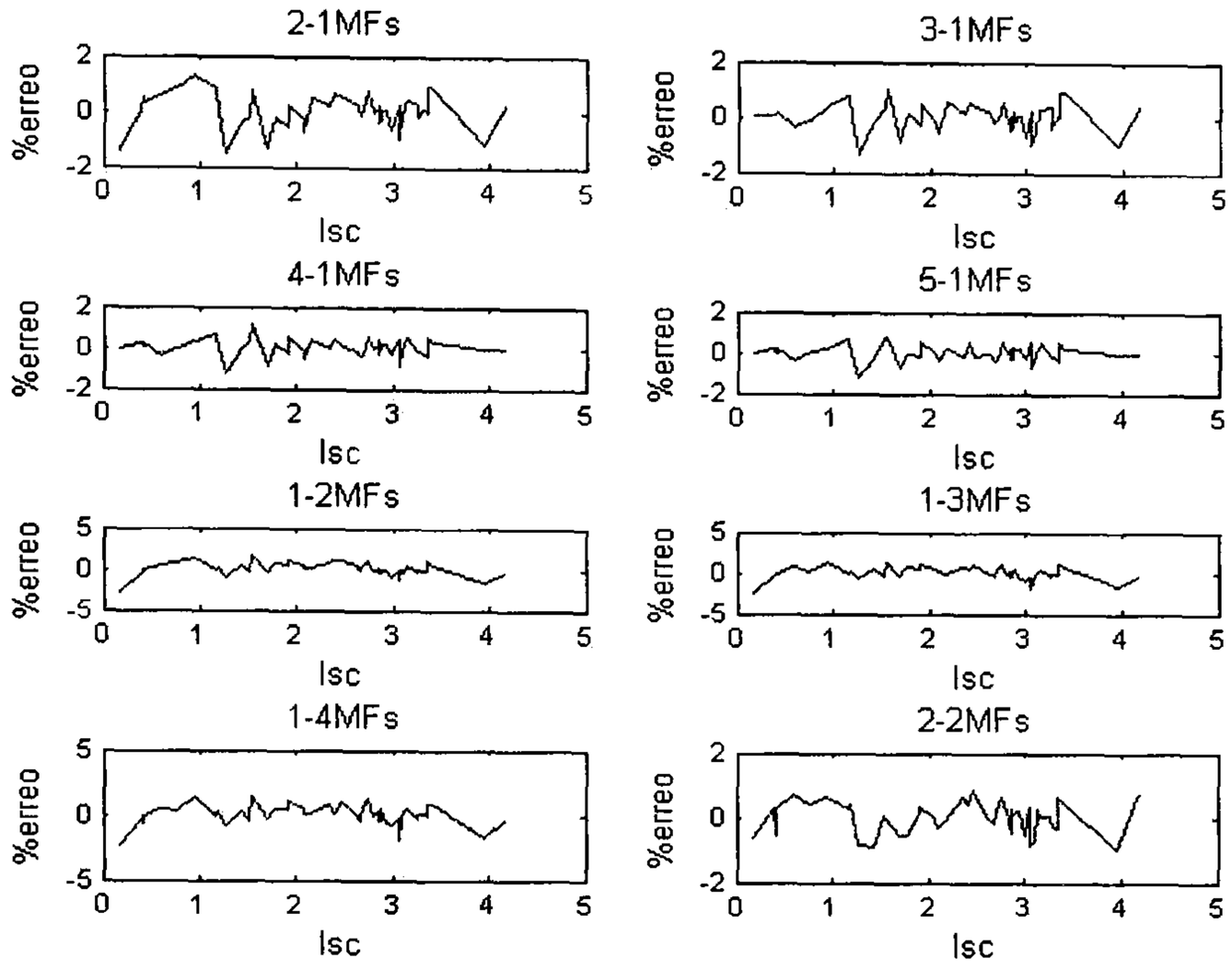

Figure 5.14: Individual errors between the actual data and outputs ANFIS models of the 51W panel

5.4.2 Selected rules for the proposed ANFIS model

By referring to the data point by point it can be observed that 4×1 model and 5×1 model achieve a very low error in both types of PV panels, however to face the extending changes in cell junction temperatures which affect V_{OC} values, it is necessary to use the 2×2 model, especially with irregular open circuit voltage points in high or low ambient temperature regions.

The 4×1 ANFIS model and the 2×2 ANFIS model that are shown in Figure 5.17 and Figure 5.18 respectively have low rules with high precision. The rules of the trained 4×1 ANFIS model of the 85W panel are:

$If\ Isc\ is\ very\ low\ and\ V_{OC}\ is\ Crisp\ THEN\ f_1 = -3.1844Isc + 3.26Voc - 46.86$

$If\ Isc\ is\ low\ and\ Voc\ is\ Crisp\ THEN\ f_2 = -0.49957Isc + 0.5935Voc + 5.4304$

$If\ Isc\ is\ high\ and\ Voc\ is\ Crisp\ THEN\ f_3 = -0.23808Isc + 1.194Voc - 7.379$

$If\ Isc\ is\ very\ high\ and\ Voc\ is\ Crisp\ THEN\ f_4 = 0.497Isc + 0.46333Voc + 3.1816$

5.4 Locating MPP voltage using an ANFIS model

Also, the training 2×2 MFs ANFIS model rules of the 51W panel are:

$If\ Isc\ is\ low\ and\ Voc\ is\ Crisp\ THEN\ f_1 = -3.8347Isc + 0.076738Voc + 13.354$

$If\ Isc\ is\ low\ and\ Voc\ is\ Crisp\ THEN\ f_2 = 0.46573Isc - 0.0.21236Voc + 21.224$

$If\ Isc\ is\ high\ and\ Voc\ is\ Crisp\ THEN\ f_3 = -2.6635Isc + 1.6051Voc - 3.7389$

$If\ Isc\ is\ high\ and\ Voc\ is\ Crisp\ THEN\ f_4 = 0.39646Isc + 1.5309Voc - 17.223$

The two models mentioned above produce a good precision with the two panels

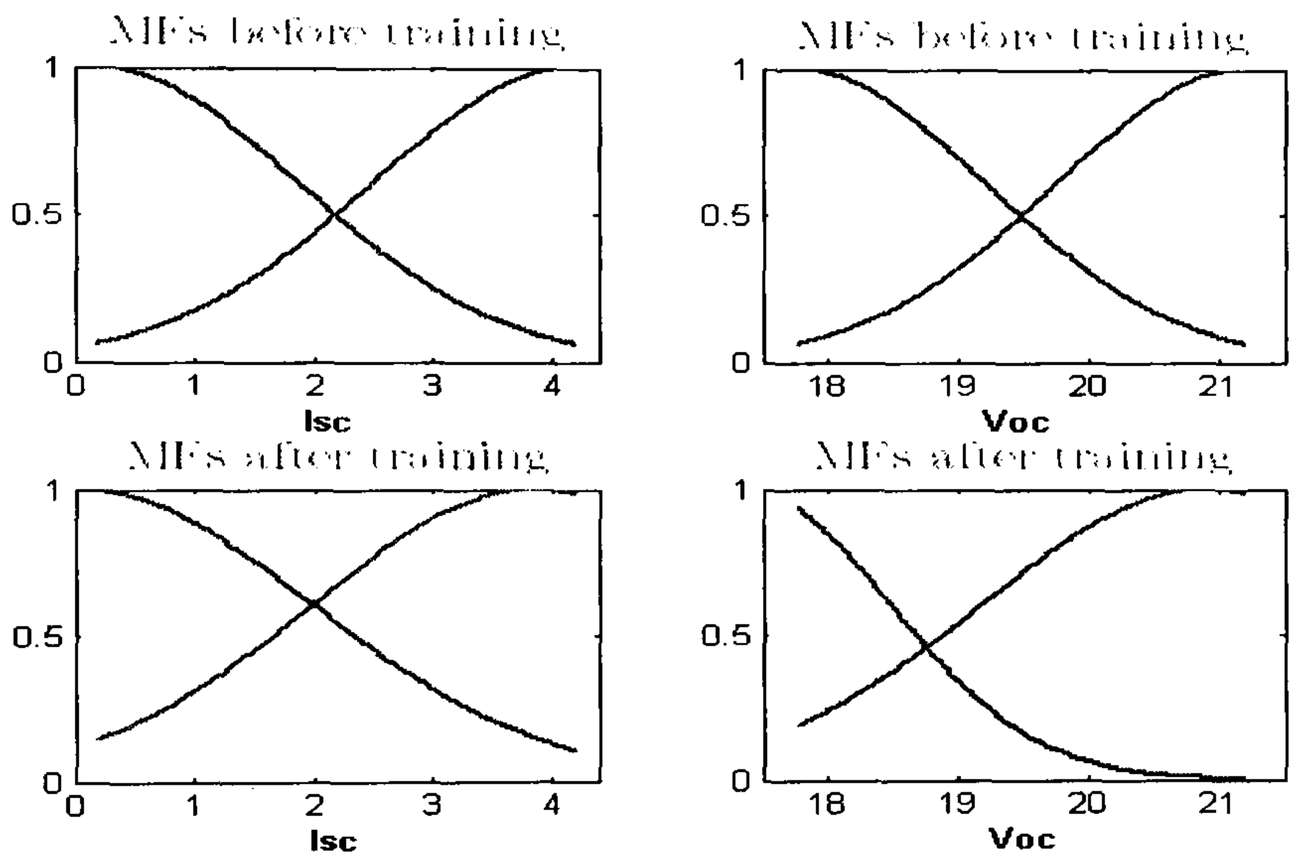

Figure 5.15: 2-2 Gaussians MFs of the 51W PV panel after 50 epochs.

that have 36 PV cells in series. When ANFIS models starts their learning, the 4×1 model produces higher RMSE than the 2×2 model. However, after few training epochs, the RMSE of 4×1 model becomes lower than that of the 2×2 model. The previous changes in RMSE take place in the two panel models as shown in Figures 5.11.a and 5.12.a.

The low initial RMSE of the 2×2 model is due to the direct proportional relationship between V_{OC} and irradiance level when the temperature effect on V_{OC} is neglected. Therefore, the V_{OC} has a limitation range change, especially at low irradiance level. Thus, dividing the data of V_{OC} in more than one MFs helps

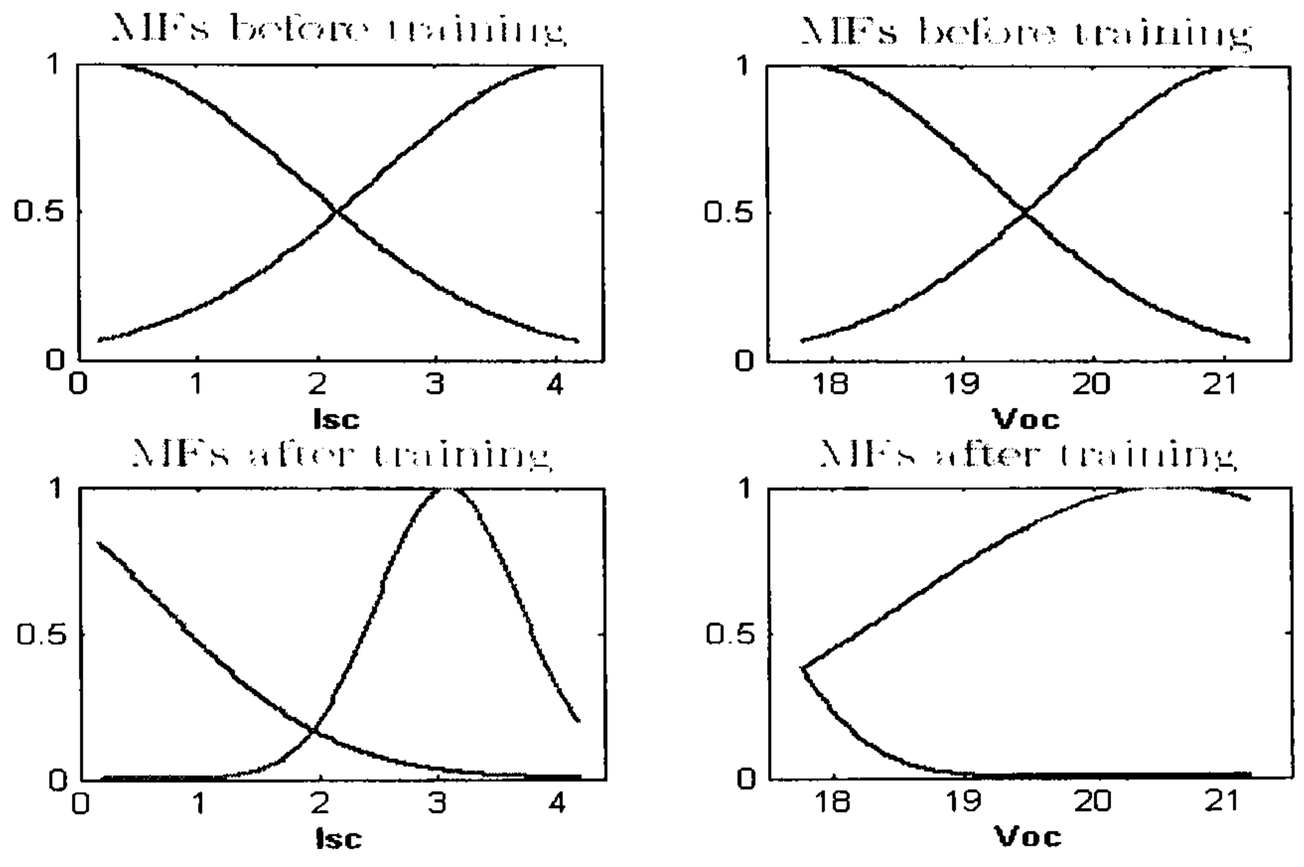

Figure 5.16: 2-2 Gaussians MFs of the 51W PV panel after 100 epochs.

the ANFIS model to learn the behaviour of PV panels at different irradiance level.

However, increasing the number of MFs of the both input parameters leads to higher number of rules. The Genfis1 function with more than two groups of two inputs generates many rules such as 9 and 16 rules, which leads to more complexity in the MPPT system. Moreover, in Genfis1 function "the backward pass gradient descent algorithm, which modifies the nonlinear premise parameters of MFs does not perform any iterative optimisation" [58]. The small improvement comes from the forward pass linear least squares estimation (LSE) algorithm modification for consequent linear parameters of ANFIS model.

Referring to data clustering, Genfis2 function in the Matlab fuzzy toolbox can generate an FIS structure using the clustering algorithm discussed in clustering methods in chapter 2."The subtractive clustering method partitions the data into groups called clusters, and generates an FIS with minimum number of rules that are required to distinguish the fuzzy qualities associated with each cluster" [58].

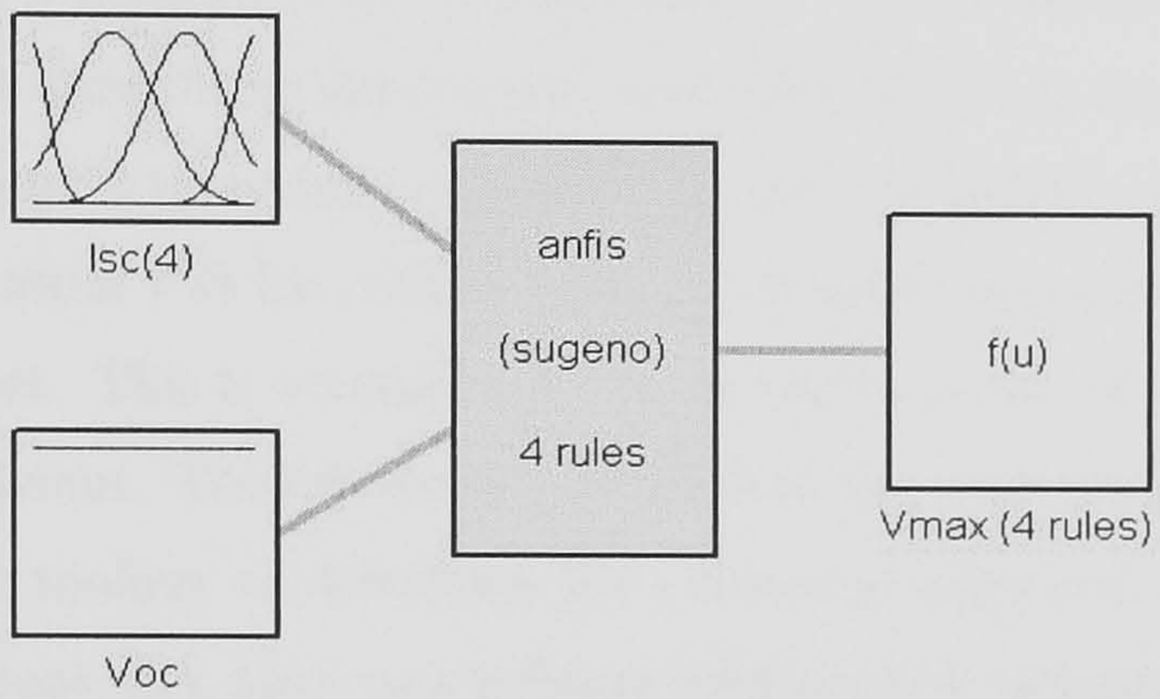

Figure 5.17: ANFIS model of 4×1MFs for the 85W PV panel

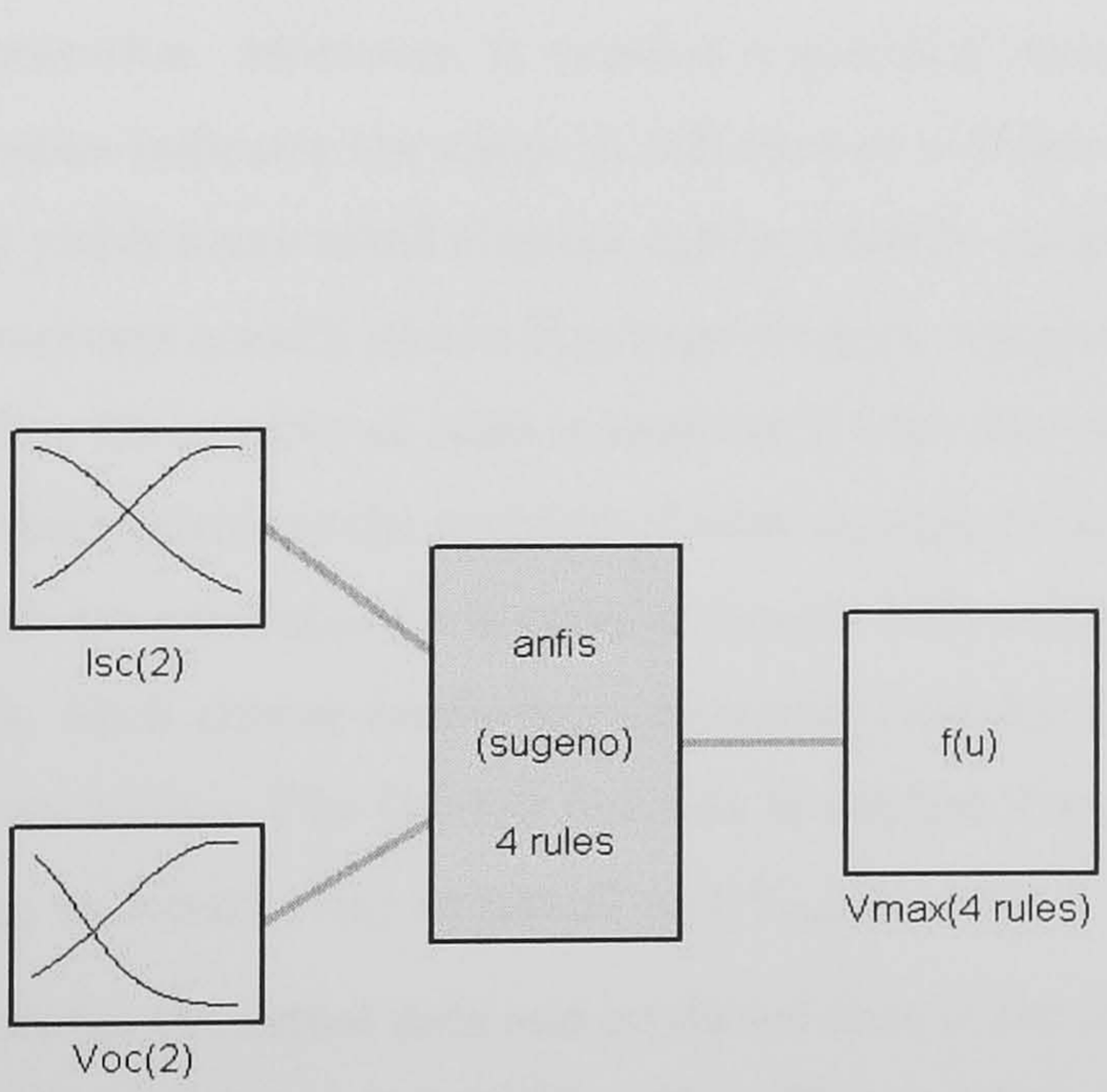

Figure 5.18: ANFIS model of 2×2MFs for the 51W PV panel

5.4.3 ANFIS models using Genfis2 function

To overcome the problem of the iterative modification in premise parameters of MFs using a gradient descent algorithm in ANFIS function, Genfis2 (generates an FIS using fuzzy subtractive clustering) function separates the input and output data in fuzzy sets when there is only one output. Genfis2 is used to generate an initial FIS for ANFIS training by applying subtractive clustering on the data set. This is accomplished by extracting a set of rules that models the data behaviour. The rule extraction method first uses the Subclust function in the Matlab toolbox to determine the number of rules and antecedent membership functions and, then uses a linear least squares estimation to determine each rule's consequent equations. This function returns an FIS structure that contains a set of fuzzy rules to cover the feature space. [58] [6] [7].

Genfis2 function is a fast and one-pass method that does not perform any iterative optimisation. Moreover, it requires a specified cluster centres range. The cluster radius indicates the range of influence of a cluster. A small cluster radius usually yields many small clusters and as a result, many rules. However, large cluster radiuses usually yield a few large clusters and generate fewer rules. This means that the number of rules is associated with the number of clusters. Accordingly, this overcomes the problem of high number of rules in the Genfis1 function, which are generated by number of input1 MFs multiplied by number of input2 MFs. Each cluster centre has a spherical neighbourhood of influence within the given radius. The Genfis2 function is applied using a cluster radius of 0.5 with I_{SC} as input1, V_{OC} as input2 and V_{max} as output.

Figure 5.19.a shows the actual data and predicted data of the 85W panel ANFIS model with cluster radius equal to 0.5. Also, Figure 5.20.a shows the actual data and the predicted data of the 51W panel ANFIS model with cluster radius equal to 0.5. The RMSE values are computed of the two models, they are 0.166 and 0.09 respectively. In addition, the individual errors between the actual

data and the predicted outputs of ANFIS models are shown in Figures 5.21.a and 5.22.a.

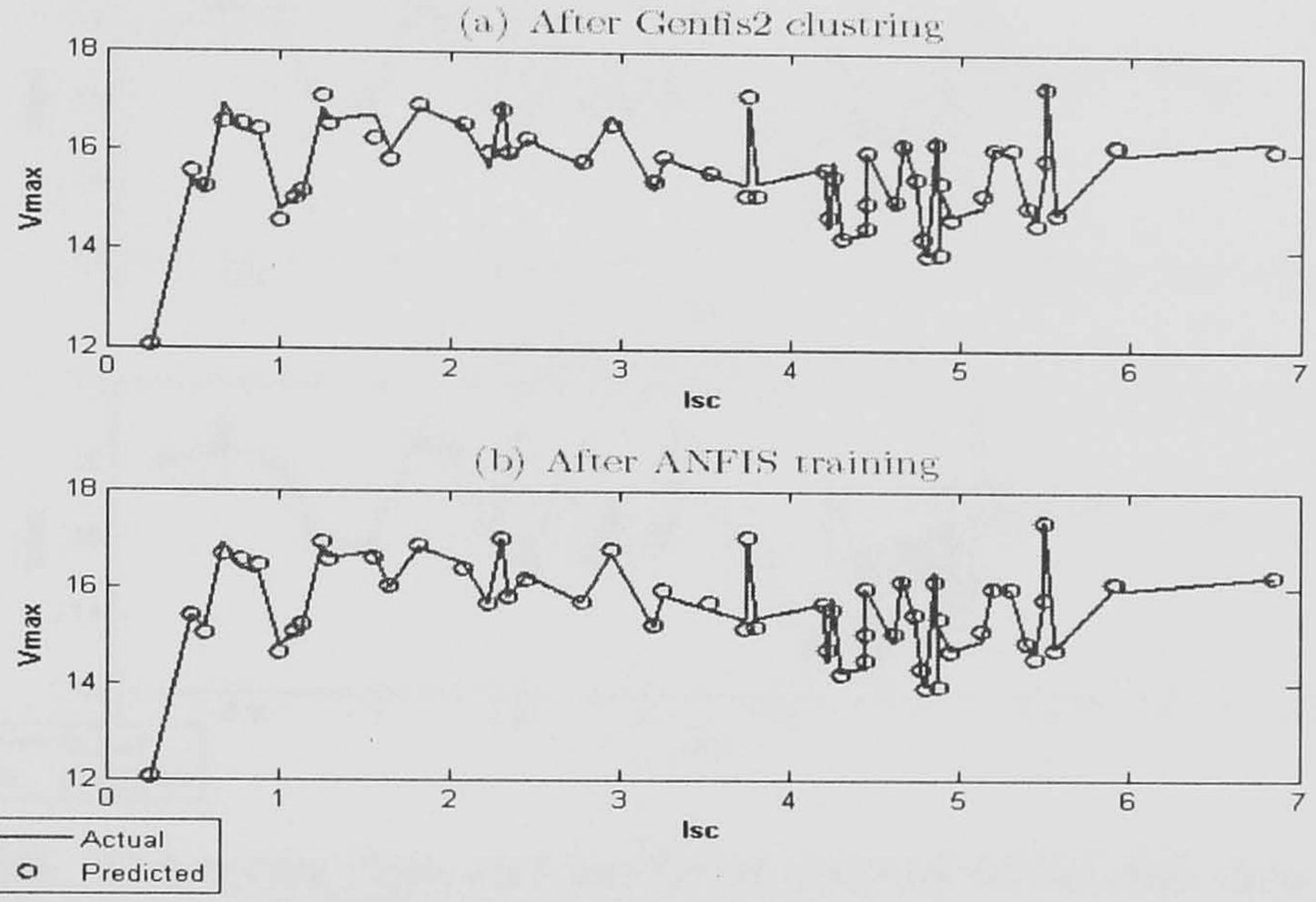

Figure 5.19: The actual data and predicted outputs of Genfis2 model data for the 85W panel before and after ANFIS function training

The two 0.5 cluster radius models have four generated rules. If the radiuses of clusters are decreased, the rules increase. The premise nonlinear parameters of the MFs are assembled by applying the subtractive clustering, which simulates the data behaviour. The Genfis2 function models achieve approximately the same RMSE compared with the selected 4×1 model and the 2×2 model that obtained with ANFIS function, which have been specified in Genfis1 models. Moreover, the individual errors between actual data and predicted outputs are less than 2% in all points that are shown in Figure 5.22.a and are roughly 2% as shown in Figure 5.21.a.

A Lower RMSE and individual errors can be achieved if the radius of cluster centre is reduced. However, decreasing the radius of clusters increases the number of clusters and, as a result, additional rules will be added. For example, if the radius of cluster centre decreases to 0.3 the RMSE decreases to 0.133 and 0.056 for an 85W and a 51W panels respectively. However, the number

5.4 Locating MPP voltage using an ANFIS model

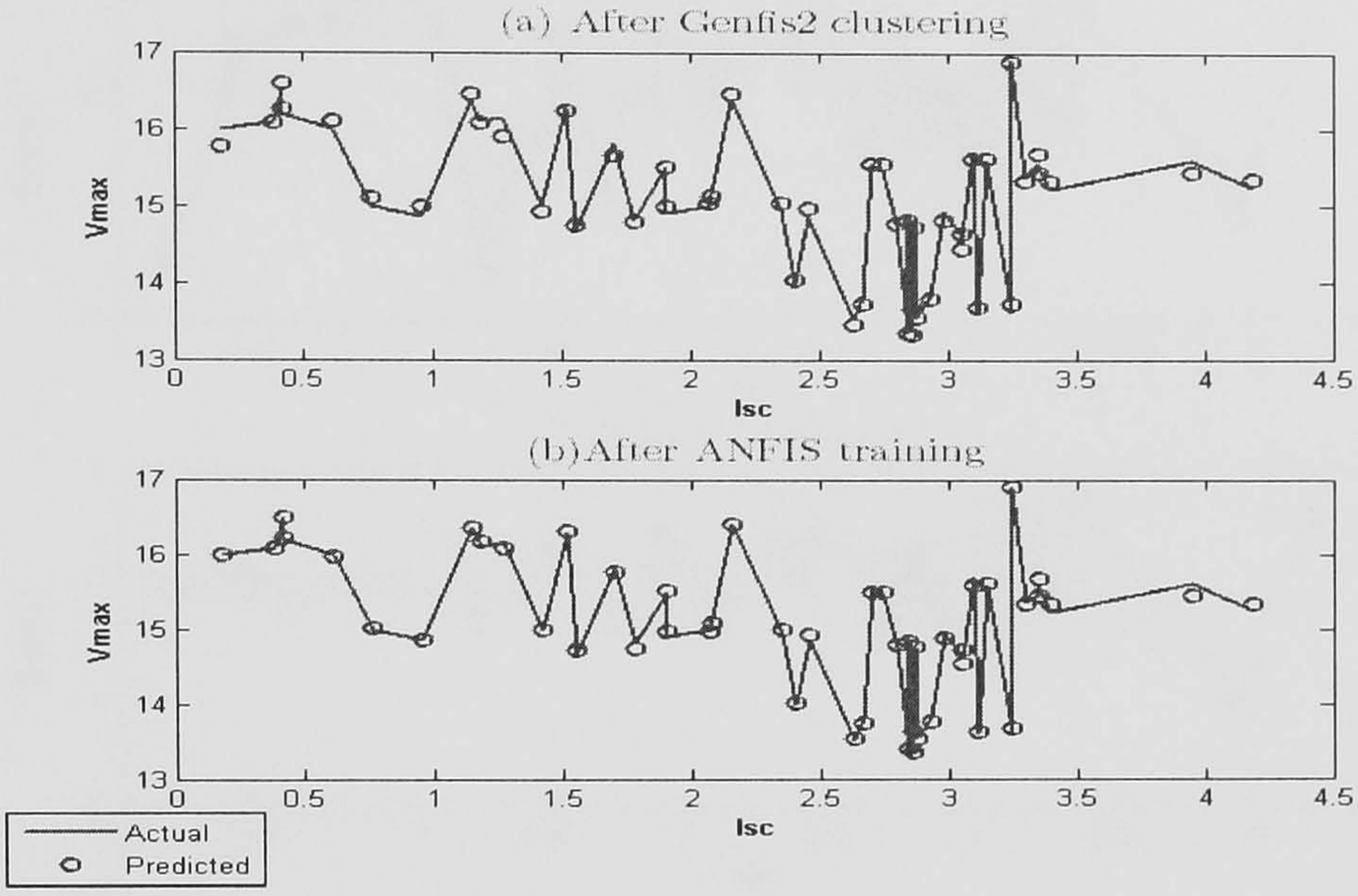

Figure 5.20: The actual data and predicted outputs of Genfis2 data for the 51W panel before and after ANFIS function training

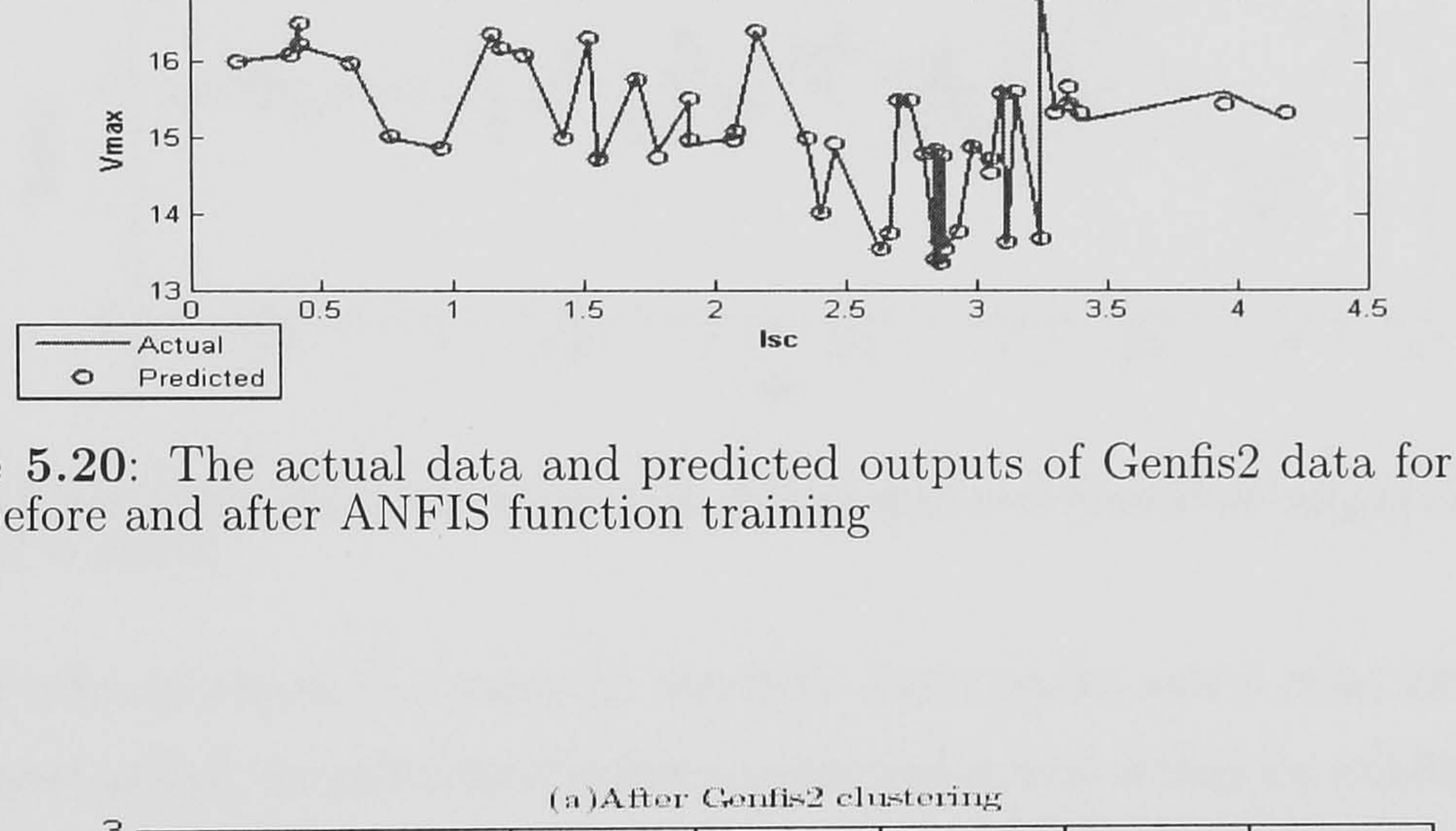

Figure 5.21: Percentage error between actual data and predicted outputs of Genfis2 of the 85W panel.

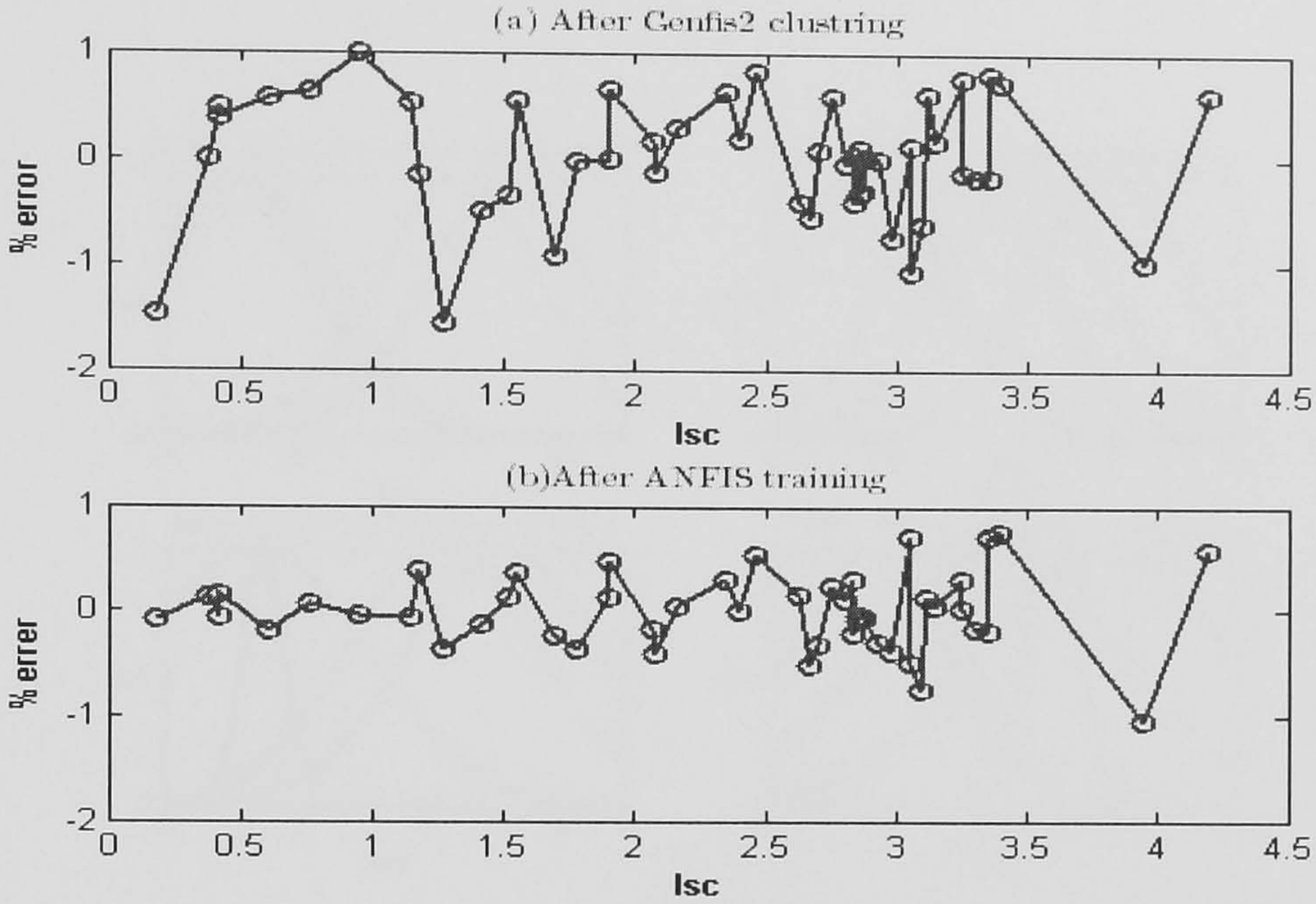

Figure 5.22: Percentage errors between actual data and predicted outputs of Genfis2 of the 51W panel.

of rules increases to 7 rules for the 85W panel model and 6 rules for the 51W panel model. As mentioned before, optimisation with minimum number of rules is very important. Thus, the output FIS structure can use the optimisation capability of ANFIS to improve the model performance. The ANFIS function can improve the consequent linear parameters applying the actual data to train the 0.5 radius model. After 100 epochs, the RMSE of Genfis2 models decrease to 0.12 and 0.054, which are better than the 0.3 radius model. The predicted data move toward the values of the actual data as shown in Figure 5.19.b and Figure 5.20.b. Moreover, the individual errors are decreased to approximately 1% in ANFIS model for 85W panel and, less than 1% in ANFIS model for the 51W panel as shown in Figure 5.19and 5.20.b. respectively.

Figures 5.23 and 5.24 show the MFs of Genfis2 models before and after applying ANFIS function training. In addition, The overall ANFIS model is shown in Figures 5.25 and 5.26.

The very low individual errors of the previous two final models achieve a good

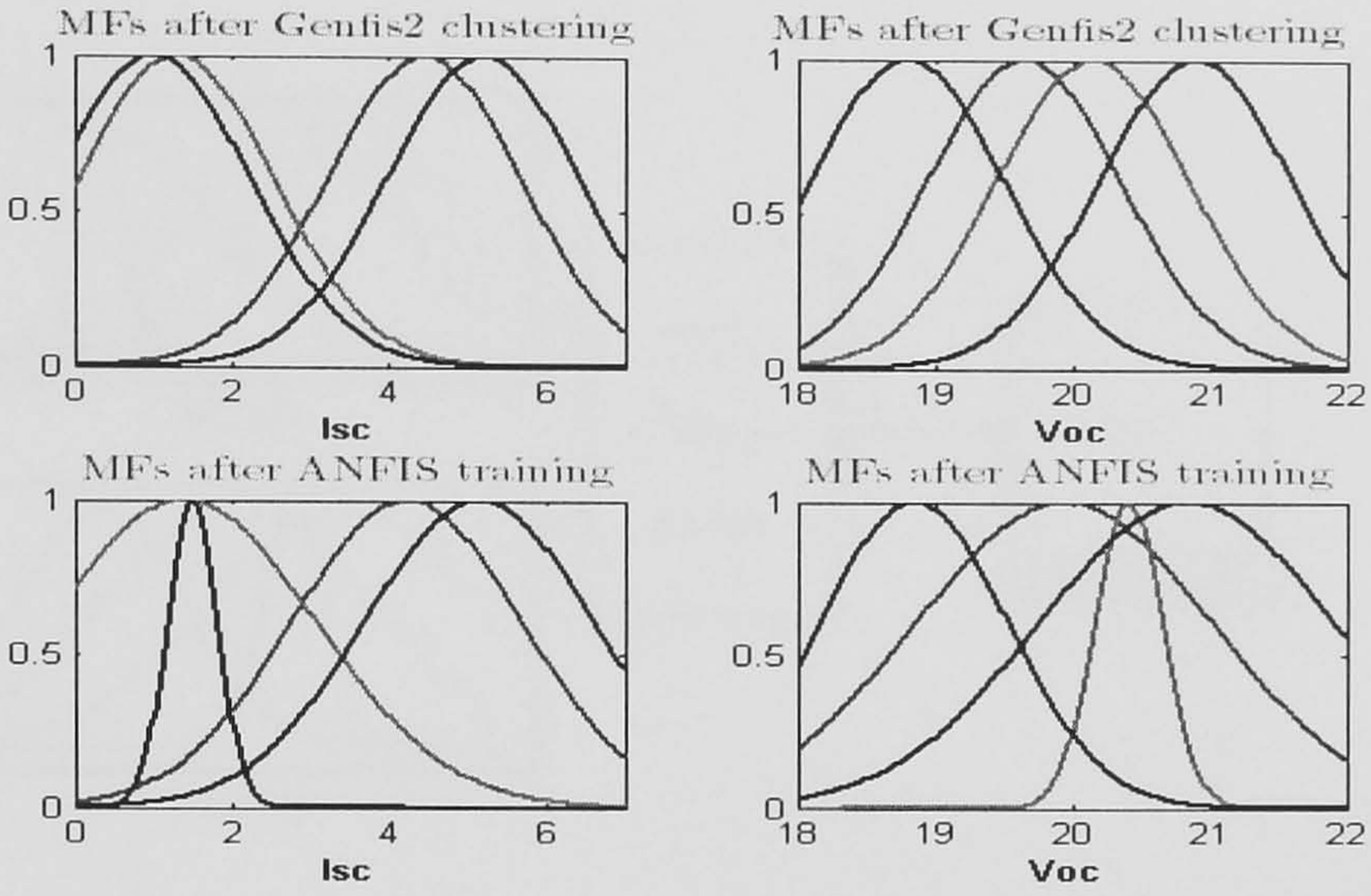

Figure 5.23: MFs of Genfis2 model for the 85W panel before and after ANFIS function training.

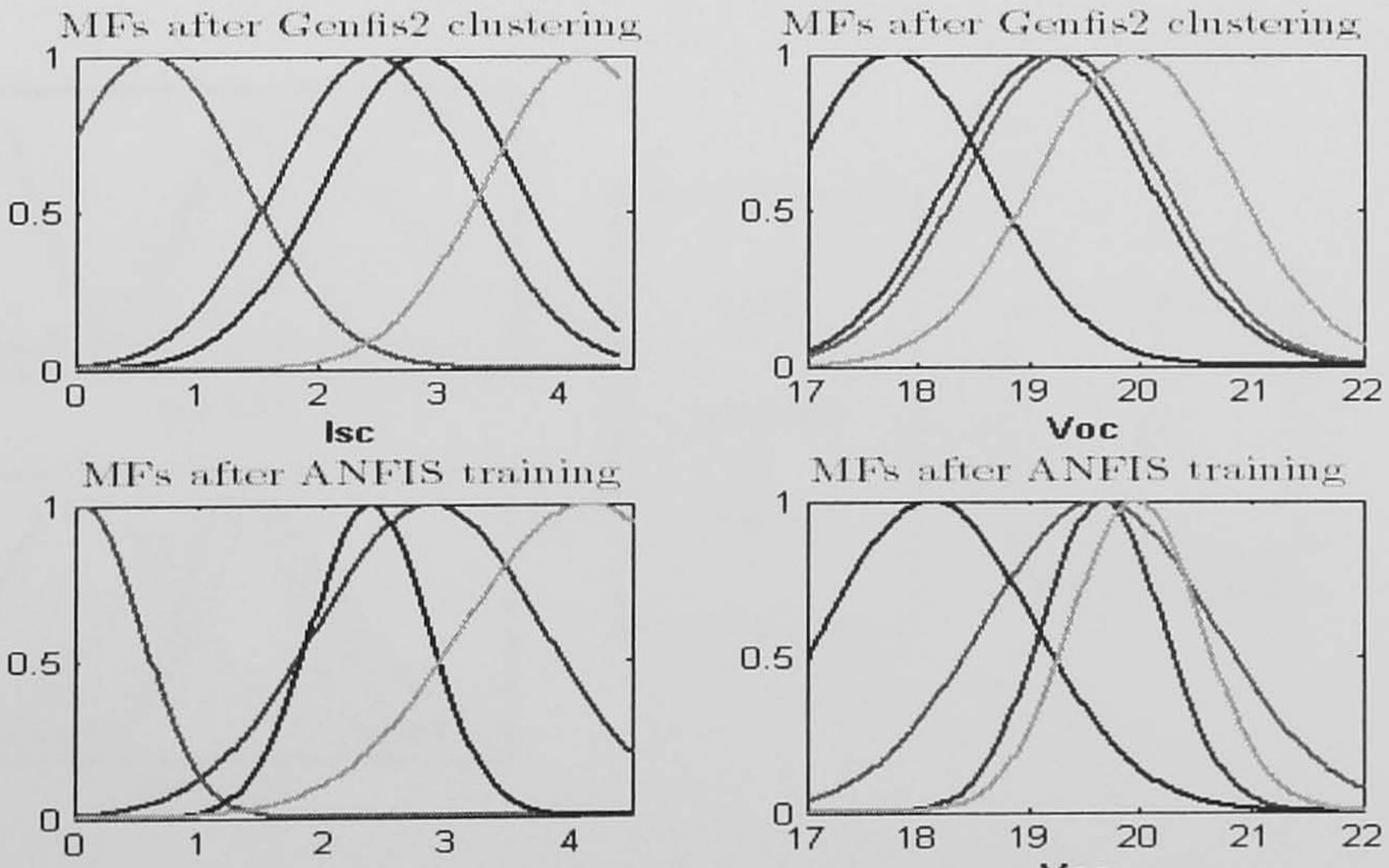

Figure 5.24: MFs of Genfis2 model for the 51W panel before and after ANFIS function training.

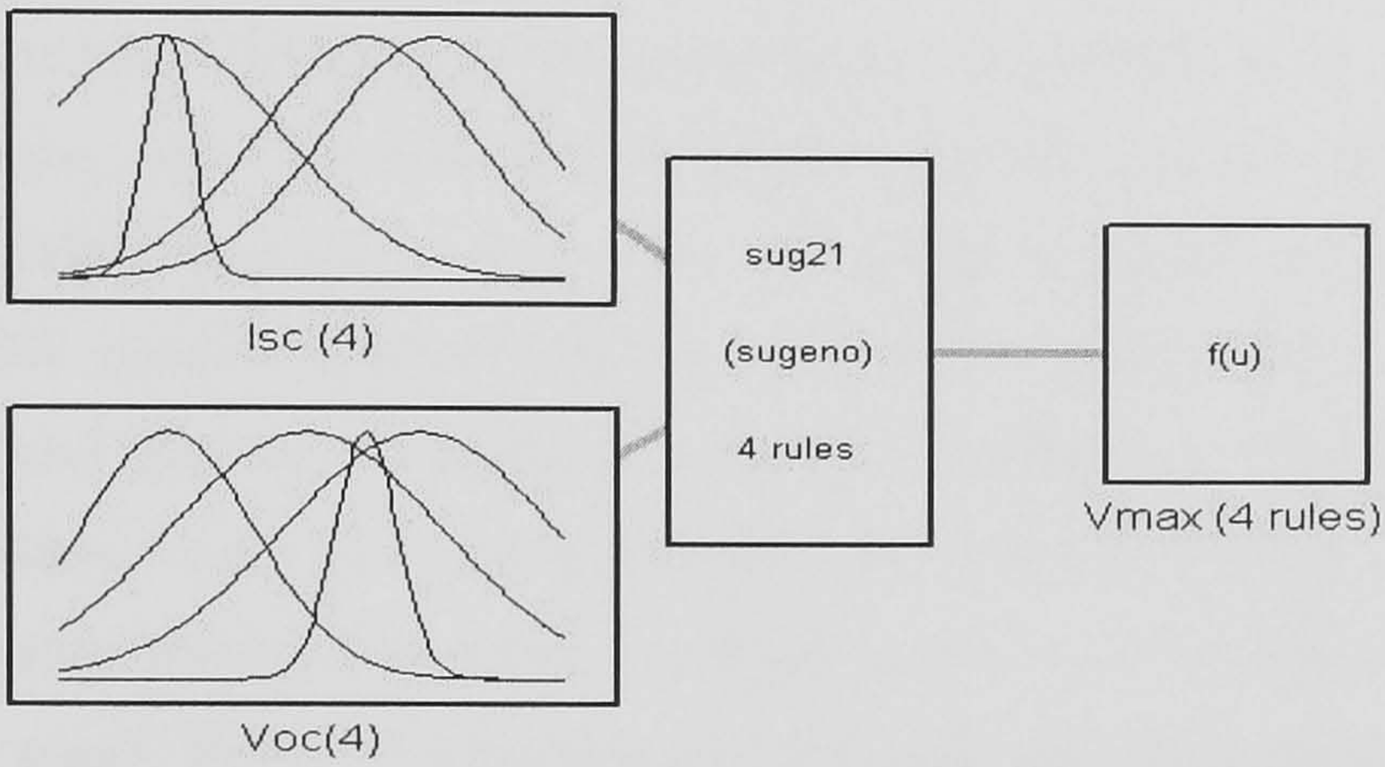

Figure 5.25: Final structure of Genfis2 ANFIS for the 85W after ANFIS function training.

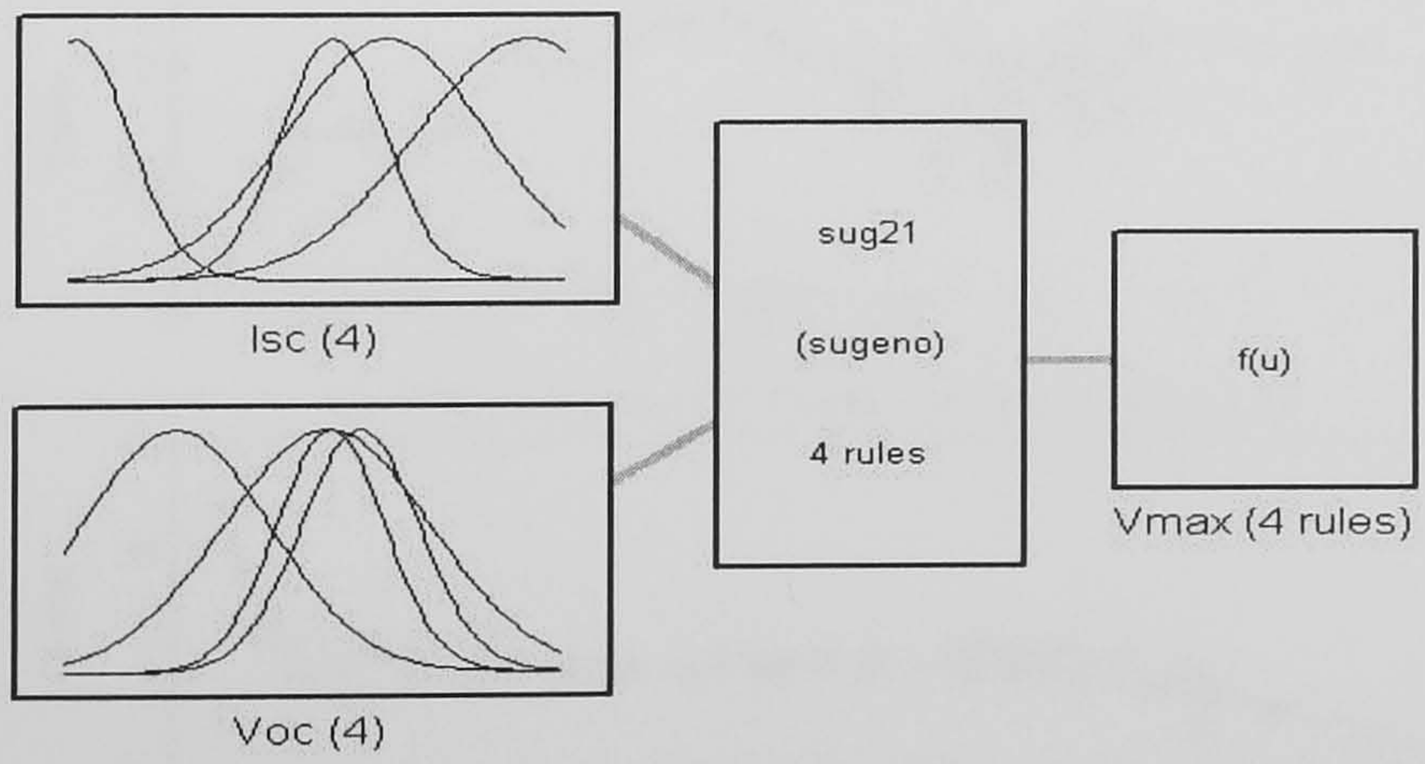

Figure 5.26: Final structure of Genfis2 ANFIS for the 51W after ANFIS function training.

performance with their own data. However, the above ANFIS models can be used only with its panel separately. To test the possibility of using the above models as a general ANFIS model, the input data of one panel is used as a test data in the ANFIS model of another panel, the RMSE becomes very high. For example, when the data of 51W panel is applied with the 85W ANFIS model the RMSE increases to 0.76. Also, the RMSE increases to 0.81 when the data of 85W panel is applied with the 51W ANFIS model. These values are very high and they are not accepted in the MPP predication. Furthermore, the high individual errors in many points that are shown in Figure 5.27 confirms the disability of using a test data of one type of PV panel on ANFIS model of other type panel. Hence, it is necessary to deal with more homogenous data to create a general ANFIS model with accepted RMSE. For generalising ANFIS model, the per-unit data can normalise the two panel data to provide a solution for the MPP predicted system generalisation. Per-Unit (pu) data provides more homogenous data, therefore it helps the cluster analysis to find the clusters that have the best relationships between input output data.

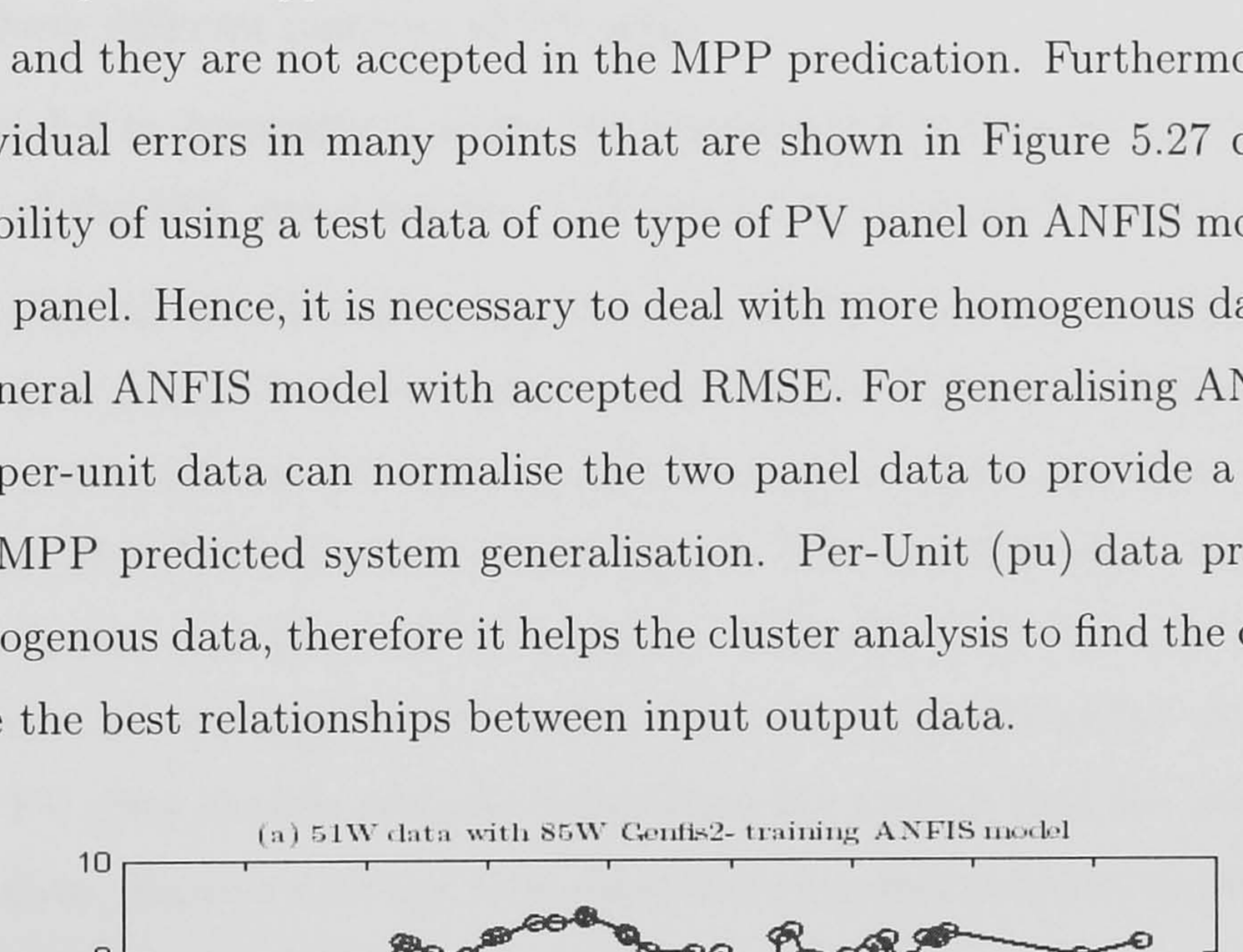

Figure 5.27: Percentage error between actual data and predicted outputs data of the two panels

5.4.4 Generalising the ANFIS models using per unit data

Single crystal PV modules and poly crystalline PV modules are the widely used PV solar systems in the market, thus, it is important to produce a general ANFIS model that can predict the MPP for these types of PV modules. Moreover, the data of 36 cells panels are used to generate the mentioned above ANFIS models, so, the general ANFIS model should be implemented for panels that can have different numbers of PV cells.

Table A.6 in Appendix A shows the normalised PU data of I_{SC}, V_{OC} and V_{max} data of the 85W panel and the 51W panel that is shown in Tables 4.3 and 4.4.

The Genfis2 model that is improved by ANFIS function is applied with per unit data using 0.5 cluster radius model. Figures 5.28 and 5.29 show the actual data and predicted PU data of ANFIS models before and after 100 training epochs of ANFIS function. Also, Figures 5.30 and 5.31 show the percentage error before and after ANFIS training. Generally, the PU data is applied to generate all training Genfis2 models that were specified earlier with real data. The PU data models perform better than the models that are generated with real data. Figures 5.30 and 5.31 show these improvements in individual errors.

As previously mentioned in this section, the ANFIS function uses a hybrid learning rule algorithm, hence, more adaptation on consequent parameters using the LSE algorithm during forward learning improves the performance of the ANFIS prediction model. However, the MFs parameters are modified by a gradient descent algorithm. The MFs parameters are assembled during the subtractive clustering by extracting a set of rules that simulate the data behaviour. Therefore, any modification within these parameters increases the error between the actual output and predicted output in one edge and decreases the error in other edge of the data as shown in Figures 5.30 and 5.31. The error in a few points at low I_{SC} is decreased and increased at high I_{SC}. To avoid this modification

5.4 Locating MPP voltage using an ANFIS model

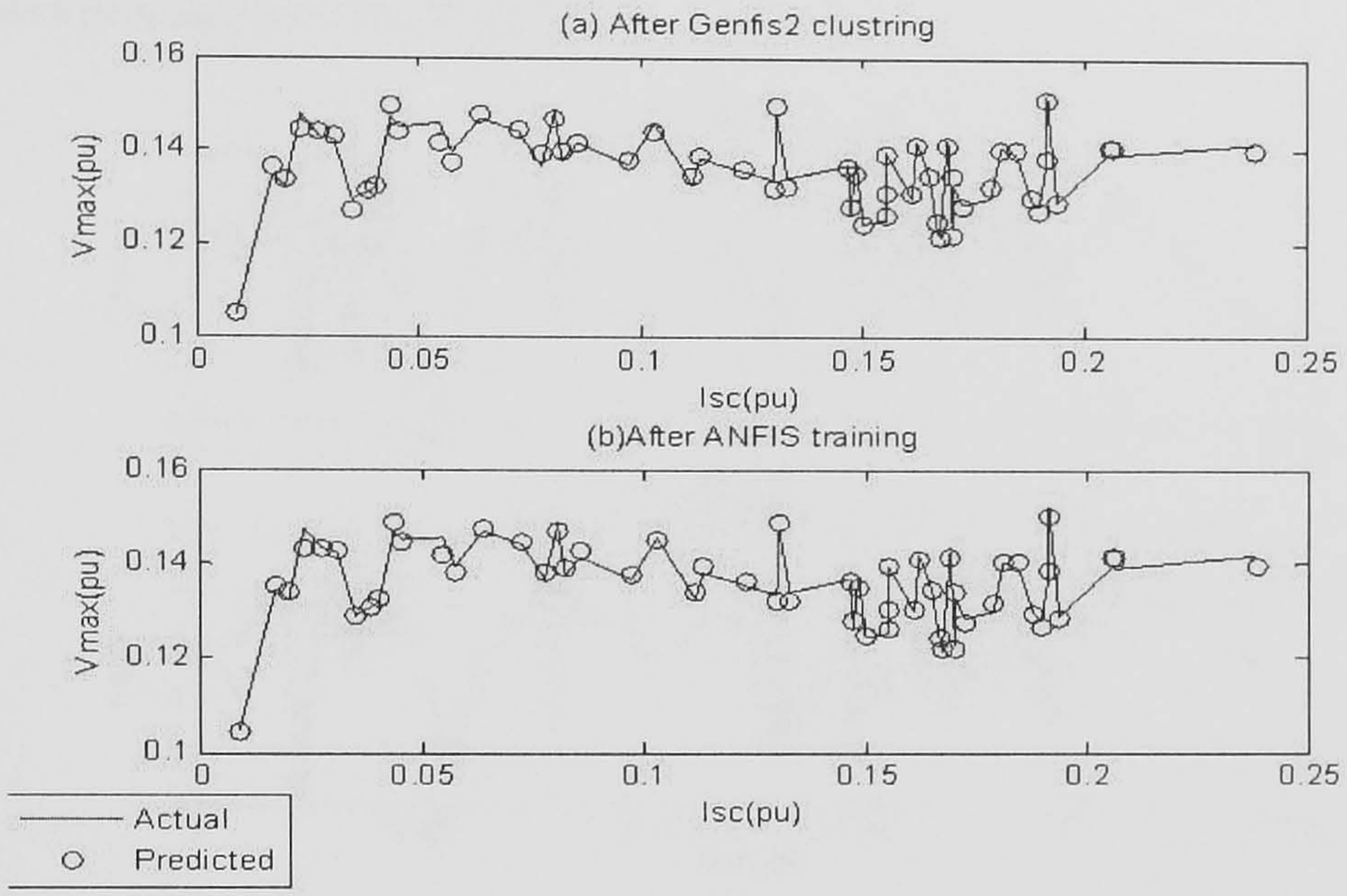

Figure 5.28: Actual data and PU predicted outputs of Genfis2 data of 85W panel before and after ANFIS function training.

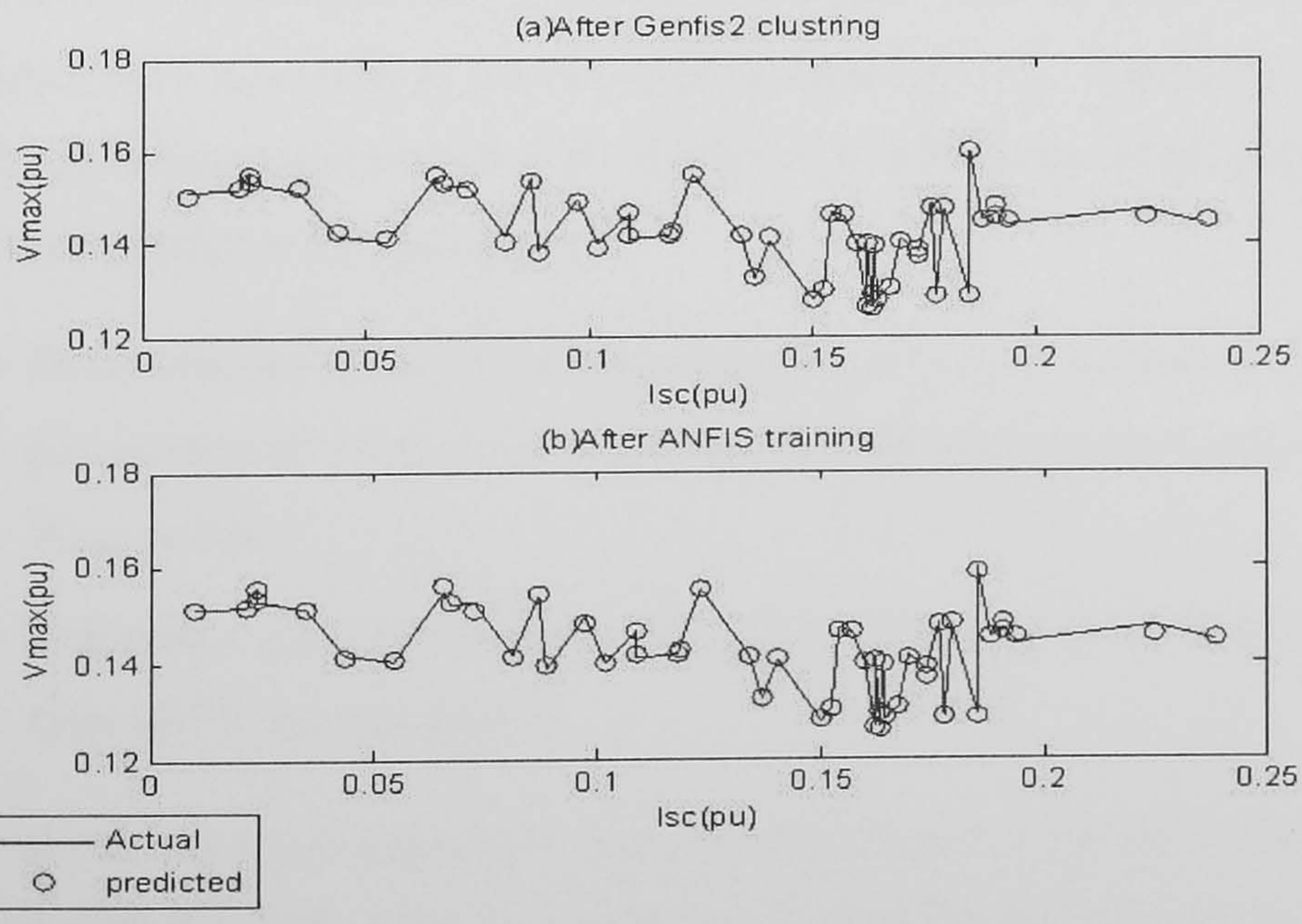

Figure 5.29: Actual data and PU predicted outputs of Genfis2 data of 51W panel before and after ANFIS function training.

in MFs parameters a very small gradient descent constant is set during the backpropagation training [45].

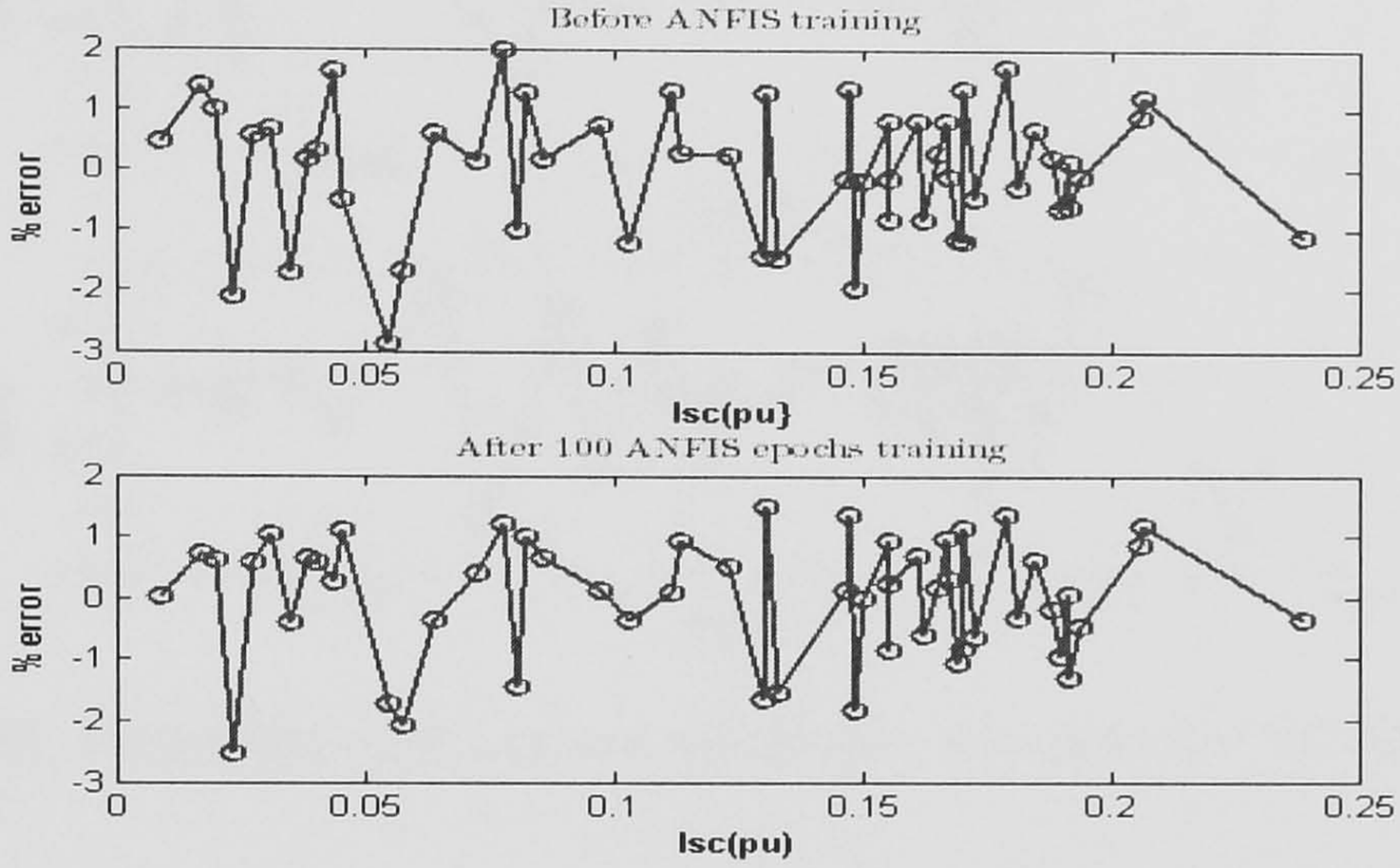

Figure 5.30: Percentage error between actual data and predicted PU outputs of the 85W panel.

Generating more clusters using a smaller radius improves the error between actual and predicted data of ANFIS models, however it decreases the associations of input MFs especially at low and high irradiance level. Generally, the clusters with big radiuses are more linked. A high linkage between large clusters of large radiuses produces two advantages:

- Decreases the effect of the actual abnormal output points on output linear parameters of rules, accordingly, the ANFIS model corrects these abnormal V_{max} points.
- Achieves a good performance, when the system is generalised for different type of PV system panels.

The above two advantages have been inferred from many models that have been tested with the 85W panel and 51W panel data. Tables A.7, A.8, A.9 and A.10 in Appendix A show part of these results.

ANFIS with a 0.5 radius predicts V_{max} with a good aspect such as:

5.4 Locating MPP voltage using an ANFIS model

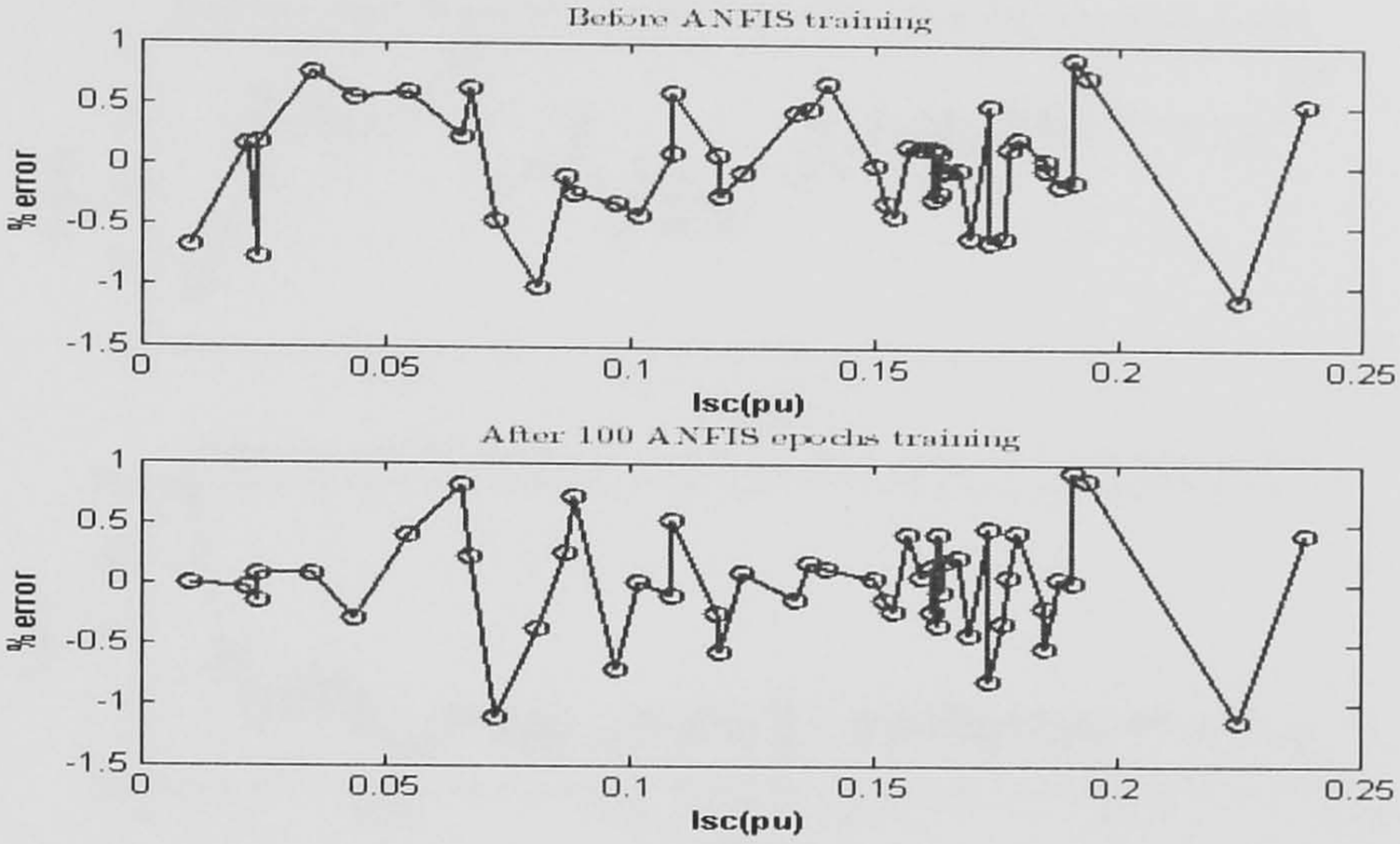

Figure 5.31: Percentage error between actual data and predicted PU outputs of the 51W panel.

- provides a small error between actual and predicted output.
- has few rules.
- corrects the abnormal data.

Figure 5.32 shows the individual voltage errors between actual data and predicted PU outputs, when the ANFIS model is used to predict the V_{max} of other PV panel. The 85W panel ANFIS model gives lower errors than the 51W ANFIS model. The predicted PU output data errors are around 2% in of 51W panel data using the 85W ANFIS model when the abnormal points are neglected. However, the predicated PU data error of 85W panel is more than 5% using the 51W panel model. The ANFIS models are improved with few numbers of epochs, but the individual errors remained around 5%. Whereas, the 85W ANFIS models are improved with very low gradient descent constant to prevent the modification in MFs and applied the LSE improving in output parameters. Figure 5.33 shows these improvements at different training epochs. However, after high modifications in input MFs by increasing the number of epochs, the performance of the model is improved at low I_{SC} (low irradiance level) and the error increases at high irradiance with 100 training epochs as

5.4 Locating MPP voltage using an ANFIS model

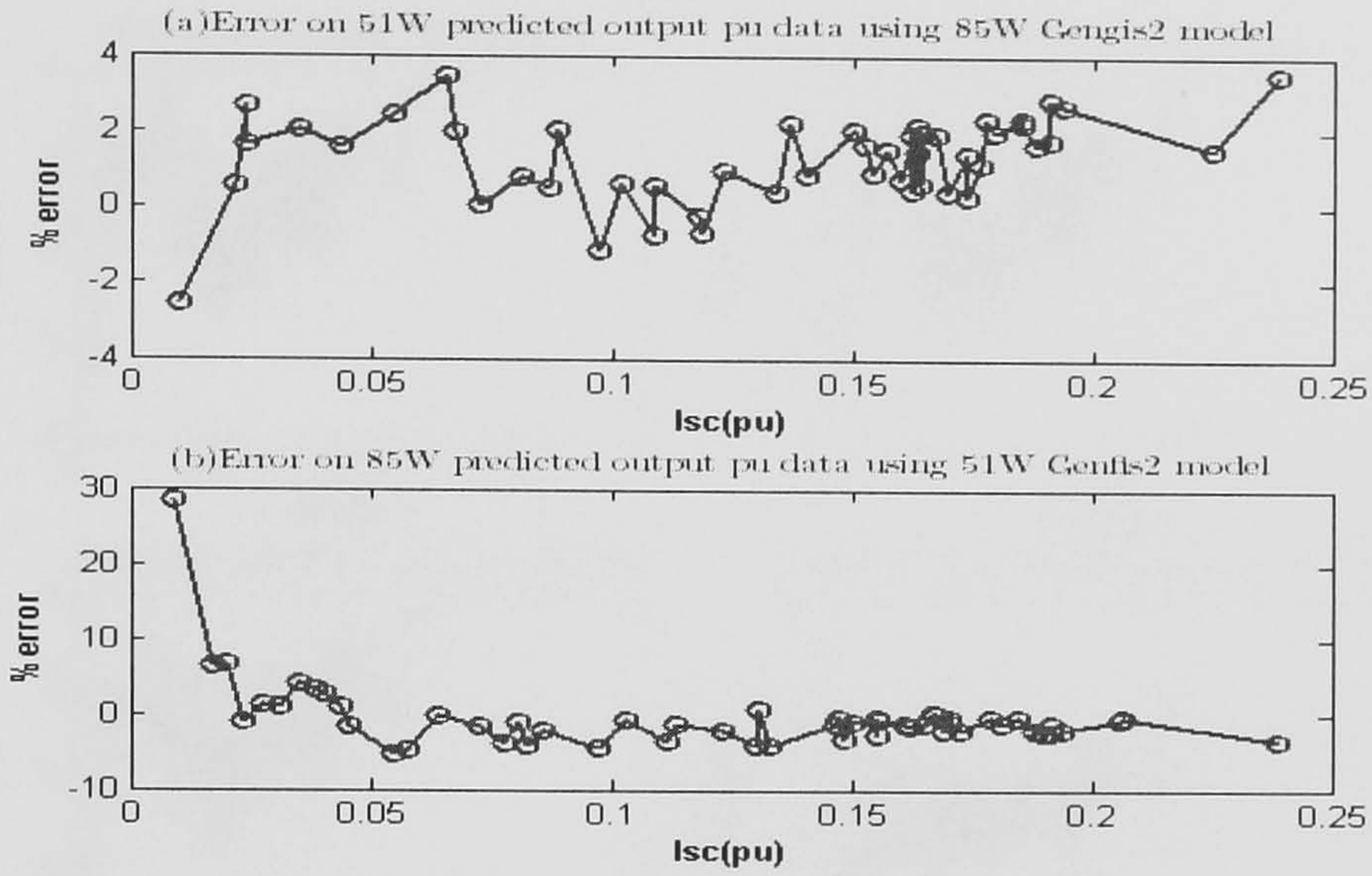

Figure 5.32: Percentage error between actual data and predicted PU outputs data of two panels

shown in Figure 5.33. This unsteadiness in the performance is due to high modifications occurred in input MFs as shown in Figure 5.34.

The 85W panel Genfis2 model with a 0.5 radius is improved after only 5 training epochs of ANFIS function. When this model is tested with PU data of 85W panel, the output predicted data is found with less than 2% error. Moreover, this error is roughly 2% for all normal PU predicted data of 51W panel as shown in Figure 5.35.Therefore, this ANFIS model can be use as general model for these two types of PV panels.

Generalising the ANFIS models for PV systems

The previous model can be generalised for the two tested 36 cells panel. However, the PV system can include panels which have different numbers of single crystal or polycrystalline PV cells. In addition, the PV systems mostly have more than one series or parallel panels. Therefore, the general ANFIS model is modified to deal with irradiance level instead of the I_{SC} to avoid the diversity of I_{SC} for different PV cell areas. In addition, the system should transact with

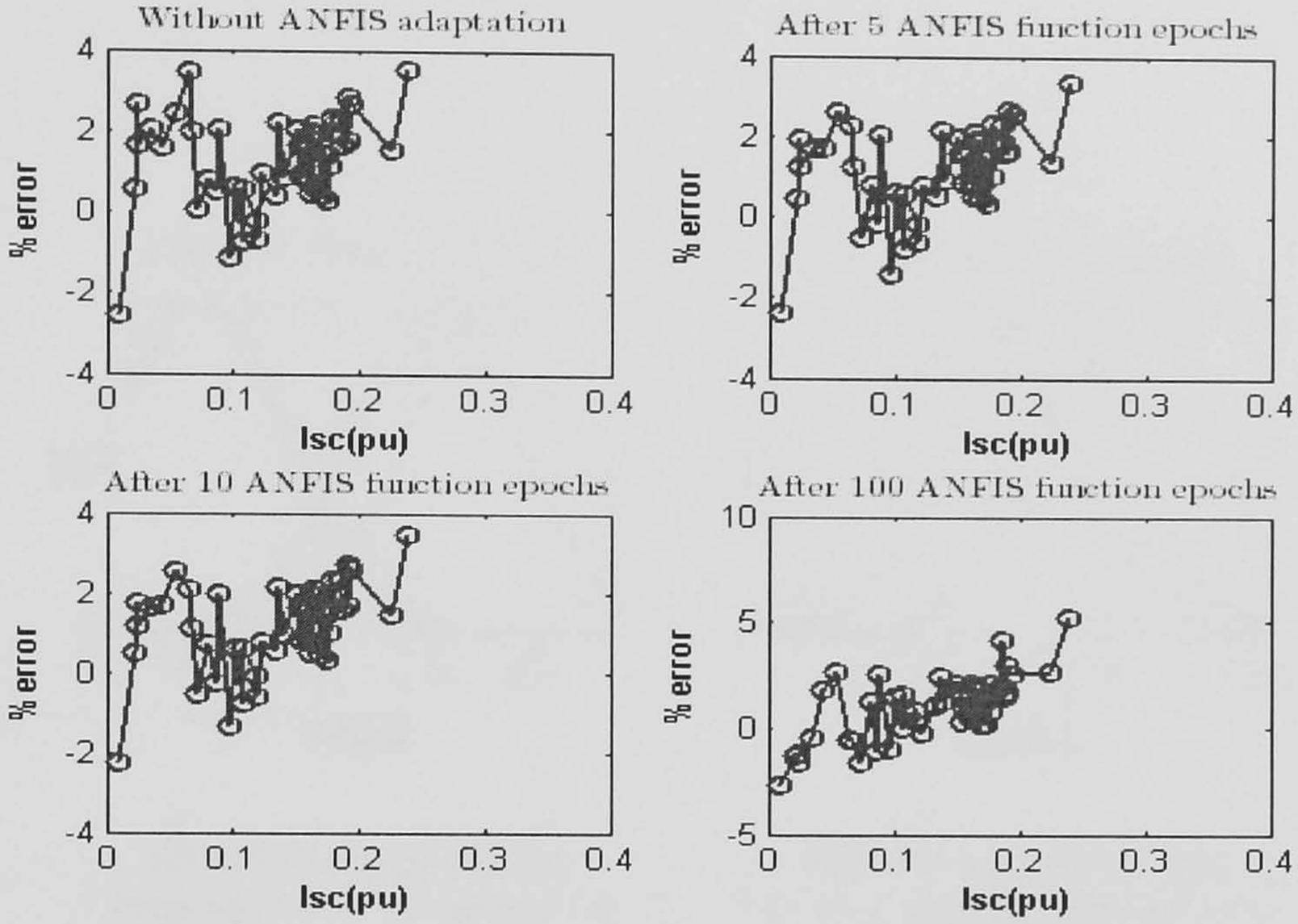

Figure 5.33: Percentage error of PU output data of the 51W panel using 85W panel ANFIS model.

only one PV cell instead of 36 cells. Hence, the learning data will be combined to provide more and common data for the general ANFIS model. To join the tested data and make it more useful in all PV systems, the following three procedures are applied.

- The open circuit voltage and V_{max} are divided by 36 to handle the voltage of one PV cell.
- The short circuit current of PV panels is divided by the short circuit current at standard test conditions. The result gives the fraction of irradiance level from 1000W/m^2.
- A per unit data is computed for the new standardised data.

The Genfis2 function is used with whole data to generate the Genfis2 model. The Genfis2 model is improved with different training epochs of ANFIS function. The model that was trained by 20 epochs is selected from different models according to minimum average absolute error. Figure 5.36 shows the actual and

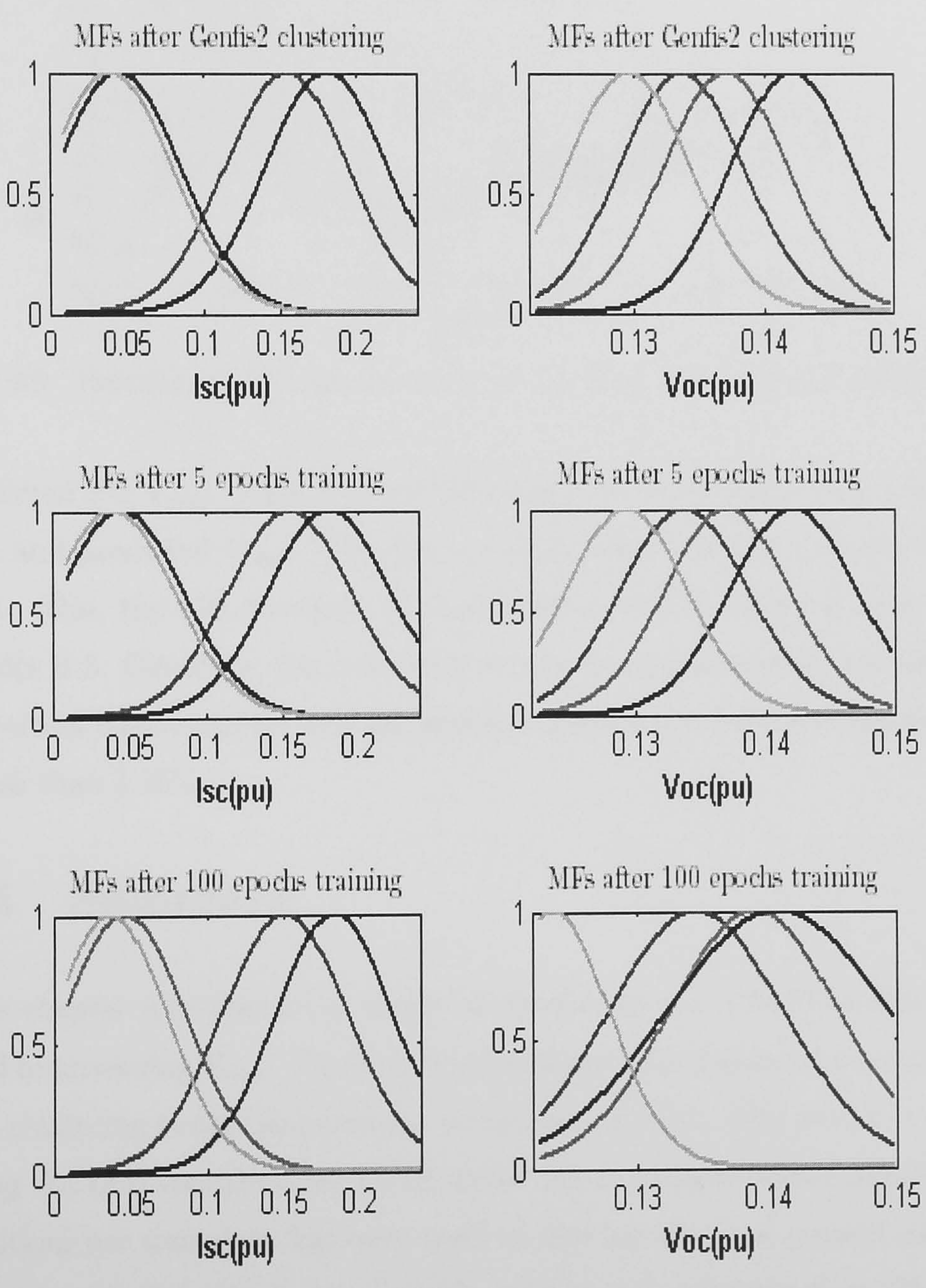

Figure 5.34: MFs of the 85W Genfis2 PU models before and after ANFIS function training.

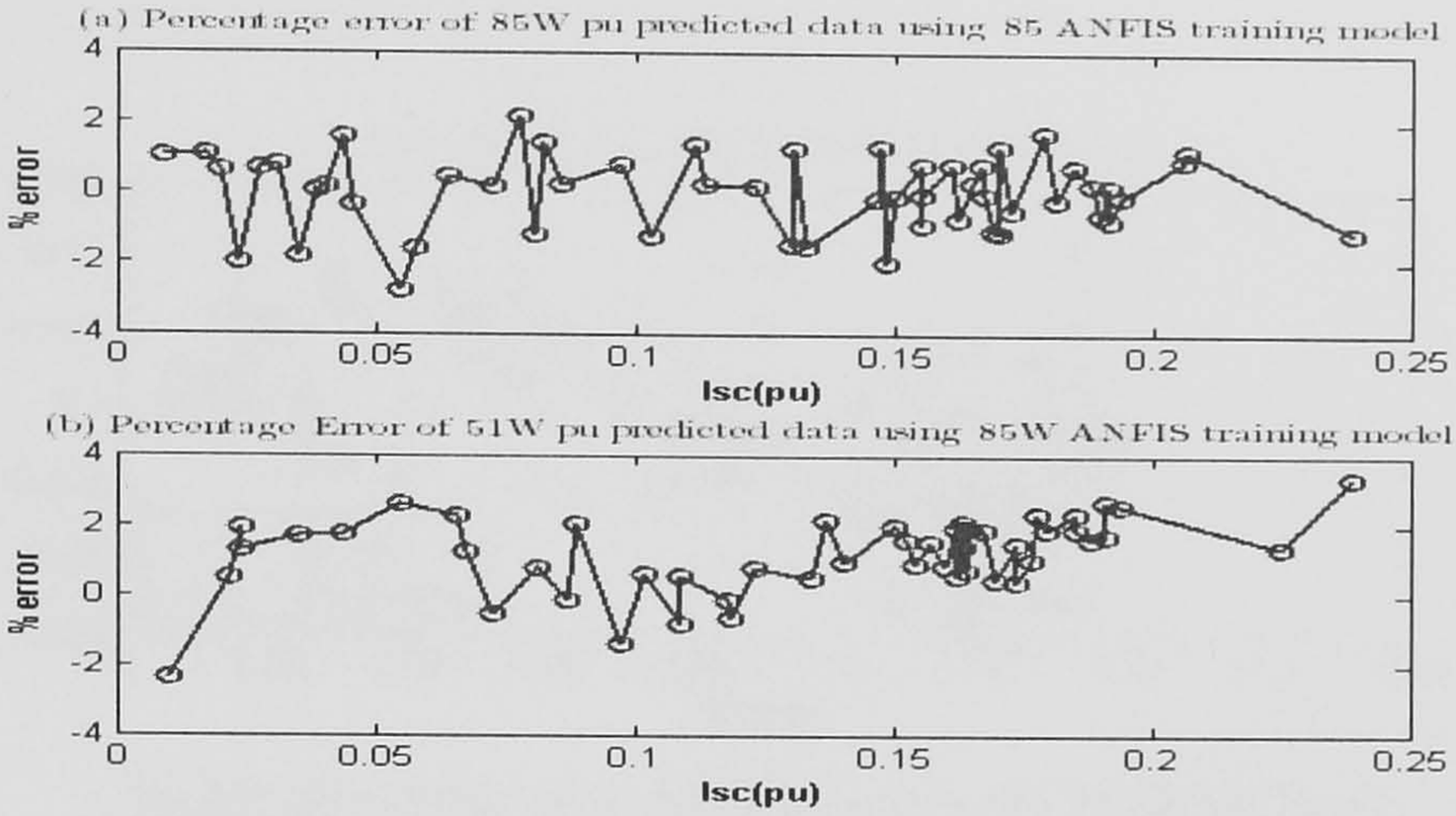

Figure 5.35: Percentage PU output error of the final 85W panel ANFIS training model.

predicted PU V_{max}. Also, Figure 5.36 shows the percentage error between actual and predicted V_{max}. The final general ANFIS model is shown in Figure 5.37. Also, the FIS structure of final general ANFIS model is shown in Appendix B.3. Generally, the individual errors are approximately less than 2% in all testing points and the average absolute percentage error is computed, which is less than 1.25%.

5.5 Summary

This chapter introduced the stages of developing the ANFIS models that are used in predicting V_{max}. The final developed model is obtained by using subtractive clustering to set the nonlinear parameters of MFs. This model is improved using the LSE algorithm modification for the consequent linear parameters. In addition, per unit data has been used to develop the final general model that is used with different types of single crystal and polycrystalline PV system. Furthermore, the final ANFIS model is tested with different types of PV panels and different data in chapter 7. In chapter 6 the predicted voltage V_{max} is used as input for FLC. The FLC will be designed to track the maximum power point of PV system.

5.5 Summary

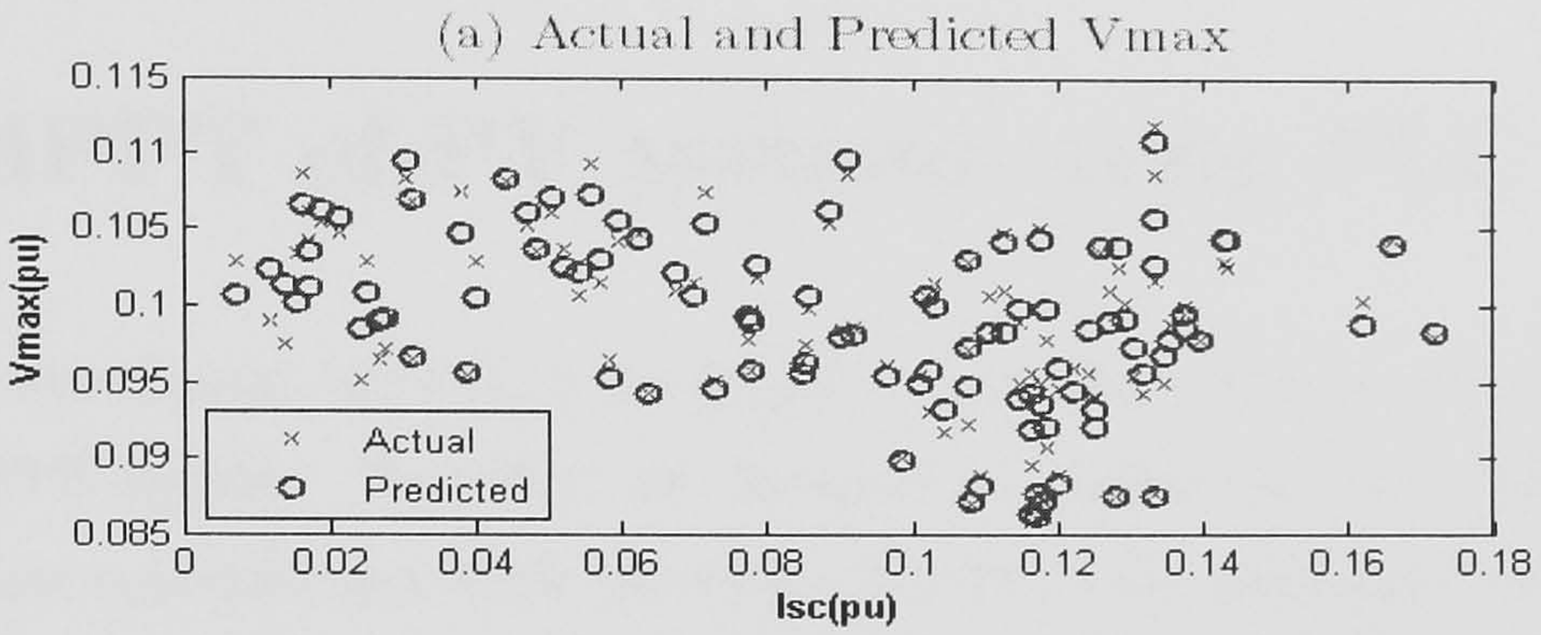

Figure 5.36: Relation between actual data and predicted output of final general ANFIS model

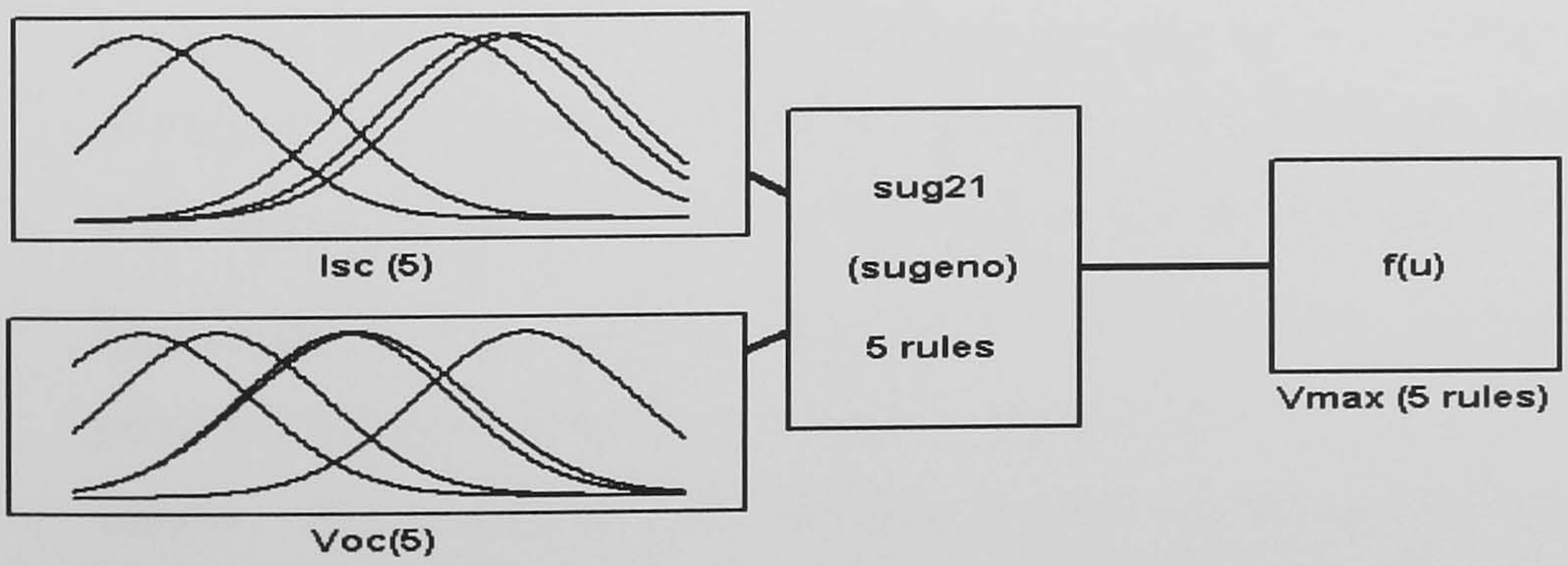

Figure 5.37: ANFIS system of general model

Chapter 6

MPPT of PV systems using FLC

In this chapter the FLC is developed to solve the problems that face the PV MPPT system. Two FLC are designed to control the duty cycle of Buck-Boost converter and Buck converter. The FLCs are generalised for all type of single crystal and poly crystalline PV panels. These two FLCs are designed for different types of load.

6.1 Introduction

The high percentage error between actual MPP parameters and estimated parameters of MPP in many proposed techniques is caused either by the shortage of data used for locating MPP parameters, or by the weakness of techniques that are implemented to find out these parameters. The ANFIS models that are developed in chapter 5 provide a solution for the high errors between predicted and actual V_{max} in other approaches.

The developed MPPT system includes three main parts: the ANFIS model, the FLC, and the DC-DC converter that can be adjusted by a square pulse signal of Pulse Width Modulation (PWM). The FLC with predicted ANFIS outputs is an off-line approach, which is described by the block diagram in Figure 6.1

The predicted V_{max} from the developed ANFIS model is used as a reference point for the FLC. The FLC is used to control the duty cycle of DC-DC converters. The output of FLC controls the rate of change in duration time of electrical square pulse which is generated by PWM. This pulse controls the duty cycle of the electronic switch of the DC-DC converter until the input voltage of converter tracks the predicted V_{max}. The developed FLC is designed to

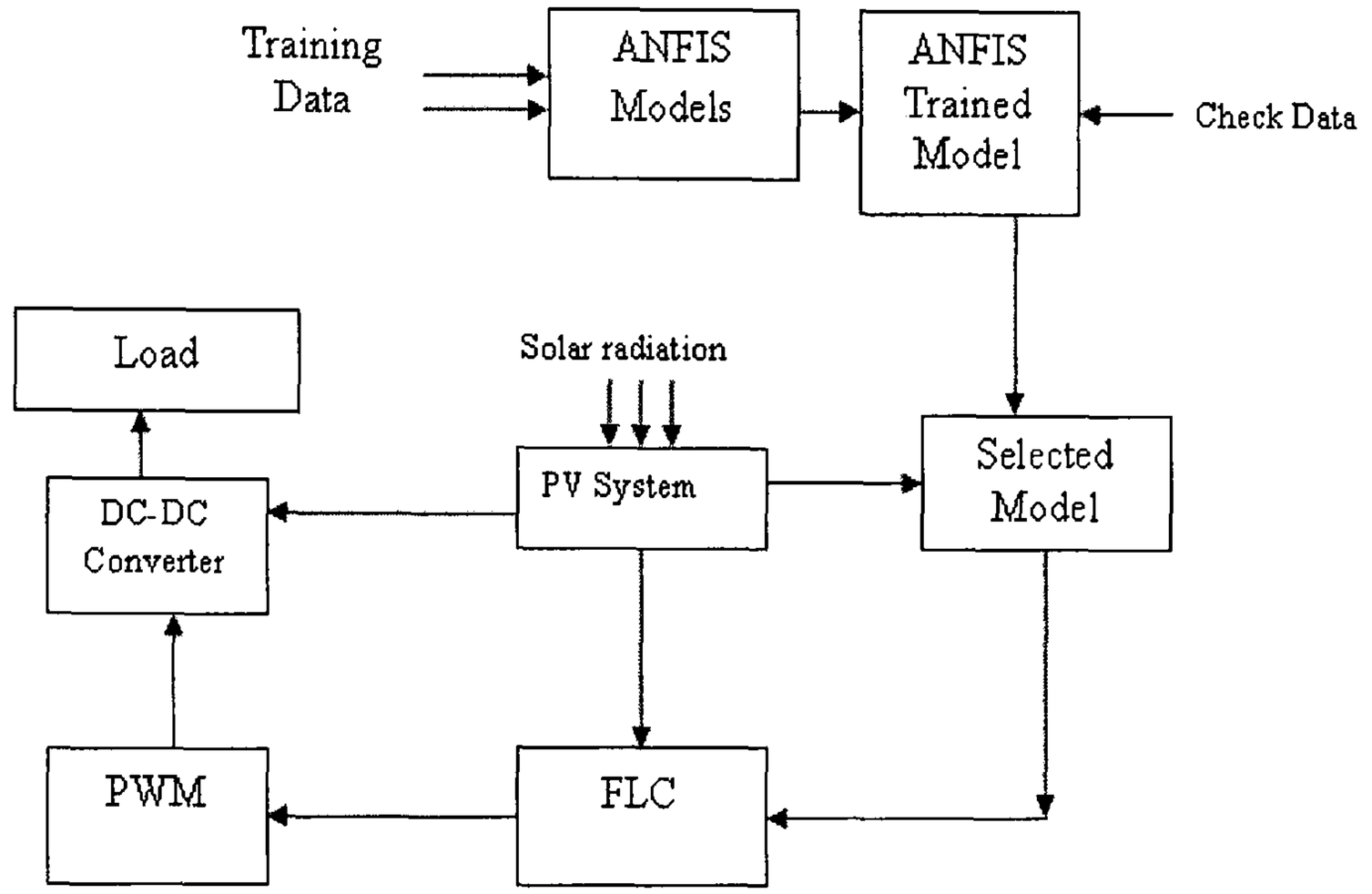

Figure 6.1: Proposed system architecture

overcome the problems in the conventional controllers and other methods based on artificial intelligence. Moreover, the developed MPPT system with the FLC is designed to balance different requisite features such as quick tracking under different environmental conditions, high accuracy, stability, simplicity, low cost, and high efficiency. The FLC is designed to achieve a good performance in different environmental conditions, different types of load, and different types of DC-DC converters.

6.2 Maximum power point tracking problems

The maximum power point tracking techniques are applied to extract maximum available power from the PV systems in different environmental conditions with different types of load. DC-DC converters are used to match the maximum power point of PV systems with different loads. The huge changes in the environmental conditions, different shapes of load line and the nonlin-

earity between duty cycle and voltage ratio of most types of converters are the problems that should be treated in MPPT systems. In this section these problems are addressed in detail.

6.2.1 Problems related to environmental conditions

Maximum power point changes on I-V curves due to any small changes in environmental conditions. These changes in environmental conditions affects the irradiance level and PV cell temperature and consequently I_{SC} and V_{OC}. Due to a fast and accurate measurment of the I_{SC} and V_{OC} the ANFIS model can predict V_{max} for any modification in these parameters. Hence, under huge changes of environmental conditions, the values of V_{max} provided from ANFIS model change quickly, which causes a rapid changes in the electrical pulse that controls the duty cycle of the electronic switch of DC-DC converter. Fast changes in the duty cycle reduce the life time of the electronic devices and generate undesirable harmonics. Three environmental influences have been detected during field data collection: wind movements, fast changes in I_{SC} and V_{OC} during cloudy conditions and sudden changes in the irradiance level.

Typically, wind affects the surface temperature of the PV cells, which increases the heat convection factor that helps in increasing the heat dissipation from the PV cells to surroundings. This improvement in heat convection due to the increase in wind speed decreases PV cell temperatures, which leads to increased V_{OC} and V_{max}. When the wind changes slightly, V_{OC} and V_{max} change slightly within a small range. Mostly, a small change in V_{max} is less than 0.3V for a short time. The drop off in generated power is roughly 1% for 0.3V deviation in V_{max} values as discussed in chapter 4. Therefore, to avoid the continuous oscillation in FLC system by wind, the FLC is designed to prevent this continuous oscillation as will be explained in section 6.3.

In addition, the short circuit current changes continuously on cloudy days. Occasionally, clouds become wobbly and dark and as a result, the irradiance

fluctuates at a low level. Hence, I_{SC} changes continuously, and consequently the V_{max}. This causes an oscillation in the MPPT system. As a result of low generated power and low percentage power losses at the low irradiance level, a higher deviation in V_{max} value can be accepted in the designing of FLC at low I_{SC} to prevent the high oscillation in cloudy time.

6.2.2 Problems related to types of load

The type of load strongly affects the range of operating point on I-V curves, as discussed in chapter 2. Generally, a battery load has a constant voltage which varies within a small range, whereas the resistive loads drive the PV panel to operate in wide interval on I-V curves as shown in Figure 2.5. The resistive load voltage is linearly dependant on the output current of the PV panels. Therefore, when the irradiance level is decreased or increased suddenly during partial cloud, the output voltage varies within a wide range. Hence, it can exceed 15V in 36 cells PV panels. On the other hand, the battery voltage depends slightly on the PV current due to the low internal resistance of batteries. The battery voltage changes roughly from 1V to 2.5V above 12V during charge time. These divergences in operating voltage due to the different load types affect the required change of duty cycle of DC-DC converter switch.

6.2.3 Problems related to DC-DC converters.

Three types of converter can be used to match PV system with different types of load: step up converter, step down converter, and dual (step up/ step down) converter. These three types were described in chapter 2. Two problems face the FLC, which are related to DC-DC converters:

- Type of the interface DC-DC converter that is needed between the load and the PV system.

- The nonlinear relationship between the change in duty cycle of the DC-DC converter and the load voltage ratio parameters.

For the applications that need either a step down or step up converter it is more efficient to use the Buck converter or the Boost converter respectively. The reason for that is the high efficiency of these two converters as mentioned in section 2.2. The Buck-Boost converter is hardly 2 or 3% lower than the buck and boost converters. However, most PV system applications need a Buck-Boost converter which is used for step up/step down the voltage of the PV system to match the V_{max} and V_O of the Buck-Boost converter.

Figure 6.2 shows the three converters that were described in section 2.2. Due to the linear relationship between duty cycle and the voltage ratio, it is easy to determine the change in duty ratio that produces 1V change in input or output voltage of the Buck converter. The difficulty encountered is computing of the change that is required in the duty cycle to produce 1V change in either V_O or V_{in} of the Boost converter and the Buck-Boost converter. This difficulty is caused by a nonlinear relationship between duty cycle and voltage ratio.

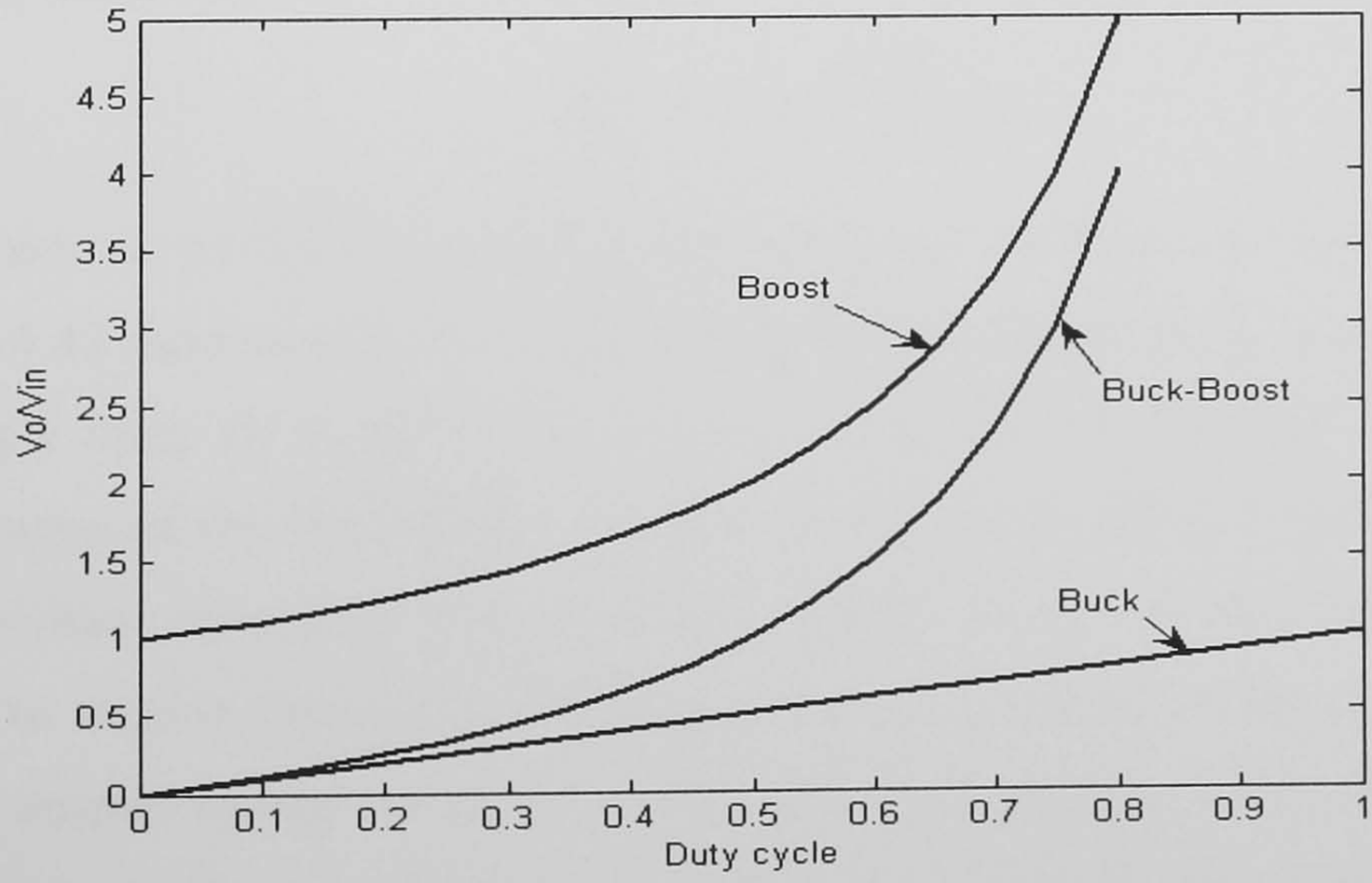

Figure 6.2: Relationship between duty cycle and voltage ratio of three types of converters

6.2 Maximum power point tracking problems

Most applications require both step-down and step-up converters at the same time. Therefore, the relationship between duty cycle and voltage ratio of the Buck-Boost converter should be analysed to establish the FLC design requirements for different load types.

To keep the input voltage of the Buck-Boost converter at the maximum power point voltage, the input voltage should be adjusted when the predicted V_{max} is changed by the variations in environmental conditions. In addition, the input voltage of the Buck-Boost converter can deviate from the value of V_{max} when the output load voltage is changed. Therefore, it is essential to study the relationship between the rate of change of duty cycle and V_{in} to help in the FLC design .

Referring to the Equation 2.17, the relationship between duty cycle and V_{in} can be derived as in Equation 6.1:

$$D = \frac{Vo}{(Vo + Vin)} \tag{6.1}$$

In addition, the rate of change of duty cycle in terms of V_{in} can be derived as in Equation 6.2:

$$\frac{\partial D}{\partial V_{in}} = \frac{-Vo}{(Vo + Vin)^2} \tag{6.2}$$

In reference to the Equation 6.2, the subfigures on Figure 6.3 and Tables A.11 and A.12 show how the duty cycle changes with respect to V_{in} when V_O changes steeply from 1V to 22V. Also, Figure 6.4 shows the standard input voltage operation of the Buck-Boost converter according to effect of resistive loads on PV voltage operation. The input and output voltage can vary from 8V to 18V due to sudden changes in irradiance level as discussed earlier in this section. The output voltage range shown in Figure 6.4, clarifies a low effect of V_O on the duty cycle. In addition, a high effect of V_{in} on the duty cycle observed in Figure 6.4. For example, when the Buck-Boost converter operates at Vin=12, the rate of change in duty cycle that is required to increase or decrease the V_{in}

by 1V is roughly 50% more than the rate of change of duty cycle at Vin= 18V. Furthermore, it is observed from Figure 6.3, the output voltage has insignificant effect on ΔD when V_O changes from 6V to 18V. It is necessary to take these dissimilar variations into consideration the $\frac{dD}{dVin}$ in when MFs and rules of FLC are designed to avoid low tracking rate or overshooting that can lead to an unstable MPPT system.

The load drives the output voltage of the converter, and consequently the input voltage of the DC-DC converter. This process occurs before adjusting the duty cycle of the electronic switch of the DC-DC converter. In addition, V_{in} varies due to changes in the PV output voltage, which is affected by environmental conditions. The duty cycle of the converter has been adjusted to track maximum power point voltage as a result of different load values and huge changes in environmental conditions.

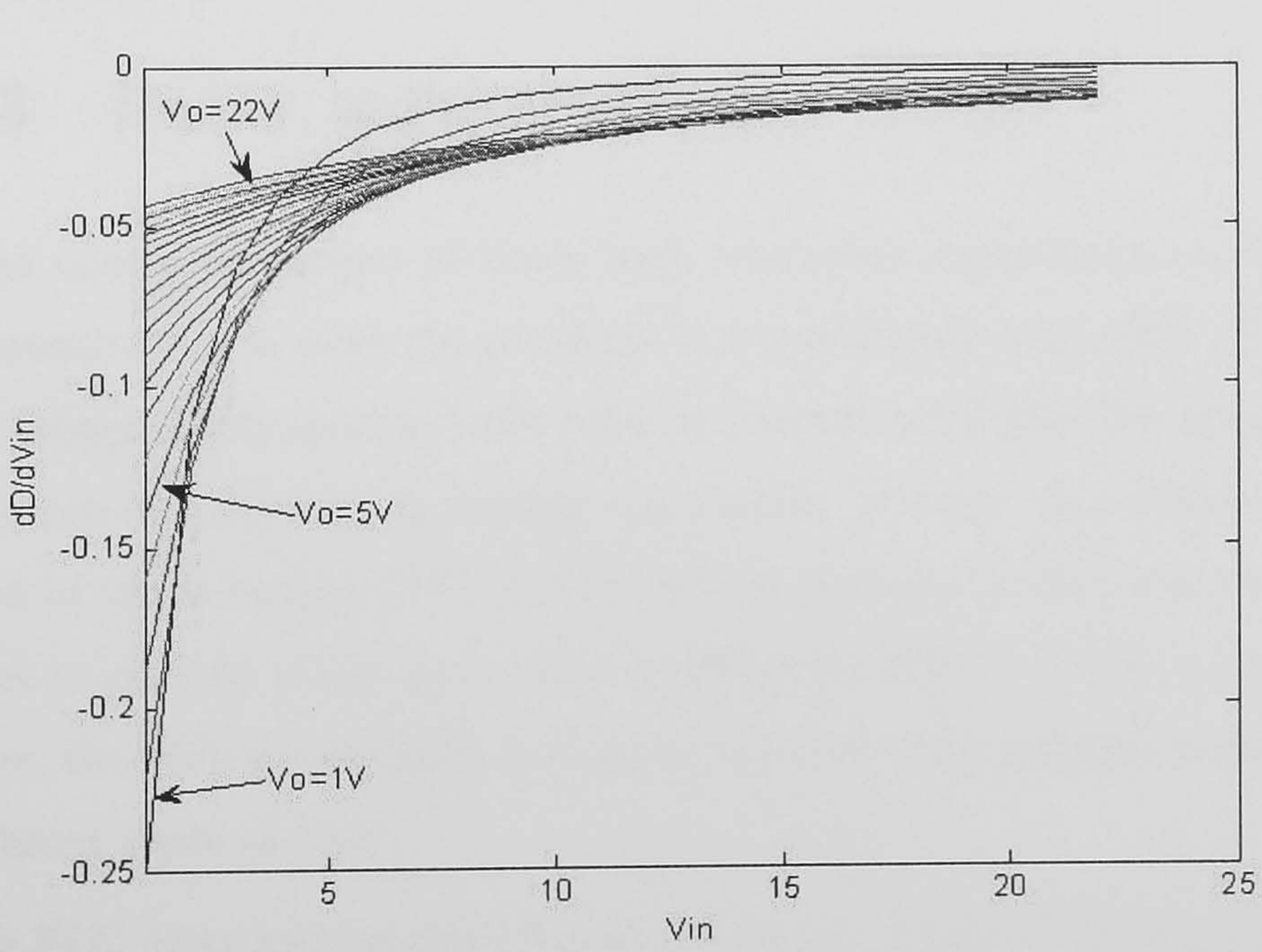

Figure 6.3: Rate of change of the duty cycle with respect to V_{in} changes within wide range of V_O

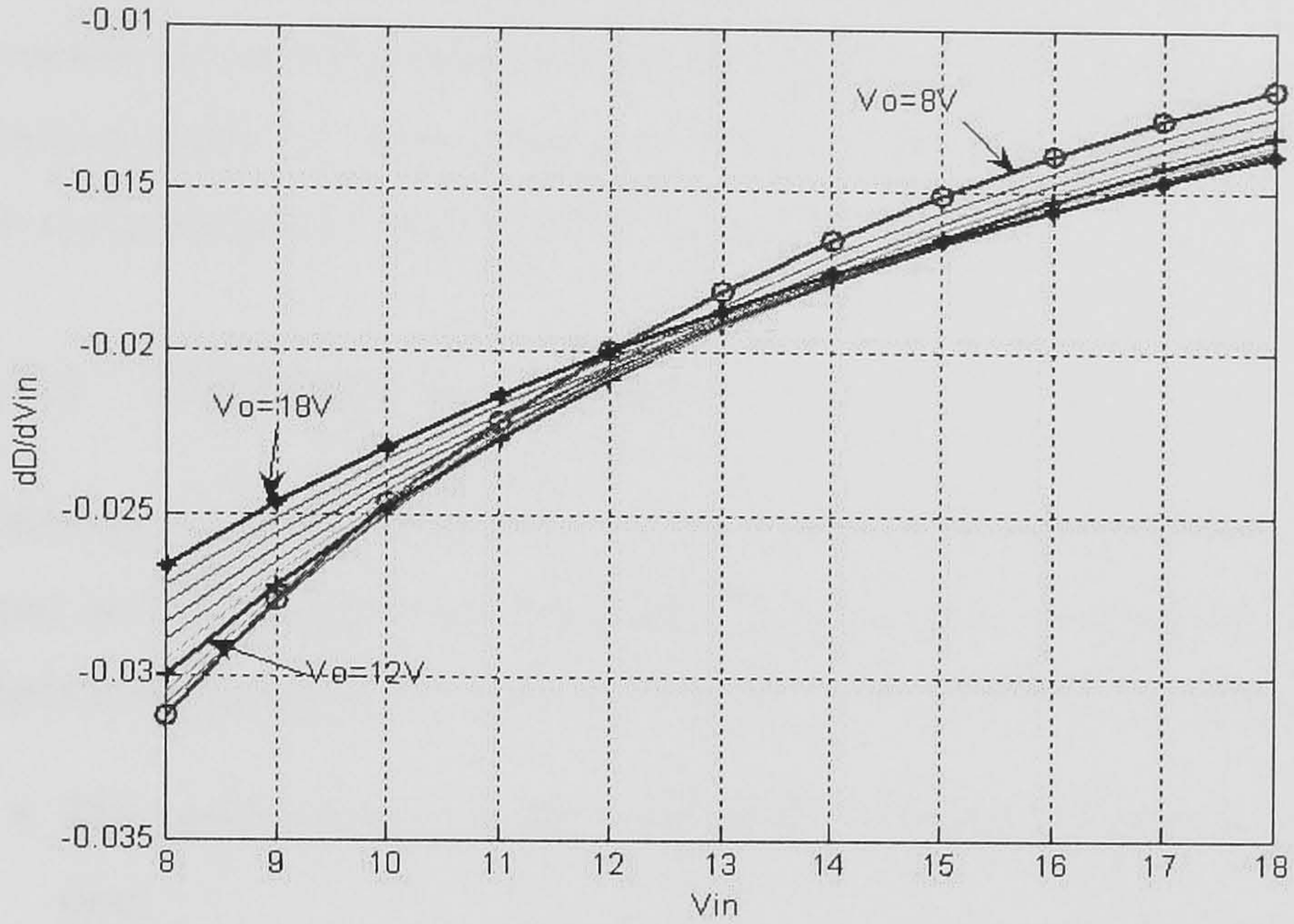

Figure 6.4: Rate of change of the duty cycle with respect to the V_{in} changes within limited range of V_O

6.3 Fuzzy logic controller design

Most control strategies of fuzzy logic controller concentrate on designing the inference rules to solve the problems in conventional controllers. The MFs that are designed incorporate with rules to provide a solution for several problems that can be solved by increasing the number of rules. In addition, the boundaries of input output MFs of FLC will be designed with minimum number of rules to provide a fast and stable tracking for MPPT of PV system. Furthermore, the MFs are designed to help on tracking the maximum power point with different types of load.

The FLC rules and membership functions are designed to face the changes in weather condition problems as a result to avoid the system fluctuation due to a small deviation of V_{max}. In addition, the MFs are modified related to the rate of changes in duty cycle of Buck-Boost converter and Buck converter at different input voltage.

The MFs are designed taking into account the behaviour of the PV panels at a variety of environmental conditions. Moreover, the developed FLC can be adjusted easily to control the duty cycle of DC-DC converters depending on the requirements of each DC-DC converter.

6.3.1 Parameters of FLC

Referring to the problems that are related to the environmental conditions, load types and DC-DC converter discussed in section 6.2, the input parameters are selected to recognise the behaviour of all parts of MPPT system as follow:

- The predicted V_{max} is the main parameter that denotes to the MPP position.
- I_{SC} is utilised to recognise the irradiance level and the amount of power that can be generated from the PV panels.
- V_{in} of the DC-DC converter indicates the operating point on the I-V curves of PV panels. It specifies the load effect on the operating point before the tracking process.

The input and output of FLC are selected carefully to give sufficient and simple information for FLC. The input voltage of DC-DC converters, and the predicted output of ANFIS model V_{max} are used to detect the deflection of operating point on the I-V curves from V_{max} . Accordingly, the first input of the FLC is Δ V which is calculated from Equation 6.3:

$$\Delta V = V_{in} - V_{max} \tag{6.3}$$

The second input is the values of I_{SC}, which represents the irradiance level. The output parameter of the FLC is the rate of change in the duty cycle dD.

6.3.2 FLC rules and membership functions

The Mamdani method is used in the FLC with max-min composition. This method is applied because it gives a steadiness response in control system and their ability to yield good results with reasonably simple mathematical operations [58] [54] [79]. The centre of area method gives a balance between the different rules outputs which generates a smooth movement towards the target [79] [18].

The generalised bell membership function is used in the fuzzy inference system. Bell membership functions are used for two important points:

- For smoothness and concise notation [58].
- The bell membership function has one more parameter than the Gaussian membership function, therefore it can approach a non-fuzzy set if the free parameter is tuned [58]. Hence, in the specific range a definite output is required with respect to a selected input, accordingly bell membership can give sufficient horizontal range with MF equals one [47].

The grid partition, tree partition and scatter partition are the main methods of partitioning input spaces to form the antecedents of fuzzy rules. The tree partition relieves the problem of an exponential number of rules. The scatter partition covers a subset of the whole input space. The grid partition is the main partition that is chosen for controller systems [39] [79]. Therefore, grid partition will be used in FLC in developed MPPT system.

As shown in Table 6.1 seven fuzzy MFs levels are chosen to control the first input variable ΔV of the fuzzy controller and only three fuzzy levels are chosen for controlling the second input variable I_{SC}. Also, seven levels are chosen for the output variable dD.

Table 6.1: MFs levels of input and output parameters of FLC

MFs of input ΔV		MFs of input I_{SC}		MFs of output dD	
NB	Negative Big	L	Low	NB	Negative Big
NM	Negative Medium	M	Medium	NM	Negative Medium
NS	Negative Small	H	High	NS	Negative Small
Z	Zero			Z	Zero
PS	Positive Small			PS	Positive Small
PM	Positive Medium			PM	Positive Medium
PB	Positive Big			PB	Positive Big

6.3.3 Fuzzy logic controller for Buck-Boost converter

To overcome the problems that have been recognised in the previous section, two methods can be suggested for FLC design. The first method is to increase the number of rules to provide the appropriate decision for each problem. Consequently, this leads to more rules, as a result more complicated control system. The second method is by design of the MFs that are incorporated with rules to provide a solution for the problems that can be solved by increasing the number of rules.

Handling the problems of environmental conditions

As discussed in chapter 4 and section 6.2 there is an insignificant effect on generated power due to small deviation from V_{max}. This aspect is utilised to prevent instability due to small changes in V_{max} by a slight wind movements or after sudden change in irradiance level.

Furthermore, when the operating voltage of PV panels deviates from V_{max} the dissipated power at high irradiance levels is more than that at low irradiance levels. Therefore, the errors between tracking voltage and V_{max} at low I_{SC} should be greater than at high I_{SC} to prevent the high oscillation of MPPT system in cloudy time.

To prevent the oscillation due to small change in predicted V_{max} the Zero MF

of ΔV in Figures 6.5 and 6.6 are assembled without any interferences with other neighbours MFs for approximate 0.3V. In addition, the rules in Table 6.2 provide a zero response in this interval. Accordingly, the FLC accepts a percentage deflection in V_{max} to avoid the system fluctuation.

In addition, at sudden change of irradiance level the PV panels need an adequate time to reach the final T_S, as a result final V_{OC}. This leads to continuous change in the predicted V_{max}. Hence, this deflection margin in V_{max} has another advantage, which awards the FLC sufficient time to track the V_{max}, as a result prevents the instability after sudden changes in solar radiation.

Moreover, the rules in Table 6.2 discriminate the second input of FLC, I_{SC} to give a suitable response at different irradiance level. Hence, it prevent the oscillation at low irradiance level (low I_{SC}). The PS and NS MFs of ΔV are assembled without interferences with PM and NM for about 0.8V around zero ΔV. Therefore, in cloudy time the rules gives a Zero dD response if the operating voltage of PV panels deviates 0.4V greater or smaller than predicted V_{max}. Consequently, within this accessibility in voltage deviation of around Zero MF of ΔV and low I_{SC}, the FLC prevents the system fluctuation due to high changes in irradiance level in cloudy weather.

Table 6.2: FLC rules

.....ΔV Isc	NB	NM	NS	Z	PS	PM	PB
H	NM	NM	NS	Z	PS	PS	PM
M	NM	NM	NS	Z	PS	PM	PM
L	NB	NM	Z	Z	Z	PB	PB

The MFs of short circuit current are designed to provide a response (weight) equal one in most I_{SC} bell MFs duration. Hence, the MFs of dD gives a response depending on ΔV, which change by either a change in V_{max} due to environmental conditions or V_{in} due to load effect (V_O of DC-DC converter). Consequently, the max-min composition of FLC mostly provides a decision

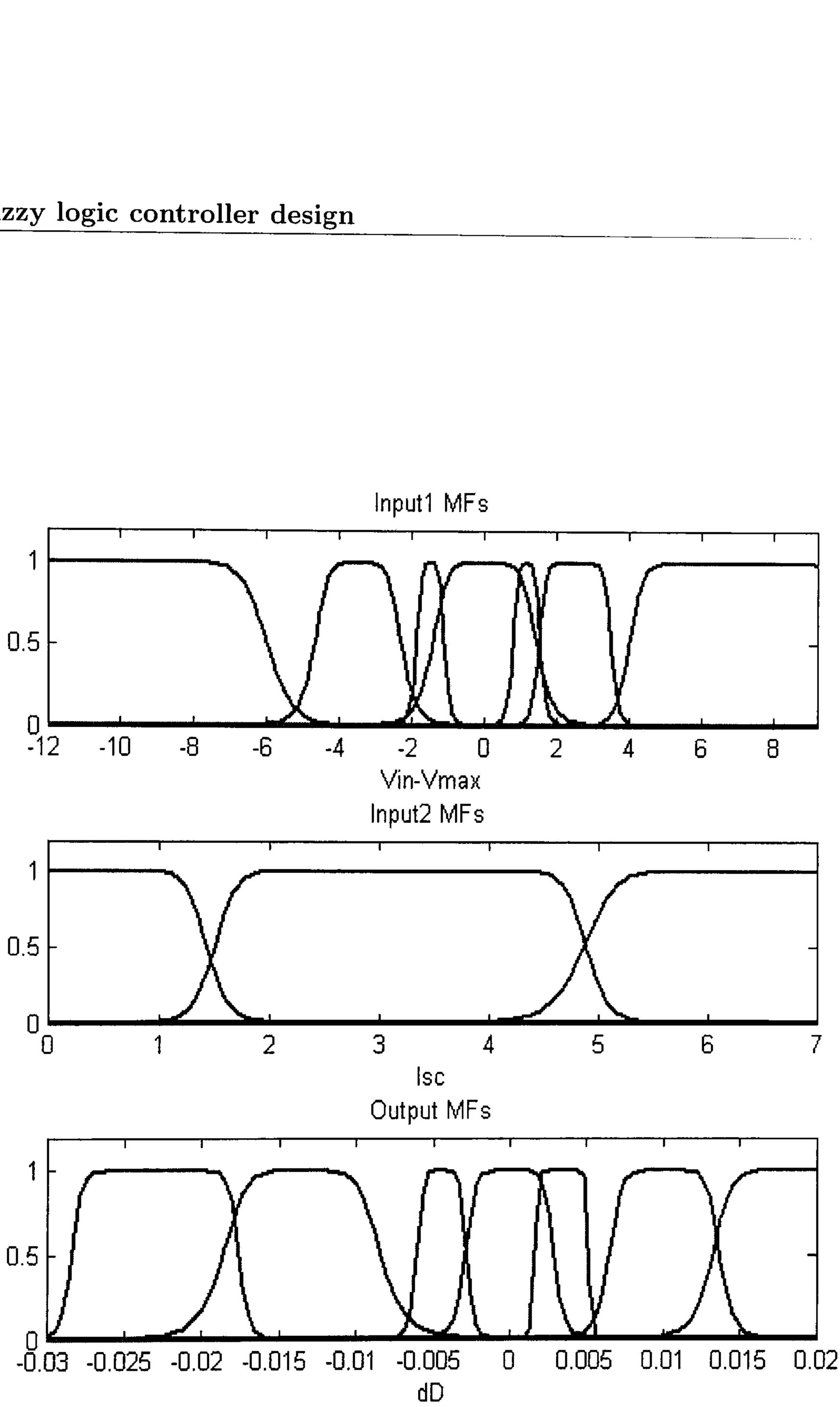

Figure 6.5: MFs of FLC system that control the duty cycle of the Buck-Boost converter for the 85W panel

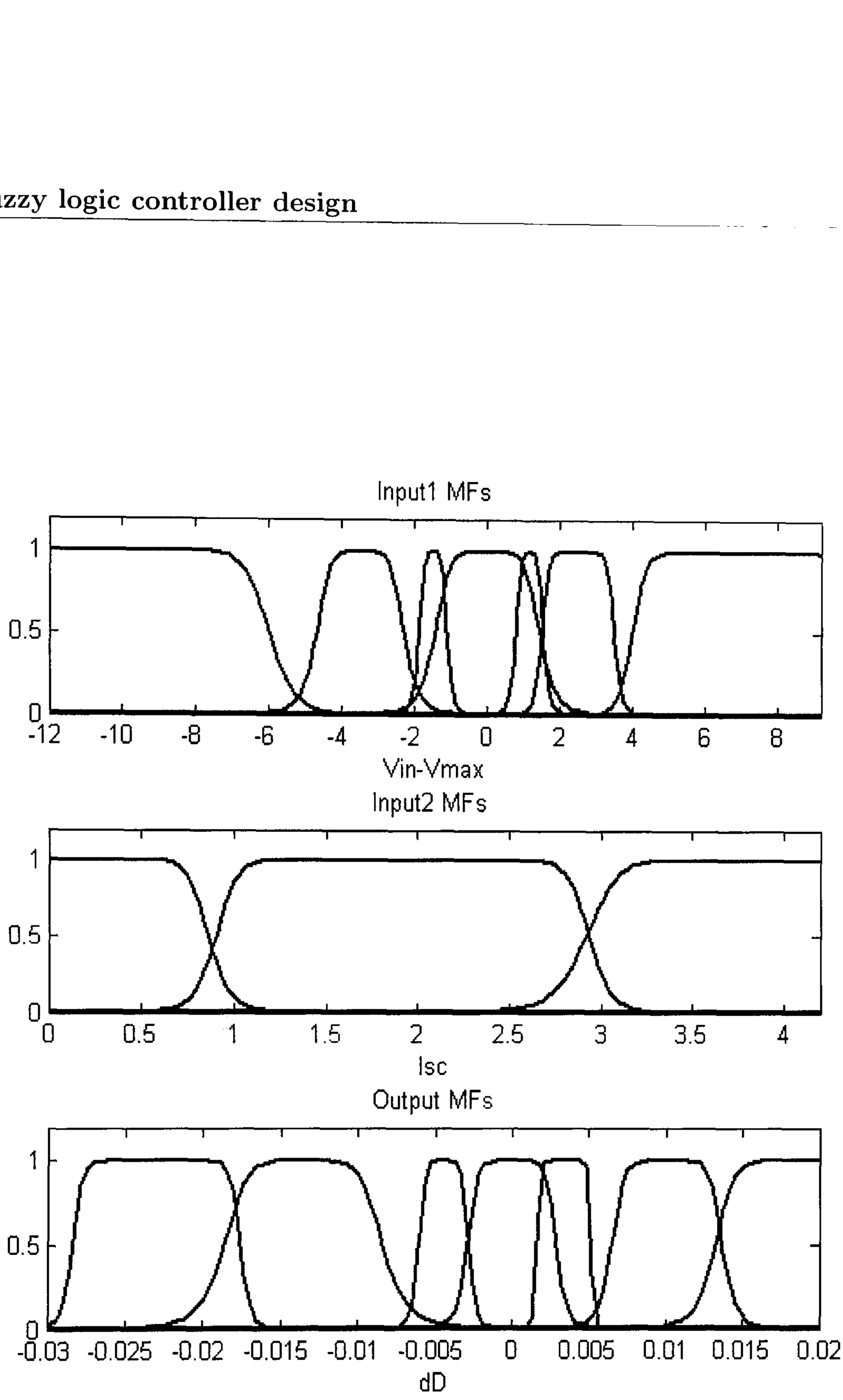

Figure 6.6: MFs of FLC system that control the duty cycle of the Buck-Boost converter for the 51W panel

according to the input variable ΔV MFs. The MFs of I_{SC} are utilised mostly to discriminate the irradiance level; therefore the rules in Table 6.2 are designed to provide a proper decision at low irradiance levels and high irradiance levels to prevent the fluctuation in different environmental conditions.

Handling problems of DC-DC converters

The unequal rate of dD at different operating voltage V_{in} of Buck-Boost converter is considered in FLC design. The MFs of output dD of FLC are assembled according to the mathematical analysis in section 6.2 which is represented in Tables A.11 and A.12 and Figure 6.4. This can be observed from the differences in negative dD and positive dD that are induced respectively by negative and positive ΔV.

Generally, the V_{max} of the two tested panels change roughly between 12V and 17V, so from Equation 6.3 when ΔV is NM or NB this means V_{in} has low values. Therefore, dD is selected carefully according to low input voltage data that is computed from Tables A.11 and A.12. Hence, according to low values of V_{in} high dD values are assembled in medium and high negative MFs of ΔV. On the other hand, the PM and PB of ΔV imply high values of V_{in}. For this reason, a low values of dD is required as shown in Tables A.11 and A.12 and Figure 6.4.

In general, the data in Tables A.11 and A.12 is used to design the range of out MFs of dD at different MFs of input ΔV. The MFs of dD and ΔV are assembled carefully to give a suitable step voltage during tracking process. Accordingly, the number of rules are minimise. The MFs of dD and the inference rules are designed to generate less than 1V change in V_{in} to prevent an induced harmonics due to high $\frac{dV}{dt}$.

Furthermore to prevent the system overshooting the range of negative small and positive small MFs of dD are carefully selected from Tables A.11 and A.12 to decrease the voltage steps when the MPPT system approaches from V_{max}.

This process prevents instability around V_{max} in the MPPT system.

Handling problems of type of load

The type of load affects the MFs and rules design. Resistive load drives the PV panel to operate within a wide interval on I-V curves. The three following points are considered when the MFs are designed.

- The output load voltage which is produced by the intersection between the resistive load and the I-V curves in Figure 2.5 can reach 5V when the irradiance level decreases suddenly by cloud effect. However, the voltage ratio $\frac{V_O}{V_{in}}$ of Buck-Boost converter is less than one. As a result, the input voltage is roughly greater than 5V.
- When the solar radiation increase suddenly, the input voltage can reach to values close to V_{OC},
- The voltage range of the V_{max} can change between 12V and 17V for two panel types in different environmental conditions.

The output MFs design

According to the above three mentioned points, the operating voltage of PV panels (V_{in} of DC-DC converter) can change from 6V to 22V and V_{max} can change between 12V and 17V. Hence, the ΔV can changes from -11V to +10V. The MFs of ΔV and dD consider the above values and the data obtained from Equation 6.2 which is represented in Tables A.11 and A.12. Thus, the following points illustrate examples of these considerations:

- The dD decreases with increasing V_{in}. Therefore, the value of dD in output MFs are designed according to maximum possible value of input voltage in different MFs of ΔV. In addition, during maximum power tracking the rules in Table 6.2 and MFs consider a maximum 1V in each step. For

example, in the MF of NB ΔV in Figures 6.5 and 6.6 the maximum V_{in} is 11V, thus to producing 1V change in V_{in} toward V_{max} the required dD from Tables A.11 and A.12 is 0.02. While the minimum V_{in} is 6V and to producing 1V response in V_{in} the required dD is 0.05. Hence the dD is set at 0.02 to avoid higher than 1V for every step.

- If the V_{in} is very low the required dD is around 0.05. Accordingly, when dD equals 0.02, the voltage step is around 0.5V for few steps and it increases until reaches 1V after few epochs. This solves the problem of a low input voltage with resistive load and applied the FLC for general applications. In addition, the rules consider this case when the irradiance is decreased suddenly by cloud to low levels by providing NB response from dD in this special situation.
- The PB of ΔV takes place when the cloud moves out, the output voltage increases suddenly to high irradiance level. Consequently, the input voltage can reach in this case to a value slightly less than V_{OC}. As shown in Tables A.11 and A.12 the high V_{in} requires a low dD response to produce maximum 1V in V_{in} as a result ΔV. Hence, the rules and MFs at high and medium I_{SC} with positive big ΔV are assembled to give a positive medium dD response due to high values of V_{in}.
- The PB response is only assembled with low I_{SC} and positive big and positive medium ΔV to solve the problem of medium values V_{in} and to give a high response before interning the interval of Zero response region at low irradiance level. Moreover, the positive big and positive medium dD are carefully selected from Tables A.11 and A.12 to provide maximum 1V step in V_{in} toward V_{max}.

The battery has a constant voltage load which varies within a small range. Therefore, the FLC can be deigned according to Figure 6.4. Therefore, five MFs of ΔV that are described with resistive load are sufficient to give the same performance as the FLC that design for all types of load. Consequently, a FLC

with 15 rules can achieve a good performance for the system that is used for the battery load system instead of the 21 rules that are used for the wide-ranging system.

6.3.4 General fuzzy logic controller for Buck-Boost converter

Figures 6.5 and 6.6 show the MFs that are used in the FLC to track the maximum power point of 85W panels and 51W panels separately. For general implementation of PV system application, it is necessary to design an FLC that has widespread implementation. The developed controller that has been described in the previous subsection can be implemented in all single crystal and polycrystalline PV models with few modifications. The required modifications can be described as follow.

- The FLC input I_{SC} should be divided by the short circuit current of PV panel at standard test conditions divided by number of parallel PV panels in PV system array. As a result, the quantities that are obtained represent a fraction of 1000 W/m^2 irradiance level.
- The FLC input ΔV should be divided by the number of PV panels that are connected in series, divided by the number of PV series cells in one PV panel. The results obtained from the last division represent the deviation operating voltage of the PV cell from its maximum power point voltage.

Figure 6.7 shows the MFs of extensive FLC, which can be implemented for all single crystal and polycrystalline PV systems. In addition, Figure 6.8 shows the structure of the general FLC system.

The performance of FLC with Buck-Boost converter and its response according previous MFs and rules design in different conditions will be shown in chapter 7.

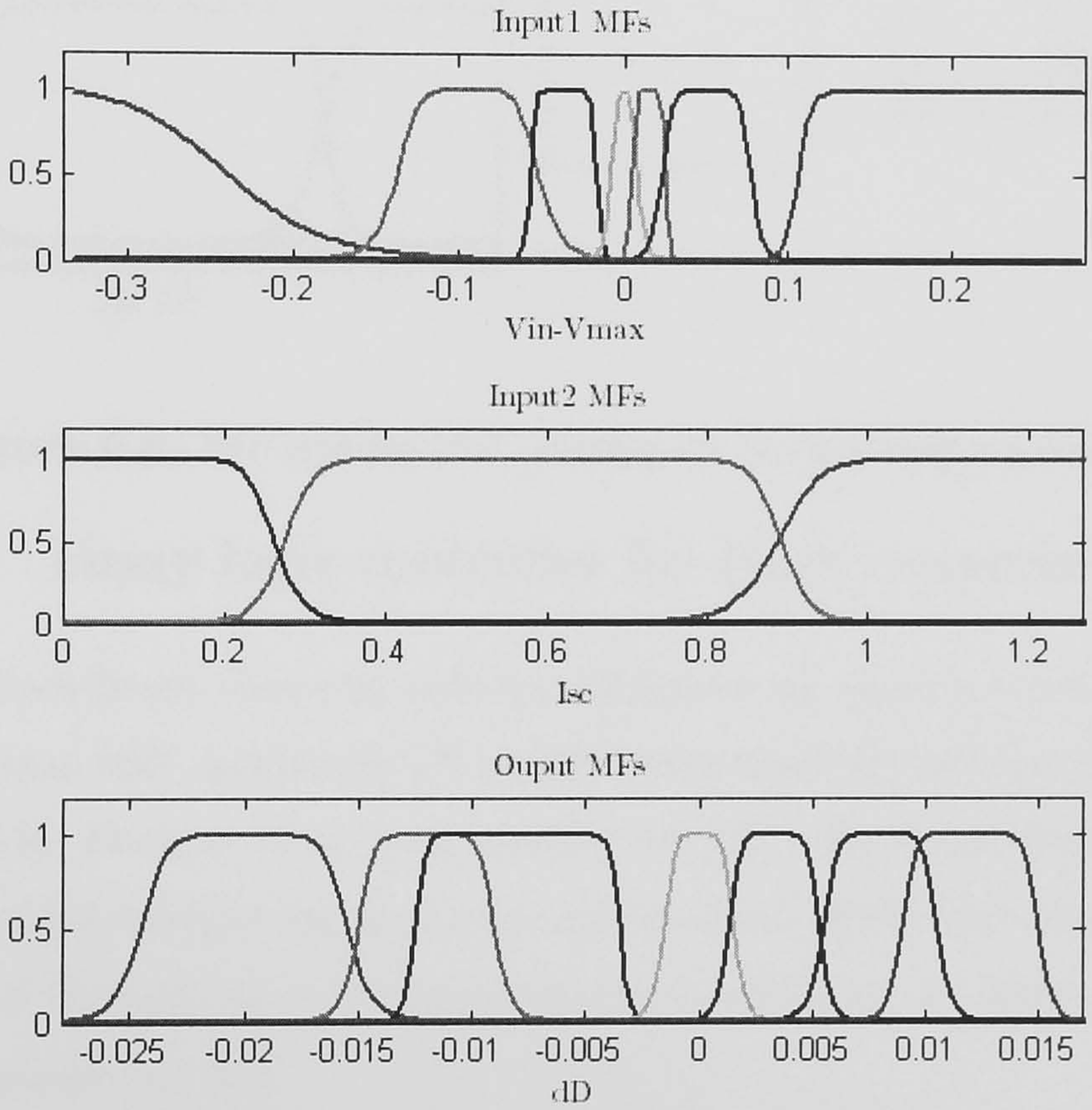

Figure 6.7: MFs of the general FLC system for Buck-Boost converter

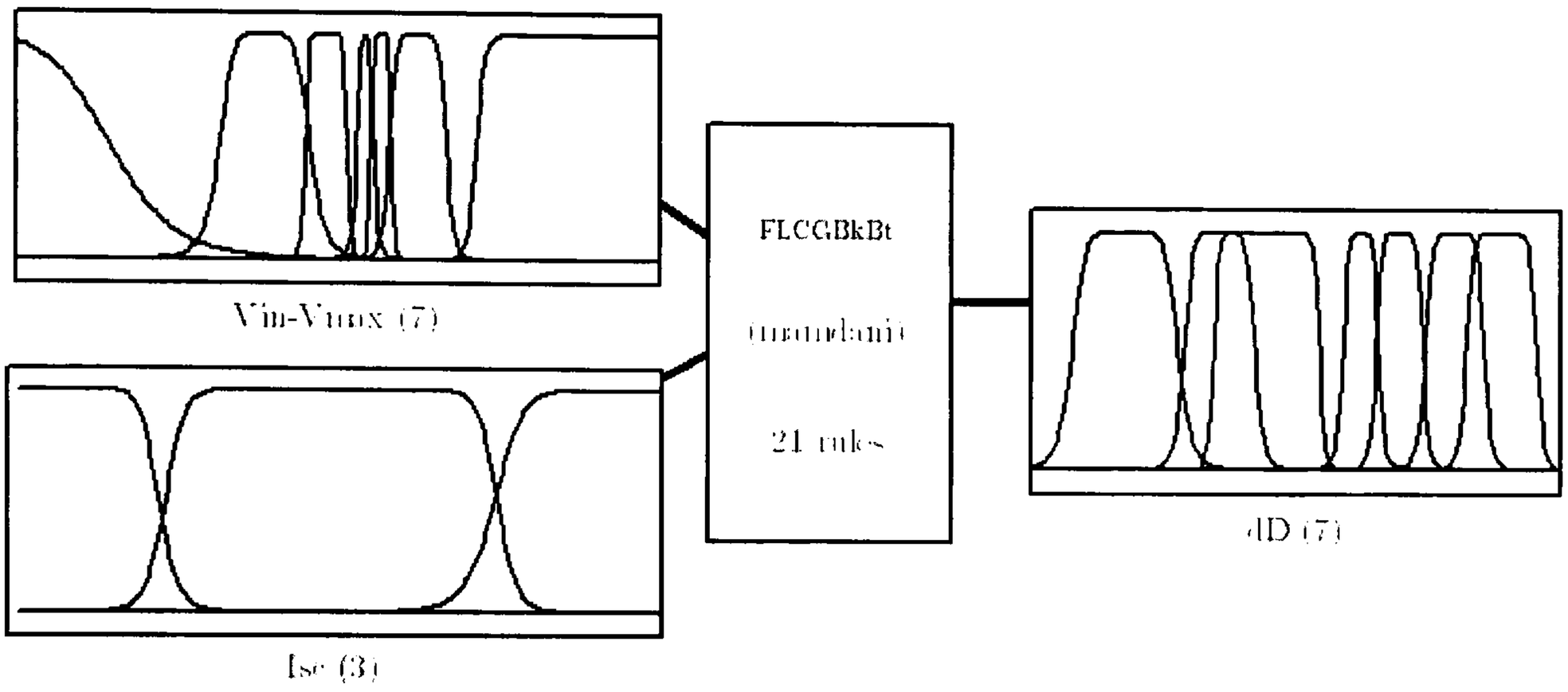

Figure 6.8: The general FLC system for Buck-Boost converter

6.3.5 Fuzzy logic controller for Buck converter

"The Buck-Boost converter achieve efficiencies as regards input rated power higher than 95% and hardly 2% or 3% lowers than the buck and boost topologies" J.M. Enrique *et al*, page number 18 [25]. Buck and Boost converters are the most efficient topologies for a given price. While the voltage flexibility varies of Buck-Boost converter is always at efficiency or, alternatively, price disadvantage [25] [65].

Some electrical applications, like water pumps can be designed to operate at voltage less than the minimum expected V_{max} of PV panels. Also, it can be observed from the data collected in high mountain areas that V_{max} is more than 16V for 85W single crystal panel and more than 15.3 for 51 polycrystalline PV panel in different summer and winter data collecting times. The full charge battery voltage is 15V during charge time. Therefore, the battery applications in low ambient temperature areas can use the Buck converter because of its high efficiency.

Moreover, the duty cycle of the Buck converter has a wider-range than the Buck-Boost converter shown in Figure 6.2 and Table 6.3. Therefore, it is easer to control the electronic devices of PWM, which control the rate of changes in duty cycle.

All points that have been identified in the design of FLC for Buck-Boost converter are considered in the FLC for Buck converter. However, the main two differences are:

- The output voltage does not exceed 15V according to the application and region that the Buck converter is implemented.
- The input voltage of PV panels is always greater than output voltage of the load.

According to equation 2.15 the rate of change in duty cycle in terms of V_{in} can expressed as:

$$\frac{\partial D}{\partial V_{in}} = \frac{-Vo}{V_{in}^2} \tag{6.4}$$

From Equation 6.4 the rate of change in duty cycle (dD) can be specified in Table 6.3, which is used to design the MFs and rules of FLC that is used in MPPT with Buck converter. Figure 6.9 shows the MFs of a general FLC for the Buck converter, which can be applied for all single crystal and polycrystalline PV systems. In addition, Figure 6.10 shows the structure of the FLC system.

To evaluate the FLC rules and the MFs, a rule viewer in Matlab fuzzy toolbox is used to test the performance of FLC under different values of ΔV and I_{SC}. The MPPT system performance is tested by applying two preceding simulation models. The early output data is utilised to develop the MFs and rules of two particular FLCs. The range of inputs MFs and the output MFs is modified to accomplish all specifications that are discussed in this section. Also, steady state movement during the tracking process is considered by modifying the MFs

Table 6.3: The rate of change in duty cycle (dD) of Buck converter at different input and output voltage

	Vo (V)										
Vin (V)	6	7	8	9	10	11	12	13	14	15	16
6	-0.167										
7	-0.122	-0.143									
8	-0.094	-0.109	-0.125								
9	-0.074	-0.086	-0.099	-0.111							
10	-0.060	-0.070	-0.080	-0.090	-0.100						
11	-0.050	-0.058	-0.066	-0.074	-0.083	-0.091					
12	-0.042	-0.049	-0.056	-0.063	-0.069	-0.076	-0.083				
13	-0.036	-0.041	-0.047	-0.053	-0.059	-0.065	-0.071	-0.077			
14	-0.031	-0.036	-0.041	-0.046	-0.051	-0.056	-0.061	-0.066	-0.071		
15	-0.027	-0.031	-0.036	-0.040	-0.044	-0.049	-0.053	-0.058	-0.062	-0.067	
16	-0.023	-0.027	-0.031	-0.035	-0.039	-0.043	-0.047	-0.051	-0.055	-0.059	-0.063
17	-0.021	-0.024	-0.028	-0.031	-0.035	-0.038	-0.042	-0.045	-0.048	-0.052	-0.055
18	-0.019	-0.022	-0.025	-0.028	-0.031	-0.034	-0.037	-0.040	-0.043	-0.046	-0.049
19	-0.017	-0.019	-0.022	-0.025	-0.028	-0.030	-0.033	-0.036	-0.039	-0.042	-0.044
20	-0.015	-0.018	-0.020	-0.023	-0.025	-0.028	-0.030	-0.033	-0.035	-0.038	-0.040

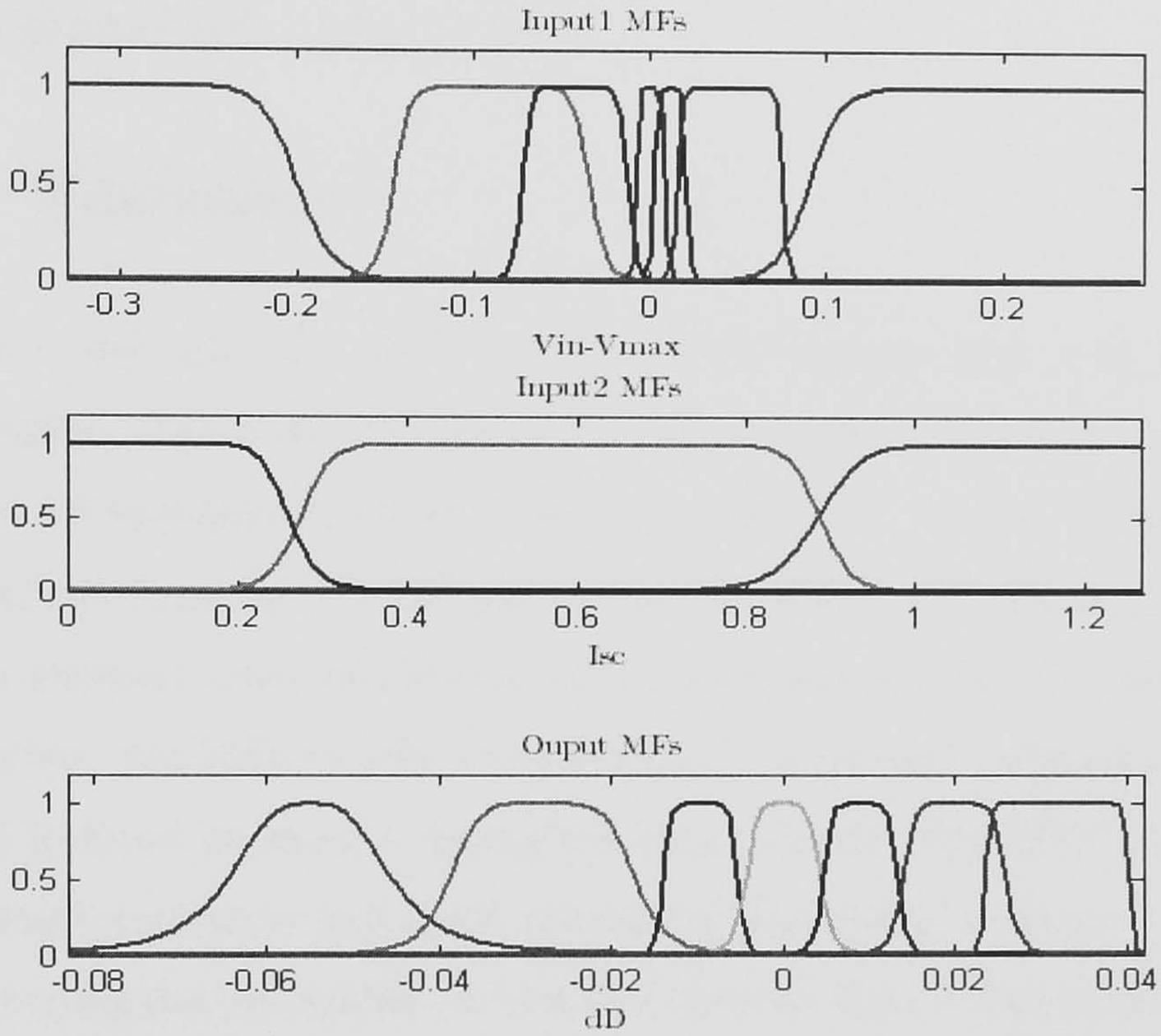

Figure 6.9: MFs of the general FLC system for Buck converter

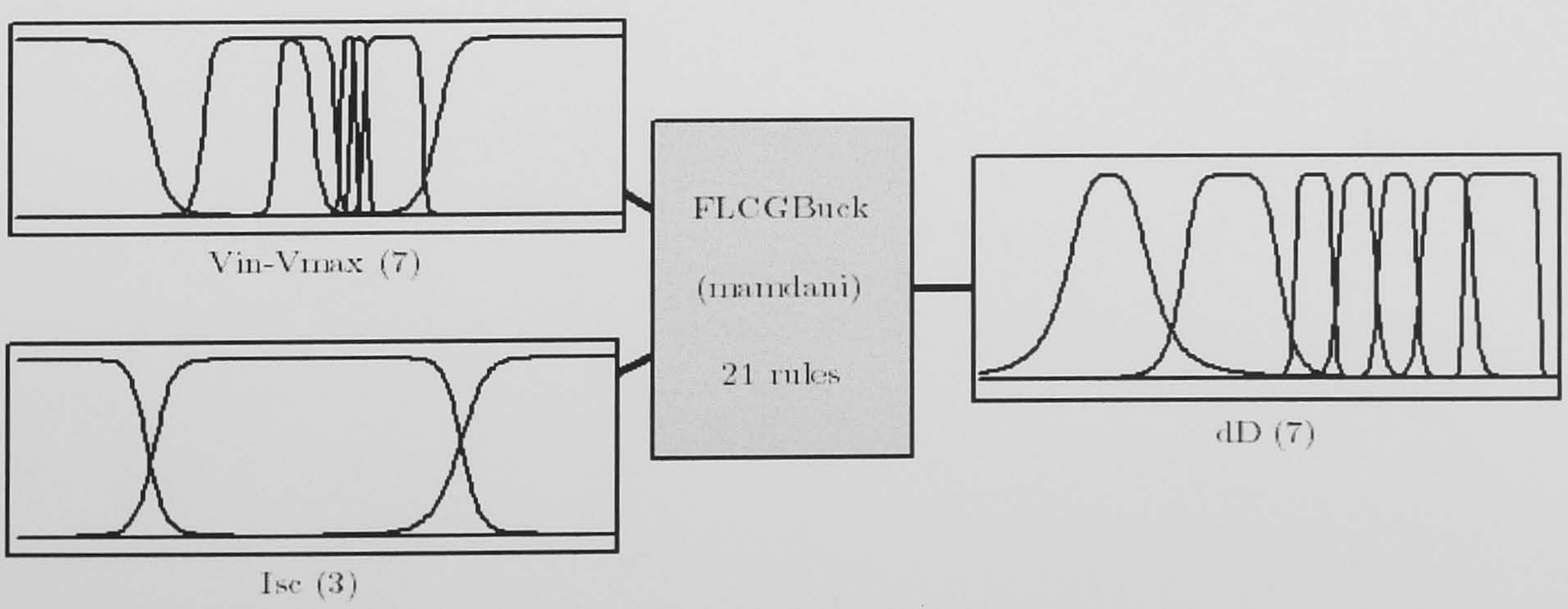

Figure 6.10: The general FLC system for Buck converter

of ΔV and the MFs of the dD. The final MFs and rules are installed as final MFs in general FLC in this section.

6.4 Summary

The FLC and problems that face the MPPT system have been addressed in this chapter. The FLC is developed in this chapter to provide a general FLC that can be implemented with different types of PV system, different types of load and two types of DC-DC converters. The MFs of FLCs are designed with rules to generate a fast and steady state movement during the tracking process. In addition, the MFs of FLCs are designed to prevent oscillation, overshooting and induced harmonics during tracking process. The MPPT systems with Buck-Boost converter and Buck converters have been evaluated in chapter 7 using two simulation models to test and develop the performance of the whole system. The simulation models are implemented to demonstrate the result of final MPPT systems.

Chapter 7

Maximum power point tracking system simulation models and results

This chapter includes the ANFIS results and performance of simulation models of MPPT with FLC. The MPPT system simulation model with Buck-Boost converter and MPPT system simulation model with Buck converter are also discussed in this chapter. In addition, evaluating the MPPT system regarding a direct coupled system with constant voltage load and resistive load are presented in the end of this chapter.

7.1 Introduction

The actual short circuit current which represents the irradiance level is used as first input of ANFIS models. In addition, the actual open circuit voltage which represents the temperature effect at certain irradiance level is used as second input of ANFIS models. The actual voltage at maximum power point V_{max} is used as output of ANFIS models.

The selected ANFIS models are developed by applying the LSE algorithm during forward learning to improve the performance of the ANFIS model by improving the consequent linear parameters. However, the iterative change on the nonlinear does not achieve a good performance in Genfis1 models. Hence, the subtractive clustering that used in Genfis2 function is used to overcome the shortage in the iterative modification in MFs premise parameters. Finally, the general ANFIS model is developed using all per unit (PU) data of the 85W single crystal panel and 51W polycrystalline panel.

The behaviour of PV panels is studied in different environmental conditions dur-

ing data collection. The problems that are related to changes in environmental conditions are recognised. In addition, the DC-DC converters relationships are analysed at different load voltages. Hence, the FLC is designed to provide fast and stable maximum power point tracking with all variations related to environment, loads and DC-DC converters.

The predicted V_{max} from ANFIS model is used with actual I_{SC} (irradiance level) as input to the FLC to control the duty cycle of DC-DC converters. The input voltage of DC-DC converter drives the operating voltage on I-V curves of PV panel. Therefore, the difference between input voltage and predicted V_{max} is the first input of FLC. Also, the measured I_{SC} is used as second input of FLC. The FLC is used to control the rate of change in duty cycle (dD) of electronic switch of DC-DC converters. This rate of change in duty cycle is studied carefully in section 6.2 applying a mathematical analysis to utilise in MFs and rule design of FLC.

Two FLCs are designed for 85W single crystal panel and 51W polycrystalline panels separately. The two models are tested using actual data and two simulation models in Matlab. Two general models with Buck-Boost DC-DC converter and Buck DC-DC converter are developed using PU data. The general FLCs are implemented for all PV single crystal and polycrystalline PV systems and different types of load.

7.2 The results of general ANFIS model

The final ANFIS model is tested by dividing the actual data into learning data and test data. Genfis2 function is applied with 75% of data to generate the ANFIS model. The generated ANFIS model is improved using the LSE algorithm modification for consequent linear parameters. The final model is tested using the remaining 25% of data. The 25% points are selected at different irradiance levels and different temperatures. Figure 7.1 shows the actual and

predicted PU V_{max} and the percentage error of between actual and predicted V_{max}. The test data selected according to temperature and irradiance levels. Figure 7.2 shows the percentage error of between actual and predicted V_{max} at low, medium and high temperatures. The percentage error is less than 2% in more than 90% and around 2.5% in remaining points.

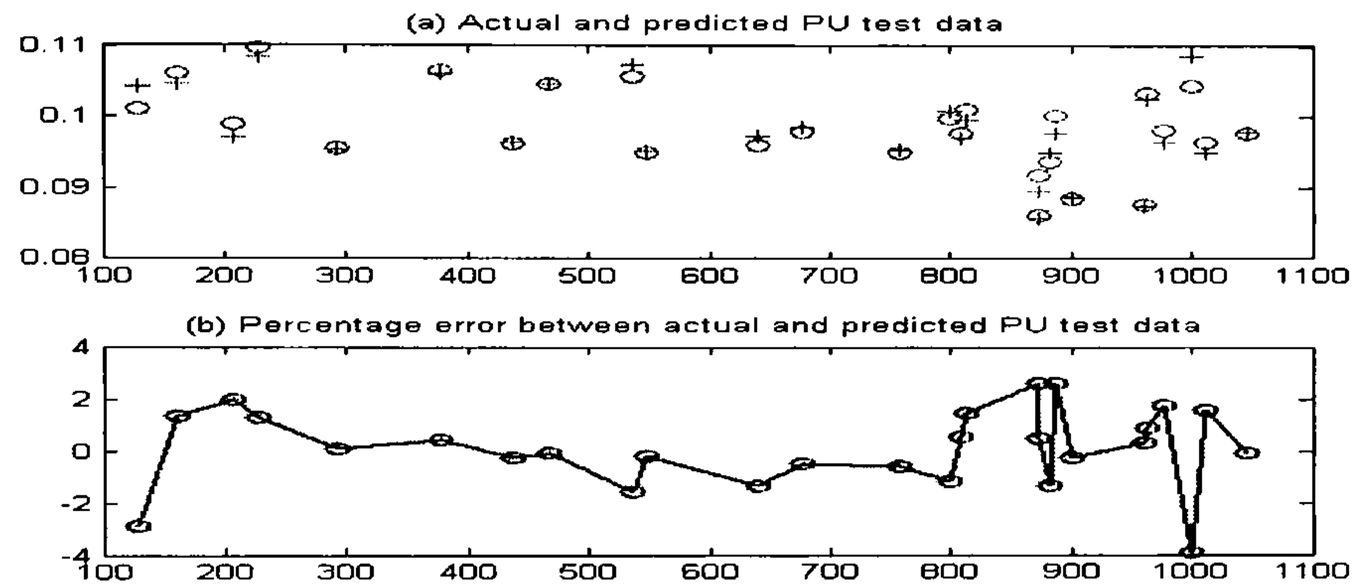

Figure 7.1: Actual data and predicted outputs of PU test data

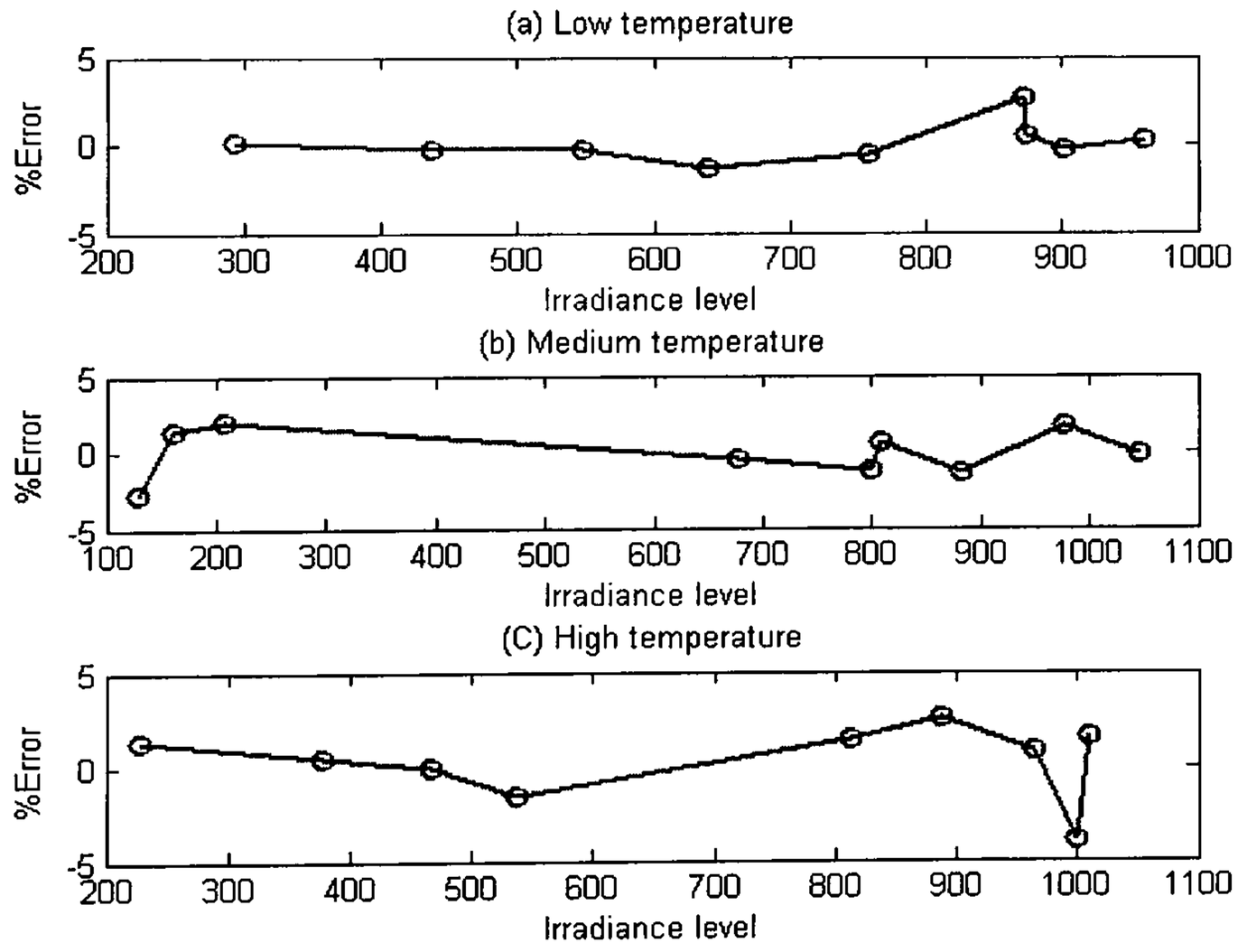

Figure 7.2: Percentage errors of PU output test data at different temperatures

In addition, the validity of general ANFIS model is tested with different types

of PV panels as shown in Figure 7.3. This data is obtained by applying the general ANFIS model to predict the V_{max} from actual I_{SC} and V_{OC} and actual V_{max} is obtained around the predicted V_{max}. The general ANFIS model provide a low error with different types of panels as will be clarify in section 7.5.

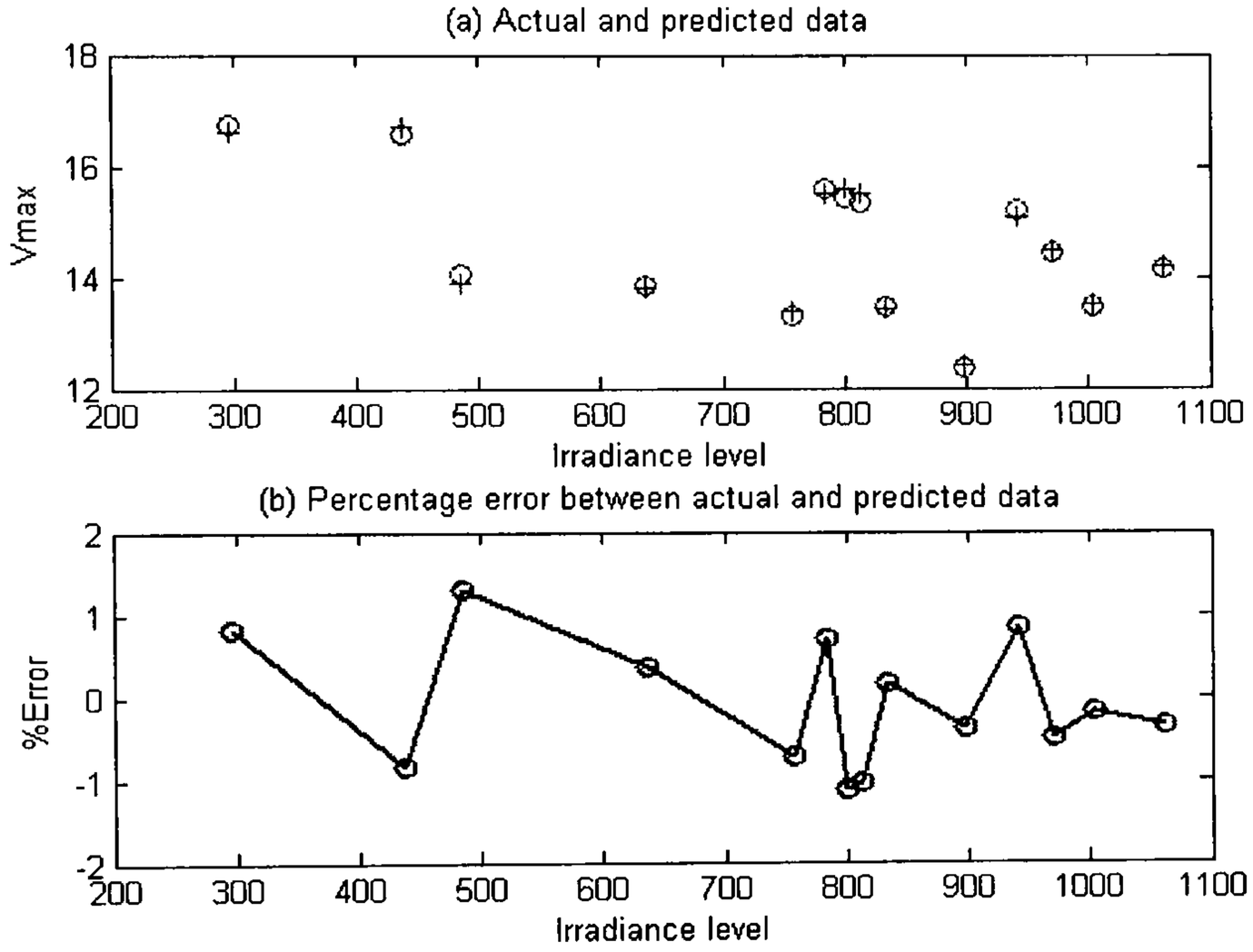

Figure 7.3: Actual and predicted V_{max} for general ANFIS model

7.3 The performance of simulation models of MPPT with FLCs

At a certain I_{SC} and V_{OC}, the ANFIS model predicts V_{max} of the PV system. The predicted voltage V_{max} with actual I_{SC} are used as inputs to the FLC to adjust the duty cycle of the electronic switch of the DC-DC converter.

The block diagram in Figure 7.4 shows the progression of matching the load voltage and maximum power point voltage of PV system. The MPPT system consists of the following three parts.

7.3 The performance of simulation models of MPPT with FLCs

- The ANFIS model, which obtains its actual input I_{SC} and V_{OC} from the PV system and it predicts V_{max} as an input for FLC.
- The FLC, which get inputs from the PV system, ANFIS model and DC-DC converter as shown in Figure 7.4. The actual I_{SC} is measured from PV system and represents the irradiance level. The second input is the difference between the simulated V_{in} from DC-DC converter and the predicted V_{max} from ANFIS model. The output of FLC is the changes in duty cycle of DC-DC converter.
- The DC-DC converter is controlled by the FLC and it interfaces between PV system and different types of load. The input voltage of DC-DC converter is a function of duty cycle and the load voltage (V_O) as shown in Equation 2.17 for Buck-Boost converter Equation 2.15 for Buck converter. The FLC changes the rate of change in duty cycle of DC-DC converter, consequently it controls the input voltage of converter. The PV panels are connected to input terminal of DC-DC converter. Therefore, the input voltage of DC-DC converter drives the operating point on I-V curve of PV system.

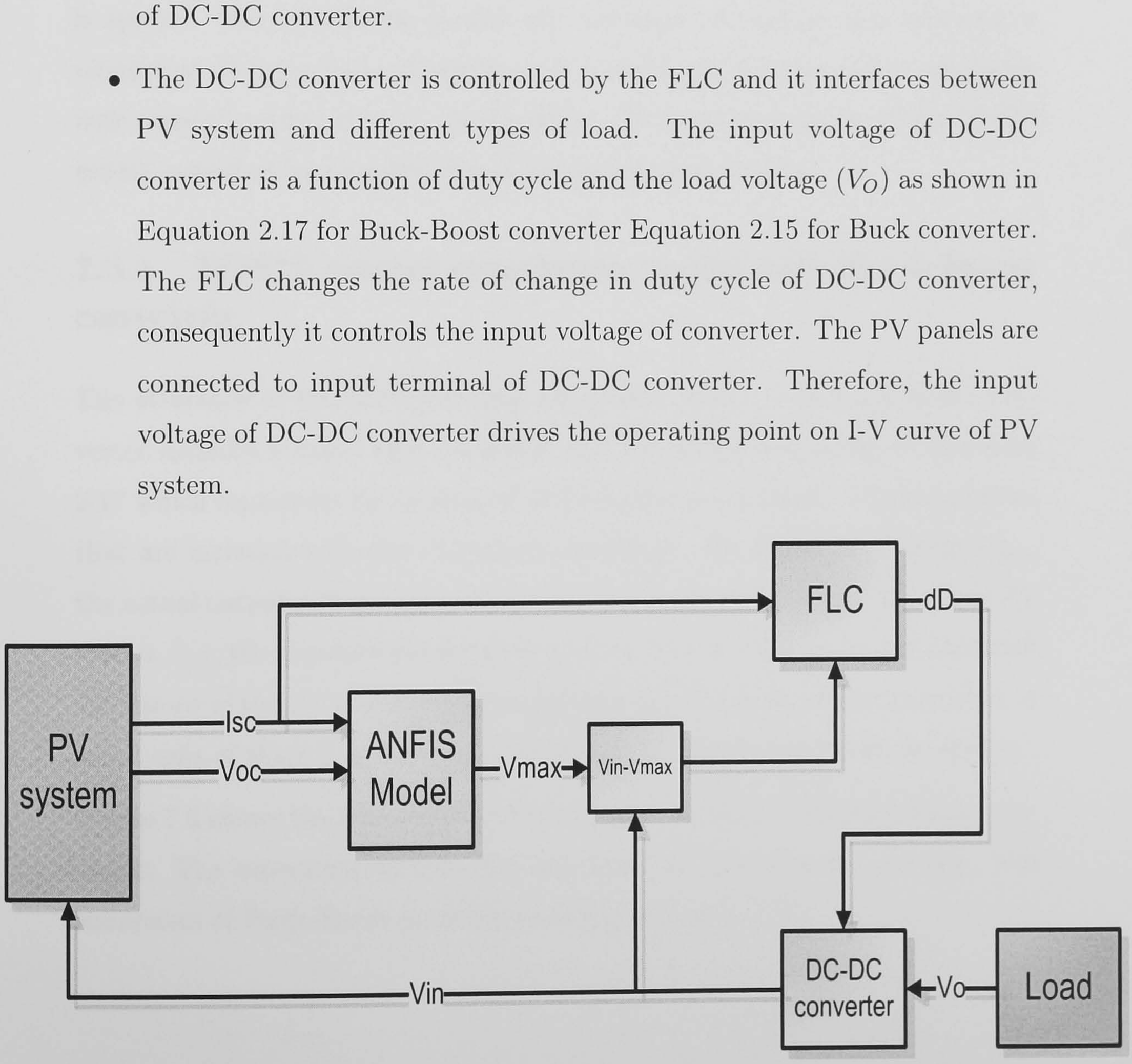

Figure 7.4: The block diagram of MPPT system

7.3 The performance of simulation models of MPPT with FLCs

The predicted voltage V_{max} changes if either V_{OC} or I_{SC} changes. Two simulation models are applied in Matlab to inspect the behaviours of the FLC with Buck-Boost and Buck converters. In addition, the simulation results are utilised to improve the MFs of the FLC to reach the optimum performance of MPPT systems with two converters.

The MPPT system is simulated in Matlab with Buck-Boost and Buck converters. The simulation process is arranged according to the type of converter that is applied. Two simulation models are introduced in this section including a simulation of fuzzy logic controller and a simple DC-DC converter operation with constant adjusted output load voltage. The predicted output of the ANFIS model is used as input parameter in two simulation models.

7.3.1 MPPT system simulation model with Buck-Boost converter

The structure of the MPPT system simulation model with Buck-Boost converter includes a fuzzy logic controller and the simulation model of Equation 2.17 which represents the behaviour of Buck-Boost converter. The parameters that are included with the simulation model are: the predicted voltage V_{max}, the actual output voltage of converter V_O, the actual short circuit current of PV system I_{SC}, the standard short circuit current that is obtained at standard test conditions of the PV panel, initial magnitude of duty cycle, the total number of series cells of the PV system and the number of parallel panels in the system.

Figure 7.5 shows the simulation model of MPPT system with Buck-Boost converter. The subsystem includes the simulation of Buck-Boost converter. The subsystem of Buck-Boost converter is shown in Figure 7.6.

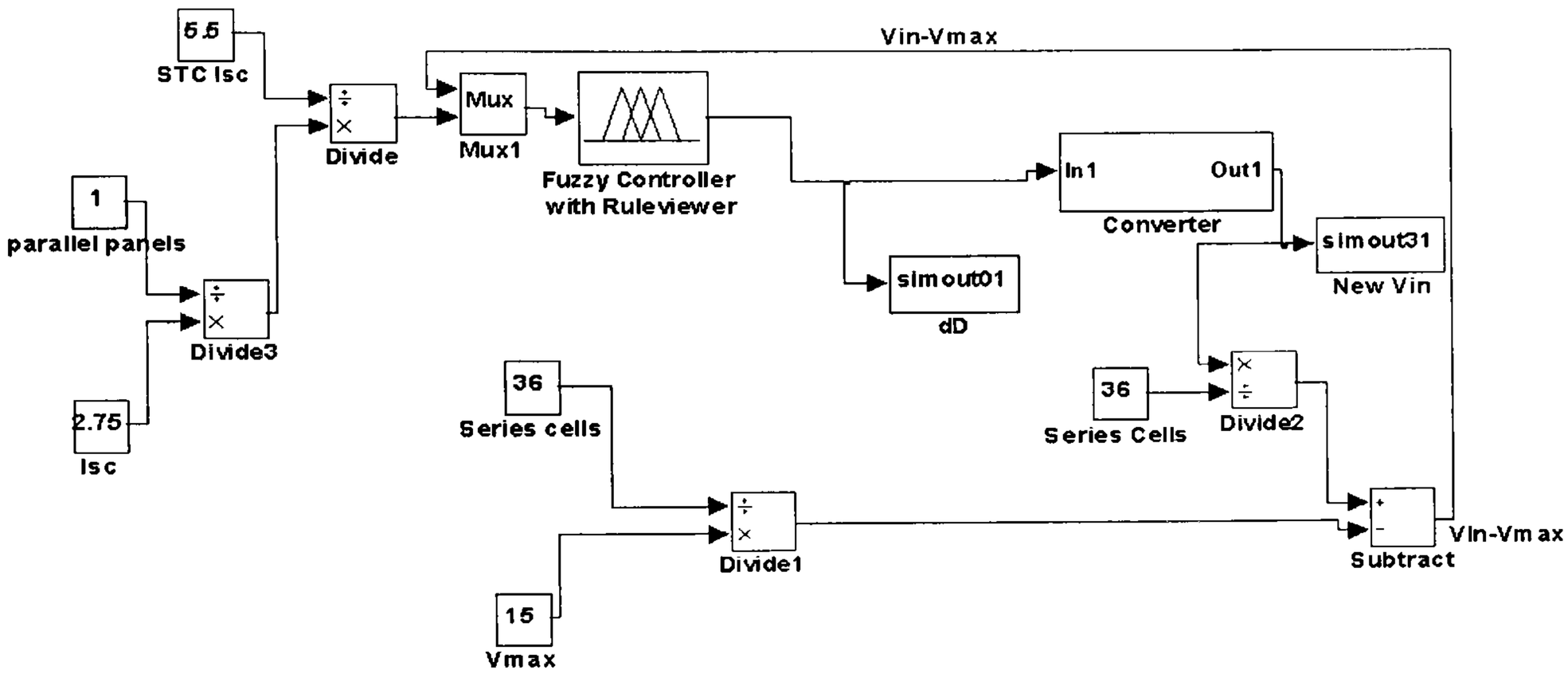

Figure 7.5: MPPT system simulation model with DC-DC converter subsystem

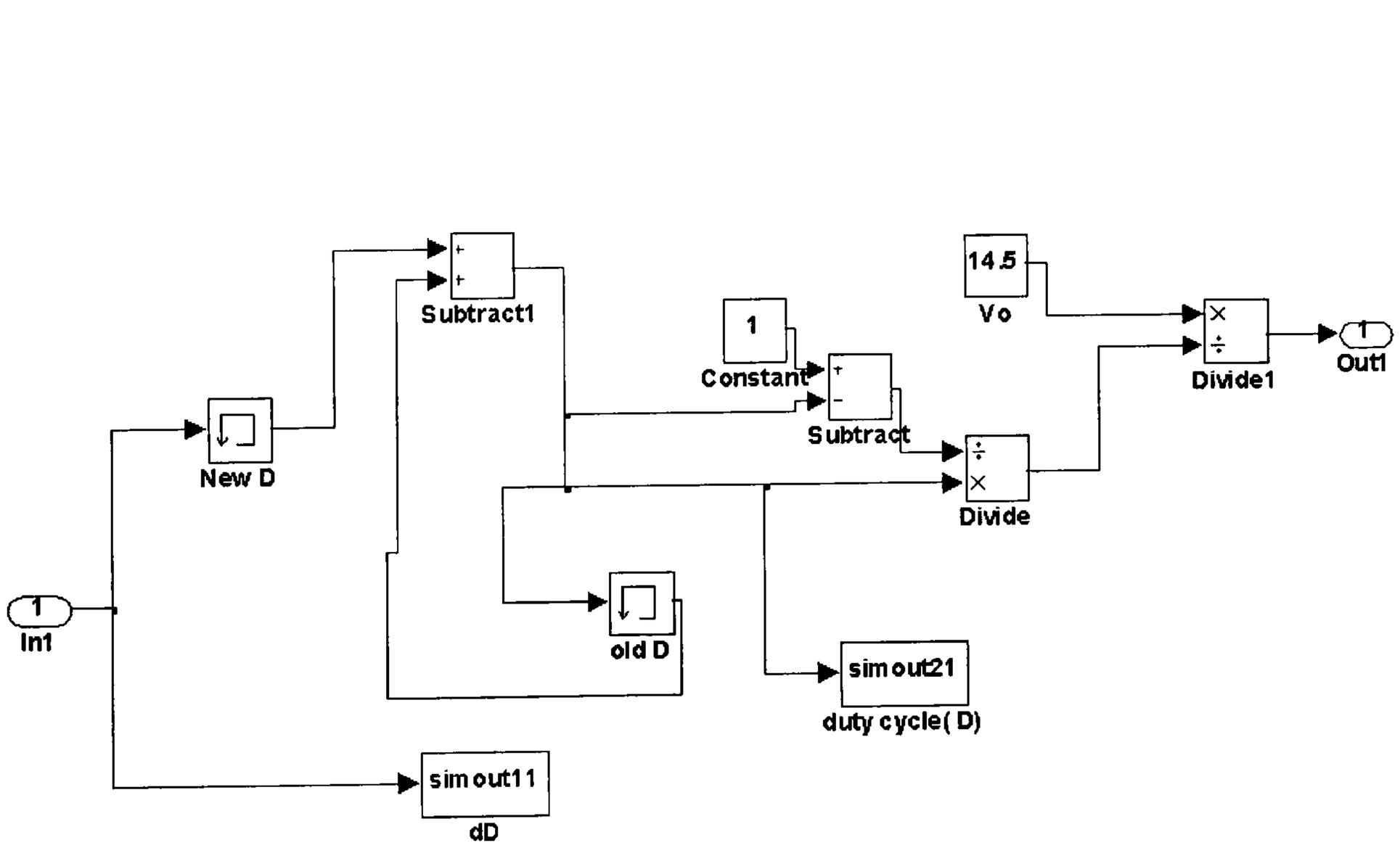

Figure 7.6: Simulation model of the Buck-Boost converter

7.3.2 MPPT system simulation model with Buck converter

The MPPT system simulation model with Buck converter has the same structure of the MPPT system simulation model with Buck-Boost converter with two main differences:

- The enclosed subsystem simulates Equation 2.15 of the Buck converter.
- The fuzzy logic controller includes the fuzzy inference system that is designed for the Buck converter.

Other variables that are mentioned in the simulation model of MPPT system with Buck-Boost converter are required in the simulation model of MPPT system with Buck converter.

Also, Figure 7.5 shows the simulation model of MPPT system with Buck converter. The subsystem includes the simulation of Buck converter. The subsystem of Buck converter is shown in Figure 7.7.

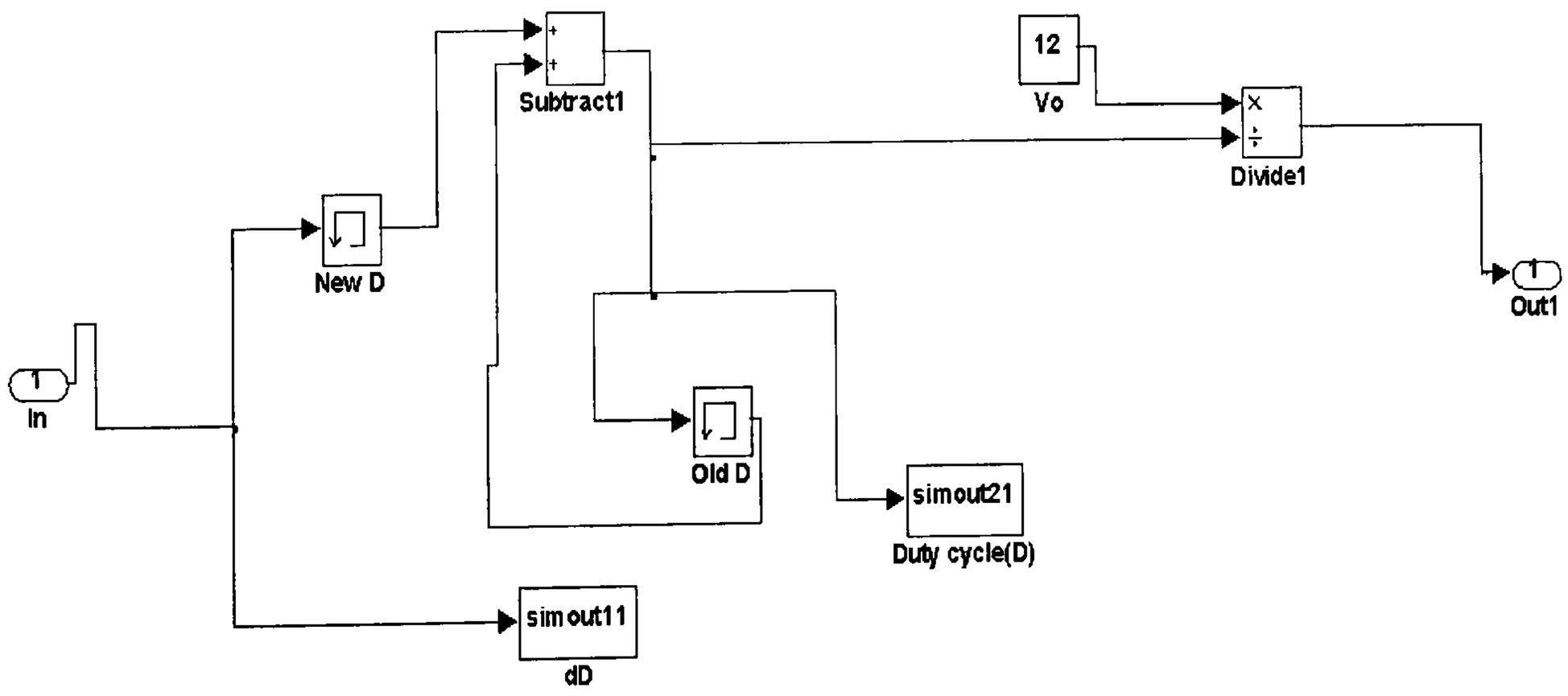

Figure 7.7: Simulation model of the Buck converter

7.4 Maximum power point tracking system results

In this section three types of results will be introduced as follows.

- The first type of result will show the performance of FLC in MPPT system. The main target in this type of result is to show how the input voltage of DC-DC converter is changed until get in touch with V_{max}. The simulation models are used to show how the FLC is tracking the predicted V_{max} at different irradiance level (I_{SC}) and different values of (V_{in}-V_{max}). The tracking steps can be described as follow:
  - The ANFIS model predicts the V_{max} at certain I_{SC} and V_{OC}.
  - The predicted V_{max} with V_{in} from DC-DC converter are used to compute the first input ΔV. Also, the measured I_{SC} is used as second input of FLC to generate the output dD.
  - The output dD of FLC is used to compute the new duty cycle of DC-DC converter.
  - The new V_{in} is modified toward V_{max} according to new duty cycle.
  - The input voltage of DC-DC converter drives the operating voltage of PV system.
  - A new ΔV is computed according to new V_{in}. As a result, the FLC generate the new dD.
  - This small simulated loop is continued until the input (V_{in}-V_{max}) reach to approximately zero.
- The second type of results will compare between the actual voltage and predicted voltage of ANFIS model and it compares between the actual power and tracked power of MPPT system.
- The third results will evaluate the MPPT system with respect to the direct coupled system.

7.4 Maximum power point tracking system results

A problem of nonzero response of bell membership functions encounters the MPPT simulation models at zero output MFs. This problem is solved by utilising the crossing area between positive and negative response of MFs to obtain approximately zero response. For this reason, the real zero response of dD should be determined.

7.4.1 The performance of FLC with Buck-Boost converter at different inputs

All possible situations in Table 6.2 have been tested. To test the FLC at different values of V_{in} three procedures are performed during testing the performance of FLC

- The FLC is tested at low and high V_{max} to driving the input voltage through all possible values of V_{in} during tracking process.
- The input voltage is selected to provide all possible negative and positive values of V_{in} - V_{max}.
- The system is tested at low, medium and high I_{SC}. These situations are all points that are required to identify the performance of FLC at different levels of irradiance levels.

Figures 7.8 and 7.9 show the performance of the simulation model of MPPT system with Buck-Boost converter at high irradiance level and different positive and negative magnitude of ΔV. In addition, Figures 7.10 and 7.11 show the performance of the simulation model of MPPT system with Buck-Boost converter at low irradiance level and different positive and negative magnitude of ΔV including special cases at low irradiance level. As shown in the Figures the FLC required few epochs to changes the values of (V_{in}) until get in touch with V_{max} as a result zero V_{in} - V_{max}. The simulation model of MPPT system with Buck-Boost converter at medium irradiance level performs similar to that at the high irradiance level.

7.4.2 The performance of FLC with Buck converter

The simulation model of MPPT system with Buck-converter is executed at different irradiance level, V_{max}, and ΔV. The main difference between FLC with Buck converter and FLC with Buck-Boost converter are the output MFs of dD which are designed depends on data that was discussed in Buck converter in section 6.3 and shown in Table 6.3. In addition, the subsystem of Buck converter which is described earlier in section 7.3 is used in simulation model of MPPT with Buck converter. The Buck converter is step down converter, therefore the output voltage of Buck converter is always less than the input voltage.

Figure 7.12 and Figure 7.13 show the performance of MPPT system with Buck-converter at low and high irradiance level and different values of (V_{in} - V_{max}).

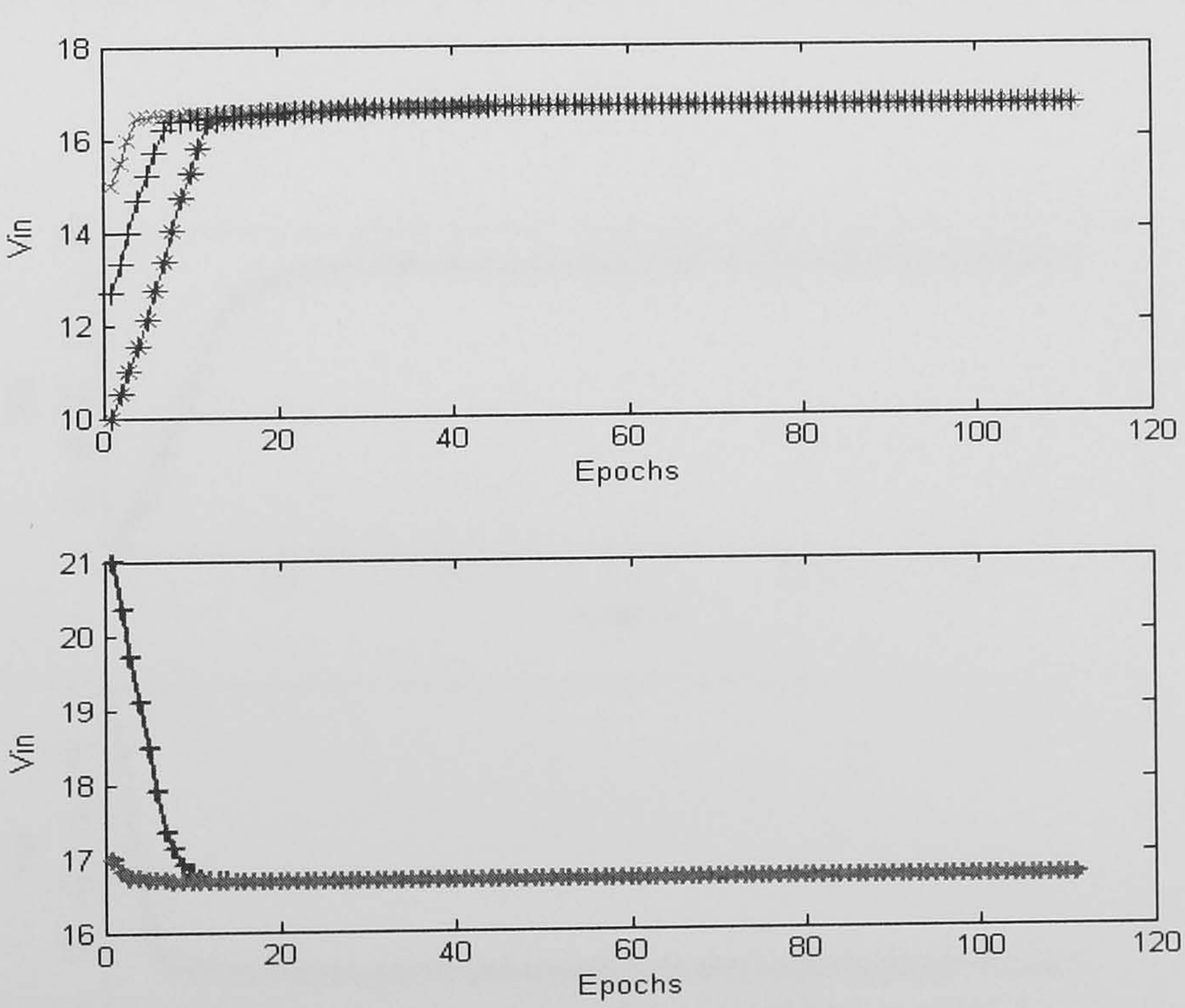

Figure 7.8: Tracking maximum power point at high irradiance and V_{max}=16.5V

7.4 Maximum power point tracking system results

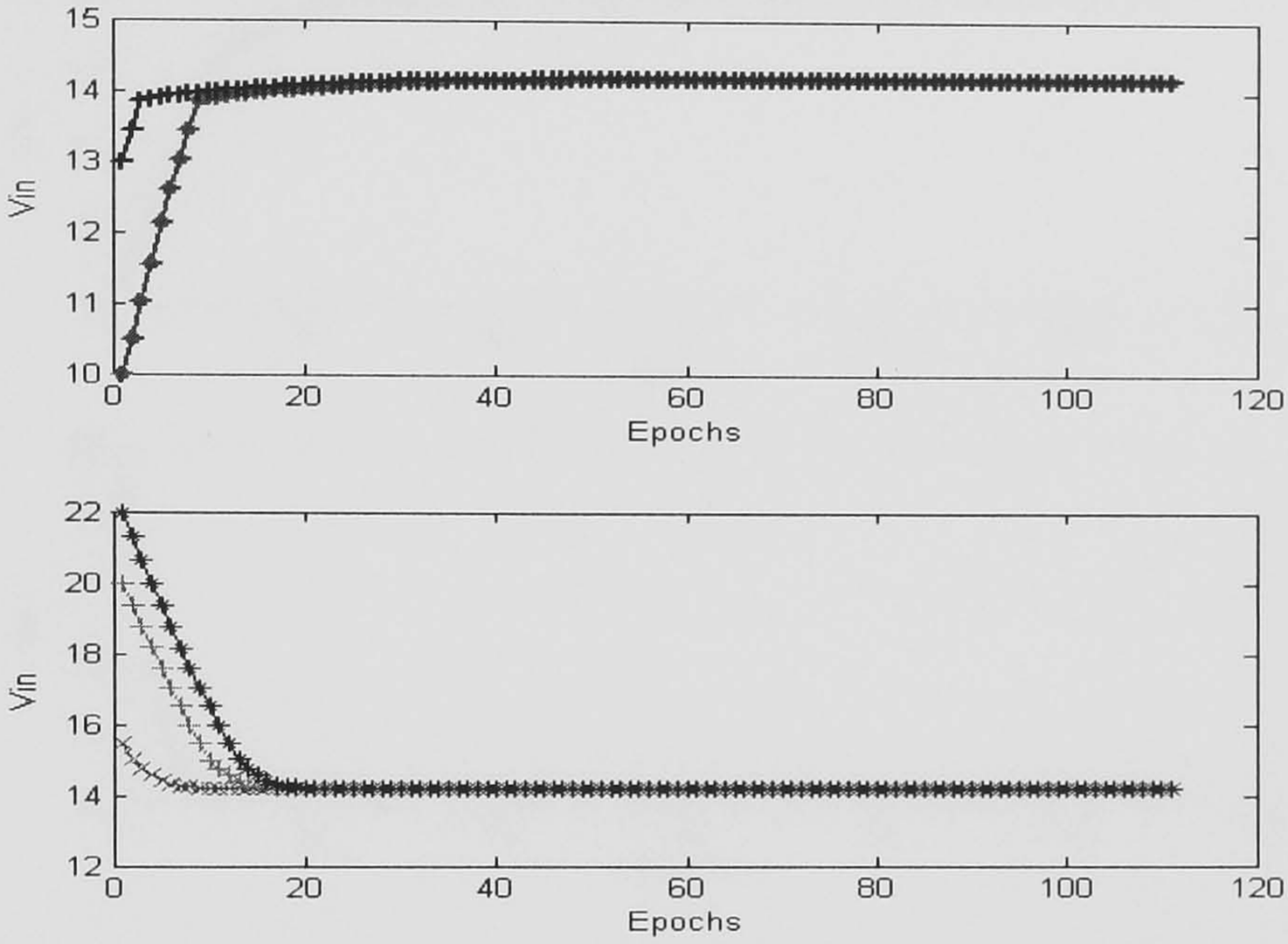

Figure 7.9: Tracking maximum power point at high irradiance and and V_{max}=14V

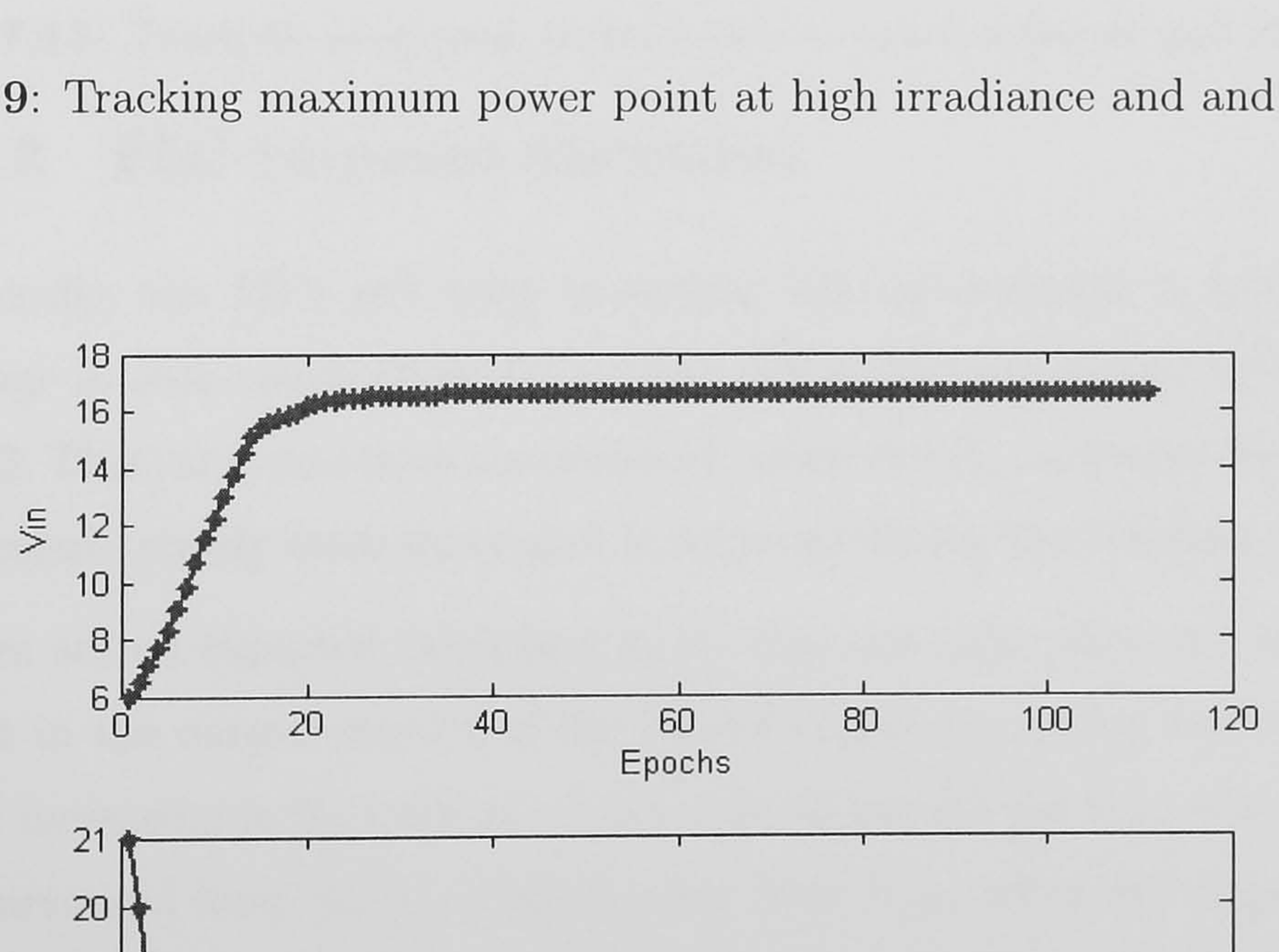

Figure 7.10: Tracking maximum power point at low irradiance and V_{max}=16.5V

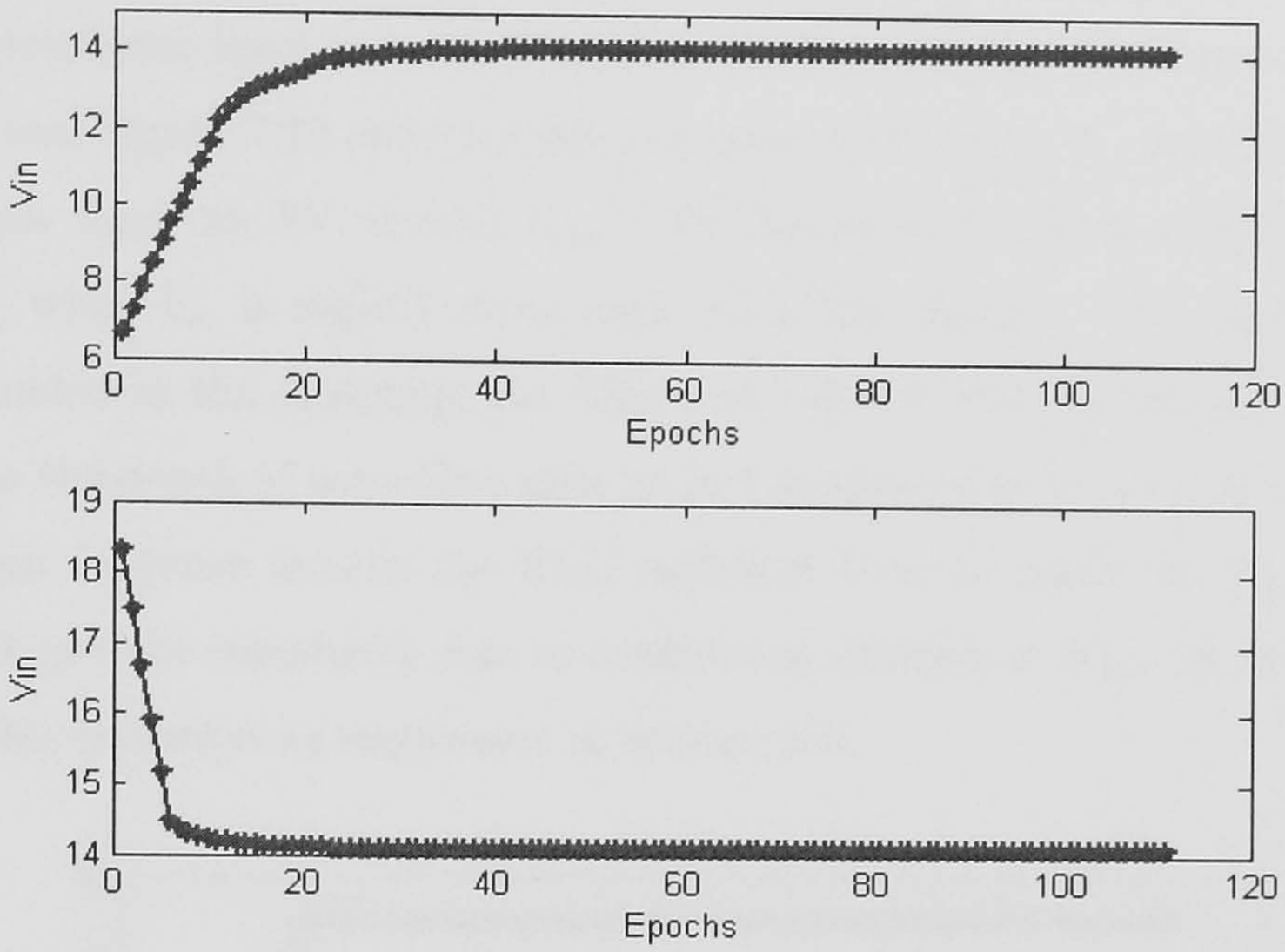

Figure 7.11: Tracking maximum power point at low irradiance and V_{max}=14V

7.4.3 FLC response discussion

Generally, the MFs and rules in section 6.3 are designed to provide a step voltage in each epoch about 0.5V when ΔV is NB and around 0.8V when ΔV is PB. This value decreases continuously, when the V_{in} converges from the V_{max}. Therefore, steady state movement is achieved during the tracking process.

There are an expected increment in V_O that can take place due to the increment in the output current of the DC-DC converter during tracking process. This increasing in V_O leads to a more moving toward the V_{max} when the ΔV is negative and force the V_{in} slightly away from V_{max} when ΔV is positive. Accordingly, there is sufficient voltage margin between the maximum step voltage and the actual step voltage, when ΔV is NB.

As discussed in section 6.3 the MFs are designed to decrease the Zero dD region from about 0.8V around V_{max} at low irradiance level to approximately 0.3V at the medium and high irradiance level as shown in Figures 7.8 and 7.9 at high irradiance level and Figures 7.10 and 7.11 at low irradiance level.

A roughly zero response of dD when ΔV changes in voltage range about 0.8V at low irradiance level and about 0.3V at medium at high irradiance level. Figure 7.14 and Figure 7.15 show a 0.001 response of dD when V_{in} diverge in a voltage margin equal to .8V around V_{max}. Furthermore, it shows a high response of FLC, when V_{in} is slightly move away from this margin. This high response is assembled in the designing the MFs and rules of FLC to strongly returns the V_{in} to the depth of zero dD region at low irradiance level. In addition, the zero margin response awards the FLC sufficient time to track the V_{max}, and as a result prevent instability due to continuous changes in V_{max} at sudden change of solar radiation as mentioned in section 6.3.

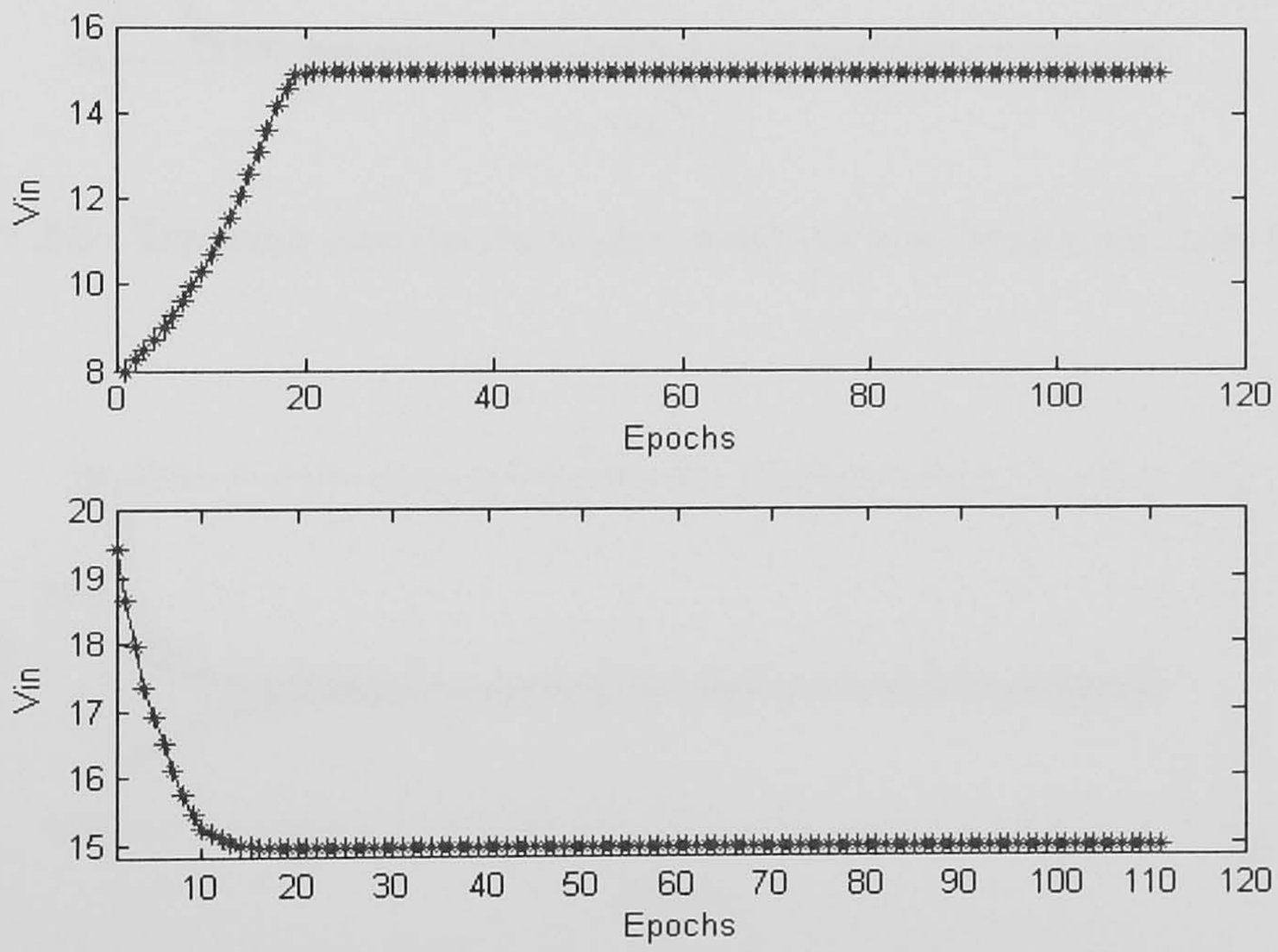

Figure 7.12: Tracking maximum power point at high irradiance and V_{max}=15V

7.5 Final results of the MPPT system with check data

The final proposed ANFIS model has been implemented with actual input check data to predict the V_{max}. Consequently, the actual V_{max} data has been mea-

7.5 Final results of the MPPT system with check data

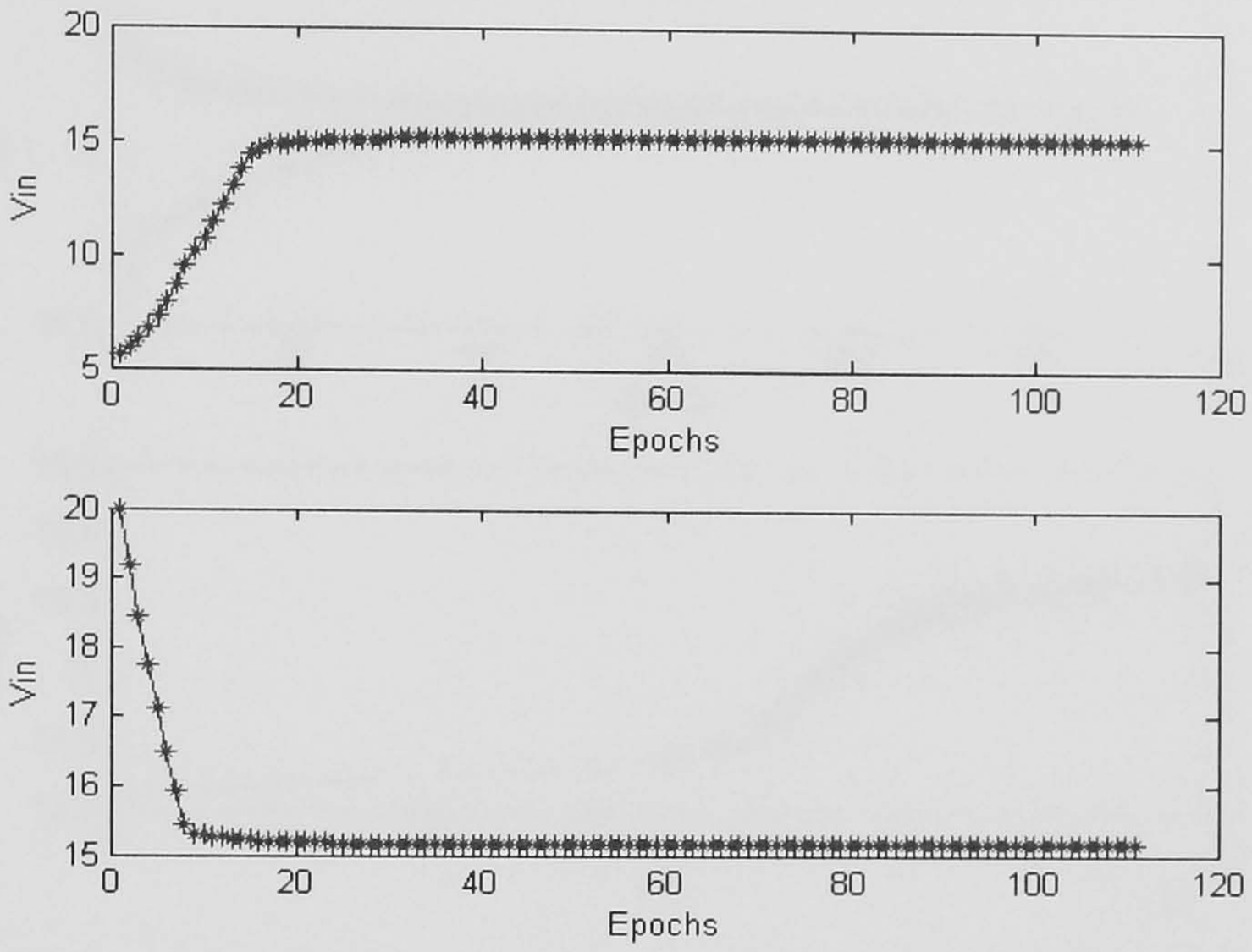

Figure 7.13: Tracking maximum power point at low irradiance and V_{max}=15V

Figure 7.14: An approximate FLC Zero response at low ΔV for Buck-Boost converter

7.5 Final results of the MPPT system with check data

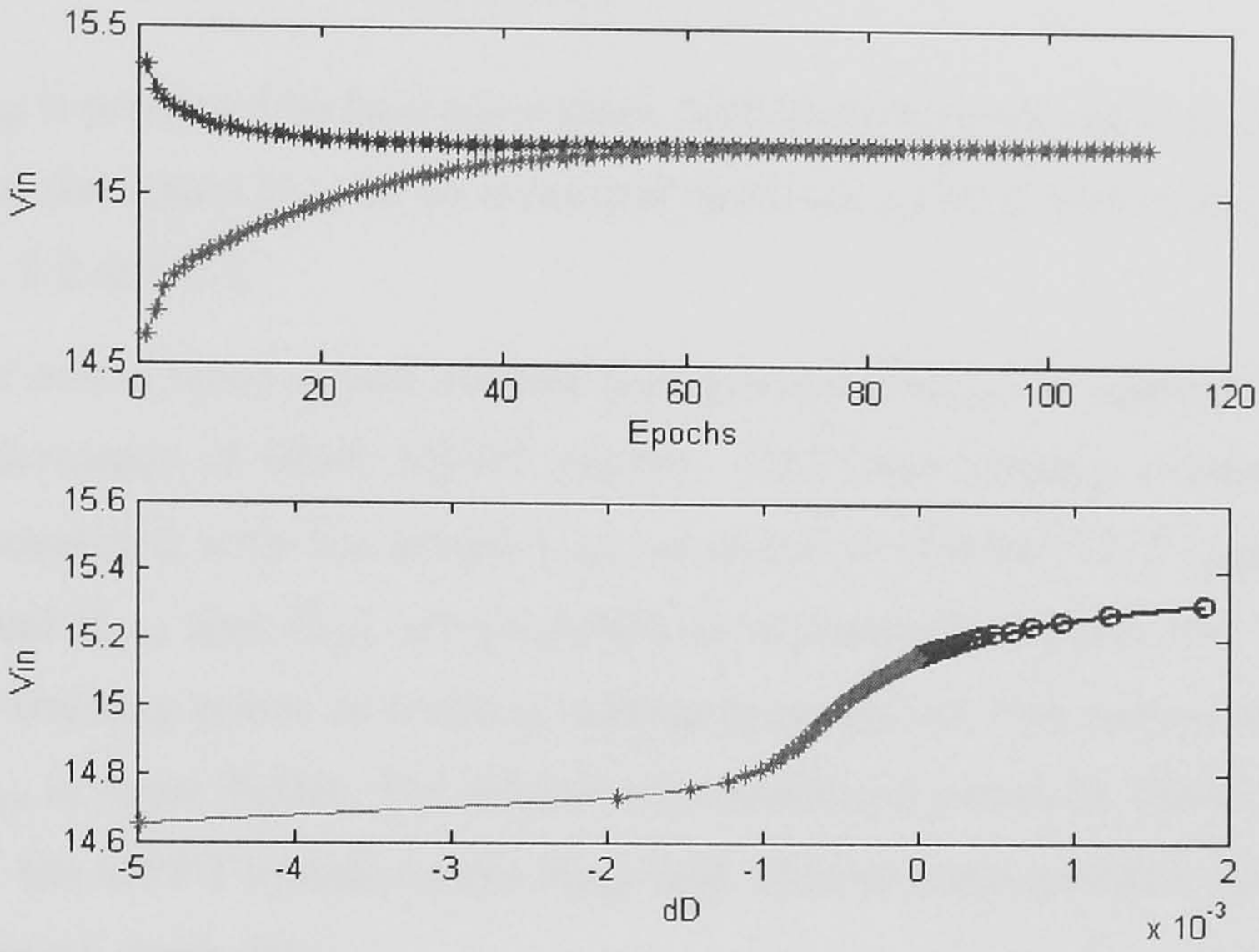

Figure 7.15: An approximate FLC Zero response at low ΔV for Buck converter

sured immediately around the predicted values. Few actual measured values are performed to get hold of position of P_{max}. Thus, P_{max} values are located using ANFIS model for three different types of PV panel.

After we provide the simulation model of MPPT system with the specification of each panel separately, the simulation model of MPPT system tracks V_{max} regardless the types of PV panel. Hence, the MPPT system cope with data in Tables 7.1, 7.2 and 7.3 as one group. Furthermore, if the PV systems consist of several numbers of parallel and series panels, the MPPT system handle only one PV cell. This process is accomplished after providing the MPPT system with numbers of PV panels in the system.

The actual data of three panels is tested with the final general ANFIS model and FLC. These points are obtained at low, medium and high irradiance level. The final tracking voltage is obtained using the actual I_{SC} and predicted V_{max} as input of FLC. The actual power is measured at tracking voltage and compared with the actual maximum power at MPP.

7.5.1 Results discussion

V_{max} is predicted by final generalised ANFIS model with less than 1% deflection from the actual V_{max} in all measured check data points that is shown in Tables 7.1, 7.2 and 7.3.

The actual short circuit current and predicted V_{max} are applied to check the performance of whole MPPT system. The final tracking voltage by MPPT is compared with the actual V_{max} as shown in Tables 7.1, 7.2 and 7.3. The actual V_{max} and P_{max} are extracted as explained in section 4.2. In addition, the tracking power at tracking voltage is compared with respect to the actual P_{max} in these Tables. For different manufactured panels in Tables 7.1, 7.2 and 7.3, the MPPT system tracks P_{max} with 1% maximum possible power losses at different check data.

Table 7.1: Actual, predicted and tracking V_{max} and P_{max} of the Kyocera poly crystalline 51W PV panel

Actual Isc	Actual V_{OC}	Actual V_{max}	Actual P_{max}	Predicted V_{max}	Tracking V_{max}	Tracking P_{max}	%Voltage deflection	%Pmax losses
3.35	19.35	14.7	46	14.751	14.9	45.9	0.35	-0.22
3.4	19.12	14.5	45.9	14.473	14.8	45.6	-0.19	-0.65
2.64	19.9	15.5	38.8	15.34	15.2	38.5	-1	-0.77
2.6	20	15.6	38.4	15.423	15.3	38	-1.1	-1
3.45	18.85	14.2	45.47	14.15	14.3	45.42	-0.35	-0.11
2.72	19.5	15.2	38.3	14.99	14.9	38.2	-1.2	-0.27
3.1	19.4	15	41.85	14.85	14.7	41.7	-1	-0.35

7.6 Evaluating the MPPT PV system along with direct coupled system

The developed MPPT system is compared with the direct coupled system. The MPPT system tracks the maximum power with less than 1% power losses in

Table 7.2: Actual, predicted and tracking V_{max} and P_{max} of the Solavolt single crystal 80W PV panel

Actual Isc	Actual V_{OC}	Actual V_{max}	Actual P_{max}	Predicted V_{max}	Tracking V_{max}	Tracking P_{max}	%Voltage deflection	%Pmax losses
5.08	19.85	15.1	63.722	15.229	15.4	63.35	0.85	-0.58
4.23	20.26	15.5	56.11	15.61	15.35	55.8	0.7	-0.55
2.36	20.65	16.7	31.563	16.561	16.4	31.25	-0.8	-0.99
1.6	20.4	16.6	19.422	16.734	16.9	19.25	0.80694	-0.88
4.1	20.3	15.6	54.29	15.653088	15.4	54.15	0.03	-0.25
4.4	20.5	15.8	58.9	15.79	15.6	58.8	0.1	-0.22
3.1	19.9	15.6	40.24	15.72	15.3	39.8	0.7	-1

Table 7.3: Actual, predicted and tracking V_{max} and P_{max} of Solec poly crystalline 90W PV panel

Actual Isc	Actual V_{OC}	Actual V_{max}	Actual P_{max}	Predicted V_{max}	Tracking V_{max}	Tracking P_{max}	%Voltage deflection	%Pmax losses
3.2	18.73	13.9	38.9	14.079	14.2	38.5	1.2	-1
5	18.5	13.4	57.75	13.301	13.2	57.5	-0.7	-0.43
5.5	18.8	13.43	64.85	13.45	13.6	64.6	0.14	-0.38
5.92	17.56	12.4	62	12.353	12.2	61.5	-0.38	-0.81
6.4	19.5	14.5	80.3	14.429	14.3	80	-0.49	-0.37
6.62	18.05	13.5	73.84	13.475	13.3	73.65	-0.18	-0.25
4.2	17.95	13.6	48.7	13.78	13.9	48.2	1.3	-1

different panel types as identified in section 7.5. The PV system can be loaded by a constant voltage load such as batteries or a resistive load system such as DC pumps. The direct coupled systems with two types of load are suggested to study the degenerated power of the PV system.

7.6.1 Degenerated power with constant voltage load

The battery voltage during charging time varies between 12V and 15V [26]. Three constant voltages are selected to evaluate the generated power from PV panels. According to additional voltage drop on the connected wires and blocking diode drop, the power losses of two tested panels are computed with 13V, 15V and 16V batteries load at a high and a low ambient temperatures. These three voltages represent the state of battery at low, medium and high battery voltage with additional voltage drop. Figures 7.16 and 7.17 show the output power of 85W single crystal panel and 51W poly crystalline panel at P_{max}, 13V and 16V operation. The output power is evaluated in high and low ambient temperature conditions as follows:

- The average power losses is around 13% when the PV panels operate in low ambient temperature and low load voltage. However, the poly crystalline panel losses decrease to 3.5% when the PV panels operate in the high ambient temperature and low load voltage. However, the single crystal panel losses decrease to 6.6% in the same mentioned conditions.
- The losses reach to 17% when the poly crystalline panel operates at high ambient temperature and 16V load voltage.

Table 7.4 shows these average losses values at 13V, 15V and 16V at low and high ambient operation conditions.

Practically, the generated power is more essential when the batteries operate at low voltage. Hence, the percentage average power losses at 13V should be considered during the system design. From Table 7.4, the average percentage

losses at 13V are around 13% at low ambient temperature regions. Accordingly, the MPPT system should be included with PV system to reduce these high losses.

Including the 1% maximum power losses in PV system with the MPPT and 2% to 5% power losses in the DC-DC converter, the degenerated power in the direct coupled system is much greater than the total power losses in PV system with the MPPT system. Nevertheless, the additional cost of the MPPT system should be investigated carefully before making any decision. The system capacity and environmental influences should be studied carefully to accomplish the best possible PV system. .

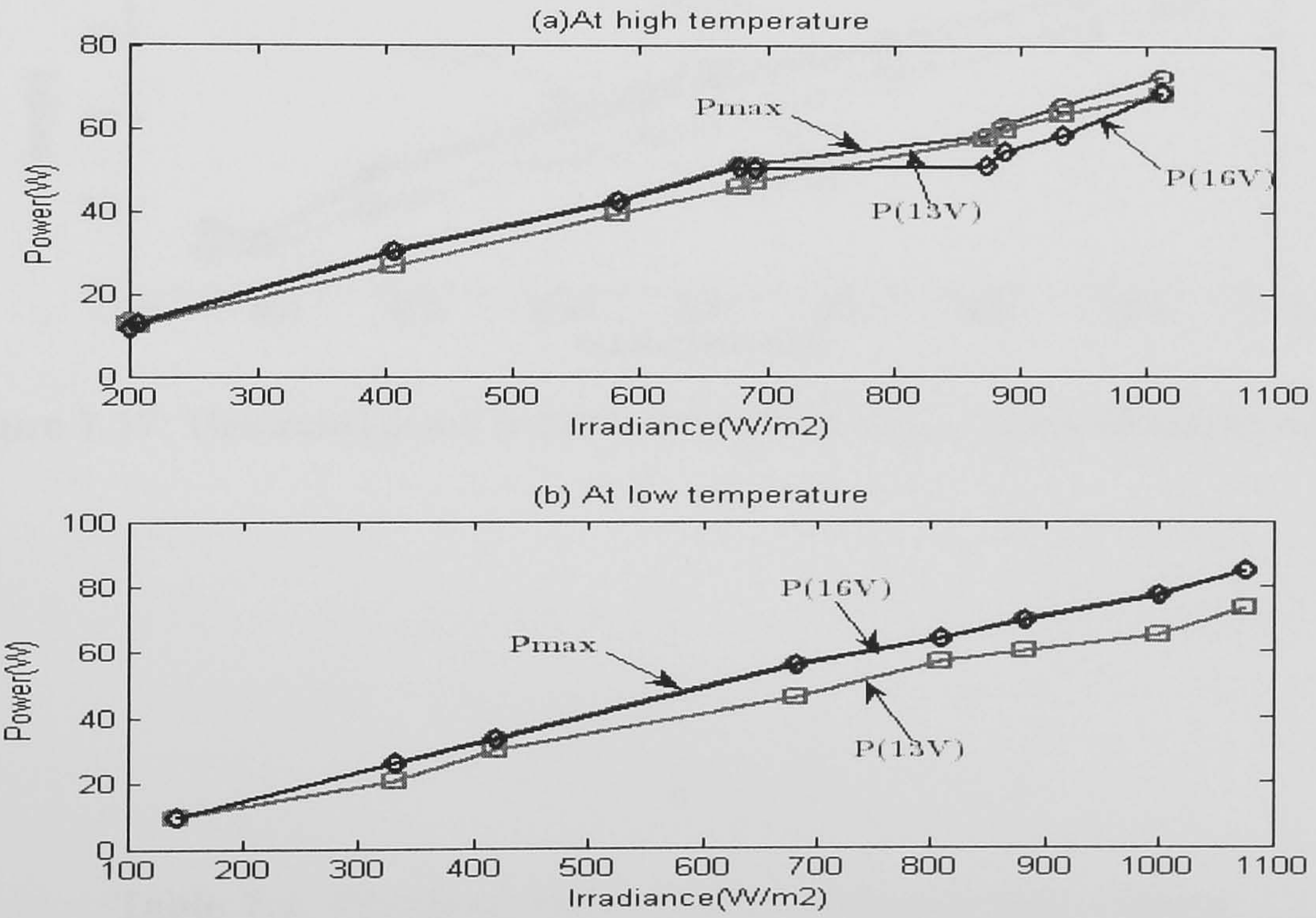

Figure 7.16: Generated power from the 85W PV at V_{max} , 13 and 16 output voltage

7.6.2 Degenerated power with resistive load

The PV systems which are loaded with resistive loads operate in extensive range of I-V curve as addressed in chapter 2 and chapter 6. Typically, the

7.6 Evaluating the MPPT PV system along with direct coupled system

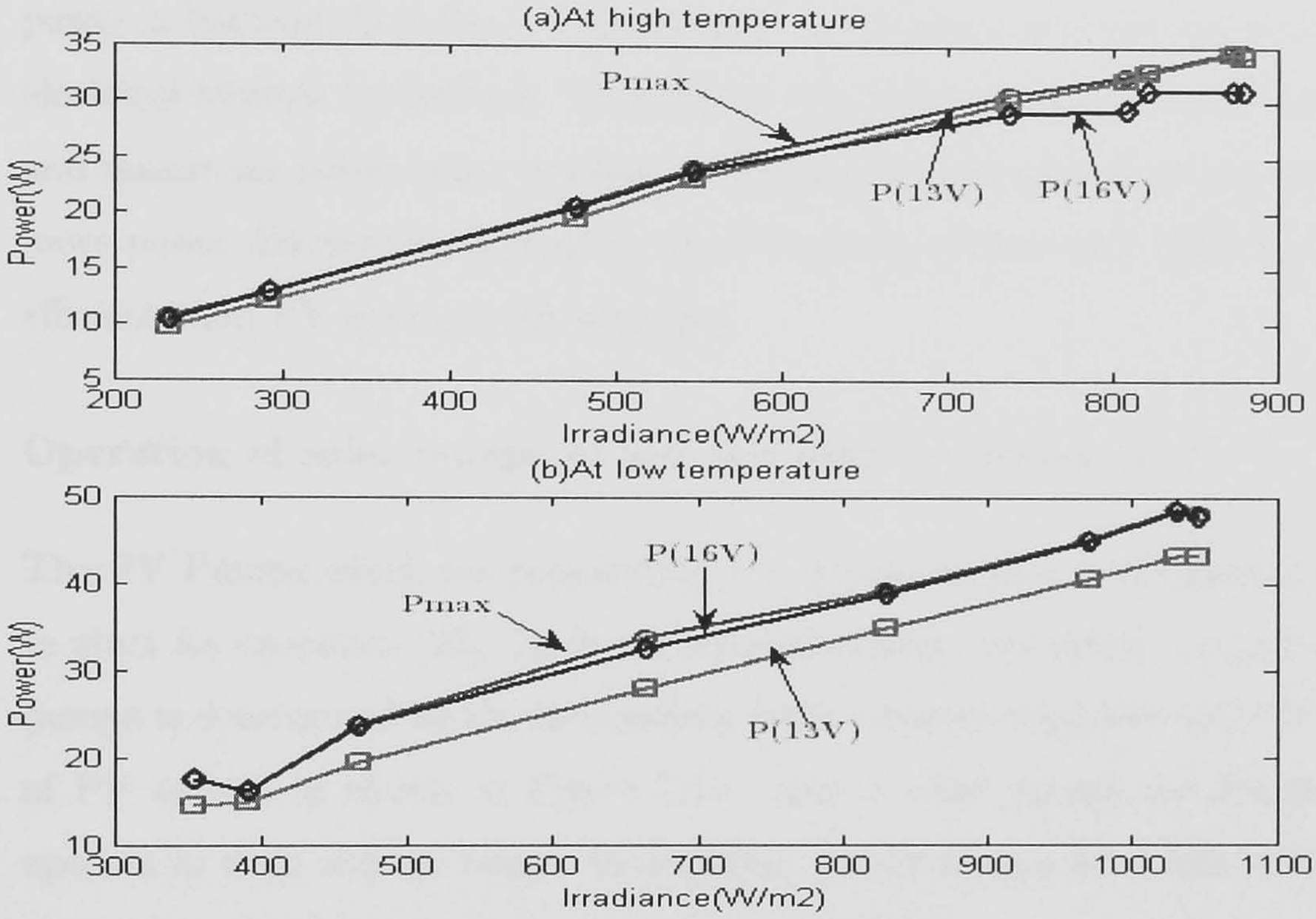

Figure 7.17: Generated power from the 51W PV at V_{max} , 13 and 16 output voltage.

Table 7.4: Percentage power losses at three operating voltages

PV panel	**Single crystal panel**			**Polycrystalline panel**		
Operating voltage	13	15	16	13	15	16
At High Ta	-6.67	-1.6	-6.7	-3.5	-5.1	-17.5
At Low Ta	-13.5	-3.8	-0.78	-12.8	-2.8	-1

direct coupled systems are useful when the centrifugal pumps are used. The positive displacement pumps usually required a MPPT or need to operate with electrical storage to perform effectively [26] [35]. Generally, the 20% dissipated power in batteries hold the system designer to use water tank storage instead of electrical storage on daytime. In addition, the mismatching between batteries and maximum power point position in different environmental conditions adds more power dissipation. Therefore, the PV pump system with MPPT is more efficient than PV system with batteries.

Operation of solar pumps at low and high irradiance level

The PV Pumps which are supplied by PV system require a minimum current to start its operation [26]. In direct coupled system, the motor current of the pumps is determined by the intersection point between load line and I-V curve of PV system as shown in Figure 7.18. Hence, solar pumps are designed to operate in wide voltage range. In addition, the irradiance level has to reach a threshold value before the pump starts its operation.

The direct coupled PV pump system can be either designed to operate at low threshold irradiance, as a result a poor operation at high irradiance level. Otherwise it is designed to achieve a good performance at high irradiance level, consequently a high threshold and poor performance at medium and low irradiance level as shown in Figure 7.18. It can be observed in Figure 7.18, the load line intersects the I-V curves of PV panel in high voltage at low irradiance level. This indicates to a significant threshold voltage at low irradiance level, however the operating point at high irradiance level is very far from the P_{max} . On the other hand, the load line which performs a good operation at high irradiance level drives the PV panels to operate at the point bellow 10V, when the irradiance level is less than $600\text{W}/m^2$. This leads to more than 30% in maximum available power at these irradiance levels.

When the PV system is designed with resistive load to operate at low threshold

irradiance level, the operating point is faraway from MPP as shown in Figure 7.18. Therefore, a high percentage of available generated power is lost at medium and high irradiance due to the poor operation on the I-V curves.

Operation of solar pumps at low and high ambient temperature

Moreover, the deviation of the operating point due to the high variations in position of V_{max} in different ambient temperatures leads to more degenerated power at constant irradiance level. Figure 7.19 shows the voltage deviation in operating voltage at low, medium and high surface temperature of 85W PV panel in different selected load lines. The voltage deflects more than 1V between minimum and maximum Ts at the same load line.

Furthermore, when the load is selected according to I-V curves at a high ambient temperature, V_{max} at low ambient temperature deviates about 2V as shown in Figure 7.19. Consequently, about 8% power drop from the maximum available generated power of PV panel. Additionally, 5% decline in maximum available generated power is computed when the load line is selected according to the low T_S when PV panels operate in low ambient temperature regions.

The significance of using MPPT system with solar pumps

In solar pumps system, it essential to study carefully the capacity of PV system that generates the power for the solar pump. In addition, the effect of solar irradiance and ambient temperature on power generated should be considered during system designing. Thus, there are two main benefits of using MPPT system:

- To operate the pumps for long time during daytime.
- To operate the PV panel at MPP in different irradiance levels and ambient temperatures.

7.6 Evaluating the MPPT PV system along with direct coupled system

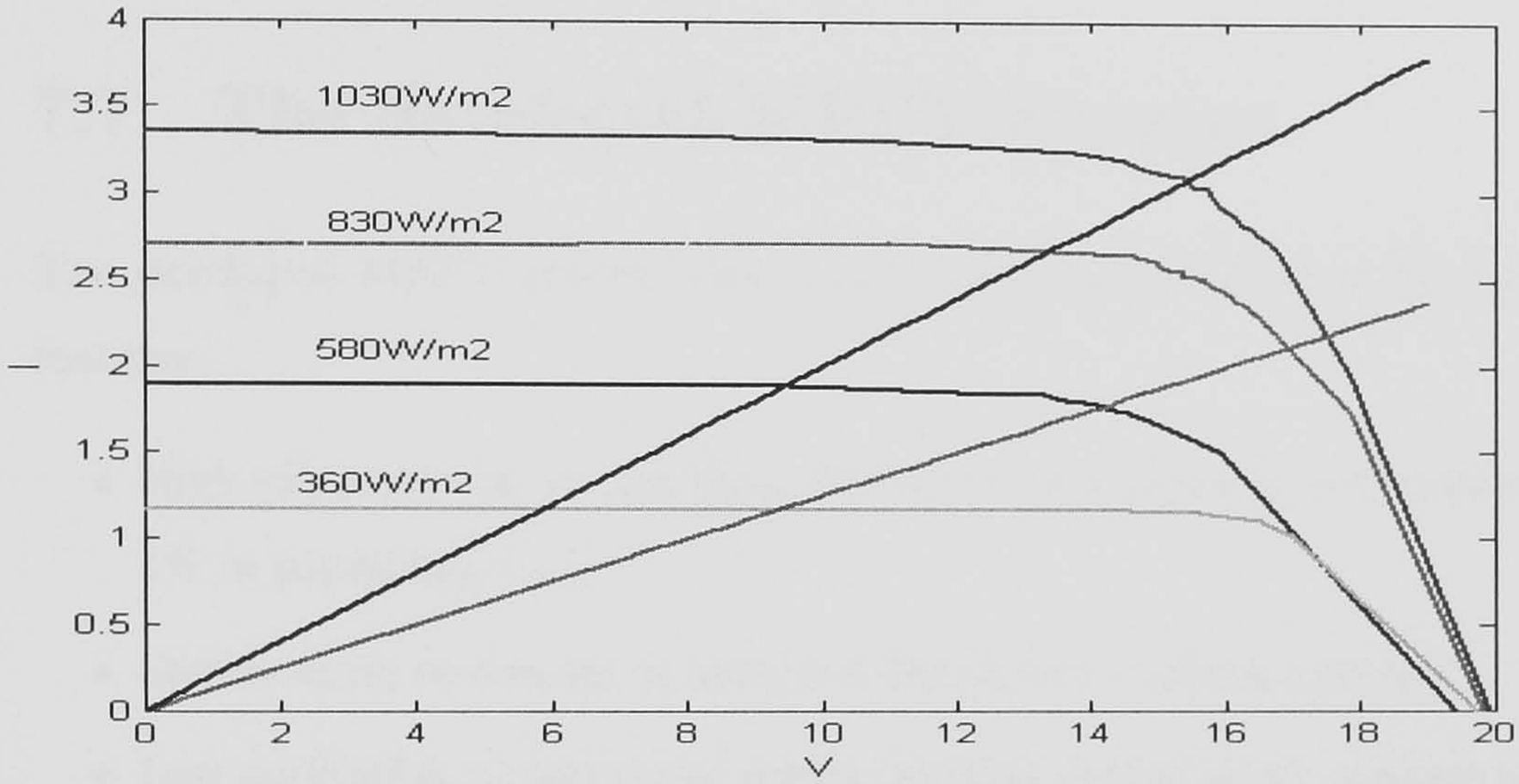

Figure 7.18: Operating point at different resistive loads and different irradiance levels

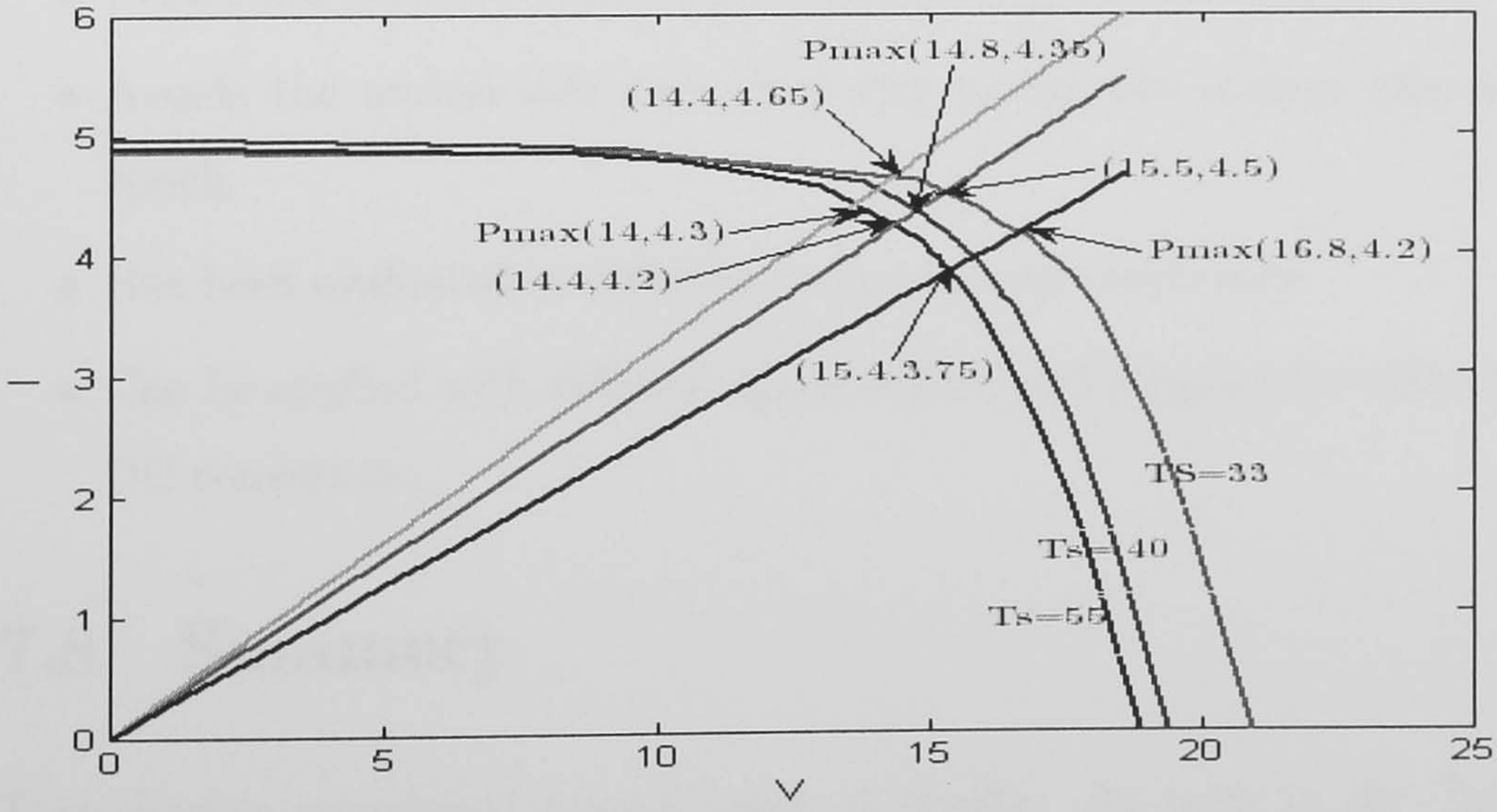

Figure 7.19: Operating point for resistive load at constant irradiance level and different Ts

Finally, more than one recommendation will be included in chapter 8 depending on pervious analysis.

7.7 The developed MPPT features

The developed MPPT system with ANFIS model and FLC has the following features.

- High efficiency due to less than 1% error in maximum power tracking and 1% in predicting V_{max} .
- Steady state movement is achieved during thc tracking process.
- Low oscillation in maximum power tracking during quick changes in environmental conditions.
- Avoids the fluctuation around MPP.
- It doesn't need external sensors to locate and track the maximum power point.
- Provides a fast and stable maximum power point tracking.
- Avoids the undesirable harmonics due to the low voltage step in each epoch.
- Has been evaluated in different environmental conditions.
- Can be applied with different types of load and adapted for different DC-DC converters.

7.8 Summary

This chapter introduced several types of results. As been in the Table 4.2 section 4.2 the result is used for validation purposes. The first type is the general ANFIS model result. The second type shows the performance of FLC. The third shows the final output of MPPT parts and it compared with actual

output. In the fourth the MPPT system has been evaluated with respect to the direct coupled system. Finally, more than one recommendation are extracted from the results in this chapter will be introduced with conclusions and future work in next chapter.

Chapter 8

Conclusion, Recommendations and Future Work

8.1 Summary

It is necessary to study the environmental conditions in which the PV system is installed. The high alteration in the environmental conditions affects the location of MPP. Hence, it is important to design the PV system depending on sufficient knowledge to perform the excellent PV design to save the generated power from PV panels.

To study the behaviour of PV panels in different environmental conditions, the field data was collected in different seasons in Yemen. This data was collected from three main different regions in different climates for the period of two years. The first region is the mountain areas, the second is the desert areas, and the third is the coastal areas. Two thirty-six single crystal and polycrystalline PV solar panels were used to collect the field data.

Actual I_{SC}, V_{OC}, V_{max} and I_{max} are the main electrical parameters that were measured during data collection. The actual short circuit current and open circuit voltage are used as inputs of ANFIS models instead of solar irradiation and cell junction temperature to predict the maximum power point voltage. More than one ANFIS models are tested to reach the best model that can predict the accurate V_{max}. The selected ANFIS models are developed with per unit data and learning algorithms to reach the final ANFIS model which can be implemented with different single crystal and poly crystalline PV systems.

The predicted V_{max} from ANFIS model is used with actual I_{SC} as input for the FLC to control the duty cycle of DC-DC converters. The FLC is used

to control the rate of change in duty cycle of electronic switch of Buck-Boost converter and Buck converter. These DC-DC converters are used to interface between the load voltage PV panels. The duty cycle of the electronic switch of the DC-DC converter is adjusted until the input voltage of a converter tracks the predicted V_{max} of the PV system.

Two simulation models are designed to test and improve the performance of final FLC. The simulation models are utilised to improve the MFs and rules of FLC to reach the best performance of MPPT system. The performance of final FLC model has been tested to show the maximum power point tracking performance at different irradiance levels and different values of V_{max}. In addition, the performance of developed MPPT has been compared with direct coupled PV systems.

The following contributions demonstrate the novelties in this thesis.

8.2 Contributions

The main contributions in this thesis are:

- The contribution in the methodology of data collection and its evaluation in this thesis provides sufficient and appropriate parameters for the developed MPPT system. The acquisition choice is accomplished in order to reach sufficient knowledge of PV panel behaviour in different environmental conditions. In addition, data was evaluated three times after design the initial ANFIS models. More data was added to fill the shortage in the collected data and as a result the performance of ANFIS model is improved at different irradiance levels and PV cell temperatures.
- The contribution in the methodology of utilising the statistical analysis methods and observation in the PV panels behaviour during data collection is highly used to select the simple input paramcters for the ANFIS models and FLC.

- The methodology of developing the ANFIS model is one of the main important novelties in this research. More than one ANFIS model were tested to reach the best model that can predict the accurate V_{max} with minimum error. Subtractive clustering has been used to overcome the shortage in the iterative modification of MFs premise parameters which is performed by gradient descent learning algorithm. Furthermore, the selected ANFIS models is developed by applying the LSE algorithm during forward learning to improve the accuracy of the ANFIS model prediction by modifying the consequent linear parameters of ANFIS model.

- The novel MPPT system with FLC are designed to balance the different requirements features of PV system such as, quick tracking in different environmental conditions, high accuracy, stability and high efficiency. The FLC is designed to achieve the most promising performance in different environmental conditions, different types of load and two types of DC-DC converters. In addition, the MFs of the developed FLC are designed jointly with the rules to minimise the number of rules that are used in FLC.

In the next section a number of recommendations will be introduced. These recommendations help in PV systems design.

8.3 Recommendations

The following recommendations are based on data analysis and final results in chapter 7:

- It is better to design the PV system that is used in solar pumps according to the highest possible T_S at the highest possible irradiance level in certain region. This keeps V_{max} over operating voltage at different environmental conditions. Hence, the MPPT system with Buck converter is preferred because it is more efficient than Buck-Boost converter.

- It is more efficient to use the single crystal panels which have higher operating V_{max}, in high climate temperature regions. These high operating voltages help the PV panels to operate near the maximum power point especially with batteries load.
- To overcome the problem of low V_{max} at high ambient temperature, it is recommended to increase the PV cells in the PV panel to 40 cell to make V_{max} higher than the load voltage. Hence, the step down voltage converter becomes more available in MPPT system especially with batteries load. On the other hand, in low ambient temperature regions it is better to use PV panels that have less than 36 cells to reduce the cost of PV system and as a result the total cost of PV system.
- The cost of MPPT system and power losses in DC-DC converter are the critical features that should be studied carefully. In addition, the capacity of PV system and the total power saving by MPPT system should be considered in the feasibility study.
- Two solutions are introduced for the small PV system to reduce the degenerated power. The first solution is by matching the number and type of PV panel cells with load voltage according to the range of V_{max} that can be expected in this region. The second solution is by using a sun tracker especially with pumps load to maintain the irradiance at high levels during daytime. Consequently, the sun tracker prevents a poor operation at low and medium irradiance levels as discussed in section 4.6.

In addition to these recommendations the next section will introduce the suggested future work for other researchers.

8.4 Future work

Four areas are recommended to enhance the developed MPPT system that is introduced in this thesis.

- The developed MPPT system is implemented with single crystal and poly-crystalline PV panel which are the wide used panels in the market. An amorphous panel is a different type of PV panels which has different behaviour from the two types that are investigated in this research. However, the proposed technique in this thesis can be modified to implement with amorphous panels and its data.
- After a long time the PV panels will be degraded. Therefore, the behaviour of PV panels will be slightly changed [26]. Accordingly, if PV panels are tested after 15 continuous operating years, the ANFIS model can be enhanced with a factor to adjust the output nonlinear parameters. Also, the Perturb and observation method can be utilised to modify the learning data of ANFIS model which is affected by degradation. Perturb and observation method can be used for sufficient time to renew the learning data of ANFIS model. This operation can be performed one or two times during PV life time.
- The behaviour of different PV pumps should be studied at different operating power and voltage. The effect of environmental conditions on V_{max} and P_{max} can be matched with the operating voltage and power of PV pumps. Consequently, the PV pump can be selected according to the available options.
- ANFIS can be used to design the MFs of FLC. The input-output data relationship can be determined by experts according to the system requirements. ANFIS can help on designing more options of MFs that can be used in FLC. In addition, ANFIS does not require a long time to reach the best MFs structure of FLC [5].
- The electronic simulation programs can provide more details about the behaviour of DC-DC converters. Hence, it can be used to determine the accurate effect of V_O on input voltage of DC-DC converter during the tracking process.

Bibliography

[1] Abd El-Shafy A. Nafeh, Faten H. Fahmy, Osama A. Mahgoub and Essam M. Abou El-Zahab (1999), "Microprocessor control system for maximum power operation of PV arrays", International Journal of Numerical Modelling: Electronic Networks, Devices and Fields Jun 1999, Vol. 12, Issue 3, pp. 187-195.

[2] Altas, I.H. Sharaf and A.M. (1994), "A novel fuzzy logic controller for maximum power extraction from a PV array driving a three-phase induction motor", 7th Mediterranean Electrotechnical Conference, 12-14 Apr, Vol. 2, pp. 853-856.

[3] I. H. Altas and A. M. Sharaf 1(1996), "A novel on-line MPP search algorithm for PV arrays", IEEE Trans. Energy Convers, Dec, Vol. 11, no. 4, pp. 748-754.

[4] Altas, I.H. Sharaf and A.M. (2007), "Novel Control Strategies Using Load Matching for Maximum Photovoltaic Energy Utilization", Canadian Conference on electrical and Computer Engineering, 22-26 April, pp. 1578-1581.

[5] Angelov P.P., V. I. Hanby, J. A. Wright (2000), "HVAC Systems Simulation: A Self-Structuring Fuzzy Rule-Based Approach, International Journal of Architectural Sciences, Vol.1, No1, 2000, pp. 30-39.

[6] Angelov P., D. Filev (2004), "An Approach to On-line Identification of Takagi-Sugeno Fuzzy Models", IEEE Transactions on System, Man, and Cybernetics, part B - Cybernetics, Vol.34, No1, 2004, pp. 484-498. ISSN 1094-6977.

[7] Angelov P. P., "A Fuzzy Controller with Evolving Structure, Information Sciences, ISSN 0020-0255, vol.161, 2004, pp.21-35.

[8] Antonio Luque and Steven Hegedus (2003), "Handbook of Photovoltaic Science and Engineering", John Wiley and Sons Ltd, Chichester, West Sussex PO19 8SQ, England.

[9] A. Aziz Aldobhani (2001), "Study of the Factors Affecting the Efficiency of the Photovoltaic Systems", University of Science and Technology-Yemen, Master thesis, May.

[10] A. Aziz Aldobhani (2004), "Power Output improvement by Using Two Axis Tracking Solar System", Yemen scientific research foundation, Science Conference 11-13 Oct..

[11] A. Aziz Aldobhani (2002), "Solar pump in Yemen", Journal of Science and Technology, Vol. 12, no. 1, Issue 1, pp. 1670-1673.

[12] A. Aziz Aldobhani, Fahr H. and A. R. Assad (2001), " Factors Affecting the efficiency of PV systems", Sharjah solar conference, 19-22 Feb, 189-PVPH08

[13] A. B. G. Bahgat, N. H. Helwa, G. E. Ahmad and E. T. El Shenawy (2005), "Maximum power point tracking controller for PV systems using neural networks", Renew. Energy, Vol. 30, pp. 1257-1268.

[14] Bezdek and J.C. (1981), "Pattern Recognition with Fuzzy Objective Function Algorithms", Plenum Press, New York.

[15] Boutalis, Yiannis S. Karlis, Athanassios D. Kottas and Theodoros L. (2006), "Fuzzy Cognitive Networks + Fuzzy Controller as a self adapting control system for Tracking Maximum Power Point of a PV-Array", IEEE 32nd Annual Conference on Industrial Electronics, IECON 2006, Issue Nov., pp. 4355-4360.

[16] Brambilla, A. Gambarara, M. Garutti, A. Ronchi and F. (1999), "New approach to photovoltaic arrays maximum power point tracking", 30th Annual IEEE Power Electronics Specialists Conference, Vol. 2, Issue 1999, pp. 632-637.

[17] Cai, C.H. Du, D. Liu and Z.Y. (2003), "Battery state-of-charge (SOC) estimation using adaptive neuro-fuzzy inference system (ANFIS)", The 12th IEEE International Conference on Fuzzy Systems, 25-28 May, Vol. 2, pp. 1068-1073.

[18] J. Casillas, O. Cordon, F. Herrera, L. Magdalena and J. V. De Oliveira (1999), "Semantic constraints for membership function optimization", IEEE Trans. Syst., Man, Cybern. Part A-Systems and Humans, Vol. 29, pp. 128-138.

[19] Chiu S. (1994), "Fuzzy Model Identification Based on Cluster Estimation", Journal of Intelligent and Fuzzy Systems, Sept., Vol. 2, no. 3.

[20] Chung, H.S.-H. Tse, K.K. Hui, S.Y.R. Mok, C.M. Ho and M.T. (2003), "A novel maximum power point tracking technique for solar panels using a SEPIC or Cuk converter", IEEE Transactions on Power Electronics, May, Vol. 18, Issue 3, pp. 717-724.

[21] M. N. Cirstea, A. Dinu, J. G. Khor and M. MC (2000), "Neural and Fuzzy logic control of drives and power system", Newnes, Oxford, England.

[22] David Linden and Thomas B. Reddy (2002), "Hand Book of Batteries", Third edition, MC Grow-Hill, USA.

[23] De Medeiros Torres, A. Antunes, F.L.M. dos Reis and F.S. (1998), "An artificial neural network-based real time maximum power tracking controller for connecting a PV system to the grid", Proceedings of the 24th Annual Conference of the IEEE, 31 Aug.-4 Sept., Vol. 1, pp. 554-558.

[24] El-Sayed and M.A.H. (1997), "Fuzzy clustering and fuzzy sets for reliability analysis of recent distribution systems", IEEE International Conference on Intelligent Engineering Systems, 15-17 Sept., pp. 277-282.

[25] M. Enrique, E. Duran, M. Sidrach-de-Cardona and J.M. Andujar (2007), "Theoretical assessment of the maximum power point tracking efficiency of photovoltaic facilities with different converter topologies", Solar Energy, January, Vol. 81, Issue 1, pp. 31-38.

[26] Florida solar energy center (1996), "Photovoltaic system Design", April 1996.

[27] Friedrich Sick and Thomas Erge (1996), " Photovoltaic in building", International Energy Agency.

[28] Gwon-Jong, Yu Myung-woong Jung, Jinsoo Song, In-Su Cha and In-Ho Hwang (1996), "Maximum power point tracking with temperature compensation of photovoltaic for air conditioning system with fuzzy controller", Twenty Fifth IEEE Conference on Photovoltaic Specialists, 13-17 May, pp. 1429-1432.

[29] R. M. Hilloowala and A. M. sharaf (1992), "A Rule-Based Fuzzy Logic Controller for A PWM Inverter in Photovoltaic Energy Conversion Scheme", Proceedings of the IEEE Industry Application Society Annual Meeting, Oct., pp. 762-769.

[30] Hilloowala R.M. and Sharaf A.M. (1996), "A rule-based fuzzy logic controller for a PWM inverter in a standalone wind energy conversion scheme", IEEE Transactions on Industry Applications, Jan/Feb, Vol. 32, Issue 1, pp. 57-65.

[31] T. Hiyama, S. Kouzuma and T. Iimakudo (1995), "Identification of optimal operating point of PV modules using neural network for real time maximum power tracking control", IEEE Trans. Energy Conversion, June, Vol. 10, pp. 360-367.

[32] T. Hiyama and K. Kitabayashi (1997), "Neural network based estimation of maximum power generation", IEEE Trans. Energy Conversion, Sept., Vol. 12, pp. 241-247.

[33] C. Hua and C. Shen (1998), "Study of maximum power tracking techniques and control of dc-dc converters for photovoltaic power system", in Proc. 29th Annu. IEEE PESC, 17-22 May, Vol. 1, pp. 86-93.

[34] C. Hua, J. Lin and C. Shen (1998), "Implementation of a DSP-controlled photovoltaic system with peak power tracking", IEEE Trans. Ind. Electron., Feb., Vol. 45, pp. 99-107.

[35] Ibrahim, H.E.-S.A. Houssiny, F.F. El-Din, H.M.Z. El-Shibini and M.A. (1999), "Microcomputer controlled buck regulator for maximum power point tracker for DC pumping system operates from photovoltaic system", Fuzzy Systems Conference Proceedings, 22-25 Aug., Vol. 1, pp. 406-411.

[36] J. S. R. Jang (1993), "ANFIS: Adaptive-network-based fuzzy inference systems", IEEE Transactions Systems, Man and Cybernetics, May, Vol. 23, no. 3, pp. 665-685.

[37] Jang, J.-S. R. and N. Gulley (1994), "Gain scheduling based fuzzy controller design", Proc. of the International Joint Conference of the North American Fuzzy Information Processing Society Biannual Conference, the Industrial Fuzzy Control and Intelligent Systems Conference, and the NASA Joint Technology Workshop on Neural Networks and Fuzzy Logic, San Antonio, Texas, Dec..

[38] Jang, J.-S. R. and C.-T. Sun (1995), "Neuro-fuzzy modeling and control", Proceedings of the IEEE, March.

[39] J.-S. R. Jang, C.-T. Sun and E. Mizutani (1997), "Neuro-Fuzzy and Soft Computing", Prentice Hall, USA.

[40] John A. Duffie and William A. Beckman (1991), "Solar engineering thermal processes", second edition, A Wiley- international publication, USA.

[41] G. J. Yu, Y. S. Jung, J. Y. Choi and G. S. Kim (2004), "A novel two-mode MPPT control algorithm based on comparative study of existing algorithms", Solar Energy, Vol. 76, pp. 455-463.

[42] N.Kasa, T.lida and H. Lwamoto (2000), "Maximum power point tracking with capacitor identifier for PV power system", IEEE Procd-Electr. Power application, Nov., Vol. 147, no 6.

[43] N.Kasa, T.lida and H. Lwamoto (2000), "Maximum power point tracking with capacitor identificator for PV power system", IEE Power electronic and variable speed drives 18-19 Sep..

[44] N. Kasabov, Q. Song (2002), "DENFIS: Dynamic Evolving Neural-Fuzzy Inference System and Its Application for Time-Series Prediction", IEEE Trans. on Fuzzy Systems, Vol.10 (2), pp. 144-154.

[45] K. Kim, J. Baek, E. Kim, M. Park (2005), "TSK Fuzzy model based on-line identification, Proc. 11th IFSA World Congress, Beijing, China, pp. 1435-1439.

[46] A. Kislovski and R. Redl (1994), "Maximum-power-tracking using positive feedback", in Proc. IEEE Power Electron. Spec. Conz, pp. 1065-1068.

[47] G. F. Klir and T. A. Folger (1988), "Fuzzy Sets, Uncertainty, and Information" Englewood Cliffs, NJ: Prentice-Hall.

[48] T. Kottas, Y. Boutalis and M. Christodoulou (2005), "A new method for weight updating in Fuzzy cognitive maps using system feedback", in Proc. 2nd ICINCO, Barcelona, Spain, Sep. 13-17, pp. 202-209.

[49] Kottas, T.L. Boutalis, Y.S. Karlis and A.D. (2006), "New maximum power point tracker for PV arrays using fuzzy controller in close cooperation with fuzzy cognitive networks", IEEE Transaction on Energy Conversion, Sept., Vol. 21, Issue 3, pp. 793-803.

[50] E. Koutroulis, K. Kalaitzakis and N. C. Voulgaris (2001), "Development of a microcontroller-based, photovoltaic maximum power point tracking control System", IEEE Trans. Power Electron, Jan, Vol. 16, no. 1, pp. 46-54.

[51] F Lasnier and TG Ang. (1990), "Photovoltaic Engineering Handbook", IOP Publishing Ltd, Bristol, England.

[52] E. Lorenzo (1994), "Solar Electricity- Engineering of Photovoltaic Systems", PROGENSA, S.A., Sevilla, Spain.

[53] A.M.A. Mahmoud, H.M. Mashaly, S.A. Kandil, H. El Khashab and M.N.F. Nashed (2000), "Fuzzy Logic Implementation For Photovoltaic Maximum Power Tracking", Proceedings 9th IEEE International Workshop on Robot and Human Interactive Communication, pp. 155-160.

[54] Mamdani, E.H. and S. Assilian (1975), "An experiment in linguistic synthesis with a fuzzy logic controller", International Journal of Man-Machine Studies, Vol. 7, no. 1, pp. 1-13.

[55] Mashaly, H.M. Sharaf, A.M. Mansour, M.M. El-Sattar and A.A. (1993),"Fuzzy logic controller for maximum power tracking in line-commutated photovoltaic inverter scheme", Canadian Conference on Electrical and Computer Engineering, 14-17 Sep, pp. 1287-1290.

[56] Mashaly, H.M. Sharaf, A.M. Mansour, M.M. El-Sattar and A.A. (1994), "A photovoltaic maximum power point tracking using neural networks", 3rd-IEEE-Control application, 24-26 Aug., Vol. 1, pp. 167-172.

[57] Masoum, M.A.S. Dehbonei, H. Fuchs and E.F. (2002), "Theoretical and experimental analyses of photovoltaic systems with voltage and current-based maximum power-point tracking", IEEE Transaction on Energy Conversion, Dec., Vol. 17, Issue 4, pp. 514-522.

[58] MATLAB help (2004), Version 7, May 2004.

[59] Mellit A. (2006), "Development of an expert configuration of stand-alone power PV system based on adaptive neuro-fuzzy inference system (ANFIS)", Electro Technical Conference, MELECON 2006. IEEE Mediterranean, Issue 16-19 May, pp. 893-896.

[60] Mellit, A. Kalogirou and S.A. (2006), "Neuro-Fuzzy Based Modeling for Photovoltaic Power Supply System", Power and Energy Conference, PECon '06. IEEE International, 28-29 Nov.

[61] Mellit A. (2006), "Artificial intelligence based-modeling for sizing of a Stand-Alone Photovoltaic Power System: Proposition for a New Model using Neuro-Fuzzy System (ANFIS)", 3rd International IEEE Conference on Intelligent Systems, Sept., pp. 606-610.

[62] Mohan and Robbins (1989), "Power electronics converter application design", John Willy, USA.

[63] Momoh, J.A. Ofoli and A.R. (2001), "Load management and control of the photovoltaic (PV) system using fuzzy logic", Conference on Engineering Systems and Power Engineering, Issue 2001, pp. 184-188.

[64] Muhammad Iqbal, Valnicek B. (1983),"An Introduction to Solar Radiation", Space Science Reviews V.39.

[65] Muhammdi H. Rashid (1993), "Power electronics- Converter application", Prentice Hall international edition, New Jercy, USA.

[66] Mummadi Veerachary and Tomonobu Senjyuand Katsumi Uezato (2002), "Feedforward Maximum Power Point Tracking of PV Systems Using Fuzzy Controller", IEEE Transactions on aerospace and electronic system, July, Vol. 38, no. 3, pp. 969-981.

[67] Patcharaprakiti and S. Premrudeepreechacharn (2002), "Maximum Power Point Tracking Using Adaptive Fuzzy Logic Control for Grid-Connected Photovoltaic System", IEEE Power Engineering Society Winter Meeting, pp. 372-377.

[68] Khaehintung, N. Pramotung, K. Tuvirat and B. Sirisuk (2004), "RISC-microcontroller built-in fuzzy logic controller of maximum power point tracking for solar-powered light-flasher applications", 30th Annual Conference of IEEE Industrial Electronics Society, 2-6 Nov., Vol. 3, pp. 2673-2678.

[69] Khaehintung, N. Pramotung, K. Sirisuk and P. (2004), "RISC microcontroller built-in fuzzy logic controller for maximum power point tracking in solar-powered for battery charger", 2004 IEEE Region 10 Conference, 21-24 Nov, Vol. D., pp. 637-640.

[70] Khaehintung, N. Sirisuk and P. Kurutach W. (2003), "A novel ANFIS controller for maximum power point tracking in photovoltaic systems", The Fifth International Conference on Power Electronics and Drive Systems, 17-20 Nov., Vol. 2, pp. 833-836.

[71] Robert John, "ANFIS note", Centre for Computational Intelligence, DE Montfort University, UK.

[72] Salameh and Taylor D. (1990),"Step-up maximum power point tracker for photovoltaic arrays", Solar Energy Journal, Vol. 44, pp. 51-57.

[73] Senjyu, T. Uezato and K. (1994), "Maximum power point tracker using fuzzy control for photovoltaic arrays", Proceedings of the IEEE International Conference on Industrial Technology, 5-9 Dec, pp. 143-147.

[74] Simoes, M.G. Franceschetti, N.N. Friedhofer and M. (1998), "A fuzzy logic based photovoltaic peak power tracking control", Industrial Electronics, IEEE International Symposium, 7-10 Jul, Vol. 1, pp. 300-305.

[75] Simoes, M.G. Franceschetti and N.N. (1999), "Fuzzy optimisation based control of a solar array system", IEE Proceedings on Electric Power Applications, Sep., Vol. 146, Issue 5, pp. 552-558.

[76] Simon Roberts (1991), " Solar electricity", Prentice Hall international, UK.

[77] Spath H. (1985), "Cluster Dissection and Analysis: Theory, FORTRAN Programs, Examples", Translated by J. Goldschmidt, Halsted Press, New York.

[78] Sugeno, M. (1985), "Industrial applications of fuzzy control", Elsevier Science Pub. Co..

[79] Timothy J. Ross (2004), "Fuzzy logic with engineering application", Wiley, Chichester, West Sussex PO19 8SQ, England.

[80] Veerachary, M. Senjyu, T. Uezato and K. (2003), "Neural-network-based maximum-power-point tracking of coupled-inductor interleaved-boost-converter-supplied PV system using fuzzy controller", IEEE Transactions on Industrial Electronics, Aug., Vol. 50, Issue 4, pp. 749-758.

[81] Wai, Rong-Jong Wang, Wen-Hung Lin and Jun-You (2006), "Grid-Connected Photovoltaic Generation System with Adaptive Step-Perturbation Method and Active Sun Tracking Scheme", 32nd Annual Conference on IEEE Industrial Electronic, Nov., pp. 224-228.

[82] Wai, R.-J. Wang and W.-H. (2008),"Grid-Connected Photovoltaic Generation System", IEEE Transactions on Circuits and Systems, April, Vol. 55, pp. 953-964.

[83] Witold Pedry Cz. (1995), " Fuzzy Sets Engineering", CRC Press, USA.

[84] S. Wolf and J. Enslin (1993), "Economical, PV maximum power point tracking regulator with simplistic controller", in Proc. IEEE Power Electron. Sep, pp. 581-587.

[85] Wilamowski, B.M. and Xiangli Li (2002), "Fuzzy system based maximum power point tracking for PV system", 28th IEEE Annual Conference on Industrial Electronics Society, 5-8 Nov., Vol. 4, pp. 3280-3284.

[86] C.-Y. Won, D.-H. Kim, S.-C. Kim, W.-S. Kim and H.-S. Kim (1994), "A new maximum power point tracker of photovoltaic arrays using fuzzy controller", in 25th IEEE PESC., 20-25 Jun., Vol. 1, pp. 396-403.

[87] Wu, T.-F. Chang, C.-H. Chen and Y.-K. (1999), "A fuzzy logic controlled single-stage converter for PV powered lighting system applications", IEEE Conference on Industry Applications, Vol. 3, pp. 1685-1692.

[88] www.powerdesigners.com/InfoWeb/design-center/articles/DC-DC/converter.shtm.

[89] web.mit.edu/10.001/Web/Course-Notes/Statistics Notes/Correlation/node2.html.

[90] www.nyu.edu/its/socsci/Docs/correlate.html.

[91] www.statsoft.com/textbook/stbasic.html.

[92] www.psychstat.missouristate.edu/multibook/mlt04.htm.

[93] www.clustan.com/what is cluster analysis.html.

[94] www.statsoft.com/textbook/stcluan.html.

[95] www4.eas.asu.edu/PowerZone/FuzzyLogic.

[96] www.seattlerobotics.org/encoder/Mar98/fuz/flindex.html.

[97] Yaragatti, U.R. Rajkiran, A.N. Shreesha and B.C. (2005), "A novel method of fuzzy controlled maximum power point tracking in photovoltaic systems", IEEE International Conference on Industrial Technology, 14-17 Dec., pp. 1421-1426.

[98] Ying-Tung and Hsiao China-Hong Chen (2002), "Maximum power tracking for photovoltaic power system", Industry Applications Conference, 37th IAS Annual Meeting, Oct., Vol. 2, 13-18, pp. 1035-1040.

Appendix A

Data Tables

Table A.1: Clustering the PU data of the 85W PV panel and the 51W PV panel.

PU data of the 85 PV solar panel				**pu data of the 51 PV solar panel**			
Isc(pu)	Voc(pu)	Clus-Num	Vmax	Isc(pu)	Voc(pu)	Clus-Num	Vmax
0.042	0.151	6	14.67	0.057	0.154	5	14.85
0.044	0.152	6	14.64	0.069	0.169	5	16.36
0.048	0.165	6	16.85	0.076	0.164	5	16.14
0.064	0.154	6	15.33	0.085	0.157	4	14.93
0.070	0.166	2	16.59	0.091	0.168	4	16.28
0.080	0.163	2	16.50	0.093	0.156	4	14.66
0.085	0.156	2	15.65	0.102	0.163	4	15.80
0.088	0.167	2	17.00	0.107	0.157	4	14.80
0.090	0.157	2	15.80	0.114	0.163	4	15.50
0.106	0.158	2	15.70	0.125	0.160	1	15.15
0.113	0.167	4	16.70	0.130	0.172	1	16.40
0.122	0.155	4	15.20	0.141	0.161	1	14.94
0.124	0.162	4	15.85	0.144	0.153	1	14.00
0.143	0.156	4	15.32	0.148	0.160	1	14.85
0.143	0.174	4	16.90	0.158	0.150	2	13.52
0.145	0.157	4	15.35	0.160	0.152	2	13.62
0.161	0.154	5	14.47	0.162	0.166	2	15.53
0.170	0.153	5	14.29	0.165	0.166	2	15.45
0.170	0.157	5	15.10	0.168	0.160	2	14.77
0.170	0.165	5	16.00	0.170	0.149	2	13.35
0.177	0.157	5	14.87	0.170	0.161	2	14.87
0.178	0.167	5	16.28	0.172	0.149	2	13.36
0.181	0.161	5	15.40	0.172	0.151	2	13.50
0.183	0.152	5	14.15	0.172	0.160	2	14.76
0.184	0.150	5	13.93	0.173	0.151	2	13.55
0.185	0.167	5	16.35	0.176	0.153	2	13.72
0.187	0.150	5	14.11	0.179	0.161	2	14.93
0.187	0.161	5	15.20	0.183	0.160	6	14.62
0.189	0.155	5	14.72	0.186	0.168	6	15.70
0.196	0.159	1	14.88	0.187	0.152	6	13.60
0.199	0.167	1	16.11	0.189	0.168	6	15.59
0.203	0.167	1	15.95	0.195	0.152	6	13.62
0.208	0.155	1	14.49	0.198	0.166	6	15.36
0.210	0.165	1	15.82	0.201	0.167	6	15.47
0.213	0.156	1	14.76	0.201	0.168	6	15.55
0.226	0.167	3	16.00	0.204	0.166	6	15.22
0.226	0.167	3	15.95	0.237	0.167	3	15.60
0.262	0.167	3	16.24	0.252	0.167	3	15.24

Table A.2: Actual and predicted V_{max} at different numbers of inputs MFs of 85W panel

Actual	**Predicted output at different number of MFs of inputs**							
V_{max}	2×1 MFs	3×1 MFs	4×1 MFs	5×1 MFs	1×2 MFs	1×3 MFs	1×4 MFs	2×2 MFs
12	12.049	12.006	12.009	12.002	12.049	12.04	12.002	12.014
15.4	15.315	15.571	15.572	15.561	15.315	15.936	15.735	15.512
15.16	15.169	15.047	15.04	15.063	15.169	15.625	15.423	15.055
16.9	16.497	16.716	16.724	16.722	16.497	16.642	16.683	16.626
16.4	16.504	16.486	16.488	16.498	16.504	16.577	16.625	16.59
16.29	16.43	16.272	16.268	16.273	16.43	16.471	16.542	16.519
14.8	14.896	14.625	14.61	14.602	14.896	14.542	14.794	14.678
15	15.194	15.134	15.139	15.132	15.194	14.975	15.016	15.098
15.1	15.266	15.276	15.288	15.288	15.266	15.069	15.021	15.218
16.85	17.374	17.105	17.084	16.998	17.374	16.932	16.921	16.906
16.6	16.612	16.531	16.531	16.496	16.612	16.522	16.526	16.573
16.7	16.122	16.28	16.305	16.372	16.122	16.128	16.226	16.294
16	15.484	15.883	15.941	16.095	15.484	15.399	15.222	15.798
16.83	17.079	16.903	16.869	16.863	17.079	16.811	16.808	16.808
16.5	16.595	16.574	16.558	16.599	16.595	16.537	16.516	16.548
15.65	15.523	15.824	15.856	15.753	15.523	15.595	15.667	15.882
17	16.962	16.812	16.771	16.896	16.962	16.782	16.794	16.775
15.8	15.651	15.889	15.907	15.792	15.651	15.759	15.884	15.946
16.22	16.259	16.304	16.291	16.292	16.259	16.302	16.28	16.324
15.7	15.528	15.714	15.716	15.548	15.528	15.667	15.743	15.777
16.7	16.716	16.598	16.57	16.682	16.716	16.686	16.699	16.626
15.2	15.123	15.307	15.299	15.162	15.123	15.241	15.218	15.345
15.85	15.946	15.961	15.948	15.923	15.946	16.022	15.997	16.012
15.53	15.54	15.584	15.572	15.613	15.54	15.65	15.629	15.628
15.32	15.034	15.114	15.094	15.304	15.034	15.145	15.222	15.103
16.9	17.292	17.081	17.116	16.892	17.292	16.92	16.906	17.138
15.35	15.077	15.137	15.118	15.323	15.077	15.188	15.32	15.131
15.66	15.677	15.63	15.644	15.676	15.677	15.682	15.652	15.66
14.47	14.699	14.71	14.682	14.632	14.699	14.746	14.651	14.614
15.8	15.509	15.468	15.477	15.494	15.509	15.529	15.488	15.492
14.25	14.328	14.343	14.298	14.212	14.328	14.238	14.292	14.172
14.35	14.544	14.518	14.487	14.432	14.544	14.553	14.437	14.409
15.1	14.987	14.948	14.939	14.918	14.987	15.041	15.109	14.924
16	16.068	15.998	16.045	16.106	16.068	16.074	16.078	16.026
14.87	15.002	14.945	14.943	14.937	15.002	15.035	15.049	14.929
16.28	16.224	16.165	16.229	16.286	16.224	16.307	16.311	16.185
15.4	15.453	15.391	15.418	15.436	15.453	15.402	15.357	15.396
14.15	14.383	14.3	14.271	14.254	14.383	14.348	14.233	14.261

Table A.3: Actual and predicted V_{max} at different numbers of inputs MFs of 85W panel

Actual	**Predicted output at different number of MFs of inputs**							
V_{max}	2×1 MFs	3×1 MFs	4×1 MFs	5×1 MFs	1×2 MFs	1×3 MFs	1×4 MFs	2×2 MFs
13.93	14.104	14.011	13.97	13.946	14.104	13.946	13.958	13.979
16.35	16.215	16.176	16.246	16.283	16.215	16.315	16.317	16.185
14.11	14.129	14.021	13.985	13.975	14.129	13.993	14.063	14.034
15.2	15.405	15.341	15.37	15.387	15.405	15.335	15.286	15.34
14.72	14.695	14.6	14.596	14.602	14.695	14.702	14.717	14.611
14.88	15.124	15.046	15.069	15.08	15.124	15.058	14.991	15.044
16.11	16.072	16.072	16.13	16.131	16.072	16.111	16.115	16.06
15.95	16.054	16.068	16.117	16.112	16.054	16.089	16.093	16.051
14.85	14.882	14.783	14.819	14.821	14.882	14.813	14.772	14.829
14.65	14.598	14.468	14.515	14.516	14.598	14.555	14.584	14.649
15.82	15.823	15.842	15.866	15.859	15.823	15.718	15.724	15.816
17.4	17.097	17.274	17.252	17.243	17.097	17.388	17.397	17.245
14.76	14.754	14.642	14.725	14.721	14.754	14.679	14.729	14.763
16	16.049	16.177	15.999	15.985	16.049	16.16	16.156	16.136
15.95	16.045	16.178	15.986	15.972	16.045	16.156	16.152	16.136
16.24	15.843	16.149	16.238	16.239	15.843	15.867	15.864	16.133

Table A.4: Actual and predicted V_{max} at different numbers of inputs MFs of 51W panel

Actual	**Predicted output at different number of MFs of inputs**							
V_{max}	2×1 MFs	3×1 MFs	4×1 MFs	5×1 MFs	1×2 MFs	1×3 MFs	1×4 MFs	2×2 MFs
16	15.77	16.001	15.992	15.994	15.54	15.582	15.629	15.9
16.07	16.06	16.076	16.091	16.09	15.967	16.013	16.003	16.108
16.5	16.572	16.507	16.501	16.498	16.42	16.407	16.394	16.404
16.2	16.252	16.217	16.225	16.223	16.174	16.194	16.176	16.246
16	16.088	15.943	15.938	15.936	16.077	16.096	16.081	16.116
15	15.121	14.984	14.995	15.003	15.09	15.032	15.038	15.06
14.85	15.034	14.913	14.887	14.881	15.06	15.039	15.054	14.942
16.36	16.492	16.485	16.473	16.47	16.344	16.348	16.351	16.406
16.1	16.093	16.092	16.088	16.087	16.143	16.137	16.139	16.167
16.14	15.894	15.927	15.933	15.949	15.997	15.998	16	16.001
15	14.937	14.975	14.983	14.964	15.055	15.056	15.046	14.862
16.28	16.238	16.328	16.337	16.397	16.218	16.216	16.214	16.282
14.66	14.762	14.807	14.817	14.778	14.881	14.862	14.852	14.656
15.8	15.592	15.658	15.666	15.674	15.735	15.743	15.754	15.717
14.8	14.773	14.815	14.826	14.788	14.903	14.888	14.868	14.721
15.5	15.411	15.453	15.459	15.471	15.553	15.565	15.578	15.519
14.9	14.933	14.967	14.977	14.975	15.067	15.066	15.053	14.948
15	14.948	14.965	14.967	15	15.07	15.071	15.063	14.989
15.15	15.044	15.062	15.062	15.092	15.168	15.175	15.175	15.104
16.4	16.479	16.496	16.472	16.434	16.41	16.396	16.401	16.381
14.94	14.971	14.963	14.933	14.915	15.058	15.062	15.068	15.03
14	14.091	14.081	14.059	14.074	14.148	14.052	14.02	14.056
14.85	14.922	14.907	14.859	14.831	14.989	14.991	14.997	14.977
13.52	13.546	13.535	13.502	13.516	13.562	13.506	13.501	13.513
13.8	13.781	13.769	13.737	13.747	13.792	13.752	13.746	13.775
15.53	15.555	15.527	15.489	15.486	15.607	15.615	15.628	15.554
15.45	15.563	15.534	15.532	15.528	15.609	15.617	15.628	15.552
14.77	14.762	14.743	14.769	14.764	14.757	14.748	14.751	14.797
13.35	13.361	13.359	13.374	13.373	13.343	13.378	13.376	13.349
14.87	14.813	14.794	14.84	14.833	14.801	14.798	14.809	14.843
13.36	13.312	13.311	13.327	13.326	13.29	13.324	13.324	13.298
13.64	13.67	13.665	13.689	13.688	13.646	13.676	13.681	13.68
14.76	14.72	14.703	14.756	14.75	14.699	14.685	14.686	14.75
13.55	13.558	13.555	13.578	13.577	13.531	13.604	13.604	13.562
13.8	13.804	13.801	13.831	13.832	13.766	13.717	13.707	13.824
14.93	14.837	14.823	14.881	14.884	14.794	14.796	14.816	14.847

Table A.5: Actual and predicted V_{max} at different numbers of inputs MFs of 51W panel

Actual	**Predicted output at different number of MFs of inputs**							
V_{max}	2×1 MFs	3×1 MFs	4×1 MFs	5×1 MFs	1×2 MFs	1×3 MFs	1×4 MFs	2×2 MFs
14.62	14.658	14.65	14.685	14.693	14.593	14.574	14.574	14.667
14.6	14.455	14.451	14.478	14.486	14.388	14.337	14.308	14.473
15.7	15.646	15.627	15.68	15.689	15.672	15.666	15.655	15.592
13.6	13.634	13.647	13.621	13.628	13.558	13.621	13.639	13.636
15.59	15.655	15.64	15.673	15.681	15.681	15.673	15.658	15.6
13.62	13.646	13.669	13.592	13.593	13.54	13.575	13.591	13.627
16.9	16.868	16.84	16.865	16.869	16.889	16.898	16.9	16.899
15.36	15.363	15.363	15.316	15.315	15.319	15.338	15.361	15.309
15.47	15.469	15.471	15.404	15.398	15.445	15.453	15.459	15.415
15.55	15.696	15.694	15.633	15.628	15.725	15.705	15.675	15.65
15.22	15.349	15.357	15.264	15.252	15.292	15.311	15.333	15.293
15.6	15.411	15.438	15.599	15.6	15.351	15.35	15.339	15.442
15.24	15.291	15.31	15.24	15.24	15.187	15.195	15.195	15.361

Table A.6: Per unit core data of solar PV panels

Per unit test data of solar PV panels								
I_{SC} (pu)	V_{OC} (pu)	V_{max} (pu)	I_{SC} (pu)	V_{OC} (pu)	V_{max} (pu)	I_{SC} (pu)	V_{OC} (pu)	V_{max} (pu)
0.0074	0.0934	0.1029	0.0540	0.0986	0.1006	0.1374	0.1015	0.1000
0.0156	0.0961	0.1033	0.0557	0.1057	0.1093	0.1394	0.0999	0.0979
0.0172	0.0991	0.1061	0.0569	0.0994	0.1016	0.0855	0.1008	0.0999
0.0172	0.0973	0.1042	0.0964	0.0967	0.0961	0.0904	0.0985	0.0985
0.0119	0.0980	0.0990	0.0984	0.0925	0.0900	0.0909	0.1101	0.1087
0.0138	0.0972	0.0975	0.0594	0.1026	0.1043	0.0921	0.0988	0.0987
0.0250	0.0973	0.1029	0.1009	0.0967	0.0955	0.1620	0.1008	0.1003
0.0162	0.1011	0.1087	0.1078	0.0903	0.0869	0.1718	0.1006	0.0980
0.0312	0.0927	0.0964	0.1095	0.0915	0.0887	0.1018	0.1024	0.1007
0.0189	0.1009	0.1055	0.1107	0.1001	0.1006	0.1023	0.0974	0.0930
0.0216	0.1006	0.1047	0.1128	0.1002	0.1010	0.1030	0.1016	0.1016
0.0390	0.0931	0.0955	0.0674	0.0996	0.1010	0.1042	0.0955	0.0916
0.0242	0.0948	0.0952	0.1148	0.0964	0.0950	0.1078	0.0968	0.0923
0.0267	0.0958	0.0964	0.1165	0.0897	0.0858	0.1078	0.0991	0.0971
0.0276	0.0961	0.0971	0.1165	0.0967	0.0956	0.1078	0.1046	0.1029
0.0472	0.1016	0.1052	0.1173	0.0895	0.0859	0.1127	0.1056	0.1047
0.0484	0.0996	0.1035	0.1173	0.0913	0.0877	0.1146	0.1018	0.0990
0.0303	0.1046	0.1083	0.1177	0.0963	0.0949	0.1163	0.0949	0.0896
0.0521	0.0988	0.1038	0.1181	0.0908	0.0871	0.1175	0.1058	0.1051
0.0315	0.1016	0.1067	0.1201	0.0920	0.0887	0.1182	0.0951	0.0907
0.0582	0.0943	0.0964	0.0715	0.1059	0.1074	0.1182	0.1017	0.0977
0.0623	0.1014	0.1047	0.1222	0.0970	0.0960	0.1199	0.0981	0.0946
0.0636	0.0938	0.0943	0.1251	0.0963	0.0940	0.1243	0.1004	0.0957
0.0378	0.1000	0.1074	0.1251	0.0953	0.0939	0.1260	0.1054	0.1036
0.0400	0.0973	0.1029	0.1271	0.1010	0.1010	0.1284	0.1054	0.1026
0.0697	0.0985	0.1016	0.1279	0.0915	0.0874	0.1306	0.0994	0.0955
0.0730	0.0945	0.0952	0.1292	0.1011	0.1002	0.1318	0.0980	0.0942
0.0441	0.1049	0.1082	0.0775	0.0983	0.0977	0.1333	0.1044	0.1017
0.0779	0.0980	0.0997	0.0787	0.1025	0.1019	0.1333	0.1109	0.1119
0.0779	0.0956	0.0958	0.1333	0.0918	0.0876	0.1347	0.0989	0.0949
0.0849	0.0961	0.0964	0.1333	0.1069	0.1087	0.1430	0.1059	0.1029
0.0504	0.1034	0.1061	0.1353	0.0999	0.0988	0.1434	0.1059	0.1026
0.0853	0.0966	0.0974	0.1374	0.1004	0.0995	0.1660	0.1056	0.1044
0.0886	0.1074	0.1055						

Table A.7: Percentage errors beween actual and predicted V_{max} of 85W data

85 ANFIS model		51 ANFIS model		
r = 0.5	r = 0.25	r = 0.5	r = 0.25	r = 0.4
0.46	-0.08	28.44	-9.05	27.49
1.39	-0.03	6.37	-2.84	5.85
0.99	0.00	6.68	-5.21	5.68
-2.11	-1.71	-0.98	-1.63	-1.64
0.56	0.99	1.33	0.31	0.43
0.67	1.30	1.08	-1.06	0.02
-1.70	-0.01	4.15	-18.96	1.51
0.18	0.03	3.28	-16.65	0.93
0.30	0.01	2.64	-16.53	0.38
1.64	0.35	0.93	3.34	0.22
-0.50	-0.21	-1.69	-2.23	-2.45
-2.89	-0.67	-5.34	-11.87	-5.87
-1.66	-0.05	-4.60	-20.80	-5.76
0.59	-0.20	-0.12	2.36	0.03
0.13	-0.57	-1.55	0.01	-1.04
1.97	0.39	-3.92	-17.87	-3.69
-1.01	0.10	-1.06	-0.03	-0.61
1.26	0.15	-4.25	-15.38	-3.67
0.18	0.78	-2.19	-2.26	-1.48
0.72	-0.66	-4.48	-13.53	-4.02
-1.19	-0.01	-0.62	-0.23	-0.67
1.31	0.08	-3.49	-3.73	-3.30
0.27	-0.45	-1.22	-1.73	-1.38
0.24	0.66	-2.13	-2.16	-2.22
-1.43	0.07	-4.16	-3.65	-4.02
1.27	-0.16	0.71	-9.89	0.92
-1.47	-0.20	-4.02	-3.56	-3.90
-0.15	0.53	-1.22	-2.37	-1.46
1.34	0.26	-0.36	-0.34	-0.39
-1.95	-0.74	-3.40	-3.84	-3.58
-0.17	-0.15	-0.89	-1.41	-1.26

Table A.8: Percentage errors beween actual and predicted V_{max} of 85W data

85 ANFIS model		51 ANFIS model		
0.82	-0.14	-0.41	-0.63	-0.57
-0.83	-0.79	-2.76	-2.65	-2.73
-0.14	0.01	-0.60	-1.35	-0.67
0.83	1.13	-1.16	-1.09	-1.13
-0.82	0.00	-1.50	-1.52	-1.44
0.29	0.13	-1.27	-1.59	-1.41
0.79	0.32	0.02	-0.48	-0.28
-0.13	0.66	0.08	-0.91	-0.57
-1.14	-0.02	-2.00	-1.77	-1.92
-1.19	-0.72	-1.09	-2.03	-1.70
1.34	-0.26	-0.38	-0.63	-0.49
-0.48	-0.44	-2.15	-2.27	-2.19
1.70	0.33	-0.47	-0.52	-0.45
-0.30	-0.41	-1.37	-0.85	-1.34
0.67	0.43	-0.50	0.06	-0.49
0.22	-0.46	-2.00	-2.05	-1.94
-0.64	0.24	-2.42	-2.67	-2.47
0.13	-0.01	-1.22	-0.22	-1.21

Table A.9: Percentage errors beween actual and predicted V_{max} of 51W data

85 ANFIS model		51 ANFIS model		
r = 0.5	r = 0.25	r = 0.5	r = 0.25	r = 0.4
-0.67	0.01	-2.54	-2.31	-4.81
0.16	0.00	0.59	-0.63	-4.38
-0.78	0.00	2.67	2.84	-7.32
0.18	0.00	1.63	0.36	-5.21
0.76	0.00	2.06	1.23	-3.27
0.54	-0.01	1.57	1.85	2.55
0.59	-0.01	2.46	2.91	3.37
0.23	-0.03	3.48	249.25	-3.74
0.62	0.08	2.02	23.47	-2.14
-0.47	-0.07	0.07	11.71	-2.33
-1.01	0.01	0.78	0.39	1.24
-0.10	0.01	0.50	340.69	-2.09
-0.24	0.01	2.04	2.60	2.22
-0.33	0.00	-1.15	35.45	-1.14
-0.41	-0.12	0.64	0.16	1.33
0.09	0.06	-0.76	10.30	-0.53
0.60	0.40	0.55	-1.16	1.54
0.08	-0.32	-0.21	-13.23	0.51
-0.27	-0.22	-0.69	-25.74	-0.16
-0.06	0.01	0.96	265.56	0.55
0.43	0.16	0.40	-81.79	0.42
0.47	0.08	2.19	1.71	2.77
0.68	0.21	0.83	-60.76	0.75
0.00	0.17	2.02	1.83	2.12
-0.31	-0.25	1.66	2.64	1.69
-0.42	-0.45	0.89	-367.86	0.78
0.16	0.57	1.55	-429.10	1.44
0.14	0.00	0.76	1.00	0.58
0.15	0.14	1.93	1.58	1.74
-0.27	-0.23	0.46	-3.09	0.30
-0.23	-0.28	1.46	1.06	1.27
0.11	0.14	2.14	2.91	1.88
-0.04	-0.06	0.64	2.99	0.47
-0.03	0.02	1.99	2.31	1.72
-0.03	-0.12	1.92	2.57	1.62
-0.59	-0.37	0.38	-7.80	0.28
0.49	0.85	1.42	2.77	1.29

Table A.10: Percentage errors beween actual and predicted V_{max} of 51W data

85 ANFIS model		51 ANFIS model		
r = 0.5	r = 0.25	r = 0.5	r = 0.25	r = 0.4
-0.62	-0.35	0.28	-7.33	0.09
-0.59	-0.38	1.10	-390.86	1.01
0.15	0.12	2.33	1.45	2.00
0.22	0.17	1.97	-319.00	1.88
0.05	0.01	2.33	-0.30	2.08
-0.04	-0.48	2.20	673.54	1.73
-0.17	-0.49	1.66	-277.49	1.65
-0.13	0.40	1.77	-148.28	1.74
0.88	0.04	2.84	14.95	2.75
0.73	0.26	2.67	-151.40	2.67
-1.11	-0.31	1.53	616.83	1.54
0.51	0.19	3.55	302.82	3.59

Table A.11: The rate of change in duty cycle (dD) of Buck-Boost converter at different input and output voltages

	Vo (V)										
Vin (V)	1	2	3	4	5	6	7	8	9	10	11
1	-0.250	-0.222	-0.188	-0.160	-0.139	-0.122	-0.109	-0.099	-0.090	-0.083	-0.076
2	-0.111	-0.125	-0.120	-0.111	-0.102	-0.094	-0.086	-0.080	-0.074	-0.069	-0.065
3	-0.063	-0.080	-0.083	-0.082	-0.078	-0.074	-0.070	-0.066	-0.063	-0.059	-0.056
4	-0.040	-0.056	-0.061	-0.063	-0.062	-0.060	-0.058	-0.056	-0.053	-0.051	-0.049
5	-0.028	-0.041	-0.047	-0.049	-0.050	-0.050	-0.049	-0.047	-0.046	-0.044	-0.043
6	-0.020	-0.031	-0.037	-0.040	-0.041	-0.042	-0.041	-0.041	-0.040	-0.039	-0.038
7	-0.016	-0.025	-0.030	-0.033	-0.035	-0.036	-0.036	-0.036	-0.035	-0.035	-0.034
8	-0.012	-0.020	-0.025	-0.028	-0.030	-0.031	-0.031	-0.031	-0.031	-0.031	-0.030
9	-0.010	-0.017	-0.021	-0.024	-0.026	-0.027	-0.027	-0.028	-0.028	-0.028	-0.028
10	-0.008	-0.014	-0.018	-0.020	-0.022	-0.023	-0.024	-0.025	-0.025	-0.025	-0.025
11	-0.007	-0.012	-0.015	-0.018	-0.020	-0.021	-0.022	-0.022	-0.023	-0.023	-0.023
12	-0.006	-0.010	-0.013	-0.016	-0.017	-0.019	-0.019	-0.020	-0.020	-0.021	-0.021
13	-0.005	-0.009	-0.012	-0.014	-0.015	-0.017	-0.018	-0.018	-0.019	-0.019	-0.019
14	-0.004	-0.008	-0.010	-0.012	-0.014	-0.015	-0.016	-0.017	-0.017	-0.017	-0.018
15	-0.004	-0.007	-0.009	-0.011	-0.013	-0.014	-0.014	-0.015	-0.016	-0.016	-0.016
16	-0.003	-0.006	-0.008	-0.010	-0.011	-0.012	-0.013	-0.014	-0.014	-0.015	-0.015
17	-0.003	-0.006	-0.008	-0.009	-0.010	-0.011	-0.012	-0.013	-0.013	-0.014	-0.014
18	-0.003	-0.005	-0.007	-0.008	-0.009	-0.010	-0.011	-0.012	-0.012	-0.013	-0.013
19	-0.003	-0.005	-0.006	-0.008	-0.009	-0.010	-0.010	-0.011	-0.011	-0.012	-0.012
20	-0.002	-0.004	-0.006	-0.007	-0.008	-0.009	-0.010	-0.010	-0.011	-0.011	-0.011
21	-0.002	-0.004	-0.005	-0.006	-0.007	-0.008	-0.009	-0.010	-0.010	-0.010	-0.011
22	-0.002	-0.003	-0.005	-0.006	-0.007	-0.008	-0.008	-0.009	-0.009	-0.010	-0.010

Table A.12: The rate of change in duty cycle (dD) of Buck-Boost converter at different input and output voltages

	Vo (V)										
Vin (V)	12	13	14	15	16	17	18	19	20	21	22
1	-0.071	-0.066	-0.062	-0.059	-0.055	-0.052	-0.050	-0.048	-0.045	-0.043	-0.042
2	-0.061	-0.058	-0.055	-0.052	-0.049	-0.047	-0.045	-0.043	-0.041	-0.040	-0.038
3	-0.053	-0.051	-0.048	-0.046	-0.044	-0.043	-0.041	-0.039	-0.038	-0.036	-0.035
4	-0.047	-0.045	-0.043	-0.042	-0.040	-0.039	-0.037	-0.036	-0.035	-0.034	-0.033
5	-0.042	-0.040	-0.039	-0.038	-0.036	-0.035	-0.034	-0.033	-0.032	-0.031	-0.030
6	-0.037	-0.036	-0.035	-0.034	-0.033	-0.032	-0.031	-0.030	-0.030	-0.029	-0.028
7	-0.033	-0.033	-0.032	-0.031	-0.030	-0.030	-0.029	-0.028	-0.027	-0.027	-0.026
8	-0.030	-0.029	-0.029	-0.028	-0.028	-0.027	-0.027	-0.026	-0.026	-0.025	-0.024
9	-0.027	-0.027	-0.026	-0.026	-0.026	-0.025	-0.025	-0.024	-0.024	-0.023	-0.023
10	-0.025	-0.025	-0.024	-0.024	-0.024	-0.023	-0.023	-0.023	-0.022	-0.022	-0.021
11	-0.023	-0.023	-0.022	-0.022	-0.022	-0.022	-0.021	-0.021	-0.021	-0.021	-0.020
12	-0.021	-0.021	-0.021	-0.021	-0.020	-0.020	-0.020	-0.020	-0.020	-0.019	-0.019
13	-0.019	-0.019	-0.019	-0.019	-0.019	-0.019	-0.019	-0.019	-0.018	-0.018	-0.018
14	-0.018	-0.018	-0.018	-0.018	-0.018	-0.018	-0.018	-0.017	-0.017	-0.017	-0.017
15	-0.016	-0.017	-0.017	-0.017	-0.017	-0.017	-0.017	-0.016	-0.016	-0.016	-0.016
16	-0.015	-0.015	-0.016	-0.016	-0.016	-0.016	-0.016	-0.016	-0.015	-0.015	-0.015
17	-0.014	-0.014	-0.015	-0.015	-0.015	-0.015	-0.015	-0.015	-0.015	-0.015	-0.014
18	-0.013	-0.014	-0.014	-0.014	-0.014	-0.014	-0.014	-0.014	-0.014	-0.014	-0.014
19	-0.012	-0.013	-0.013	-0.013	-0.013	-0.013	-0.013	-0.013	-0.013	-0.013	-0.013
20	-0.012	-0.012	-0.012	-0.012	-0.012	-0.012	-0.012	-0.012	-0.013	-0.012	-0.012
21	-0.011	-0.011	-0.011	-0.012	-0.012	-0.012	-0.012	-0.012	-0.012	-0.012	-0.012
22	-0.010	-0.011	-0.011	-0.011	-0.011	-0.011	-0.011	-0.011	-0.011	-0.011	-0.011

Appendix B

Programs and Codes

B.1 Clustering Program

```
norm51 =normc(data)
[cidx651,cmeans6] = kmeans(norm51,6,'dist','sqeuclidean')
tsymb = {'Ks','K^','kd','ko','k+','k*'};
for i = 1:6
clust = find(cidx651==i);
plot(norm51(clust,1),norm51(clust,2),ptsymb{i});
hold on
end
plot(cmeans6(:,1),cmeans6(:,2),'ko');
plot(cmeans6(:,1),cmeans6(:,2),'kx');
hold off
xlabel('Isc(per unit)'); ylabel('OCV(per unit)');
grid on
```

B.2 ANFIS Function Program

```
x = [cdata85(:,1) cdata85(:,2)] ;
y = cdata85(:,3);
trnData = [x y];
numMFs = [4 1];
mfType = 'gaussmf';
epoch_n = 200;
in_fismat = genfis1(trnData,numMFs,mfType);
[out_fismat,trnerror85Gauss51_05] = ANFIS(trnData,in_fismat,[200 0.05]);
cdata85(:,6)=evalfis(x,out_fismat);
```

```
[x1,mfin1] = plotmf(in_fismat,'input',1);
subplot(2,2,1),plot(x1,mfin1);
xlabel('input1(Isc) (gaussmf)');
title('MFs befor training');
[x2,mfin2] = plotmf(in_fismat,'input',2);
subplot(2,2,2),plot(x2,mfin2);
xlabel('input2(OCV) (gaussmf)');
title('MFs befor training');
[x1, mfout1] = plotmf(out_fismat,'input',1);
subplot(2,2,3),plot(x1,mfout1);
xlabel('input1(Isc) (gaussmf)');
title('MFs after training');
[x2, mfout2] = plotmf(out_fismat,'input',2);
subplot(2,2,4),plot(x2,mfout2);
xlabel('input2(OCV) (gaussmf)');
title('MFs after training');
```

B.3 FIS Structure

```
[System]
Name='G2G1struutureG_thesis'
Type='sugeno'
Version=2.0
NumInputs=2
NumOutputs=1
NumRules=5
AndMethod='prod'
OrMethod='probor'
ImpMethod='min'
AggMethod='max'
DefuzzMethod='wtaver'
[Input1]
```

B.3 FIS Structure

Name='in1'

Range=[0.0073807 0.1718]

NumMFs=5

MF1='in1mf1':'gaussmf',[0.0290888063512544 0.107814272589563]

MF2='in1mf2':'gaussmf',[0.0290686522123429 0.0483974255600078]

MF3='in1mf3':'gaussmf',[0.0290564204000468 0.120142120900253]

MF4='in1mf4':'gaussmf',[0.029061071480828 0.12599102547254]

MF5='in1mf5':'gaussmf',[0.0290381335173562 0.0242065385415515]

[Input2]

Name='in2'

Range=[0.089547 0.11093]

NumMFs=5

MF1='in2mf1':'gaussmf',[0.0037020704914013 8 0.0991266618360669]

MF2='in2mf2':'gaussmf',[0.0039006343528395 4 0.0995501215896314]

MF3='in2mf3':'gaussmf',[0.0037985503653792 7 0.0920262581510554]

MF4='in2mf4':'gaussmf',[0.0037844173833104 7 0.10536153579982]

MF5='in2mf5':'gaussmf',[0.0037296540815444 4 0.0946462858535078]

[Output1]

Name='out1'

Range=[0.085837 0.11188]

NumMFs=5

MF1='out1mf1':'linear',[0.0284587670940233 0.953426845771906 -6.29434793431661e-005]

MF2='out1mf2':'linear',[-0.089668440325274 8 -0.149200575923581 0.130010956663389]

MF3='out1mf3':'linear',[-0.046790210073274 8 0.759940337542289 0.0234497465379686]

MF4='out1mf4':'linear',[-0.0040072184994376 49 1.25867557269035 -0.0282479509226493]

MF5='out1mf5':'linear',[-0.257628075633 57 -0.736976195520495 0.169417515183569]

[Rules]

1 1, 1 (1) : 1

2 2, 2 (1) : 1

3 3, 3 (1) : 1

4 4, 4 (1) : 1

5 5, 5 (1) : 1